Burial and Regeneration of Phosphorus in the Northern and the Central Indian Ocean: Linkage to Iron Geochemistry

A Thesis submitted to the Goa University for the Award of the Degree of

DOCTOR OF PHILOSOPHY

In Marine Sciences

By

LINSY P

Research Supervisor: **Dr. B. Nagender Nath**

Co-Guide: **Dr. Sridhar D. Iyer**

(CSIR) National Institute of Oceanography

Dona Paula, Goa-403004

Goa University,

Taleigao, Goa

September 2020

Dedicated to Ehan Adam

CONTENTS

Statement

As required under the University ordinance OA-19.8 (v), I state that the present thesis entitled *"**Burial and Regeneration of Phosphorus in the Northern and the Central Indian Ocean: Linkage to Iron Geochemistry**"*, is my original contribution and the same has not been submitted on any previous occasion. To the best of my knowledge, the present study is the first comprehensive work of its kind from the area mentioned.

The literature related to the problem investigated has been cited. Due acknowledgements have been made wherever facilities and suggestions have been availed of.

Linsy P

CSIR - National Institute of Oceanography

Dona Paula, Goa-403004

September 2020

Certificate

This is to certify that the thesis entitled *"**Burial and Regeneration of Phosphorus in the Northern and the Central Indian Ocean: Linkage to Iron Geochemistry**"*, submitted by Mrs. Linsy P for the award of the degree of Doctor of Philosophy in Marine Sciences is based on her original studies carried out by her under my supervision. The thesis or any part thereof has not been previously submitted for any other degree or diploma in any university or institution.

Dr. B. Nagender Nath
Research Guide

CSIR – National Institute of Oceanography

Dona Paula, Goa, 403004

Dr. Sridhar D. Iyer

Co - Guide

CSIR – National Institute of Oceanography

Dona Paula, Goa, 403004

Place:

Date:

Acknowledgements

The work presented in this thesis would not have been possible without the support of many people. I take this opportunity to extend my sincere gratitude and appreciation to all those who made this thesis possible.

Firstly, I would like to express my sincere gratitude to my guide, Dr. B. Nagender Nath for introducing me to this exciting field of geochemistry and for his patience, motivation and continuous support throughout my Ph.D. His guidance helped me throughout my research and thesis writing. His enthusiasm, dedication on research and his mission for providing high-quality work, has made a deep impression on me. Dr. Nath's wealth of knowledge in the field of marine geochemistry, in particular, is inspiring. Thank you for allowing me to work with you and thereby familiarizing me with the sampling techniques and analysis during the oceanographic expeditions. I could not have imagined a better advisor and mentor for my Ph.D. study.

My special words of thanks should also go to my research co-guide Dr. Sridhar D. Iyer for his continuous support, guidance, cooperation, and encouragement during my Ph.D. and related research. His guidance greatly improved the manuscripts and this thesis. Thank you for giving me the wonderful opportunity to work with you.

I express my gratitude to Vice Chancellor's nominee Dr. Parthasarathi Chakraborty for his invaluable suggestions during DRC meetings and evaluating my work and progress report from time to time. My sincere gratitude also goes to Vice Chancellor's nominee Prof. Vishnu Murty Matta, Goa University for his suggestions.

I express my heartfelt gratitude to Dr. Maria Brenda Mascarenhas Pereira for being with me as an elderly figure throughout. Her scientific inputs, personal help, and friendly nature have always made me feel at ease with her and I could always look back on her for any support during my Ph.D.

I am indebted to my project leaders Dr. Rahul Sharma and Dr. N.H Khadge for their continuous support during my stay at NIO. I am thankful to Dr. Prakash Babu and Dr. Parthiban for providing the analytical facilities like Coulometer, C-N analyzer and ICP-MS for my research work and helping me in various analyses.

I am also thankful to Dr. Yatheesh, Dr. V.K Banakr, Dr. Durbar Ray, Dr. Sibi Kurian, Dr. Kocherla, Dr. Abhay Mudholkar, Dr. Kamesh Raju and Mr. B.R Rao for their support during my stay at NIO.

I am also grateful to my fellow labmates Kazip, Pavan, Arindam, Jayesh, Pushkaraj, Peeyush, Manuel, Ajeesh, Robin, Chandan, Avinash, Sushil, Sneha, Latha, Sarun, Sooraj, Tanvi, Amol, Bagyasree, Ankeeta, Sucharita, Archana, Surabhi, Simontini, Hellen, Manimaran and Veersen for helping me in every possible way.

I thank Saranya, Aswini, Kartheek, Krushna, Suresh, Darwin, Jubin, Aswini M.A, Arathy, Nikhil, Kabeer, Sarath, Suja, Prajith, Sameena, Teesha, Sherin, Srinivas and Savithri, for all the fun we had in the last seven years. I am also thankful to the Malayali community of NIO colony who made this journey wonderful.

I am grateful to people of ship cell and ship crew for their help during onboard sampling. Brother Vikas, still I can't believe you are gone, will never forget you. Rest in peace.

I gratefully acknowledge, MOES-supported PMN-EIA (GAP2128), Council of Scientific and Industrial Research (CSIR)-supported GEOSINKS (PSC0106) projects for the funds to carry out this research. My sincere gratitude goes to the former and present Directors, of CSIR-NIO for providing all the research facilities to carry out my doctoral research work.

Finally, I acknowledge the people who mean a lot to me, my parents, Achan, and Amma for supporting me throughout my life. Your hard work and sacrifice made me what I am today. Thanks to my

brother Lijoy, for his love, care and support. I express my gratitude to Ranjiettan for helping me and my family in every possible way. My heartfelt regard goes to my father-in-law, mother-in-law, Denish, and Doniya for their love and moral support.

I owe thanks to my husband, Tyson, for being so understanding and for putting up with me through the toughest moments of my life. His continued and unfailing love and support made this thesis possible. I greatly value his contribution and deeply appreciate his belief in me. I appreciate my son, Chanku (Ehan) for abiding my absence and the patience he showed during my research. Words would never say how grateful I am to both of you.

...Linsy P

Preface

Phosphorus (P) is a limiting nutrient in the oceanic system and exerts a major control on the primary productivity in geological time scale (Tyrrell, 1999). Its burial within the sediments is an important process by which P is removed from the oceanic nutrient pool (Ruttenberg, 2003). Thus, it is important to understand the ability of sediments to regenerate and/or retain bio-available P. The biogenic P is delivered to the sediments mainly in association with organic matter. During degradation of organic matter, P is released to interstitial waters. Phosphate in interstitial waters appears to be involved in various biogeochemical processes. The released P may either be adsorbed onto grain surfaces, bound to iron (oxy)hydroxides or diffused back to bottom waters or may be available for formation of authigenic carbonate fluorapatite (CFA) which is eventually buried in the bottom sediments (Babu and Nath, 2005 and references therein). The dominant sink for oceanic P is deposition and burial in marine sediments (after transformation from dissolved to particulate forms). A significant diagenetic reorganization of P has been observed in the lacustrine, continental margin, and deep-sea sediments of various areas (Filippelli, 2001 and references therein).

The cycling of P is strongly coupled with Fe cycling through iron oxyhydroxide, one of the dominant reactive Fe phases in sediments. The iron oxyhydroxides, due to their high adsorption capacity, scavenge dissolved phosphate mainly in oxic condition (Slomp et al., 1996). On the other hand, under reducing conditions, they undergo reductive dissolution and release P to the overlying water (Froelich et al., 1988; Van Cappellen and Berner, 1988) and this released phosphate may also facilitate the formation of CFA within the sediments (e.g., Ruttenberg and Berner, 1993). Most of the reduced Fe undergoes re-oxidation, a portion of which reacts with other elements to form minerals such as Fe(II) sulfides (FeS - iron mono sulfide, FeS_2 - pyrite), Fe(II) carbonates (siderite, ankerite), Fe(II) phosphates (vivianite), and Fe(II)-bearing authigenic clays, depending on the diagenetic conditions (Aller et al., 2004b, 2004a; Zhu et al., 2013; Egger et al., 2015; Ma et al., 2018). Though the role of Fe on the benthic release of P and CFA

formation was studied extensively (e.g., Slomp et al., 1996; Marz et al., 2008; Noffke et al., 2012), questions still remain concerning the controlling factors which link the P and Fe oxide geochemistry, especially due to variable bottom water oxygenation. Also, the affinity of P towards different Fe bearing minerals (especially among the Fe-oxide/oxyhydroxides) is poorly known.

Among the sources and sinks of P, the regeneration fluxes from sediments are not well constrained. There are very few global estimates of diffusive regeneration/return fluxes of phosphate from marine sediments to overlying bottom waters. The most comprehensive global estimate is based on only 193 published pore water phosphate profiles (Coleman and Holland, 2000). The total pre-agricultural return flux of P from marine sediments was estimated by those authors to be ca. 12 x 10^{11} mol P/yr, which is more than an order of magnitude larger than the riverine flux of total dissolved P to the oceans (ca. 0.3 x 10^{11} mol P/yr). As the estimates are based on less than 200 locations, the estimates need revision with new measurements and collation with other results published in the last 18 years. One of the major gaps is a lack of quality data from the Indian Ocean, which make the global estimates incomplete.

Thus, in view of the prevailing gap in our understanding, this study is undertaken on the P cycling in the Northern and the Central Indian Basin. These are two contrasting areas, with former having varying bottom water oxygenation and the latter having typically oxic bottom water. The study by Colman and Holland (2000) and others have also found that the phosphate return fluxes, scaled to carbon regeneration fluxes, are significantly greater from highly reduced sediments than from highly oxidized sediments. Hence, the present study in the Northern Indian Ocean assumes importance, as both the Arabian Sea and the Bay of Bengal have intense intermediate water oxygen minimum zones.

A minor sink for P is uptake through seawater-oceanic crust interactions associated with hydrothermal activity on the oceans floor (Paytan and McLaughlin, 2007). Removal of phosphate by coprecipitation with Fe-rich particles in hydrothermal plumes along ridge axes accounts for ~18–33% of the dissolved riverine flux and the oceanic hydrothermal systems remove about 50% of the pre-industrial

dissolved riverine flux of phosphate (Wheat et al., 1996). While the P removal in hydrothermal plume is known, the phosphorus geochemistry during the hydrothermal alteration of sediments is not clearly identified.

In view of the prevailing gaps, some of which are described above, and the importance of geochemical cycling of P for ocean functioning in general, a comprehensive study of sedimentary cycling of P in the Northern and the Central Indian Ocean has been undertaken with the following objectives.

1. compare the variability of regeneration processes and quantify the phosphate fluxes at the sediment-water interface in the Northern and Central Indian Ocean.

2. quantify the phosphorus bound to chemically separable phases to understand the burial pattern and pathways in shelf and slope sediments of the Northern Indian Ocean and the abyssal areas of the Central Indian Basin.

3. study the influence of redox chemistry of iron on benthic pore water fluxes and authigenic formation of calcium fluorapatite in the northern Indian Ocean.

4. investigate the binding of phosphorus in different phases of iron using sequential extraction protocol.

In order to achieve these objectives, bottom sediments and porewater collected from the Northern and Central Indian Ocean were studied. The Northern Indian Ocean is one of the most dynamic tropical region of the world. These dynamic conditions are driven by the diverse conditions prevailing in the area such as high river runoff in the northeast and large excess evaporation over precipitation and river runoff in the northwest (Gupta and Naqvi 1984). These unique characteristics make the Northern Indian Ocean an interesting site for studying the variability of sedimentary cycling of P which is expected to vary with the changes in the character of sediments and the depositional environment. The Central Indian Basin (CIB) is a large abyssal basin, which is rich in ferromanganese nodules. The sediments of the CIB are low in organic matter due to oxygen rich bottom waters, low export fluxes from surface oceans, and low

sediment accumulation rate (leads to increased oxygen exposure time) (Nath and Mudholkar, 1989; Gupta and Jauhari, 1994; Nath et al., 2012). The P cycling in the sediments overlain by oligotrophic waters, in general, is poorly known. Thus, the study on P geochemistry of CIB sediments undertaken here, contributes to the very few studies of abyssal oceans available so far. Earlier studies have reported the occurrence of hydrothermally altered sediments from the flank of a seamount in the CIB.

The porewater geochemical data and sequential chemical extraction tools are used here to understand the fate and sink pathways of P, sink switching after the deposition, P authigenesis and the geochemical control of iron on P cycling. Quantification of the diffusive flux of phosphate in the studied areas helped assess the P regeneration processes within a depositional environment as well to compare between different depositional environments. The data presented in this thesis represent the single largest benthic flux data base for the Indian Ocean region, and will contribute to the global budgeting of diagenetic flux of P in the oceans.

The entire work has been presented in eight chapters and a brief outline of each of these chapters is presented below.

Chapter 1

This chapter is based on extensive literature survey and provides a general introduction to the importance of P in the marine realm and its cycling in the ocean and also describes the linkage of P and Fe in marine sediments. In the light of gaps in our understanding of P cycling at the sediment-water interface, the scientific rationale to undertake this work will be defined and the objectives drawn for this study will be presented.

Chapter 2

This chapter describes the features of the study area, materials used and methods employed for the fulfillment of the research objectives. A detailed description of the oceanography and geological settings of the study areas viz., the Arabian Sea, Bay of Bengal, and the CIB is presented. Following that, a detailed description of the sampling techniques employed and location map of the sampling stations are provided in this chapter. To accomplish the scientific objectives, benthic fluxes of phosphate are calculated at 98 stations from different water depths (28-5307 m) using porewater phosphate data. Thirty six surface sediments and sixteen short cores are used for the sequential chemical extraction study in order to understand the pathways of P incorporation and redistribution in sediments.

This chapter also provides the details of the analytical procedures used in this study. These include the determination of dissolved oxygen (DO) in the seawater by Winkler's method and dissolved inorganic phosphate (DIP) in porewater and seawater by spectrophotometric method. Sequential chemical extraction of phosphorus, modified by Babu and Nath (2005) using the original method developed by Ruttenberg (1992), subsequently modified by Anderson and Delaney (2000) and Schenau and De Lange (2000), was used for the separation of different phases of P from the sediments. The different phases of P extracted are 1) easily exchangeable or loosely sorbed or biogenic P (P_{bio}), 2) iron bound P (P_{Fe}), 3) authigenic P (P_{auth}), 4) detrital P (P_{det}) and the 5) Organic P (P_{org}). The sequential extraction procedure developed by Poulton and Canfield (2005) was used for Fe fractionation. The six phases intended for separation of iron represent the possible Fe-bearing minerals which could be amorphous or crystalline and are as follows: 1) carbonate bound Fe ($Fe_{AVS+carb}$), 2) ferrihydrite and lepidocrocite (Fe_{ox1}), 3) goethite, akaganeite and hematite (Fe_{ox2}), 4) magnetite (Fe_{mag}), 5) nontronite, chlorite, glauconite, and biotite (Fe_{PRS}) and 6) un-reactive silicate Fe and pyrite Fe (Fe_{U+py}).

Chapter 3

This chapter details the P speciation study of the Eastern Arabian Sea. This study attempts to assess the P burial pathways and investigate if any present day phosphogenesis is on-going in the oxygen-depleted sediments of the Eastern Arabian Sea. Results of this study provide convincing evidence of present-day phosphogenesis in the study area. This finding contrasts with previous reports of the occurrence of only old phosphorites along the Indian margin. Extensive benthic P regeneration is observed in the sediments that are deposited on topographic highs in the western Indian continental margin, which are impinged by a perennial oxygen minimum zone (OMZ). The phosphate flux from the sediments ranged between 1.1 and 22 mmol m^{-2} yr^{-1}. Among the P reservoirs, biogenic P (P_{bio}) is the major pool of P within the upper 30 cm of the sediments. P released from organic matter decomposition and fish debris dissolution mainly control benthic P regeneration while the role of redox cycling of iron is weak.

The change in authigenic P (P_{auth}) with depth in the sediment and a concomitant decrease in porewater dissolved inorganic phosphate (DIP), solid phase P_{bio} and organic P (P_{org}) content collectively indicate the transformation of P from labile phases to an authigenic phase. Molar C_{org}/P_{org} and $C_{org}/P_{reactive}$ ratios also support the notion of ongoing phosphogenesis in the area. To quantify the P_{auth} formation from P_{org} and P_{bio} depletion, best-fit curves were drawn and the area under the curves was calculated by integration. This study is the first report of ongoing phosphogenesis in the Indian continental margin. In one of the sites, eolian deposition and water column authigenesis were found to be responsible for elevated CFA content. The estimated burial efficiency of P at the sediment-water interface at two locations is only about 2% and this indicates extensive P regeneration in this area.

Chapter 4

This chapter pertains to the sedimentary cycling of P in the Bay of Bengal and represents the first detailed investigation of sedimentary cycling of P in the Bay of Bengal.

In this study, the benthic cycling of P in the western Bay of Bengal is investigated where the sediments are impinged by oxygen-depleted water. The results suggest that the sedimentary cycling of P in Bay of Bengal sediments is largely regulated by the influx of fluvially derived lithogenic material. P_{org} exerts a minor role on the benthic release of P owing to the low decomposition rate of organic matter and abundance of terrestrially derived organic matter. Low input of reactive P (P_{react}) and high input of non-reactive P through river runoff and their rapid burial by ballast effect hinders sink switching of P from the labile to authigenic phase. Despite the oxygen-depleted conditions, low bacterial respiration limits microbial reduction of iron oxyhydroxide and makes the redox cycling of iron a weak player in sedimentary cycling of P. Compared to the eastern Arabian Sea, the western Bay of Bengal shows a large variability in P cycling owing to low primary productivity, high lithogenic flux and possibly due to different sediment physical properties.

Chapter 5

This chapter concerns the distribution and diagenesis of P in the deep-sea sediments of the CIB. The results show that P enrichment is in the order of $P_{bio} > P_{auth} > P_{Fe} > P_{det} > P_{org}$. The higher concentrations of P_{bio} are found in siliceous oozes, which are attributed to high biological productivity in the overlying waters compared to pelagic clay region. High P_{auth} and P_{det} contents with low molar C_{org}/P_{react} ratios in the pelagic/red clays indicate the deposition of calcium fluorapatite and refractory material from the atmospheric input. The oxygenated bottom water promotes adsorption of P onto iron oxyhydroxides making the P_{Fe} an important sink in the CIB. Remobilization of P within the sediments is limited in the CIB because of well-oxygenated conditions and efficient adsorption by iron oxyhydroxides and clay-sized sediments. A twofold increase in P_{total} and P-species is observed in hydrothermally altered,

ferruginous sediments from a seamount flank suggesting an important role of hydrothermal processes in P cycling. The calculated P accumulation rate in the present study ranges between 0.6 and 11.7 μmol·cm^{-2}·kyr^{-1}. The burial flux of P for the entire CIB (5.7 × 106 km^2) is 0.01 × 10^{10} mol P per year which accounts for 0.05% of the global flux.

Chapter 6

The first comprehensive study of the benthic diffusive flux of phosphate covering large parts of the Northern Indian Ocean and the CIB is presented in this chapter. Diffusive flux of phosphate at 98 stations using porewater phosphate concentration is estimated to compare the variability of benthic regeneration processes in the shelf slope sediments of the Northern Indian Ocean and abyssal areas of the CIB. Along with this, the factors controlling the benthic release of P in sediments are assessed. The results suggest that the continental margin sediments of the Northern Indian Ocean are an important source for P to the global oceans. In the Northern Indian Ocean, high fluvial input and high input of photosynthetically produced organic matter and their degradation lead to the enhanced release of P from sediments. Highest fluxes are measured at shallow stations in which the coastal seasonal hypoxia prevail which coincide with the highest Fe concentration indicating that microbial reduction of iron oxyhydroxides is responsible for the elevated fluxes in the shallow shelf stations. High concentrations of Fe in the shelf area may be due to the high deposition rate of iron oxyhydroxides during the periods of bottom water oxygenation.

The calculated benthic flux of phosphate for the CIB indicate that the sediments act as sink for P where well-oxygenated conditions and an efficient adsorption by iron oxyhydroxides and clay-sized sediments and low input of photosynthetically produced organic matter limits the release of P. The total annual diffusive flux of P for the entire Arabian Sea is 0.39 x 10^{11} mol/yr (this work combined with

published literature) and the flux for Bay of Bengal is 0.377 x 10^{11} mol/yr; combinedly these two areas increases the global diagenetic flux by about 6%.

Chapter 7

This chapter deals with the geochemical study of P and Fe and their linkages. For this study, in addition to P speciation, fractionation studies of Fe are also undertaken of the surface sediments along two transects across the OMZ of the Eastern Arabian Sea (EAS) to understand the effect of varying bottom water oxygen concentration on the geochemistry of both these elements individually and their linkages. The porewater profiles and solid phase speciation results of this study suggest that the precipitation of CFA is mostly restricted to the OMZ where high remobilization of P from the reductive dissolution of iron oxyhydroxides and dissolution fish debris leads to this sink-switch over. High benthic phosphate flux and high C_{org}/P_{org} ratio in the OMZ indicate the low P retention capacity of the Arabian Sea sediments. The presence of high P_{Fe} content in sediments overlain by hypoxic waters is attributed to the re-adsorption of upward diffusing phosphate at the sediment-water interface.

The results suggest that ferrihydrite is an important sink for P since ferrihydrite is poorly crystalline, and have large micropore volume and surface site density compared to other Fe oxide minerals. Thus, sorption of P is found to be higher than that for other crystalline Fe(III) oxides (e.g. goethite and hematite). The fractionation study of Fe shows that the formation of Fe(II) minerals such as siderite, iron mono-sulfide, pyrite etc., are limited in the surface sediments, even though the sediments are overlain by oxygen-depleted water due to the lack of significant sulfate reduction and abundance of iron oxide associated with metal-reducing microbial communities.

Chapter 8

This chapter summarizes the results and major conclusion drawn from this study. While all the conclusions are described in the individual chapters, the key findings of this investigation are presented below:

1. In the Northern Indian Ocean, the continental margin sediments act as a source of oceanic P and contribute to about 6% of its global diagenetic flux while the deep-sea sediments of the CIB act as a sink of P.
2. In the Arabian Sea, enhanced degradation of organic material and the dissolution of fish debris and oxygen-depleted conditions favor the present day phosphogenesis, while in the Bay of Bengal because of high input of non-reactive P through river runoff and their rapid burial by ballast effect limits the sink switch over. In the CIB, extensive water column remineralization and lack of significant diagenesis limit the phosphogenesis while the atmospheric deposition contributes a significant amount of P to the authigenic pool.
3. Even under reducing conditions, Fe plays a weak role on the benthic release of P in the Northern Indian Ocean while in the CIB, prevailing oxic condition makes Fe a major sink for P.
4. Relative proportions of Fe-bearing oxide minerals (ferrihydrite, goethite, hematite and magnetite) were found to vary with changing bottom water oxygenation.
5. Among the major iron-bearing mineral phases, ferrihydrite is found to be the major hosting phase for P in the Arabian Sea sediments.

List of tables

List of Figures

Chapter 1

Introduction

1.1 Introduction

1.1.1 Importance of Phosphorus

Phosphorus (P) is the thirteenth element in the periodic table and eleventh most abundant element in the Earth's crust (0.11 % by mass), act as an essential nutrient for energy transfer process and growth of biota. P is a structural component of deoxyribonucleic acid (DNA) and ribonucleic acid (RNA) as a phosphate ester backbone and is part of a molecule adenosine triphosphate (ATP) which carries energy in living molecules. P is an important constituent of phosphoproteins and phospholipids in the cell membrane (Paytan and McLaughlin, 2007). P is incorporated in bones and teeth of vertebrates in the form of hydroxyapatite ($Ca_{10}(PO4)_6(OH)_2$) and carbonate fluoride substitutes, respectively. P present in rocks and soils include both inorganic phosphate mineral and organic phosphate derivatives. Over 95% of the P in Earth's crust occurs as apatite ($Ca_5(PO4)_3$-(F Cl OH) (Paytan and McLaughlin, 2007). Most of the organic P derivatives in soils and sediments are orthophosphate monoester, orthophosphate diesters, and phosphonates and phosphorus anhydrides.

Generally, P bears a +5 oxidation state and in the natural environment, P is exclusively present as phosphate ($PO4^{3-}$) and a trace amount of phosphine (PH_3) have been found in aquatic sediments, soils and atmosphere (Slomp, 2011 and references therein). At neutral pH, free phosphate occurs as a mixture of mono and diprotonated P species of orthophosphate (HPO_4^{2-}

and $H_2PO_4^-$). Orthophosphate plays a key role in photosynthesis (Paytan and McLaughlin, 2007). The chemical equation representing average ocean photosynthesis can be written as

$$106CO_2 + 16HNO_3 + H_3PO_4 + 12H_2O + \text{Trace and Vitamins} \xrightarrow{\text{light}} C_{106}H_{263}O_{110}N_{16}P + 138O_2$$

Thus the marine phosphorus (P) cycle is connected to the marine carbon (C) and nitrogen (N) cycles through the photosynthesis by phytoplankton, which forms the base of the marine food web (Ruttenberg, 2003). Redfield, (1958) estimated that the marine phytoplankton, on average has molar C: N: P ratio of 106:16:1. Thus the availability of P in the marine system can strongly influence marine primary productivity and act as a limiting nutrient over a geological timescale (see Delaney, 1998; Filippelli, 2008).

1.1.2 Phosphorus in the marine realm

Phosphorus is a limiting nutrient in the oceanic system and exerts a major control on the longer-term primary production in the global ocean (Falkowski et al., 1998; Tyrrell, 1999). The major sources of P to the ocean are river input, atmospheric deposition, and volcanic activity. The major share of P supplied comes from river runoff, as a continental weathering product. The atmospheric deposition also is an important source of P, reaching the ocean through aerosols, volcanic ash and mineral dust but it is less than 10% of river input (Fig. 1.1). Hydrothermal processes like submarine high-temperature weathering and submarine low-temperature seawater-basalt exchange also can bring soluble P to the ocean (Froelich et al., 1982).

P reaching in the ocean by river runoff in dissolved and particulate matter comes in both mineral and organic forms (Baturin, 2003). Out of that most of it is in the detrital phase and buried in sediment without further alteration (Fig. 1.1). Particulate forms include living and dead plankton, detrital P, P adsorbed to particulates etc. Detrital P refers to P that present in detrital

grains such as igneous, metamorphic and sedimentary apatites as well as a trace element in other minerals (Compton et al., 2000). Detrital P is generally covalently bonded in mineral structures and not available for biological uptake or by adsorption until released by chemical weathering (e.g., Compton et al., 2000; Ruttenberg, 2003). Adsorbed P refers to the P adsorbed on iron-manganese oxide/oxyhydroxide particle surfaces and clay minerals. Adsorbed P is readily available for biological uptake through the reversible exchange. The estimated flux of average riverine discharge into the ocean ranges between 27 and 49 $\times 10^{10}$ mol/year for particulate inorganic P (PIP) and 2.9 $\times$ 10^{10}mol/year for particulate organic P (POP) (Paytan and McLaughlin, 2007).

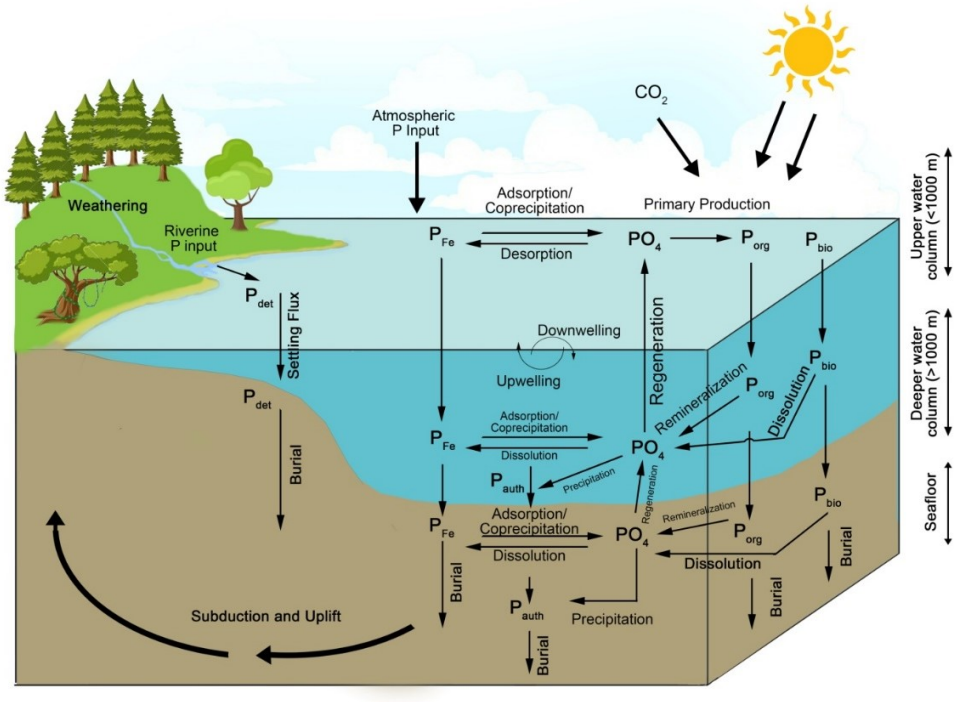

Figure 1.1 Schematic representation of the marine phosphorus cycle

Atmospheric input is the significant source of P to the open ocean as well as coastal zone and comprises 5% of the total pre-anthropogenic P input to the ocean or about 3.2 $\times 10^{10}$mol/year

(Paytan and McLaughlin, 2007 and references therein). Major sources of particulate P in the present-day atmosphere are the soil particles containing both naturally occurring and fertilizer derived, sea-salt particles and from biomass burning or industrial sources (Graham and Duce, 1979; Slomp, 2011). Thus, the dominant pre-anthropogenic atmospheric P supply to the ocean could have mainly come from soil and sea-salt sources. The deposition by aerosol is highly episodic and dependent on atmospheric circulation and location of source regions for P-containing dust (Slomp, 2011). Atmospheric P carried through the Sahara mineral dust has been found to maintain the fertility of the Amazon rainforest (e.g., Prospero et al., 1981) and the Western Ghat rainforests in India (Ramaswamy et al., 2017). A fraction of atmospheric P is water soluble and available for uptake by oceanic plankton, and the atmospheric acidification of aerosols is considered as a prime mechanism for producing soluble phosphorus from the soil-derived mineral dust (Nenes et al., 2011).

Volcanic activity is another source of P in a localized area albeit on a short timescale. The volatilization of basaltic magma produces P_4O_{10} gas which condenses to form water-soluble polyphosphates upon rapid cooling (Yamagata et al., 1991). The concentration of P in volcanic ash can reach up to 1%. wt and ash releases P to the seawater at a rate of 1.7 $\mu mol.g^{-1}h^{-1}$ (Paytan and McLaughlin 2007). In any case, this does not significantly contribute to the marine phosphorus balance (e.g., Baturin, 1988).

Sinking of organic matter is the principal source of P to the marine sediments and organic matter undergoes extensive degradation during the transport through the water column (Kraal, 2011). Released P from organic matter is eventually returned to surface water through upwelling and is re-available for biological uptake. Oceanographic settings exert a major role in the

remineralization processes in which 50% of the sinking organic matter is buried in shelf sediments under relatively shallow water column.

The majority of the organic matter reaching the sediment is oxidized mainly at or near the sediment-water interface (e.g., Filippelli and Delaney, 1996). Jahnke (1996) estimated the organic carbon burial in deep-sea sediments (at water depth > 1000 m) to be 1.25×10^{12}mol C/Yr and contributes approximately 3% of the deposition rate to the seafloor sediment. The re-mineralization of organic matter in the sediment releases phosphate to interstitial water and this phosphate either reaches back to the water column or may be adsorbed by iron oxyhydroxides; elevated concentration of dissolved P will result in authigenic precipitation. The degradation of organic matter is highly redox-dependent; in deep-sea settings where the supply of organic matter is low and bottom water is well-oxygenated which results in oxidation of more than 90% of the organic matter being deposited (Fig.1.2). But in coastal areas, the supply of organic matter is high and bottom water can be oxygen depleted which leads to the preservation of C relative to P.

The molar C_{org}/P_{org} is a good indicator of P burial in sediments and redox-dependent regeneration of P from organic matter (Babu and Nath 2005 and Kraal et al., 2012). The molar C_{org}/P_{org} ratios in anoxic sediments are higher than the oxic sediments indicating an enhanced regeneration of P from organic matter relative to organic carbon (Ingall et al., 1993). Lower C_{org}/P_{org} ratios in organic-poor pelagic sediments may either reflect the presence of stable, phosphorus-rich organic fraction or the bacterial biomass (Froelich et al., 1982). Thus, the molar C_{org}/P_{org} ratio in sediments are also used as a tool to study microbial sequestration of P (Dale et al., 2016). Some microorganism such as bacteria can store and accumulate P as polyphosphate granules (Sannigrahi and Ingall, 2005). Accumulation of polyphosphate occur under an oxic

condition but under an anaerobic environment the stored P is utilized as an energy source and eventually released to surrounding water (Sannigrahi and Ingall, 2005). The polyphosphate synthesized by bacteria are converted into nearly non-metabolizable organic P such as phosphate esters and phosphonates (Dale et al., 2016). This microbial sink switching leads to lower C_{org}/P_{org} ratios in oxic sediments (Ingall et al., 1993; Dale et al., 2016). Due to the efficient transfer of P_{org} to other sedimentary P phases C_{org}/P_{react} ratio can be used to study the diagenetic redistribution of P in sediments (Anderson et al., 2001), and it reflects the overall burial efficiency of P in sediments (Kraal et al., 2012).

Another potential source of P to the sediments is the burial of fish debris. The hard part of the fish debris consists of hydroxyapatite ($Ca_5(PO_4)_3OH$) (60-70%) which will be a significant source of P in sediments of the highly productive region and undergo dissolution and phosphate will be released to porewater. The dissolution of fish debris predominantly occurs after deposition due to its larger size and high density compared to seawater and thus sinking of fish debris is relatively fast (Schenau and De Lange, 2000). The dissolution of fish debris may regulate the benthic porewater fluxes and authigenic apatite forms in highly productive coastal upwelling areas (Suess, 1981; Van Cappellen and Berner, 1988; Schenau and De Lange, 2000). The mineral hydroxyapatite may convert into carbonate fluorapatite by replacing the hydroxyl ion by fluoride (Atlas and Pytkowicx, 1977; Schenau and De Lange, 2000). High benthic phosphate fluxes in continental margin sediments of the Arabian Sea are to a large extent the result of sedimentary fish debris dissolution (Schenau and De Lange, 2001).

Iron oxyhydroxides are a potential carrier of reactive P to the sediment. Oxic condition favor the adsorption of dissolved phosphate on surface of iron oxyhydroxides (Slomp et al., 1996b). The iron oxyhydroxides in sediment can scavenge upward diffusing phosphate released

by the dissolution processes within the sediments and limits the release of P to overlying water. In contrast, these iron oxyhydroxides undergo reductive dissolution under reducing condition and P is released to the surrounding waters (Fig.1.2). Enrichment of reactive iron may occur at sediment-water interface due to re-precipitation of upward diffusing Fe^{2+} mobilized under reducing condition, as the oxic-suboxic interface is located close to the sediment surface (Schenau and De Lange, 2001). Thus, under the oxygen-depleted condition, dissimilatory Fe (III) reduction may lead to the enrichment of porewater phosphate and is conducive to the formation of authigenic apatite (Fig 1.2).

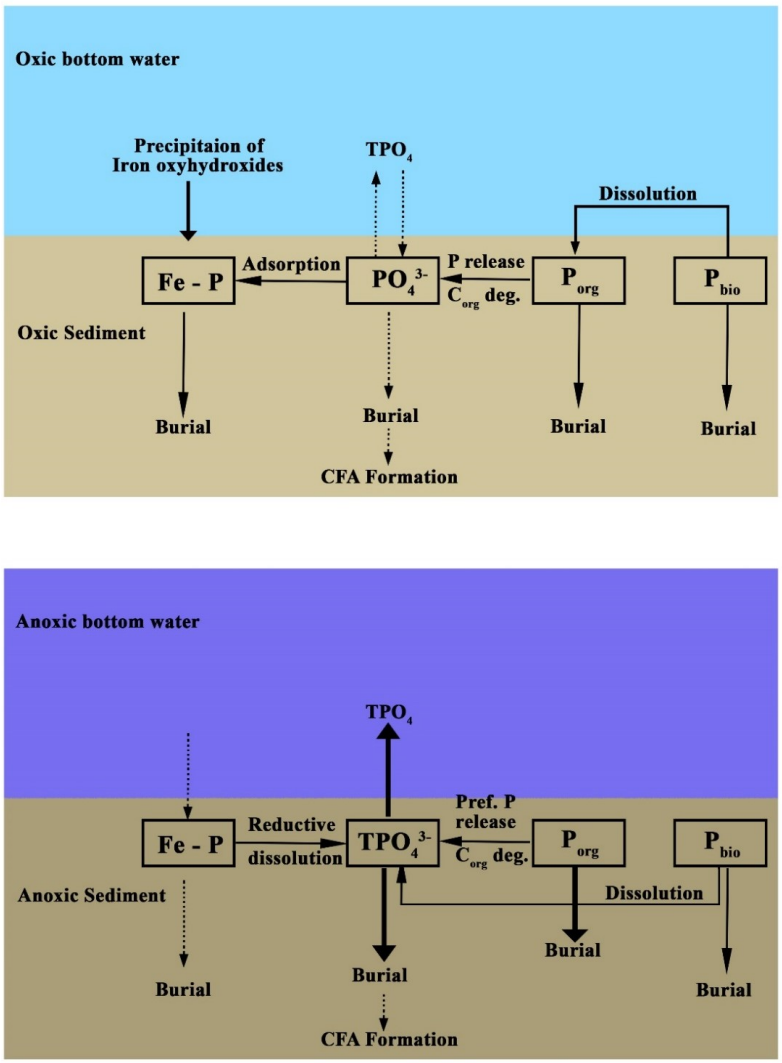

Figure 1.2 Schematic diagram showing variation of P dynamics under oxic and anoxic conditions (modified from Noffke, 2014).

The major sink of P from the ocean is through the formation of authigenic apatite (calcium fluorapatite- CFA) (Ruttenberg and Berner, 1993). Phosphate released from organic matter degradation (e.g. Froelich et al., 1988; Ruttenberg and Berner, 1993), reductive dissolution of iron oxyhydroxides (e.g. Sundby et al., 1992; Slomp et al., 1996a) and dissolution of fish debris (Suess, 1981; Schenau and De Lange, 2001) may lead to the precipitation of CFA in sediments, and the process is called sink switch over. Two prerequisites for authigenic P formation are saturation of porewater phosphate concentration and sedimentary condition that favor the nucleation of phosphate in porewater (Van Cappellen and Berner, 1988; Schenau et al., 2000; van der Zee et al., 2002). High porosity may reduce the P retention capacity by enhancing the P diffusion to bottom water (Van Cappellen and Berner, 1988; Filippelli et al., 1994; Schenau et al., 2005).

The sink switching of P from labile phase to authigenic phase is more common in upwelling areas characterized by oxygen-depleted water (Ruttenberg and Berner, 1993; Anderson et al., 2001; Ruttenberg, 2003). CFA formation was also reported in the non-upwelling areas (Long Island Sound and Mississippi Delta) where organic matter degradation and subsequent release of phosphate are conducive to the precipitation (Ruttenberg and Berner, 1993). The authigenic apatite formation is limited in oligotrophic deep sea settings where low organic matter flux and high oxygen concentration limits the release of P to the porewater (e.g., Tsandev et al., 2012). High francolite precipitation during early diagenesis and processes of sediment reworking such as redeposition and winnowing may lead to phosphorite formation (containing more than 5 wt% P_2O_5) (Kolodny, 1981; Froelich et al., 1988; Schenau et al., 2000).

1.1.3 Linkage of Fe and P in Marine Sediments

Iron oxyhydroxides are the primary constituents governing mobility of P in sediments. The binding mechanism includes adsorption on the surface of iron oxyhydroxides or co-precipitation with a metal ion (Fig. 1.3). However, the adsorption capacity of iron oxyhydroxides varies with mineralogy, crystallinity, morphology and chemical composition (Kostka and Luther, 1994; Thamdrup, 2000). P sorption is dominant on iron oxide minerals such as ferrihydrite, lepidocrocite, and goethite than minerals with characteristically lower surface areas, such as hematite (Torrent and Schwertmann, 1992; Slomp and van Raaphorst, 1993; Ruttenberg and Sulak, 2011).

The adsorption of phosphate on iron oxyhydroxides involves ligand exchange mechanism in which OH^-group on the hydrous oxides are replaced by phosphate anion in solution (Zhang and Huang, 2007).

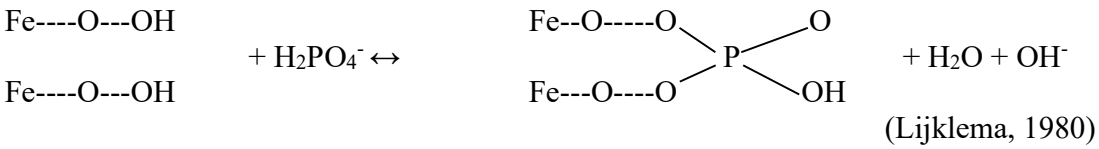

(Lijklema, 1980)

This reaction is pH dependent in which excess hydroxide ion can reduce P-retention in metal complexes (Lijklema, 1980). In anoxic settings sulfate reduction also affects the P adsorption; in which sulfate reduction produce OH^- ion and promote desorption of P (Caraco et al., 1993). But non-sulfidic reducing condition leads to precipitation of Fe-P mineral such as vivianite (Dijkstra et al., 2014). Vivianite ($Fe_3(PO4)_2$ $8H_2O$) is a reduced Fe(II) phosphate mineral and its formation occurs mostly in anoxic, non-sulfidic iron-rich environment (Gunnars

et al., 2002). However, the early diagenetic formation of vivianite is restricted to oceanographic settings with high sedimentation rate and relatively high abundance of Fe-oxides (Ruttenberg, 2003; Egger et al., 2015). Vivianite formation mostly occurs in the sulfate-methane transition zone (SMTZ), Fe^{2+} enrichment can occur in the absence of sulfide below SMTZ and the build-up of porewater phosphate from organic matter degradation may lead to supersaturation with respect to vivianite (März et al., 2008; Slomp et al., 2013; Egger et al., 2015) (Fig. 1.3). Lacustrine sediments are ideal sites for vivianite formation in which the sediments are rich in iron oxide and depleted with $SO4^{2-}$ (Fagel et al., 2005; Sapota et al., 2006; Rothe et al., 2014; O'Connell et al., 2015).

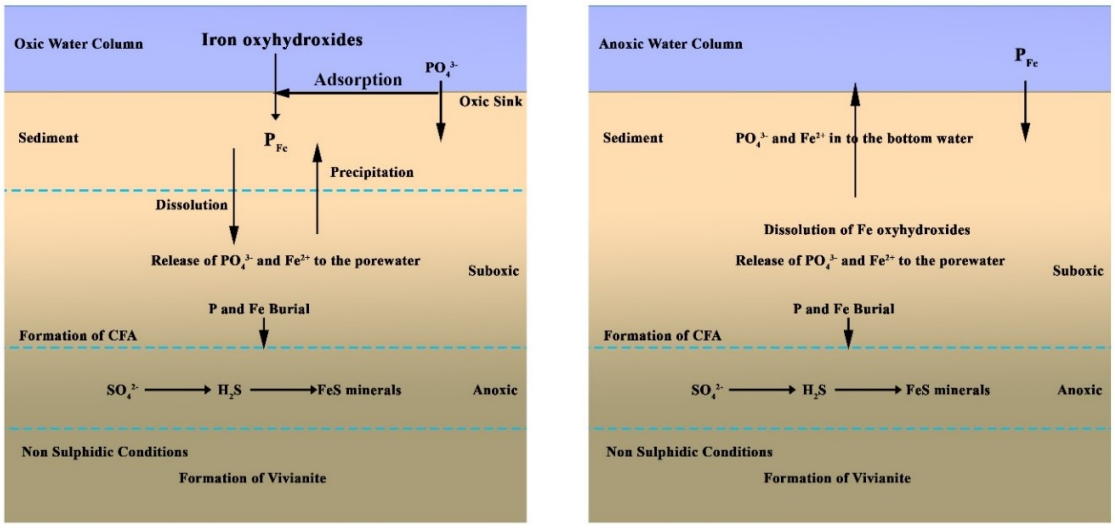

Figure 1.3: Schematic diagram showing P and Fe linkage under different oceanographic condition (modified from Lomnitz, 2017).

1.2 Scope of this work and the scientific rationale

Nearly all the major global campaigns, such as JGOFS (Joint Global Ocean Flux Study) and LOICZ (Land Ocean Interactions in the Coastal Zone), which assessed the biogeochemical

cycling of biologically essential elements in oceans have placed an emphasis on carbon leaving out phosphorus, possibly because the coastal zone is an efficient sink for carbon than for other two nutrients N and P (Wollast, 1993). However, P, though constitutes less than 1% of carbon in plankton, is an essential element and forms the base of a marine food web. Thus, the sedimentary cycling of P is important to understand the ability of sediment to regenerate or retain the bio-available P, where the enhanced regeneration may induce high primary productivity in the photic zone. Among the sources and sinks of P, the regeneration fluxes from sediments are not well constrained. There are very few global estimates of diffusive regeneration/return fluxes of phosphate from marine sediments to overlying bottom waters (e.g., Wollast, 1993; Hensen et al., 1998). But the most comprehensive global estimate is based on 193 published pore water phosphate profiles (Coleman and Holland, 2000).

The total pre-agricultural return flux of P from marine sediments estimated by those authors works out to ca. 12 x 10^{11} mol P/yr, which is more than an order of magnitude larger than the riverine flux of total dissolved P to the oceans (ca. 0.3 x 10^{11} mol P/yr). This could either be an underestimation or an overestimation, as these estimates are based on less than 200 locations. These estimates need revision with new measurements and collation with other results published in the last 18 years. One of the major gaps in the estimates is a lack of quality data from the Indian Ocean, an area which occupies ~20% of global oceans, which make the global estimates incomplete.

A minor sink for P is uptake through seawater-oceanic crust interactions associated with hydrothermal activity on the ocean floor (Paytan and McLaughlin, 2007). Removal of phosphate by co-precipitation with Fe-rich hydrothermal plume particles in the mid-oceanic ridge systems accounts for ~18–33% of the dissolved riverine flux and the oceanic hydrothermal systems

remove about 50% of the pre-industrial dissolved riverine flux of phosphate (Wheat et al., 1996). While P removal in hydrothermal plume is known, P geochemistry during hydrothermal alteration of sediments is not clearly identified. In a Fe-P co-diagenesis study in hydrothermal sediments from the East Pacific Rise, Poulton and Canfield (2006) found that a significant portion of the primary ferrihydrite precipitates are altered to goethite, which is a stable form of Fe and to clay minerals, a process involves the scavenged P release to solution but also retaining a major P fraction within the secondary goethite. Thus, the hydrothermal sediments act as sinks. Fluid flow through ridge flanks was estimated to remove 2.8×10^{10} mol P yr^{-1}, which constitutes about 35% of the sedimentary P sink (Wheat et al., 2003) which is substantial. Unlike, in active hydrothermal systems at ridge systems, Iron oxyhydroxides can act as both source and sink for P in the marine environment depending on the bottom water oxygenation. Though the role of Fe on the benthic release of P and CFA formation was studied extensively (e.g., Slomp et al., 1996; Marz et al., 2008; Noffke et al., 2012), questions still remain concerning the controlling factors which link/delink the P and Fe oxide geochemistry especially when the bottom water oxygenation vary. It is generally believed that the benthic flux of Fe increases in low bottom water oxygenation condition due to dissolution of Fe-oxyhydroxides. P bound to Fe oxyhydroxides tends to dissolve increasing the dissolved loads of both these elements. However, recently, Fe-oxides were found to precipitate in oxygen deficient zones when the dissolved Fe is oxidized back to particulate Fe(III) by nitrate or nitrite either through microbial or through abiotic catalysts (Heller et al., 2017). Also, the affinity of P towards different Fe bearing minerals (especially among the Fe-oxide/oxyhydroxides) is poorly known. Though the affinity of P for newly formed oxyhydroxides is known, the variability of different iron minerals within the suboxic-anoxic conditions is poorly known.

In view of the prevailing gaps in our understanding, this study is undertaken on the P cycling in the Northern and the Central Indian Basin. These are two contrasting areas, with former having varying bottom water oxygenation and the latter having typically oxic bottom water. The study by Colman and Holland (2000) and others have also found that the phosphate return fluxes, scaled to carbon regeneration fluxes, are significantly greater from highly reduced sediments than from highly oxidized sediments. The benthic phosphorus fluxes from the Peruvian oxygen minimum zone (OMZ), for example, are higher than the global flux from oxic margin sediments by a factor of 17 (Noffke et.al., 2012). Hence, the present study in the Northern Indian Ocean assumes importance, as both the Arabian Sea and Bay of Bengal have intense intermediate water oxygen minimum zones which can possibly reflux significant amount of P.

Over the decades, the ancient phosphorites and phosphatic grains have been reported in the continental margin of India (Nair, 1985; Rao, 1986; Borole et al., 1987; Rao and Nair, 1988; Rao et al., 1995,1998, 2000, 2002, 2007, 2008; Rao and Lamboy, 1995; Rao and Rao, 1995; Vaz, 1995; Vaz et al., 1996, 1999). Phosphorite formation is long-term sink of bio-available P in the ocean, so its formation strongly influences the availability of P for the biogeochemical processes. Thus, the present-day biogeochemical cycling, ongoing phosphogenesis and P incorporation into the sediment are important in regulating the P availability to the ocean ecosystem. Though, the phosphorites, phosphatic pellets and concretions are known to occur in the Indian continental margins, limited attempts are made to understand the benthic biogeochemical cycling of P and the prevalence of present day phosphogenesis, if any.

Owing to the presence of intense OMZ in the Arabian Sea, most of the P cycling studies in the Indian Ocean is confined to the Arabian Sea in which the OMZ strongly impacts the P-

biogeochemistry (Kraal et al., 2012). Enhanced release of P from organic matter and reductive dissolution of iron oxyhydroxides under oxygen-depleted condition leads to high benthic P regeneration in the Arabian Sea sediments. Along with this, high fish production resulted from high primary productivity also lead to this high benthic regeneration (Schenau and De Lange, 2001). Schenau and De Lange (2001) and Babu and Nath (2005) suggested that the redox cycling of iron play a weak role on the sedimentary P cycling in the Arabian Sea. In contrast, Kraal et al. (2012) suggested that redox cycling of iron plays a major role on P geochemistry in the western Arabian Sea. Thus, more detailed studies are needed to understand the role of iron on the P cycling. The information on the variation of P geochemistry within the OMZ and the contribution of the Arabian Sea to the global diagenetic flux of P are limited.

Even though the Arabian Sea and Bay of Bengal are two limbs of the northern Indian Ocean, information on sedimentary cycling of P in the Bay of Bengal is conspicuously lacking. Babu and Ramaswamy (2017) and Mohanty et al. (2018) have studied the distribution of different forms of P in the surface sediments of Bay of Bengal. Babu and Ramaswamy (2017) suggest that most of the sedimentary P phases are associated with intense diagenetic iron oxide cycling while Mohanty et al. (2018) suggest that most of the P in Bay of Bengal (BoB) sediments is associated with calcium. The published data of P-geochemistry in the BoB are limited to the surface sediments leaving a major gap in our understanding of the early diagenetic processes of P. In addition, role of large terrestrial supplies and the impact of OMZ on the sedimentary cycling of P are not known yet.

Most of the efforts to understand the P cycling at the deep-sea sediment-water interface were limited to study the pore water and diffusive flux of phosphate from the sediments the Atlantic (De Lange, 1986a, 1986b, Hensen et al., 1998, 2000; Zabel et al., 1998); the Pacific

(Emerson et al., 1980; Jahnke et al., 1982) and the Indian Ocean (Nath and Mudholkar, 1989; Grandel et al., 2000) with an emphasis to assess the early diagenetic processes. Though, the ocean floor deeper than 3000 m water depth occupies more than 50% of the ocean space, the information on pathways of P incorporation and solid phase P-speciation in deep-sea sediments, is limited to very few studies in the Pacific (Morse and Cook, 1978; Filippelli and Delaney, 1995, 1996; Tsandev et al., 2012; Ni et al., 2015) and only one in the Atlantic (Kraal et al., 2010), leaving a major gap in our understanding of other abyssal areas of the Indian and the Atlantic Oceans. In view of the prevailing gaps, some of which are described above, and the importance of geochemical cycling of P for ocean functioning in general, a comprehensive study of sedimentary cycling of P in the Northern and the Central Indian Ocean has been undertaken with the following objectives.

1.4 Objectives of the present study

5. Compare the variability of regeneration processes and quantify the phosphate fluxes at the sediment-water interface in the Northern and Central Indian Ocean.
6. Quantify the phosphorus bound to chemically separable phases to understand the burial pattern and pathways in shelf and slope sediments of the Northern Indian Ocean and the abyssal areas of the Central Indian Basin.
7. Study the influence of redox chemistry of iron on benthic pore water fluxes and authigenic formation of calcium fluorapatite in the northern Indian Ocean.
8. Investigate the binding of phosphorus in different phases of iron using sequential extraction protocol.

To achieve these objectives, 36 surface sediments and 98 short cores collected from the Central and the Northern Indian Ocean (Fig.2.4 and Table 2.2) were studied for porewater and sediment geochemistry. In addition, seawater was analyzed for dissolved oxygen and phosphate in 98 stations. For the calculation of diffusive flux of phosphate, porewater and bottom water data from 98 locations (water depths between 28 and 5307m), in areas with different oceanographic settings, was used, making this the largest single data set of benthic P regeneration presented so far for the Indian Ocean region. Porewater geochemical data and sequential chemical extraction tools were used to understand the P geochemistry and Fe-P relationship in sediments.

Three short cores collected from the marginal highs of Arabian Sea were used to assess the P burial pathways and investigate if any present-day phosphogenesis is ongoing in the oxygen-depleted sediments of the Eastern Arabian Sea. Sedimentary cycling of P in the western Bay of Bengal was assessed using four short cores. The core tops of 26 surface sediment samples collected from two sediment domains (siliceous ooze and pelagic brown clays) of Central Indian Basin were studied for assessing the spatial variability in distribution of different P phases. In addition to this, six sediment cores mainly chosen to represent a north-south transect were chosen to study the down core P geochemistry of the Central Indian Ocean (CIB). A sediment core recovered from the flanks of a seamount, in the vicinity of fracture zone where hydrothermal alteration reported earlier was used to study the influence of hydrothermal activity on the P geochemistry.

To understand the impact of varying bottom water oxygen concentration on the geochemistry of elements P and Fe and their linkages, 16 surface sediments of two transect across the OMZ of the Eastern Arabian Sea were studied. In addition to P speciation, Fe speciation was also

undertaken in the surface sediments across the OMZ to assess the major Fe-bearing mineral phases favorable for P sorption and its variability with changing oxygenation.

Chapter 2

Study area, Materials and Methods

Study Area, Materials and Methods

2.1 Study Area

2.1.1. Geological and Oceanographic settings of the Arabian Sea

The Arabian Sea is situated in the northwestern part of the Indian Ocean and is bounded by Asian and African land masses (Fig. 2.1). It covers an area of 3.86 x10^6 square kilometers with an average water depth of 2,734 m (Groves and Hunt, 1980). The Arabian Sea was formed by the collision of the Indian subcontinent with Asia within the past ~50 million years (https://www.britannica.com). The continental shelf of the Arabian Sea is "approximately 120 km wide off the southern tip of India, narrow to about 60 km off 11˚N and widens to about 350 km off the Gulf of Cambay" (Shetye et al., 1994). Compared to the Arabian Peninsula, the continental shelf is narrow along the Somali coast. In the Arabian Sea, terrigenous deposits cover the major part of the continental margin and the deeper basins (above 2700 m) are covered by the calcareous oozes (https://www.britannica.com).

The Arabian Sea experiences a semiannual reversal of wind regimes and which governs the terrestrial and oceanic climate as well as the biogeochemistry of the area. The summer south-west monsoon winds lead to an intense coastal upwelling along the NE African coast due to strong offshore Ekman Transport (e.g., Wyrtki, 1973; Slater and Kroopnick, 1984). These nutrient-rich surface upwelled waters are transported throughout the Arabian Sea and stable solar irradiance leads to a summer primary productivity bloom that produces approximately 200 g Carbon/m^2 /y (e.g., Nair et al., 1989; Brock et al., 1993). Strong North East Monsoon wind causes large-scale convective mixing and generates winter blooms. These make the Arabian Sea as the most productive region of the world ocean and it contributes nearly ~5% of the world primary production (Qasim, 1982).

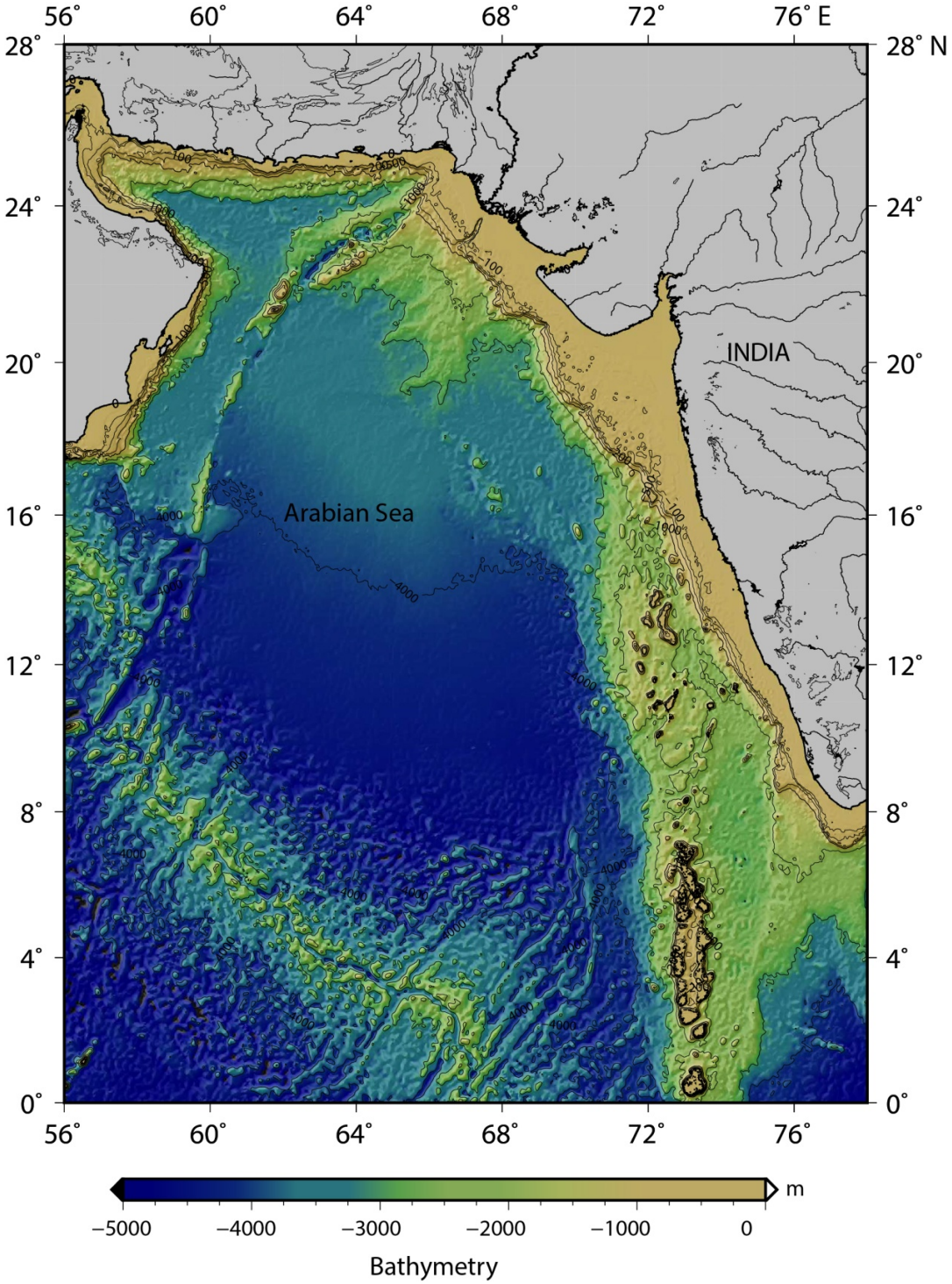

Figure 2.1. Bathymetric map of the Arabian Sea (Source: https://maps.ngdc.noaa.gov/viewers/wcs-client/)

The Arabian Sea is a negative water body in which evaporation exceeds precipitation and leads to the formation of high saline water masses called the Arabian Sea High Saline Water mass (Shetye et al., 1994). During winter monsoon, the Arabian Sea receives low salinity surface water from Bay of Bengal (Kolla et al., 1981; Swallow et al., 1983; Chauhan and Gujar, 1996). Evaporation at the surface of the Arabian Sea and horizontal advection of water from the other ocean leads to the occurrence of several water masses at intermediate depth in the Arabian Sea. Warm saline water mass from the Persian Gulf water spreads in the Northern Arabian Sea at a depth of 200-250 m (Shetye et al., 1994). The spread of Red Sea water masses in the Arabian Sea leads to a salinity maximum at about 500 m in the north and to about 800 m in the equator (Shetye et al., 1994). In the deeper layer between 1,500 and 3,500 m North Indian Deepwater is found and below that is circumpolar deep water (Schott and McCreary, 2001).

The Arabian Sea experiences a pronounced oxygen minimum zone (OMZ) at an intermediate depth of the water column, and it is one of the four known tropical OMZs in the open ocean viz., the Eastern South Pacific and Eastern Tropical North Pacific, in the Pacific Ocean; the Arabian Sea and Bay of Bengal, in the Indian Ocean (Paulmier and Ruiz-Pino, 2009 and references therein). A combination of high organic matter flux associated with high primary productivity and moderate rates of thermocline ventilation leads to this intense OMZ at intermediate water depth of between 150 and 1,000 m (Wyrtki, 1973; Dulk et al., 1998), with an oxygen concentration <22 μM (Sen Gupta et al., 1976; Naqvi, 1987) in the Arabian Sea. It is an intense denitrification zone which is estimated to be ~30 Tg N/Yr (Naqvi, 1987; Bange et al., 2000). The reducing condition is more intense during NE monsoon due to the sluggish renewal of water during this period whereas during the SW

monsoon northward-flowing subsurface current supply oxygen (Prakash et al., 2012). Even though the Arabian Sea covers ~ 2% of the global ocean area, yet 20% of the global denitrification occurs in the Arabian Sea (Gruber and Sarmiento, 1997; Howell et al., 1997).

Along with the intense OMZ at intermediate depth, presence of warm low salinity water formed through intense precipitation in the coastal zone and upwelling along the Indian coast results in strong stratification and subsequent formation of the oxygen-depleted condition along the western continental shelf of India and some part of Pakistan shelf (Banse, 1968; Sankaranarayanan, 1978; Naqvi et al., 2000, 2009; Habeebrehman et al., 2008). This covers an area of about 180,000 km^2 and which is 10 times bigger than the famous dead zone in the Gulf of Mexico (Naqvi et al., 2000, 2009).

The phosphate concentration in the Arabian Sea water ranges between 0 and 7 μM (Morrison et al., 1998). Phosphate concentration in the surface water decreases with increasing distance offshore to the oligotrophic waters (Woodward et al., 1999). Below 1,000 m depth, the concentrations of phosphate are nearly similar (Brand and Griffiths, 2009). Along with the dissolved oxygen, phosphate also shows seasonal variability in the Arabian Sea. Phosphate concentration increases during south-west monsoon and the highest phosphate concentrations are found in the coastal upwelling zone (Morrison et al., 1998; Conkright et al., 2000). Low concentration is observed in the north-west Arabian Sea and along the Arabian Peninsula during the late NE monsoon (Morrison et al., 1998). Vertical profile of phosphate concentration shows near-surface depletion and mid-depth enrichment. The maximum concentration of phosphate was observed at 600-800 m depth (Brand and Griffiths, 2009; Gupta and Naqvi, 1984).

2.1.2 Geologic and Oceanographic settings of the Bay of Bengal

The Bay of Bengal (BOB) is an embayment of the Indian Ocean, situated between latitudes 5° and 22°N and longitudes 80° and 90°E and covers an area of 2.2 x10^6 square kilometers (https://www.britannica.com). It is bounded by Indian subcontinent and Sri Lanka on the west and Burmese Peninsula and the Andaman-Nicobar island groups on the east and has a maximum depth is 4,000 m (Sarin et al., 1979) (Fig. 2.2). BOB has formed as a result of the collision of the Indian plate with Asian plate (Rao and Kessarkar, 2001 and references therein). The continental shelf of Bay of Bengal is widened towards the north and narrows towards south and which is broad of 210 km off the Ganges and is minimum 6 km off Kakinada (Rao and Kessarkar, 2001). The continental slope is steep in the central part than the northern and southern parts (Kader et al., 2013).

Morphological features of the Bay of Bengal include Bengal fan, basins, canyons, ridges and subduction zone (Rao and Kessarkar, 2001). Among these, Bengal fan is important and is the largest delta system in the world (Mohanty et al., 2008). It is formed by the turbidite deposits of Ganges-Bramhamaputra Rivers and covers an area of 3,106 km^2 with a thickness of about 20 km (Rao and Kessarkar, 2001). Sediments are tunneled to the fan via delta-front trough called Swatch of No Ground, which cuts continental shelf in a general northeast and southwest direction at the end of Bay (Mohanty et al., 2007).

BOB receives enormous sediment load (2.1×10^{12}kg/yr) and freshwater discharge (1,887 km^3/yr) from the major rivers Ganga and the Brahmaputra that drain the Himalaya and those that arise in the peninsular India (e.g. the Godavari, Krishna, Mahanadi, Cauvery) (Bird et al., 2008; Pattan et al., 2013; Tripathy et al., 2014). The river inputs are the major source of nutrients to the BOB and the river discharge constitutes 10% of world total inorganic P

(Datta et al., 1999; Stoll et al., 2007) while the dissolved silicate supplied from Ganges and Brahmaputra rivers constitute ~2% of the river input to the world ocean (Sarin et al., 1989).

The nutrient concentration in the BoB shows large spatial and vertical variations. The phosphate concentrations are very high in the surface waters of the coastal zone due to terrigenous input by the rivers (Thangaradjou et al., 2014). But in the deeper areas, surface layers are oxygen-depleted with mean phosphate concentration of 0.13 μM (Sarma et al., 2016). The lower phosphate concentration is due to the utilization of nutrients within the coastal zone (Sarma et al., 2016). Compared to north, phosphate is enriched in the south with very high concentration throughout the water column in the area south of Madras (De Sousa et al., 1981).

The BoB experiences a seasonal reversal of wind direction; a winter northeast monsoon wind (5 m/s) and summer south-west monsoon wind (14 m/s) (Stoll et al., 2007). The wind reversal establishes a large anticyclonic gyre during the spring inter-monsoon in the central Bay (Babu et al., 2003) and cyclonic gyre in the north and central Bay during south-west monsoon. This seasonal monsoon cycle affects fresh water fluxes in the BOB where high discharge occurs during south-west monsoon and leads to strong stratification (Ostlund et al., 1980). This discharge also reduces the surface water salinity by 7‰ (Pattan et al., 2013) and mixed layer depth in the northern Bay (Somayajulu et al., 2003; Stoll et al., 2007). Freshwater induced stratification and weak winds over the BOB together restrict the vertical mixing to a shallow depth and inhibit the nutrient introduction below the mixed layer. This results in a low productivity in the BoB (Kumar et al., 2002). The waters of BOB experience an intense oxygen minimum zone at an intermediate depth between 200 and 800m water depth in which the oxygen concentration reaches a very low value (<5 μM) (Rao et al.,

1994; Sardessai et al., 2007). This OMZ is mainly associated with strong stratification and high phytoplankton biomass (Sarma et al., 2013).

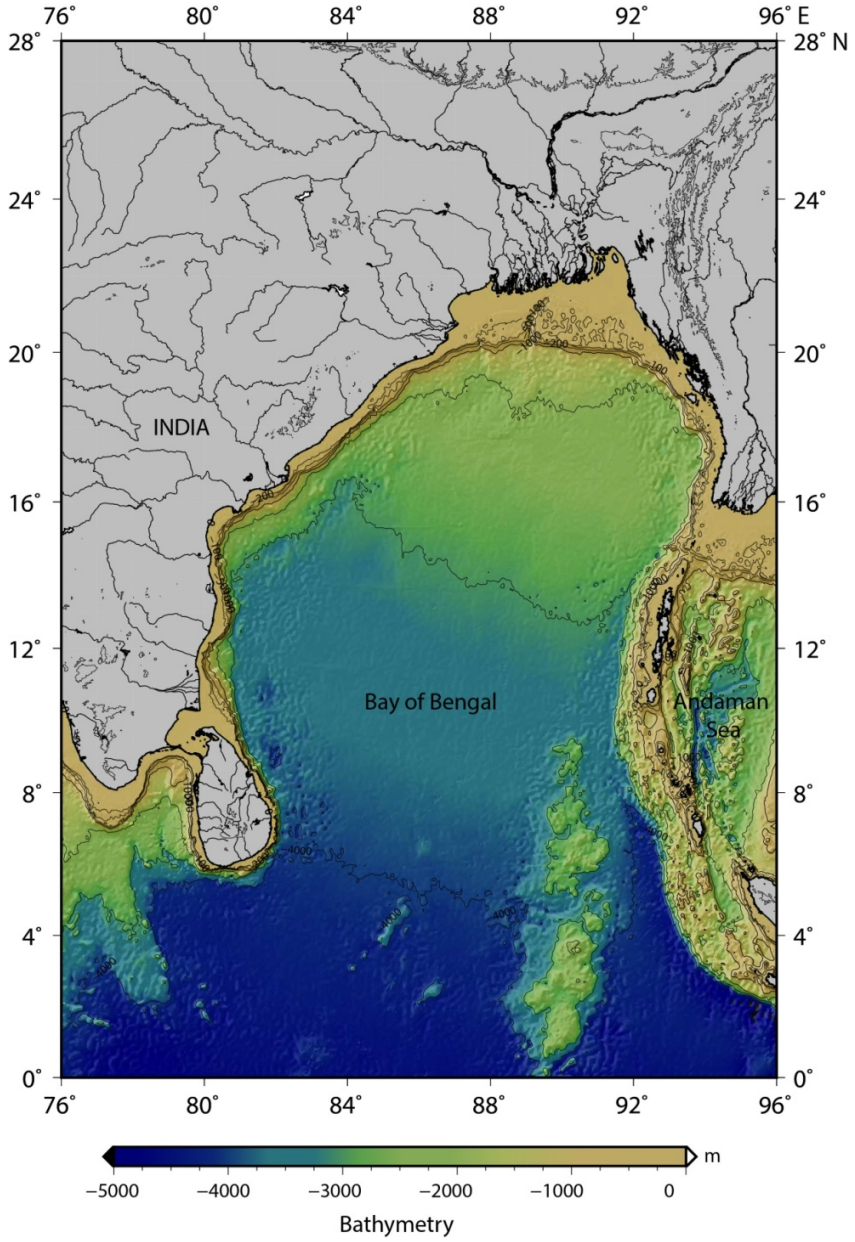

Figure. 2.2 Bathymetric map of the Bay of Bengal

(Source: https://maps.ngdc.noaa.gov/viewers/wcs-client/)

2.1.3 Central Indian Basin

The Central Indian Ocean basin (CIB) is a large abyssal basin which is a potential site of mineral resources like polymetallic nodules and covers an area of 5.7×10^6 km^2 (Nath et al., 1989). The basin is bounded by the ridge systems of which the Ninety East Ridge is on the east, the Central Indian Ridge is to the west, and South East Indian Ridge is in the south. Age of the basin is between 50 and 60 Ma (Mukhopadhyay and Batiza, 1994) (Fig. 2.3) and the average water depth of the basin is 5,100 m. The basin is open to the north towards the Indian Peninsula and bounded by Chagos-Laccadive Ridge on the northwest. The Central Indian Ridge acts as a barrier to the entry of strong bottom water currents to the CIB from the Madagascar Basin and Crozet Basin (Vineesh et al., 2009). The CIB is characterized by three equator moving water masses (De Sousa et al., 2001; Nath et al., 2013). The bottom of the basin is bathed by North Indian Deepwater formed by the mixing of Antarctic Bottom Water (AABW), North Atlantic Deep-Water (NADW) and the deep water of the Northern Indian Ocean and the depth above 4,000 m are bathed by oxygen-rich AABW (Tchernia, 1980; Nath et al., 2013).

The chemical characteristics of the CIB water vary considerably due to the presence of different water masses. The surface water is characterized by low salinity (34.67 psu) and high dissolved oxygen concentrations (223-243 μM) (DeSousa et al., 2001). The influx of low salinity Pacific water and local excess of precipitation leads to the formation of low salinity layer at the upper water column of the CIB (Warren, 1982; De Sousa et al., 2001). The subsurface waters are characterized by the salinity maximum and shallow oxygen minimum (67-112 μM) at a depth range of 125-200 m (DeSousa et al., 2001). This shallow OMZ is due to the oxidation of sinking detritus which decay rapidly with depth (Warren,

1982; De Sousa et al., 2001). Chemical characteristics (oxygen and nutrients) of the deep-water are nearly constant below 3000 m water depth.

Phosphate concentrations are low in the upper layers of the water column and compared to nitrate, phosphate is less depleted in the surface water. The oxygen minimum zone in the subsurface water is accompanied by a weak phosphate maxima (1.4-1.8 μM) in the depth range of 125-200 m resulted by the organic matter degradation (De Sousa et al., 2001). Phosphate profiles show enrichment around 800-1,200 m depth in the CIB and below that it shows a slight decrease with depth (De Sousa et al., 2001).

The sediments in the CIB are mainly of siliceous, terrigenous and pelagic red clays with the presence of calcareous sediments in areas near to the ridge (Rao and Nath, 1988; Nath et al., 1989) and on shallow seamount tops (e.g., Nath et al., 2013). The turbiditic currents in the north disperse the sediments to the south into the basin and the signature of the terrigenous sediment supply can be traced up to 8°S in the CIB (Nath et al., 1989, 1992). The terrigenous sediments dominate in the northern part, siliceous clays and ooze sediments are confined largely to the central part with pelagic red clays in the southern part of the basin (Nath et al., 1989). The circulation of cold, oxygen-rich Antarctic Bottom Water (AABW) into the CIB through the northern saddles of Ninety-East Ridge makes the bottom water oxygen-rich (Warren, 1982; Nath and Mudholkar, 1989; Vineesh et al., 2009). The sediments of the CIB are low in organic matter due to reduced sediment accumulation rate (Nath and Mudholkar, 1989; Gupta and Jauhari, 1994; Nath et al., 2012). The surface primary productivity of the CIB is low compared to other deep ocean and ranges between 9.1 and 103.4 $mgCm^{-2}day^{-1}$ (Matondkar et al., 2005). An intense erosion of the younger sediments in the CIB as a consequence of AABW has also been reported (Banakar et al.,

1991). The sedimentation rates in the basin are about 2 mm kyr^{-1} and mostly <1cm kyr^{-1} (Banakar et al., 1991; Borole, 1993; Nath et al., 2013; Mascarenhas-Pereira et al., 2016).

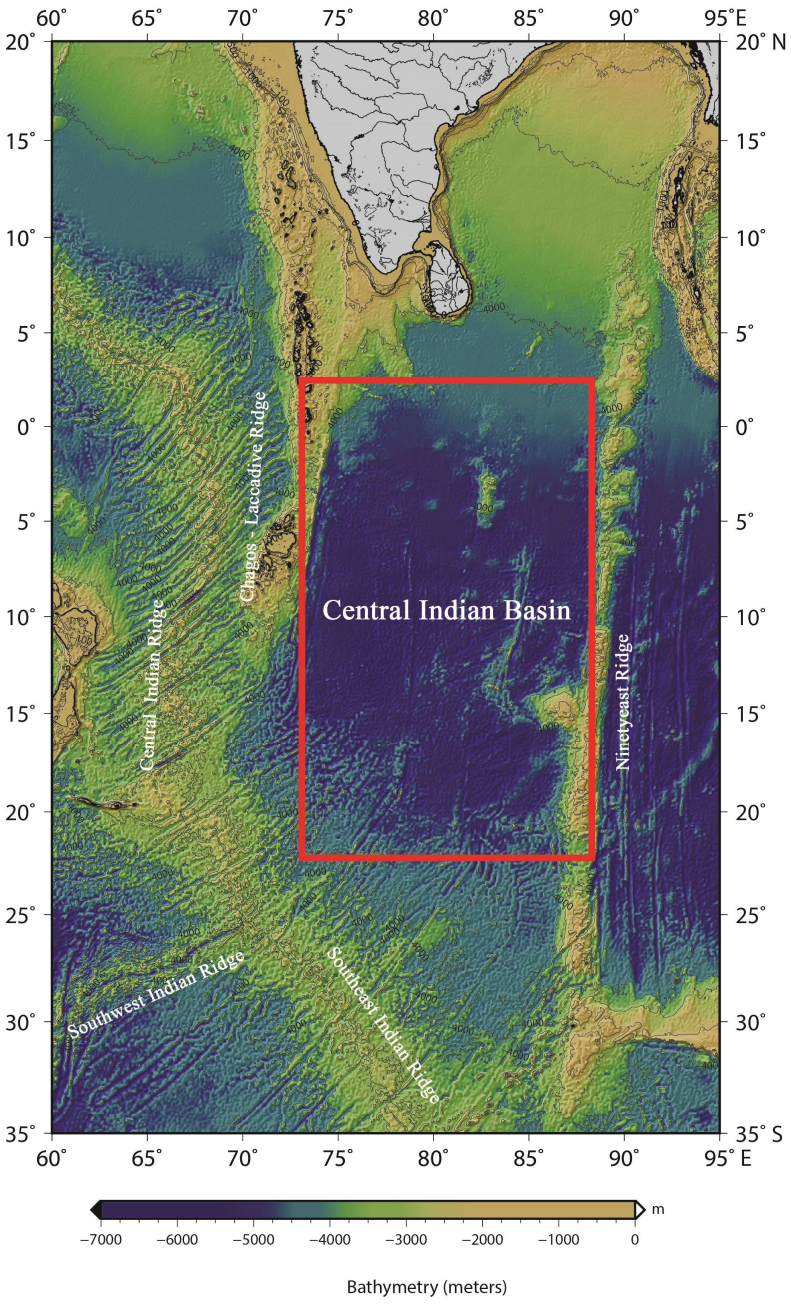

Fig. 2.3 Bathymetry map of the Central Indian Basin (Source: https://maps.ngdc.noaa.gov/viewers/wcs-client/)

2.2 Sediment Sampling

The sediment sampling was carried out in the BoB and the Arabian Sea during the several expeditions of two research vessels, viz., R.V. Sindhu Sankalp and R.V.Sindhu Sadhana, belonging to CSIR-NIO. The details of the expeditions are presented in Table 2.1. For deep-sea sediments, sampling was carried out in the CIB. The sediment sampling was mainly carried out using box/spade corer (Kasterngriefer type). To accomplish the scientific objectives, porewater and the solid phase chemistry were determined. Porewater phosphate data were used to calculate the benthic fluxes of phosphate at 98 stations from different water depths (28-5,307 m). The sampling depths and locations of the stations are detailed in Table 2.2 and Figure 2.1. Sequential solid phase speciation was carried out on 36 surface sediments and 16 short cores to understand the pathways of P incorporation and redistribution in sediments.

Table 2.1: *Details of the Oceanographic expeditions during which sediments were sampled for the present work.*

Ship & Cruise Name	Month/Year	Area
R.V.Sindhu Sankalp SSK 40	October-November/2012	Arabian Sea
R.V.Sindhu Sankalp SSK 50	May 2013	Andaman Sea and Bay of Bengal
R.V.Sindhu Sankalp SSK 59	January/2014	Bay of Bengal and Arabian Sea
R.V.Sindhu Sadhana SSD 03	September – October/2014	Bay of Bengal

R.V.Sindhu Sankalp SSK 71	November/2014	Arabian Sea
R.V.Sindhu Sankalp SSK 73	December/2014	Arabian Sea
R.V.Sindhu Sankalp SSK 80	March/2015	Arabian Sea
R.V.Sindhu Sadhana SSD 13	July 2015- August 2015	Central Indian Basin
R.V.Sindhu Sadhana SSD T14	September/2015	Arabian Sea
R.V.Sindhu Sankalp SSK 86	January/2016	Arabian sea
R.V.Sindhu Sadhana SSD 19	February/2016	Bay of Bengal
R.V.Sindhu Sadhana SSD 27	October-November/2016	Arabian Sea

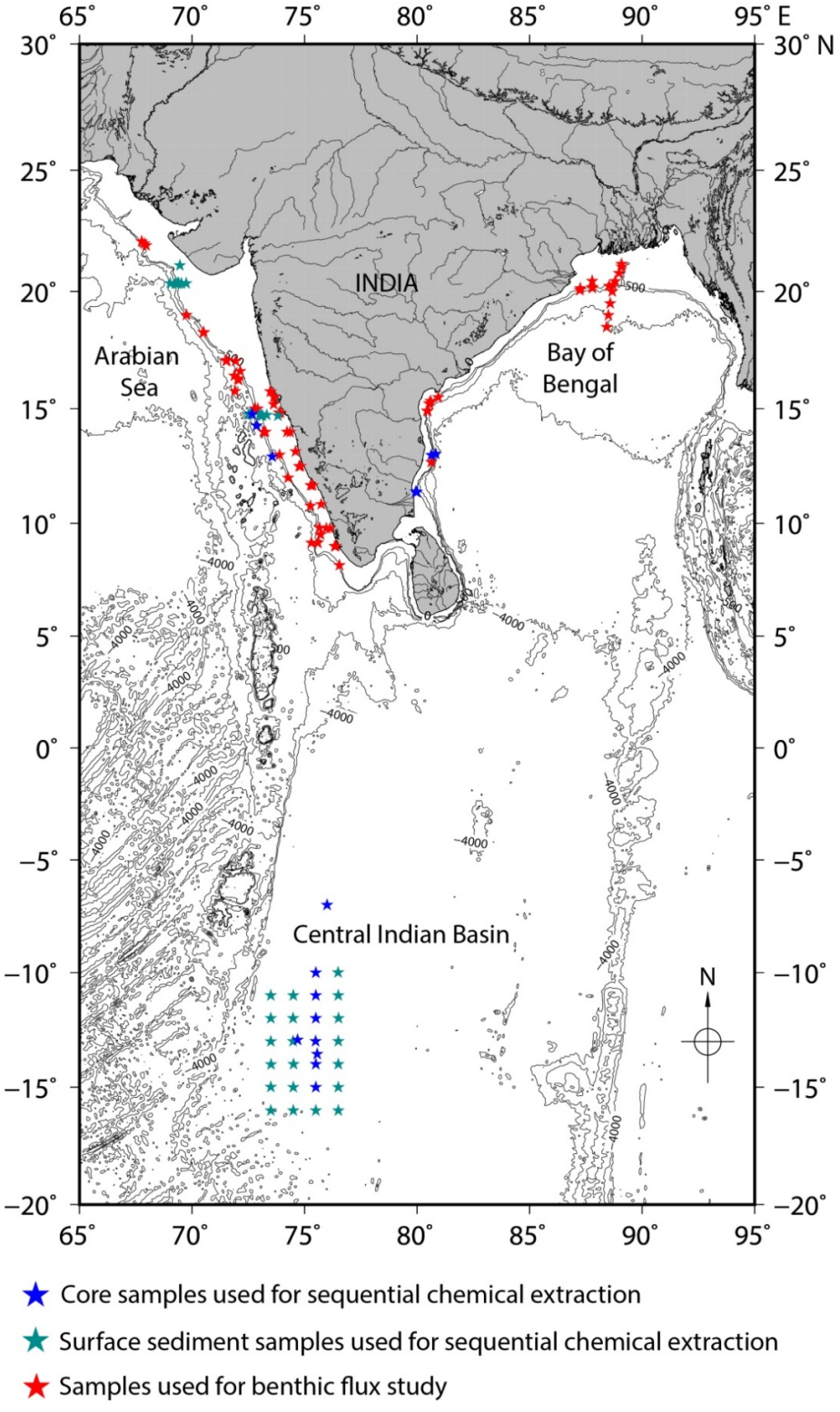

Figure 2.4: Map showing the sampling locations of the sediment samples used in this study.

Table 2.2: *Location and water depth details of samples used for the benthic flux study*

Cruise Name	Spade Core	Latitude (°N)	Longitude (°E)	Water Depth (m)
SSK40	SPC-1R	14.77	72.67	347
	SPC-2	14.27	72.87	325
	SPC4R	12.92	73.56	279
SSK50	SPC-5	13.04	80.83	269
	SPC-7	12.99	80.63	202
	SPC-9R	12.68	80.63	148
SSK-59	SPC-3	11.37	79.99	224
	SPC-4	8.15	76.55	635
	SPC-5	9.50	75.71	314
	SPC-6	10.77	75.26	260
SSD-03	SPC-1	14.91	80.47	829
	SPC-2	14.91	80.44	288
	SPC-3	15.23	80.54	620
	SPC-4	15.22	80.54	358
	SPC-5	15.33	80.60	230
	SPC-6	15.49	80.94	800
	SPC-10	20.23	88.53	632
	SPC-14	20.44	87.78	95
	SPC-15RR	20.18	87.78	260
	SPC-16	20.14	87.79	650
	SPC-17	20.13	87.25	175
	SPC-18	20.05	87.23	640
SSK-71	SPC-1	16.62	72.14	238
	SPC-2	16.42	71.88	410
	SPC-3	16.24	72.07	442
	SPC-4	17.07	71.54	630
	SPC-5	17.09	71.53	826
	SPC-6	17.05	71.52	930
	SPC-7	15.76	71.91	399
	SPC-9	16.30	72.04	1051
	SPC-10	17.05	71.94	212
	SPC-11	18.28	70.50	407
	SPC-12	18.26	70.52	751
	SPC-13	19.01	69.75	774
	SPC-15	20.34	69.74	80

Table 2.2: Continued

Cruise Name	Spade Core	Latitude (°N)	Longitude (°E)	Water Depth (m)
SSK 71	SPC-16R	20.34	69.53	98.7
	SPC-17	20.35	69.41	195
	SPC-18	20.34	69.35	297
	SPC-19	20.33	69.33	509
	SPC-20	20.34	69.25	791
	SPC-21	20.34	69.03	1544
	SPC-22	21.09	69.46	64
	SPC-24	22.00	67.88	218
	SPC-25	21.92	67.96	353
	SPC-26	22.09	67.76	415
SSK-73	SPC-1	15.00	72.78	951
	SPC-3	15.00	72.92	300
	SPC-4	14.00	73.18	826
	SPC-6	14.00	73.26	289
	SPC-7	13.00	73.89	243
	SPC-13	12.00	74.27	973
	SPC-14	11.00	75.12	158
SSK-80	SPC-1	14.70	73.82	53
	SPC-2	14.73	73.32	110
	SPC-3	14.71	73.07	294
	SPC-4	14.76	73.00	563
	SPC-5	14.76	72.67	329
	SPC-6	14.78	72.59	541
	SPC-7	14.75	72.52	1711
	SPC-8	14.71	73.13	217
SSD-13	BC-1	-7.00	76.00	5307
	BC-4	-12.94	74.69	5152
	BC-13	-13.56	75.56	5170
SSD-T14	SPC-1	15.52	73.64	28
	SPC-2	15.75	73.48	31
SSK-86	SPC-1	14.76	72.68	330
	SPC-2	15.75	73.48	34
	SPC-3	15.51	73.65	30
	SPC-4	15.19	73.63	34

Table 2.2: Continued

Cruise Name	Spade Core	Latitude (°N)	Longitude (°E)	Water Depth (m)
SSD-27	SPC-3	8.99	76.34	46
	SPC-4	9.00	76.39	32
	SPC-5	9.78	76.13	29.8
	SPC-6	9.78	75.97	49.8
	SPC-7	9.81	75.66	106.13
	SPC-8	9.14	75.30	1978.7
	SPC-10	9.14	75.58	501
	SPC-11	9.15	75.59	229
	SPC-12	10.84	75.74	32.93
	SPC-13	11.67	75.27	44.23
	SPC-14	11.67	75.36	32.37
	SPC-15	12.50	74.76	44.65
	SPC-16	12.51	74.82	33.88
	SPC-17	13.15	74.60	30.82
	SPC-18	14.00	74.22	45.61
	SPC-19	13.99	74.36	31.73
	SPC-20	14.82	73.86	44.2
	SPC-21	14.83	73.93	32.25
	SPC-22	15.52	73.64	31.6
	SPC-23	15.75	73.49	34.7
SSD-19	SPC-1	21.15	89.08	29
	SPC-2	21.03	89.09	90
	SPC-3	20.77	88.97	132
	SPC-4	20.43	88.80	226
	SPC-5	20.27	88.70	719
	SPC-6	20.00	88.67	1314
	SPC-7	19.50	88.58	1700
	SPC-8	19.00	88.50	1954
	SPC-9	18.50	88.42	2161

2.2.1 Surface Sediment

The core top of 26 sediment cores from 61stcruise of AA Sidorenko collected at a 1° interval grid (between 10 and 16°S latitude and 73.5 and 76.5°E longitude) from two sediment

domains (siliceous ooze and pelagic clays) were studied for assessing the spatial variability of P distribution in the Central Indian Basin. Sampling location and water depths are furnished in Table 2.3 and displayed in figure 2.1.

Table 2.3: *Location and water depth details of surface samples collected from the Central Indian Basin*

Station	Longitude (°S)	Latitude (°E)	Water depth (m)
AA/1R	-9.99	76.49	5355
AA/2RR	-11.00	76.50	5320
AA/3R	-12.00	76.51	5280
AA/4	-13.00	76.50	5360
AA/5	-14.00	76.50	5180
AA/6	-15.00	76.50	4980
AA/7	-16.00	76.50	5070
AA/8	-16.00	75.50	5010
AA/9	-16.00	74.50	5350
AA/10	-16.00	73.50	4900
AA/11	-14.99	73.50	5480
AA/12R	-15.00	74.50	5390
AA/13	-15.00	75.50	4840
AA/14	-14.00	75.50	5145
AA/15	-14.00	74.51	5160
AA/16	-14.01	73.51	5120
AA/17	-13.01	73.50	4810
AA/18	-13.00	74.49	5050
AA/19	-13.00	75.49	5070
AA/20	-12.00	75.50	5200
AA/21	-12.00	74.49	5055
AA/22	-12.00	73.50	4900
AAS/23	-11.00	73.50	5100
AA/24	-11.00	74.50	5050
AA/25	-11.00	75.50	5300
AA/26	-10.00	75.50	5290

In addition, 16 surface sediments (0-1cm) (Table 2.4) were collected during the 71st and 80th cruise of RV Sindhu Sankalp from the eastern Arabian Sea along two transects passing through the perennial OMZ, one-off Gujarat (SSK71) in the northern part and another off

Karwar (SSK80), the central part was used to study the variability of P and Fe fractionation and benthic P fluxes with changing bottom water oxygen concentration.

Table 2.4: *Location and water depth details of surface samples collected from the eastern Arabian Sea*

Transect Name	Station Name	Latitude (°N)	Longitude (°E)	Water Depth (m)
SSK71	SPC22	21.09	69.46	64
	SPC15	20.34	69.74	80
	SPC16R	20.34	69.53	98.7
	SPC17	20.35	69.41	195
	SPC18	20.34	69.35	297
	SPC19	20.33	69.33	509
	SPC20	20.34	69.25	791
	SPC21	20.34	69.03	1544
SSK80	SPC-1	14.70	73.82	53
	SPC-2	14.73	73.32	110
	SPC-8	14.71	73.13	217
	SPC-3	14.71	73.07	294
	SPC-5	14.76	72.67	329
	SPC-6	14.78	72.59	541
	SPC-4	14.76	73.00	563
	SPC-7	14.75	72.52	1711

2.2.2 Sediment Cores

Three short sediment cores were collected from topographic highs on the western continental margin of India in the central part of the Eastern Arabian Sea were used to study the benthic cycling of P. The cores were collected during the 40th cruise of RV Sindhu

Sankalp using a spade corer of 30 × 15× 50 cm dimensions. The cores labeled as SPC 1R, SPC 2 and SPC 4R were recovered from water depths of 347, 325 and 279 m, respectively, within the intense OMZ of the Arabian Sea (200–1200 m; Wyrtki, 1973).

In addition to this, four short cores were collected during the 50th and 59th cruises of RV Sindhu Sankalp from the eastern continental margin of India were used to study the impact of OMZ and lithogenic input on the sedimentary cycling of P in the BoB. Details of the location and water depth of the 7 short cores are provided in Table 2.5.

Table 2.5: *Location and water depth details of sediment cores collected from the Northern Indian Ocean*

Cruise Name	Spade Core	Latitude (°N)	Longitude (°E)	Water Depth (m)
SSK40	SPC-1R	14.77	72.67	347
	SPC-2	14.27	72.87	325
	SPC4R	12.92	73.56	279
SSK50	SPC-5	13.04	80.83	269
	SPC-7	12.99	80.63	202
	SPC-13	11.39	79.94	218
SSK-59	SPC-3	11.37	79.99	224

In addition, nine sediment cores were studied from the abyssal areas of the CIB for downcore P geochemistry. Six of these (AA/13, AA/14, AA/19, AA/20,AA/25, and AA/26), collected during the 61st expedition of R.V.A.A. Sidorenko, were chosen to represent an N-

S transect. Three other sediment cores were collected during the 13th cruise of Sindhu Sadhana (SS/1, SS/4, and SS/13) (Table 2.6).

Table 2.6: *Location and water depth details of sediment cores collected from the Central Indian Ocean*

Station	Longitude (°S)	Latitude (°E)	Water depth (m)
AA/13	-15.00	75.50	4840
AA/14	-14.00	75.50	5145
AA/19	-13.00	75.49	5070
AA/20	-12.00	75.50	5200
AA/25	-11.00	75.50	5300
AA/26	-10.00	75.50	5290
SS/1	-7.00	76.00	5307
SS/4	-12.94	74.69	5152
SS/13	-13.56	75.56	5170

2.3 Porewater Extraction

Undisturbed sediment cores, two from each sampling sites, were collected by pushing Plexiglas (6 cm diameter, 40 cm length) into the collected spade core sediment. The cores were immediately transferred to an onboard chemistry laboratory for the extraction of porewater. All the cores collected from the Northern Indian Ocean were extruded into an N_2 purged glove-box to provide an inert atmosphere and to avoid sediment/porewater oxidation from the ambient oxygen. Whereas, the abyssal sediments from CIB, which are from highly oxygenated environment, were sub-sectioned at ambient conditions. The cores were sub-sectioned at 2 cm interval. Porewater was extracted by centrifuging the samples at 5,000 rpm in a refrigerated centrifuge. The temperature of the centrifuge was set to the in-situ bottom water temperature (obtained using Conductivity Temperature Depth (CTD) profiler) to avoid temperature induced analytical artifacts (e.g., Bischoff et. al., 1970, Fanning and Pilson,

1971). The porewater was then collected in pre-cleaned vials after filtering through MILLEXHA -0.45 μm pore size cellulose acetate syringe filters and dissolved phosphate in the porewater was determined immediately after extraction.

2.4 Collection and analysis of Seawater

Seawater samples were collected from pre-determined depths using a Rosette Sampler connected to the CTD (SBE 25, Seabird, USA) system fitted with 10 L Niskin bottles. The temperature and salinity of water column were measured using sensors attached to the CTD profiler. Water samples from Niskin bottles were collected for dissolved oxygen (DO) and dissolved nutrient measurements. The samples for DO measurement were fixed immediately using Winkler A (manganese chloride) and B solution (alkaline potassium iodide).

2.4.1 Determination of dissolved oxygen

The dissolved oxygen concentration in the seawater samples was determined by the chemical method proposed by Winkler (1888) and modified by Strickland and Parsons (1960). The procedure involves the fixation of oxygen by manganese chloride (Winkler A) and alkaline Potassium iodide (Winkler B) and titrated against Sodium thiosulphate solution using autotitrator (Dosimat plus) at acidic pH.

2.4.2 Determination of dissolved inorganic phosphate (DIP) in seawater and porewater

DIP concentration in seawater and porewater were measured by using standard spectrophotometric method (Grasshoff et al., 1983) and it involves the formation of phosphomolybdate heteropoly acid from orthophosphate and followed by reduction to give

molybdenum blue complex. The absorbance of thus produced molybdenum blue was measured spectrophotometrically at 880 nm.

2.5 Solid phase Analysis

The sediment cores were stored at temperatures (4 °C) until they were sub-sectioned. After sub-sectioning in shore labs, they were freeze dried, ground to fine powder and used for analytical work.

2.5.1 Sequential Chemical Extraction of Phosphorus

The speciation of P in the sediments was determined using a five-step sequential extraction scheme (Table 2.5), proposed by Ruttenberg (1992) and modified by Babu and Nath (2005). 100 mg of dried and ground sediment sample was leached out with 25 ml of 2 M NH_4Cl (pH 7; 8 times; 4 hours) for extracting exchangeable or loosely sorbed, carbonate-associated phosphorus and biogenic apatite. In the second step, in order to separate easily reducible or reactive iron-bound P residue was extracted with 10 ml citrate dithionite buffer (pH 7.6; 6 hours), followed by 25 ml of 2 M NH_4Cl (pH-7; 2 hrs) and 10 ml of distilled water (2 hours). For extracting authigenic P fraction, the residue was treated with 1 M sodium acetate buffer (pH 4; 6 hours), 1 M Magnesium chloride (pH 8; 2 hours) and distilled water. P associated with detrital fraction was extracted by 1 M HCl (24 hours); the residue is dried and heated with 50% (w/v) magnesium nitrate at 80°C and extracted with 1M HCl (24 hours) after ignition at 550 °C (2 hours) Phosphorus associated with this step represents the P bound as organic matter. After step (2) and (3) the samples were rinsed repeatedly with distilled water (2 hours) for preventing the re-adsorption of phosphate. P concentrations in extraction solutions were measured spectrophotometrically by using the

phosphomolybdate method; by treating the solution with acidified molybdate solution and then reduced to blue colored complex by ascorbic acid. Absorbance was measured at 880 nm. P concentration in the citrate dithionate extracts was determined by organic extraction technique (stannous chloride reduction method of Watanabe and Olsen, 1962) and the measurement was made at 730 nm with a UV Spectrophotometer (following Filippelli and Delaney, 1996). All the extractions of P were carried out at room temperature.

***Table.2.5**: Chemical and target phase of sequential extraction procedure of P (modified by Babu and Nath (2005).*

Extraction	Target Phase	Term	Reference
1×10ml 1M $MgCl_2$ (pH 8), 2h	Loosely bound + exchangeable P	Exchange P (P_{ex})	Ruttenberg (1992)
8×25 ml. of 2M NH_4Cl (adjusted to pH 7 with ammonia), 4 h	Exchangeable or loosely sorbed P Carbonate associated P Biogenic apatite (Hydroxyapatite)	Biogenic P (P_{bio})	Schenau and De Lange (2000), Babu and Nath (2005)
1×10 ml of 0.22M Na-citrate, 0.033M sodium dithionite, 1.0M sodium bicarbonate (pH 7.6), 6 h 1×25 ml. 2M NH_4Cl, 2 h 1×10 ml. of distilled water, 2 h	Easily reducible or reactive iron bound P	Iron bound P (P_{Fe})	Ruttenberg (1992), Anderson and Delaney (2000), Schenau and De Lange (2000)
1×10 ml 1.0M Na-acetate buffered (pH 4), 2 h 2×10 ml $MgCl_2$ (pH 8), 1 h 1×10 ml of distilled water, 1h	Authigenic apatite	Authigenic P (P_{auth})	Ruttenberg (1992), Anderson and Delaney (2000)
1×13 ml of 1.0N HCl	Detrital apatite	Detrital P (P_{det})	Ruttenberg (1992), Anderson and Delaney (2000)
50% (w/v) $MgNO_3$ 1ml dry at 80 °C, ash at 550 °C (2h), 1N HCl 13 ml, 24 h	P associated with organic matter	Organic P (P_{org})	Ruttenberg (1992), Anderson and Delaney (2000)

The P_{total} content was calculated by adding all the five fractions ($P_{total} = P_{bio} + P_{Fe} + P_{auth} + P_{det} + P_{org}$) and the propagated errors for the P_{total} calculation are on an average ~8.8% with a maximum error of 12%. Reactive P (P_{react}) is the sum of all non-detrital fractions ($P_{react} = P_{bio} + P_{Fe} + P_{auth} + P_{org}$). Duplicates and standard reference material (JLk-1 of Geological Survey of Japan) were included to monitor the precision and recovery of the extraction method. The P total calculated by the sum of the five fractions in the JLk-1 standard (29.3 μmol/g) and the certified P content of this standard (29.6 μmol/g) are comparable within an error of ±1.3%. The analytical precisions calculated from the duplicate analyses of my samples were generally <9% with a mean better than 1.7%.

2.5.2 Sequential Chemical Extraction of Iron

The sequential extraction procedure developed by Poulton and Canfield (2005) was used for Fe fractionation. The extraction procedure includes the separation of operationally defined six different iron-bearing mineral phases (Table 2.6). 200 mg of dried and ground sediment samples was leached out with 1M magnesium chloride to isolate exchangeable or loosely adsorbed Fe. For separating carbonate bound iron, the residue was treated with sodium acetate for 24 hours. Mineral phases ferrihydrite and lepidocrocite were separated by treating the residue with hydroxylamine hydrochloride in the next step. In the fourth step, mineral phases like goethite, akaganeite and hematite were targeted by adding sodium dithionate. For isolating magnetite, the residue was treated with ammonium oxalate. Nontronite, chlorite, glauconite and biotite were separated by boiling the residue with 12N HCl. The residue left after the sixth step was digested with 7:3:1 HF: HNO_3: $HClO_4$ mixture and measured for iron content. After each step of the extraction, the residue was washed three times with ultrapure water. Fe measurements in all leaches were carried out by using a Solar S4 Atomic Absorption Spectrophotometer. All the Fe extractions were carried out at room temperature.

***Table.2.6**: Chemical and target phases of sequential extraction procedure of Fe developed by Poulton and Canfield (2005).*

Extraction	Target Phase	Term	Reference
1×10ml 1M CH_3COONa (pH-4.5) 24hrs	Carbonate Iron and acid volatile sulfide	$Fe_{AVS+carb}$	(Poulton and Canfield, 2005)
1×10ml 1M hydroxylamine-HCl (in 25% v/v acetic acid)	Ferrihydrite and lepidocrocite	Fe_{ox1}	(Poulton and Canfield, 2005)
1×10ml sodium dithionite (50g/l) (pH-4.8)	Goethite, akaganeite and hematite Ferrihydrite and lepidocrocite	Fe_{ox2}	(Poulton and Canfield, 2005)
1×10ml 0.2M Ammonium oxalate/0.17 M oxalic acid	Magnetite	Fe_{mag}	(Poulton and Canfield, 2005)
Boil with 12N HCl	Poorly reactive sheet silicate	Fe_{PRS}	(Poulton and Canfield, 2005)
Digestion with concentrated HF, HNO_3 and $HClO_4$ mixture and final dissolution in 2 % (v/v) HNO_3.	Un-reactive silicate and Pyrite Fe	Fe_{U+py}	

2.5.3 Total Phosphorus

The total P content was determined by combustion method wherein the sediments were combusted at 550 °C (2 hours,) cooled, and P was extracted with 1 N HCl (24

hours—slightly modifying the method described by Ostrofsky, 2012). The blue color developed (Strickland & Parsons, 1972) was measured for P at 880 nm with an UV Spectrophotometer. Duplicates and international geochemical reference materials (JSd-1 and Jlk-1 from Geological Survey of Japan) were included in the extraction steps to monitor the precision and recovery of the extraction.

2.5.4 Total inorganic carbon and Total organic carbon

Total inorganic carbon (TIC) in the sediments was measured by using CO_2 coulometer. Ground sediment samples were treated with 1N HCl and evolved CO_2 from sediment samples were swept into the coulometric cell. The accuracy of the analysis was established using pure calcium carbonate as standard reference material as well as internal standards with varying TIC content. Elemental analyzer (Thermo Scientific Flash 2000) was used to measure the total carbon (TC) and total nitrogen concentrations in the samples. The accuracy of the analysss was within ±3% for NC soil standard. Total organic carbon (C_{org}) was calculated by subtracting TIC from TC values (C_{org} = TC - TIC).

2.5.5 Total Iron

Total iron (Fe_{total}) concentration was determined using Solar S4 Atomic Absorption Spectrophotometer after digestion with 7:3:1 HF: HNO_3: $HClO_4$ acid mixture. The accuracy of the measurements was assessed using Marine Mud (MAG-1), the geochemical standard procured from the United States Geological Survey.

2.5.6 Trace Metal Analysis

For the determination of trace metals in sediments, ground sediment samples were digested with 7:3:1 HF: HNO_3: $HClO_4$ acid mixture (MERCK - Suprapur grade HF and HNO_3) and evaporated to dryness on a hot plate at a temperature 180-200 °C. Then

the residue was re-dissolved in 2% HNO_3 and analyzed by an Inductively Coupled Plasma Mass Spectrometer (Thermo FischerICPMS, X Series 2, Germany) at NIO, Goa, with Rh as an internal standard. The accuracy of the measurements was monitored by analyzing Marine Mud (MAG-1) standard of the United StatesGeological Survey.

2.6 Benthic flux and burial efficiency calculation

Diffusive flux of phosphate at the sediment-water interface was calculated by Fick's law of diffusion using the equation

$$J_P = -\phi D_S(\delta C/\delta Z)$$

where J_P is the benthic flux of phosphate, ϕ is the porosity calculated from the moisture content data, D_S is the molecular diffusion coefficient of phosphate in the sediment and $\delta C/\delta Z$ represents the gradient in DIP concentration between the overlying seawater (5 m above the sea floor) and the porewater of surface sediments (0-2cm).

$$D_S = D^*/\theta^2$$

where D* is the diffusion coefficient of HPO_4^{2-} in seawater calculated at in situ bottom water temperature (Li and Gregory, 1974), and θ is the tortuosity calculated using the equation

$\theta^2 = 1 - \ln \phi^2$ (Boudreau, 1997).

The mass accumulation rate of phosphorus (PAR) in sediment was calculated using sedimentation rate (S), dry bulk density and P content (C) in sediments

PAR=Cx Sx dry bulk density

Phosphorus burial efficiency (PBE) in sediments was calculated using the equation

PBE=100 x PAR/ (PAR+J_P) (Fang et al., 2007)

where PAR is the phosphorus mass accumulation rate and J_P is the benthic flux of phosphate.

Chapter 3

Benthic cycling of phosphorus in the Eastern Arabian Sea

Chapter 3

3.1 Introduction

The Arabian Sea is a highly productive ocean owing to the intense upwelling caused by the southwest monsoon (Qasim, 1982). The high production of organic matter leads to an intense oxygen minimum zone (OMZ) at 150-1200 m water depth in the Arabian Sea (Wyrtki, 1973, DeSousa et al., 1996). In addition, the high phytoplankton and zooplankton productivity leads to high fish production in this area (Schenau and De Lange, 2000). All these characteristics make the Arabian Sea a suitable site for studying the pathways of P accumulation in sediments.

The variation in total P in the Arabian Sea sediments has been extensively studied (Murty et al., 1968; Setty and Rao, 1972 and Rao et al., 1978, 1987). Detailed studies of P fractionation into different binding phases and P cycling in the area were undertaken, much later, in the Eastern Arabian Sea (Babu and Nath, 2005; Acharya et al., 2016; Sudheesh et.al., 2017), northern part of the Eastern Arabian Sea and the Oman Margin (Schenau et al., 2000; Schenau and De Lange, 2001), and the Western Arabian Sea (Kraal et al., 2012, 2015). The results have shown that the high benthic flux of phosphate in the OMZ is associated with the dissolution of fish debris and degradation of organic matter which may lead to sink switching of P to authigenic phases (Schenau and De Lange, 2001, Babu and Nath, 2005). In addition to organic matter, iron also was found to play a major role in the P cycling and authigenesis in the Arabian Sea sediments (Kraal et al., 2012). A high rate of francolite formation (using porewater fluoride and phosphate gradients and molar P/F ratios in the authigenic fraction) was observed by Schenau et al. (2000) in Oman Margin sediments. This lead to the formation of a Holocene phosphorite deposit which contrasted

with earlier reports of the occurrence of only old phosphorites in this area (e.g., Rao and Lamboy, 1995).

Rao et al. (1990) have studied the phosphatised limestones from the outer continental shelf of India between Goa and Ratnagiri in the Arabian Sea and found that the algal nodules grew with microbial mats formed by trapping and binding of sediment particles, which were subsequently phosphatised. The phosphatised material of the algal nodules contained terrestrial siliciclastic detritus and those authors asserted that the impact of present-day upwelling is insignificant in the phosphatisation of the limestones. On the other hand, Vaz et al. (1996) have attributed the formation of phosphorites in the upper continental slope off Kutchchh to early diagenesis in shallow waters.

Rao et al. (1995) and Rao and Rao (1996) reported the occurrence of phosphatic concretions in the marginal high area off Goa (see **Fig.3.1** for the reported occurrences of phosphorites, phosphogenesis and sediments with high authigenic P). Rao et al. (1995) suggested that the phosphorite in this area is from fish coprolite which was phosphatized under low terrigenous sedimentation rate and calm environmental conditions. They interpreted the phosphorite to be of Pleistocene age and ruled out the possibility of recent formation. Rao and Rao (1996) recovered phosphatic concretions and grains from a sediment core on the same topographic high at different depths but the top 1 m sediments did not contain any concretions. The concretions from this core were dated using the U/Th equilibrium method and their ages were estimated to be over 250 ky, no modern concretions were recovered. Nair (1985) has reported the occurrence of Holocene nodular algal limestones containing francolite in other areas of the Eastern Arabian Sea, which he attributed to have been formed from diagenetic processes with the enrichment of phosphate

in limestones by microorganisms that built the algal mats. These algal carbonate nodules **(Fig. 3.1)** with ~ 1 mm thick phosphorite coatings were dated by Borole et al. (1987) using the $^{230}Th/^{234}U$ method and were found to have ages of 13.9-5.8 ky and interpreted to indicate that phosphorite deposition started soon after the carbonate nodule formation.

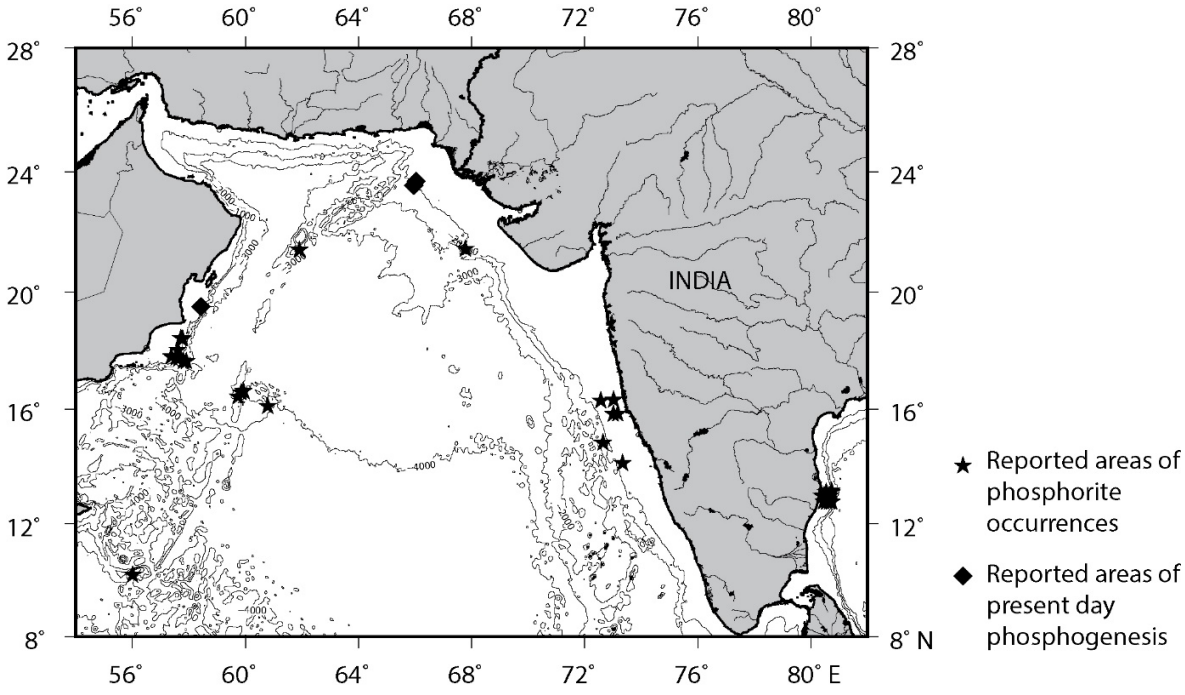

Figure 3.1: Map showing the reported areas of phosphogenesis and phosphorite occurrences along with the areas of high P_{auth} content.

Rao and Lamboy (1996) have however, argued that the phosphatization of these limestones from the eastern Arabian Sea has occurred during a short event in the Early Holocene (at about 8,300 yr B.P) influenced by microbial processes following an event of increased terrigenous sediment flux. In a recent study of P speciation in Eastern Arabian Sea sediments, Acharya et al. (2016) have argued for the absence of active phosphatization due to the low total P content and the dominance of a detrital non-reactive fraction of P which would inhibit the formation of authigenic P. All these interpretations are based on the

occurrence of hard geological evidences, yet no clear information is available if the prevailing benthic biogeochemical conditions are conducive for phosphogenesis to take place. Thus, this study is undertaken to assess the P burial pathways and investigate if the present-day phosphogenesis is occurring in the oxygen-depleted sediments of the Eastern Arabian Sea using an approach to study the buildup of phosphate in sediment pore fluids, diffusion across sediment-water interface and the pathways of P accumulation and its transformation in the sediments.

Three short sediment cores (SPC-1, SPC-2 and SPC-4) raised from three topographic highs from the central western continental margin of India **(Fig. 3.2 and Table 3.1)**. (On one of which the old phosphatic concretions were recovered before by Rao et al. 1995 and Rao and Rao, 1996) are studied here. As they are from topographic highs, they are free from slumping and turbiditic sedimentation. Porewater extracted from sediment cores in inert conditions was studied for P geochemistry. In addition, seawater collected from various depths at the same locations was also analysed for phosphate content in order to assess the direction of diffusion at the sediment-water interface. Diffusive fluxes were calculated to quantify the magnitude and direction of P flux (see section 2.6 in Chapter 2 for the equations used). In addition to estimating P, organic and inorganic carbon content in bulk sediments, sequential extraction of sediments was carried out to determine P content in five chemically separable fractions (see Table 2.5 in Chapter 2 for details).

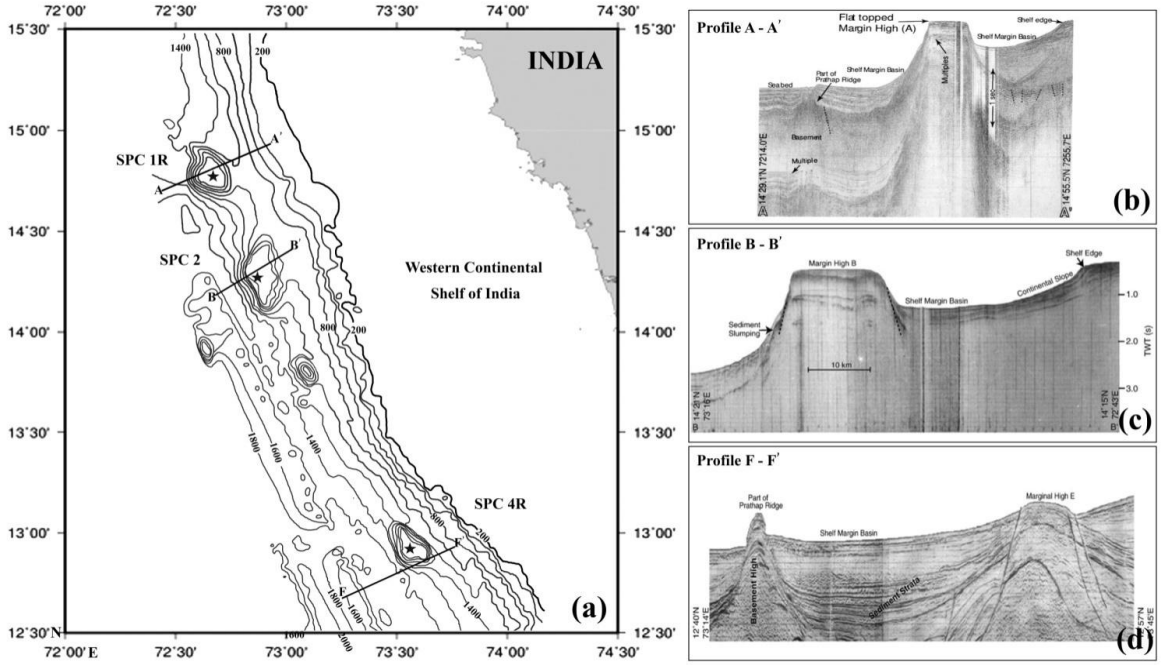

Figure 3.2: *a) The core locations are plotted on a swath bathymetric depth contour map (contour interval 200 m) showing the mid-slope/marginal highs along with the geophysical transects (modified from Rao et al., 2010); b and c) single-channel seismic reflection images of profiles A-A', B-B'; d) multi-channel seismic image of profile F-F' on the southern edge of topographic high (Rao et al., 2010 and references therein)*

3.2 Results

Porewater and seawater phosphate

The dissolved inorganic phosphate (DIP) profiles of the porewater and seawater samples are shown in **Fig. 3.3**. The porewater DIP profiles of SPC 1R and SPC 2 show similar trends with high concentration in the top 6 cm and low concentration down the core. The porewater DIP concentration in SPC 1R varies between 2 and 23 µmol/L, whereas in SPC 2 it is between 7 and 35 µmol/L **(Table 3.2)**. In both profiles, highest concentration is observed in the 4-6 cm section. While SPC 1R shows a gradual decrease in DIP concentration after 6 cm, the decrease is more rapid in SPC 2 and becomes almost constant by 10 cm. In SPC 4R, the maximum DIP concentration is observed in the surface (0-2 cm section) and shows a downcore decrease. The concentrations are also low (0.2-7 µmol/L) in this core.

For seawater, the DIP concentration were measured in CTD 1, CTD 2 and CTD 3 corresponding to locations of sediment cores SPC 1R, SPC 2 and SPC 4R, respectively. The DIP concentrations at surface are low **(Fig. 3.3)**, with a gradual increase with depth. The values range between 0.6 and 5.3, 0.03 and 2.5 and 0.1 and 2.8 µmol/L in CTD 1, CTD 2 and CTD 3, respectively. The bottom water DIP values are much lower than those in the porewater of all locations **(Fig. 3.3)**.

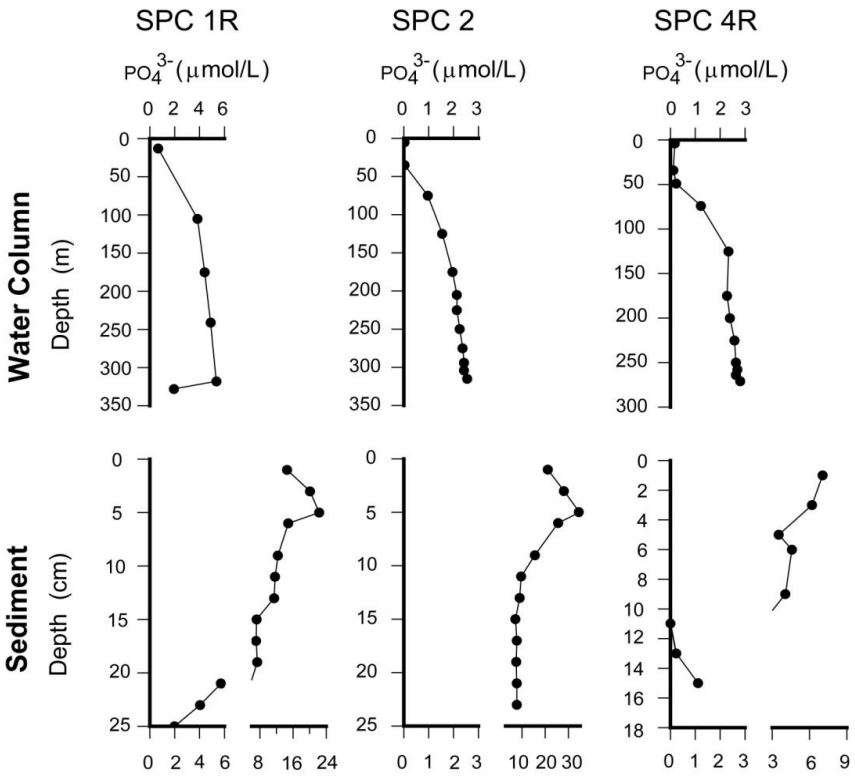

Figure 3.3: *Dissolved phosphate (µmol/L) in seawater (with depth) and porewater (with sediment depth).*

Benthic flux of phosphate

The magnitude of benthic flux that are calculated from Fick's law of diffusion for SPC 1R, 2 and 4R are in the order of 16, 22 and 1.1 mmol m^{-2} yr^{-1} respectively. Compared to the other two cores SPC 4R has a low benthic flux. However, in all the three locations, the fluxes display negative values, indicating that the flux of phosphate is from the sediment to the water column **(Table 3.1)**.

Downcore solid-phase phosphorus profiles

Downcore variations of sequentially extracted P fractions and total P contents in three cores are shown in **Fig. 3.4. and Table 3.3.**

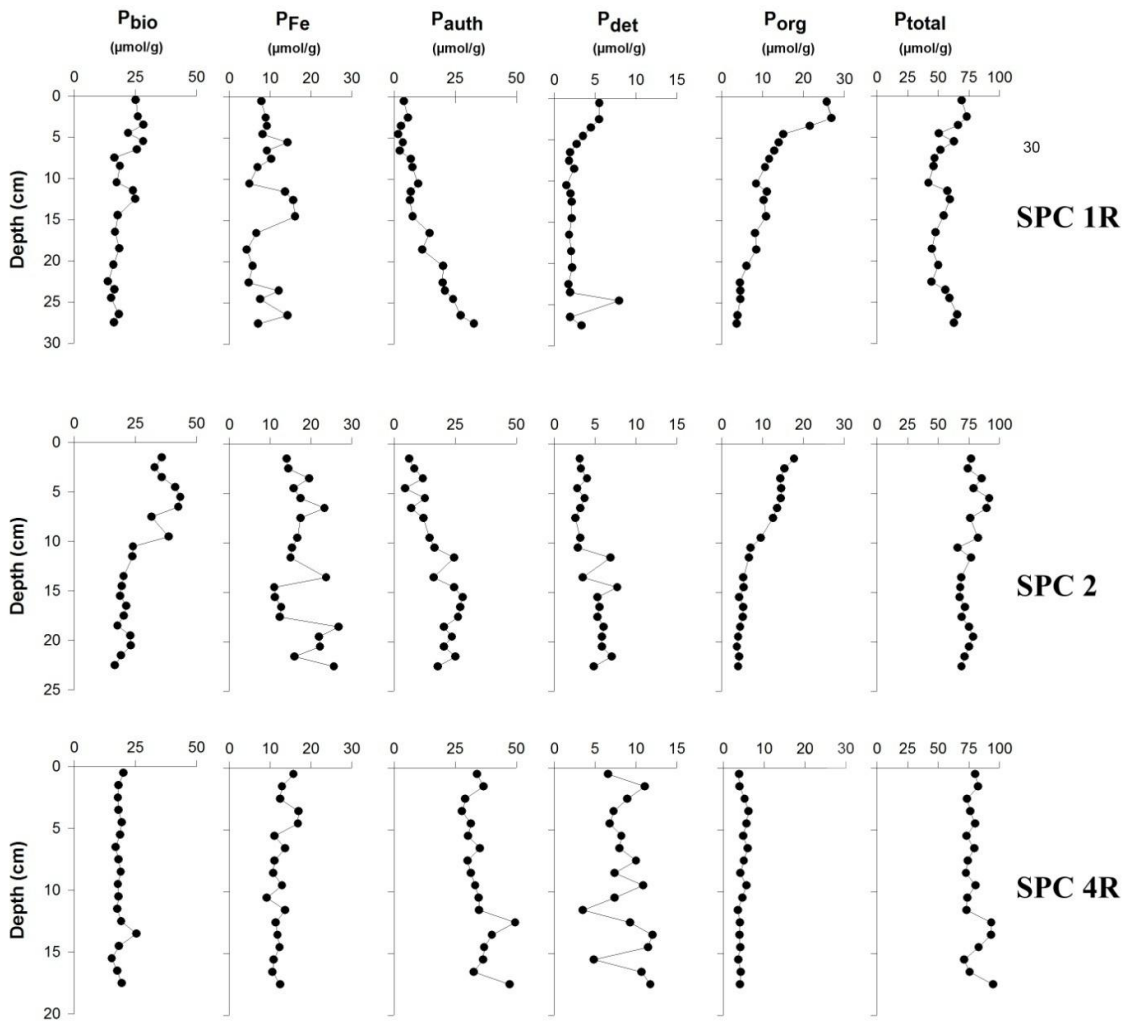

Figure 3.4: *Down core variation of total phosphorus and P in five geochemically separable phases (units in µmol/g)*

The total P content in the study area ranges between 42 and 95 µmol/g. Compared to SPC 1R and SPC 2, total P contents are relatively high in SPC 4R and range from 71 to 95 µmol/g.

The biogenic P (P_{bio}) content in sediment cores SPC 1R and 2 accounts for 25-50% of total P **(Fig.3.5 and Table3. 4)** and varies between 14 and 28 and 17 and 43 µmol/g, respectively.

In SPC 1R, P_{bio} fraction shows broad increase at three subsurface depths (at 3-4, 5-7 and 11-13 cm below sea floor (bsf)). In SPC 2, P_{bio} content is highest at 5.5 cm bsf (43.3 µmol/g) and then decreases down the core gradually. In SPC 4R, P_{bio} accounts for 20-27% of the total P with values ranging between 15 and 25 µmol/g. The P_{bio} fraction is nearly constant throughout the core with an exception at 13.5 cm bsf, where an increase to 25 µmol/g is observed.

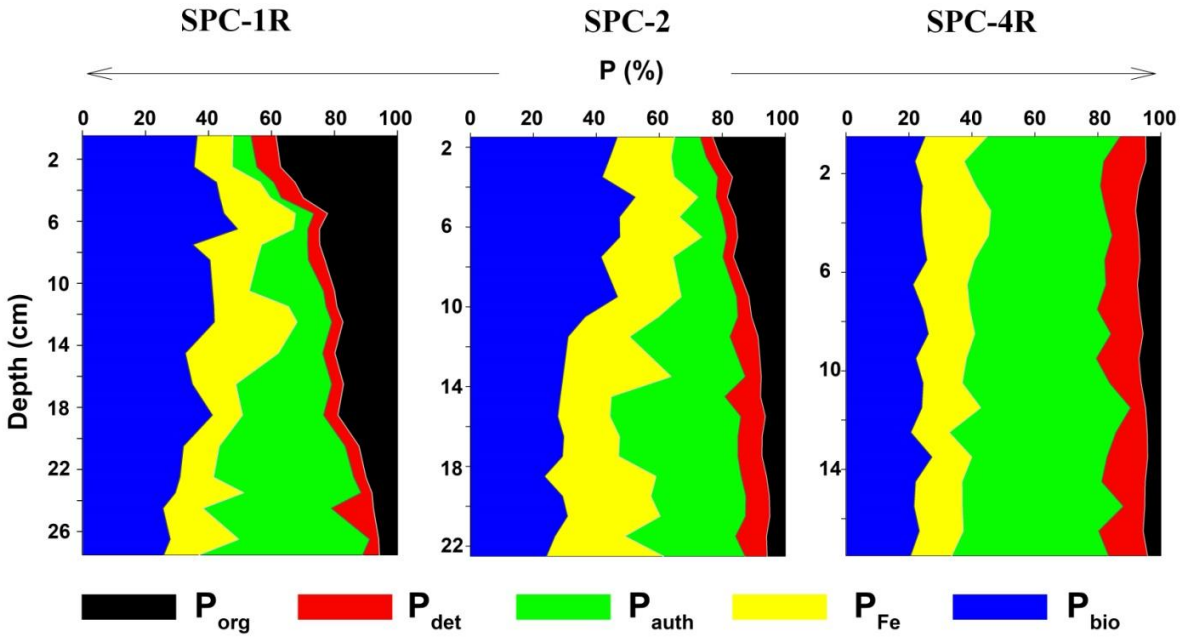

Figure 5: *Relative percentages of solid P phases with sediment depth.*

The Fe-bound P content (P_{Fe}) in SPC 1R accounts for 9-29 % of total P and varies between 4 and 16 µmol/g. The P_{Fe} content is approximately 9 µmol/g in the top 4 cm with a spike at 5.5 cm (14 µmol/g) followed by a gradual decrease with depth down to 11 cm with a broad maximum between 11 to 15 cm. The minimum values (4.2 to 6.5 µmol/g) are found between 16.5 and 22.5 cm with a third increase close to the bottom of the core. In SPC 2, P_{Fe} content

ranges from 11 to 27 µmol/g (16-37% of the total P) with a general trend of downcore increase. In SPC 4R, the values ranged between 9 and 17 µmol/g accounting for 12-22% of the total P.

The authigenic P (P_{auth}) ranges from 2 to 49 µmol/g. In SPC 1R, the P_{auth} content shows significant variation from 2 to 33 µmol/g. The P_{auth} content accounts for 3-7% of the total P at the core top but increases up to 51% in the bottom of the core. In SPC 2, the value ranges from 5 to 28 µmol/g with an increasing trend down core. P_{auth} fraction is very high in SPC 4R and it contributes 36-53% of the total P with values ranging between 28 and 49 µmol/g.

The detrital (P_{det}) content in the three cores ranges between 1 and 12 µmol/g and accounts for not more than 14% of total P. In SPC 1R, the P_{det} content is high near the surface and decreases until 8 cm bsf and is then nearly similar for the rest of the core except for a peak at 25 cm bsf. In SPC 2, the values range from 2.6 to 7.7 µmol/g, accounting for 3-11% of total P. When compared to other two cores, SPC 4R shows higher P_{det} content with values ranging between 3.5 and 12 µmol/g.

The organic P (P_{org}) content ranges from 4 to 27 µmol/g. In SPC 1R, it is a major contributor to the total P (5-38%) in the surface along with P_{bio}. P_{org} decreases downcore with values reducing from 27 to 3.6 µmol/g with depth. In SPC 2, the values vary between 4 and18 µmol/g. In SPC 4R, the variation is less pronounced with values ranging between 3.6 and 6.1 µmol/g.

Total iron

In SPC 1R, the total iron content in carbonate-free basis decreases with depth until 5 cm and then remains nearly constant till 21.5 cm before showing a bottom enrichment (**Fig.**

3.6 and Table 3.5) The values range between 3 and 4.8 wt.%. A similar bottom enrichment is seen in core SPC 2 also with values ranging between 3.2 and 7.2 wt%. In SPC 4R, the values lie between 4.6 and 7.2 wt.%

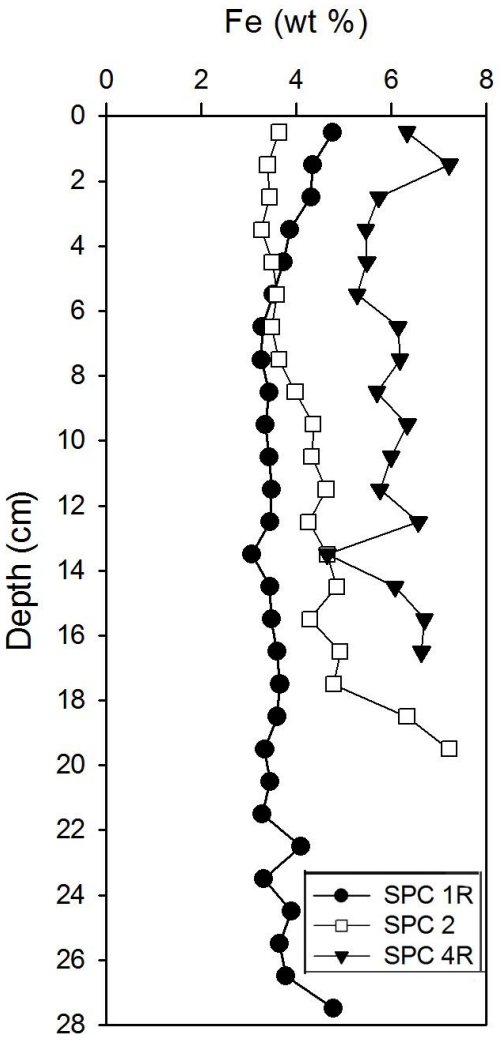

Figure 3.6: *Downcore variation of total Fe content (wt.% on a carbonate-free basis) in the sediment cores*

Organic and inorganic carbon

The down core variations of total organic and inorganic carbon (TOC and TIC) are presented in **Fig.3.7 and Table 3.5.** The TOC content varies between 2.1 and 10.2 wt%, 1.3 and 8.8 wt.% and 1.7 and 2.6 wt.% in SPC 1R, 2 and 4R, respectively. The TOC profiles of SPC 1R and 2 are similar and illustrate a downward decrease from surface. In contrast, the TOC content in SPC 4R is relatively low and shows no downcore change. The TIC profiles of these three cores mirror image the TOC profiles with values varying between 3.93 and 9.36 wt.%, 4.7 and 8.6 wt.% and 9 and 10 wt.% in SPC 1R, 2 and 4R, respectively.

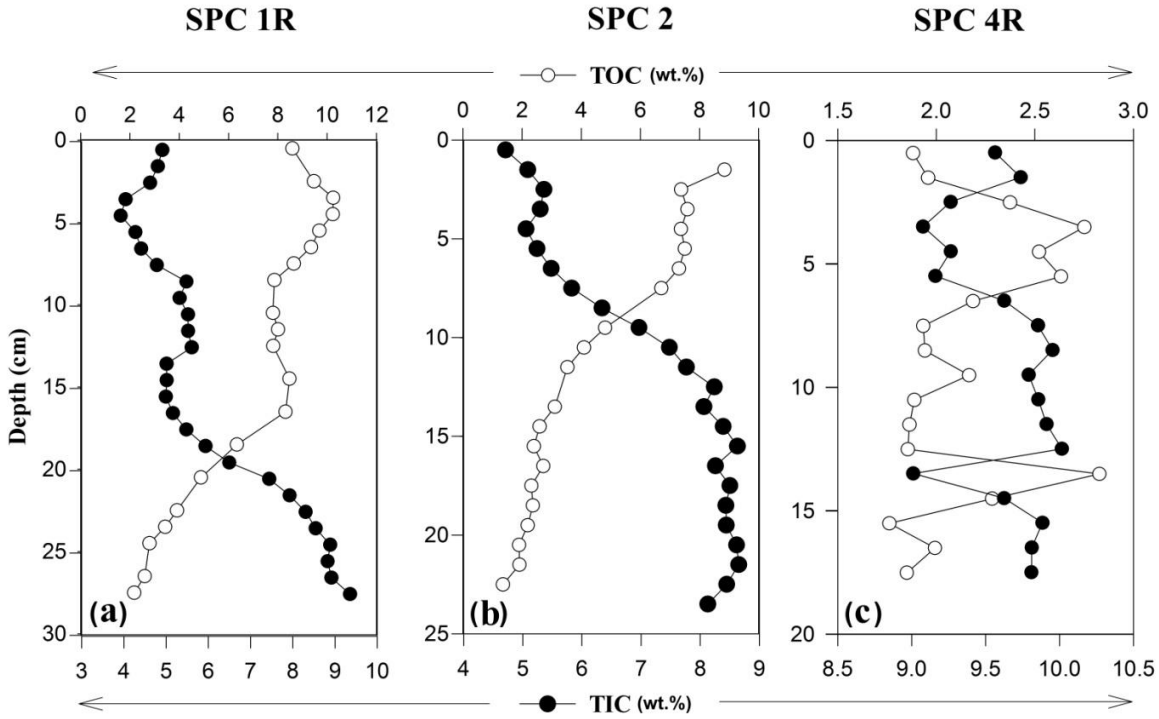

Figure 3.7: *Downcore variation of total organic and inorganic carbon (TOC and TIC in wt%) in a) SPC 1R, b) SPC 2 and c) SPC 4R.*

3.3 Discussion

Benthic flux and solid phase P speciation

The benthic porewater flux values are similar to the previously reported values from the Arabian Sea and Peruvian OMZ (Schenau and De Lange, 2001; Noffke et al., 2012). Benthic fluxes of phosphate in OMZ sediments are high compared to the sediments below the OMZ, indicating the rapid regeneration of phosphorus in sediments impinged by oxygen depleted waters (Schenau and De Lange, 2001). Compared to SPC 1R and SPC 2, the phosphate flux is less at the location of SPC 4R **(Table 3.1),** which may be due to the low organic matter and fish debris content (P_{bio}). The high porewater phosphate concentration

(**Fig. 3.3**) in the top layers of the cores may either be due to the increased remineralization of phosphate from organic matter or the release of phosphate from the dissolution of biogenic apatite. The downcore decrease in porewater P concentration is likely the result of the formation of calcium fluorapatite (Jahnke et al., 1983; Ruttenberg and Berner, 1993; Schenau et al., 2000).

Solid phase fractionation results of the studied cores indicate that P_{bio} is the major fraction of sedimentary P in the top sections of SPC 1R and 2 while P_{auth} is the dominant phase in the bottom depths. SPC 4R is an exception to this pattern with P_{auth} as the major fraction throughout the core **(Fig. 3.5)**. Incidentally, the sediment characteristics of this core (SPC 4R) which was recovered from a marginal high off Mangalore region (south of SPC 1R and 2 - **Fig. 3.2**) differ in the texture (more coarser), sedimentation rate (faster) and TIC content (higher) compared to SPC 1R and 2. The possible reasons are explained in the later part of the paper.

The Arabian Sea is characterized by intense coastal upwelling and high productivity. High amounts of fish debris are found in sediments of upwelling areas (De Vries and Pearcy, 1982), which is likely the reason for higher P_{bio} contents. The decrease in P_{bio} content with depth sediment depth indicates dissolution of biogenic apatite. Even though dissolution of fish debris is proposed to explain the downcore decrease in P_{bio}, no increase in DIP is seen in the porewater profiles (Fig. 3.3), implying that phosphate released from fish debris is leading to precipitation of authigenic apatite (e.g., Suess, 1981, Schenau et al., 2000) as reflected in the downcore increase in P_{auth} content in SPC 1R and SPC 2. Though P_{org} forms the third largest P pool in these sediments, a distinct downcore decrease (**Fig. 3.5**) suggests a major role of this phase in P diagenesis (please see Filippelli et al., 1994; Ingall and Jahnke, 1994;

Filippelli and Delaney, 1995, 1996; Filippelli, 2001). The downcore decrease in TOC and P_{org} in the cores indicates the degradation and release of P to the porewater, which would enhance the benthic flux of P and would facilitate the formation of authigenic apatite (Froelich et al., 1988; Filippelli et al., 1994; Ingall and Jahnke, 1994; Filippelli and Delaney, 1995,1996; Filippelli, 2001; Arning et al., 2009a, 2009b).

Molar C_{org}/P_{org} ratios in general are greater than the Redfield ratio (C:P= 106:1) in all the three cores (Fig. 3.8) indicating the preferential release of P relative to carbon during organic matter degradation (Schenau and De Lange, 2001; Babu and Nath, 2005). To account for P bound to other reactive forms (such as biogenic, iron bound and authigenic), $C_{org}/P_{reactive}$ has also been used (Anderson et al., 2001). The molar $C_{org}/P_{reactive}$ ratio in SPC 1R and SPC 2 is close to the Redfield ratio at surface and decreases down the core (**Fig. 3.8**), indicating that the transformation of P is taking place from labile to authigenic phase. Such a sink switching phenomenon from labile to authigenic P phase has been reported before (Ruttenberg and Berner, 1993; Slomp et al., 1996; Louchouarn et al., 1997; Babu and Nath, 2005). Much lower $C_{org}/P_{reactive}$ ratios in SPC 4R **(Fig. 3.8)** are driven by high P_{auth} content **(Fig. 3.4)**.

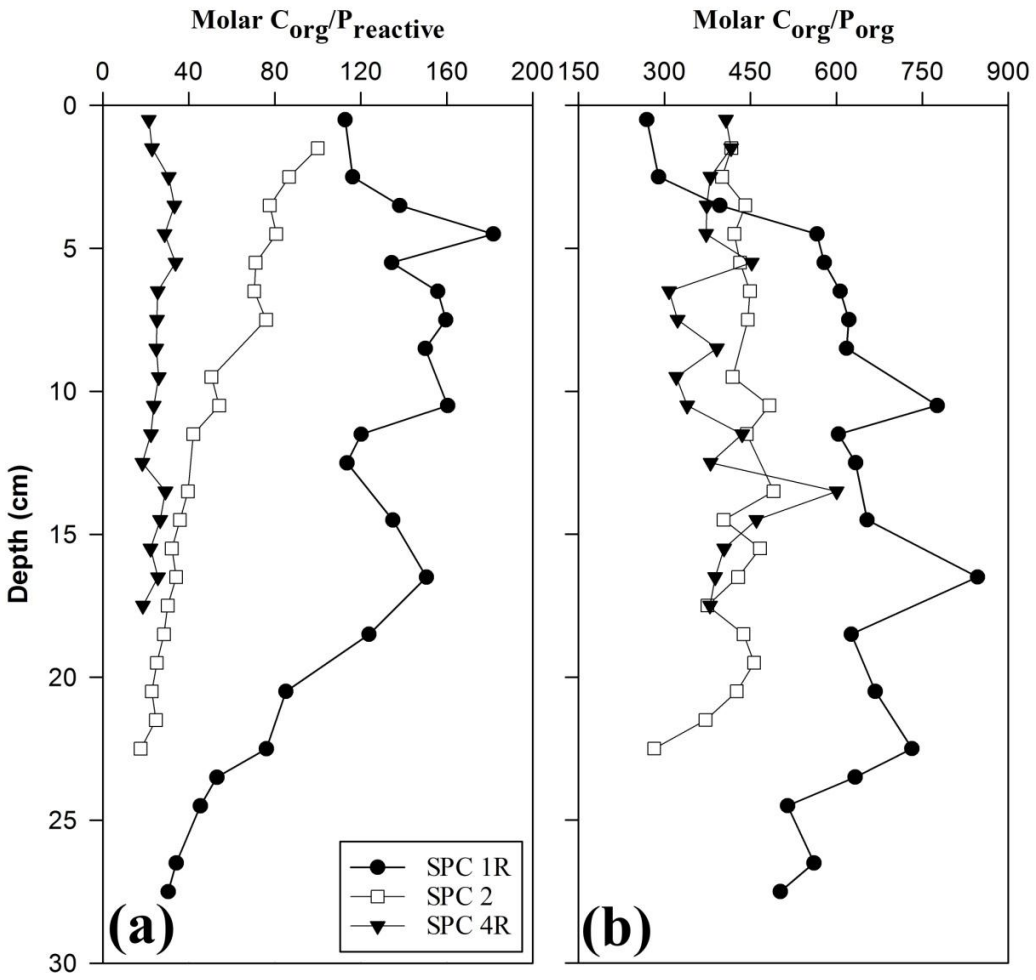

Figure 3.8: *Downcore variation of a) molar $C_{org}/P_{reactive}$ and b) molar C_{org}/P_{org} ratios.*

Iron oxyhydroxides play a major role in the benthic cycling of P. The presence of Fe-oxyhydroxides in the sediment acts as an effective trap of reactive P. In oxic environments, Fe-oxyhydroxides scavenge the dissolved P from seawater and porewater. Under reducing conditions, it undergoes reductive dissolution and releases P to porewater and thereby enhancing the benthic P flux and fueling P_{auth} formation (Slomp et al., 1996; Filippelli, 2001). But in this study, even under the reducing conditions as deduced from the bottom water oxygen concentration, the P_{Fe} content does not show a prominent downcore decrease but accounts for 9-37% of the total P **(Fig. 3.4)**. The possible reason for the high P_{Fe} content

at subsurface depths may be the formation of vivianite since the P_{Fe} fraction can contain Fe-P mineral phases (such as vivianite) along with P associated with iron-oxyhydroxides. It is pertinent to mention here the recent finding of Kraal et al. (2017) that the P extracted during the step targeting Fe-bound P can also extract $CaCO_3$-associated P.

The formation of vivianite is likely to occur in non-sulfidic environments such as below the sulphate methane transition zone (März et al., 2008; Slomp et al., 2013). Dissolved oxygen in the present day Arabian Sea is almost completely consumed, which is accompanied by significant denitrification in the OMZ (150-1200m) (e.g., Naqvi et al., 1993), with no sulfate reduction taking place in the outer shelf (hypoxia) and over the mid shelf (suboxia) (Naqvi, 2008). Also, no euxinic conditions were found to develop in the OMZ in the Arabian Sea during the last 120 kyr (Schenau et al., 2002). The permanent oxygen minimum zone and non-sulfidic condition of the Arabian Sea allows the availability of dissolved Fe for the formation of vivianite. Vivinite would be in the range of 0.11 to 0.66% even if all the P_{Fe} is converted to vivianite. However, no direct evidence of presence of vivianite can be presented, because it is below the detection capacity of X-ray diffractometry (~5%). The possibility of Fe oxidation during sample handling may lead to a possible increase in P_{Fe} fraction (Kraal et al., 2009; Dijkstra et al., 2014; Kraal and Slomp, 2014). The prevalence of non-sulfidic conditions in the study area precludes Fe sulfide formation ruling out the possibility of oxidation effects on P speciation.

In sediments, the ratio of Fe to P can reflect the changing redox conditions (Louchouarn et al., 1997). Schenau and De Lange (2001) use the molar ratio of Fe_{CDB}/P_{Fe} as a proxy for the reductive dissolution of iron oxyhydroxides. In the absence of Fe_{CDB} data, Fe_{ex}/P_{Fe} ratio was used in this study, in which Fe_{ex} represents the proportion of Fe in excess

of what can be contributed by the residual phase (calculated using Fe and Ti to account for Fe which is non-lithogenic; Murray and Leinen, 1993). The Fe_{ex}/P_{Fe} shows low values in SPC 2 (7.7-34.8, average 20.6) and SPC 4R (8.9-50.9, average 27.6) (**Fig. 3.9)**. The top 5 cm of sediment at stations SPC 1R stands out in two ways: (1) a down-core decrease in Fe_{ex}/P_{Fe} from about 46 to 10 **(Fig. 3.9)** and (2) corresponding increase in porewater DIP **(Fig. 3.3)** suggesting that a reductive dissolution of iron bound P releases phosphate to the porewater. This interpretation is consistent with the redox conditions within the core. Water column DO values and moderately high porewater nitrate (secondary terminal electron acceptor for organic matter decomposition) plus nitrite values in surface sediments indicate suboxic conditions **(Fig. 3.9)**. The drastic decrease in porewater nitrate plus nitrite values below the surface indicates the near complete utilization of oxygen for the mineralization of organic matter. This is also supported by the increasing U/Th ratio down core from suboxic at surface to anoxic at about 5cm bsf **(Fig. 3.9).** The ratio of U to Th is commonly used as a redox indicator (Wright et al., 1984; Jones and Manning, 1994 and references therein, Nath et al., 1997; Pattan et al., 2017 and references therein). Since Th is immobile in low-temperature environments, the ratio is sensitive to changes in U supplied from seawater. In turn, U variation depends on the redox state of seawater, with fixation of low valency U under reducing conditions. U/Th ratios above 1.25 have been used to infer suboxic and anoxic conditions and those below 0.75 are indicative of oxic conditions (Jones and Manning, 1994).

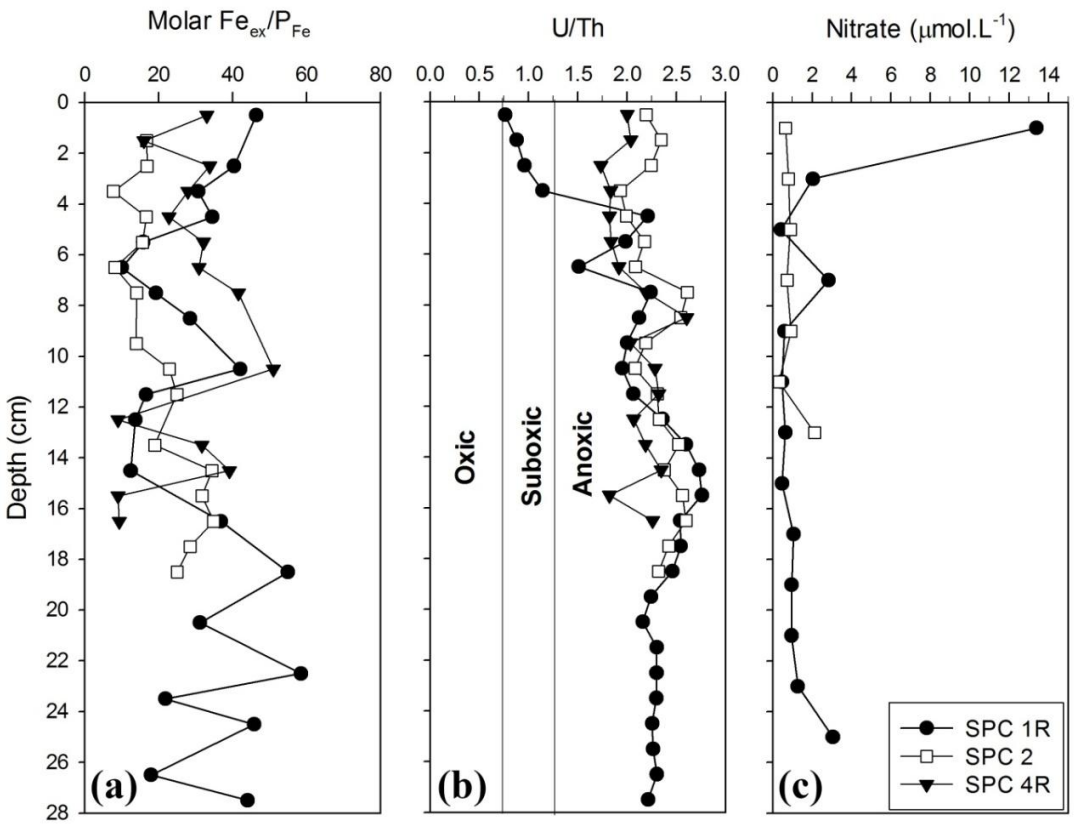

Figure 3.9: *Downcore variation of molar Fe_{ex}/P_{Fe}ratios and U/Th ratio in sediments. Fe_{ex} represents the empirically calculated excess Fe concentrations over that found in lithogenic fraction. Also shown are porewater nitrate (μmol/L) in SPC1R and SPC2.*

High porewater nitrate, lower U/Th ratio and higher Fe_{ex}/P_{Fe} in the core top of SPC 1R collectively indicate that P is probably bound to Fe-oxides/oxyhydroxides in the surface sediments **(Fig. 3.9)**. Such high Fe_{ex}/P_{Fe} is not found at the other two locations. A gradual reduction in P_{Fe} content from 5 to 10 cm at SPC 1R is followed by a small increase in P_{auth} **(Fig. 3.4)** at about 10 cm indicating that P_{Fe} dissolution is contributing to the formation of a small amount of authigenic apatite. Two subsurface P_{Fe} peaks are observed, a distinct high occurs at 11-15 cm and the second close to the bottom of the core **(Fig. 3.4).** Though, Fe

redox cycling seems to have a role here, Fe bound P seems to play limited role in P diagenesis compared to that of P bound to organic carbon and biogenic fractions. The documented scenario at the lower boundary of OMZ in the western Arabian Sea (Kraal et al., 2012) is different to the proposed processes (interpreted from reactive transport modeling), where Fe redox cycling was postulated to play an important role in P retention and subsequent authigenesis (Kraal et al., 2012).

The P_{det} constitutes only a minor fraction of TP in the study area. The P_{det} fraction undergoes burial into the sediment without undergoing any alterations and may indicate the changes in depositional conditions. Major detrital P input on these topographic high areas would be through the settling of suspended materials and atmospheric input. In SPC 1R, P_{det} is high in top 5 cm and nearly uniform until the bottom of the core except for a peak at ~25 cm bsf **(Fig. 3.4)** which coincides with increased Fe content **(Fig. 3.6)** possibly representing an episode of increased dust deposition. Similarly, two subsurface peaks in SPC 2 and a large fluctuation in SPC 4R likely represent periods of increased atmospheric input. One subsurface P_{det} peak in SPC 2 co-occurs with a high P_{auth} **(Fig. 3.4)**. One possible reason could be an increased nutrient input associated with detrital input. Recently, the SEDEX extraction method was found to extract a part of P_{auth} as P_{det} leading to under estimation of P_{auth} (Kraal et al., 2015). This may not be the case here, as the downcore P_{det} variation **(Fig. 3.4)** in this study mimics the variability of refractory elements such as Ti, Th and Zr **(Fig. 3.10)**, with the co-occurring peaks representing periods of increased detrital input.

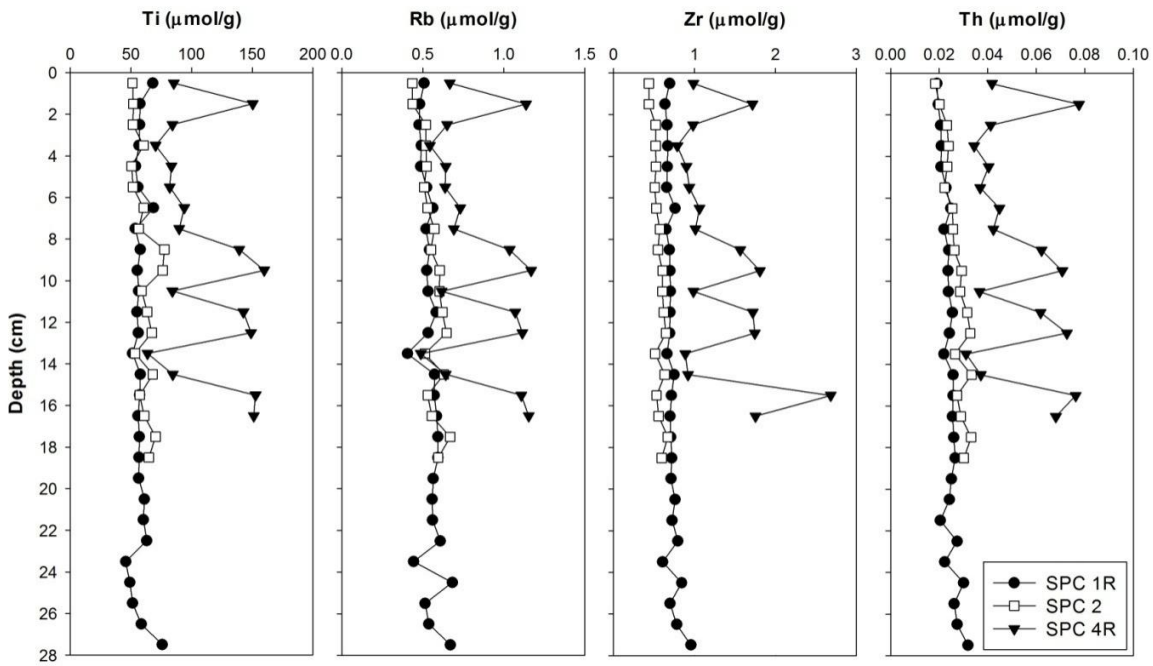

Figure 3.10: Downcore variation of elements Ti, Th, Zr and Rb (in carbonate-free basis) in the three cores showing a large fluctuation in SPC 4R.

The P burial efficiency (PBE) was calculated (see Section 2.6 for the formula used) to evaluate the relative roles of regeneration and burial of P in this part of the Arabian Sea. PBE is very low (2.1 and 2.6%) in SPC 1R and SPC 2 compared to that in SPC 4R (90%). Lower burial efficiencies correspond to lower sedimentation rates (3.8 cm/ky in SPC 1R and 2.1 cm/ky in SPC 2 compared to 26.5 cm/ky in SPC 4R (unpublished sedimentation rates estimated based on AMS ^{14}C of foraminifera) and higher porewater phosphate fluxes out of sediments (16 mmol m^{-2} yr^{-1}in SPC 1R and 22 mmol.m^{-2}.yr^{-1} in SPC 2 compared to 1.1 mmol m^{-2} yr^{-1} in SPC 4R) indicating higher P regeneration. These burial efficiencies (in SPC 1R and SPC 2) in the eastern Arabian Sea are much lower than those reported for the Oman and Pakistan margins (27 -74%, Schenau and De Lange, 2001) and Murray Ridge in the northern Arabian Sea (14%, Kraal et al., 2012) indicating significant P regeneration in this

part of the Arabian Sea. Lack of significant diagenesis (see the section of SPC 4R) and high sediment accumulation may be the reason for the higher PBE (90%) in the southern station.

Evidence of ongoing phosphogenesis

The concurrent decrease in P_{org} and P_{bio} with increase in P_{auth} suggests that P_{auth} is forming at the expense of P_{org} and P_{bio} (Ruttenberg and Berner, 1993) and is a direct indication of phosphogenesis occurring in the study area. To quantify the P_{auth} formation from P_{org} and P_{bio} depletion, best fit curves were drawn and the area under the curves was calculated by integration **(Fig. 3.11)**. The best fit curve was made through the logarithmic fit of the form y=m0+m1*ln(x) where "ln" is the natural (base e) logarithm function **(Fig. 3.11**).

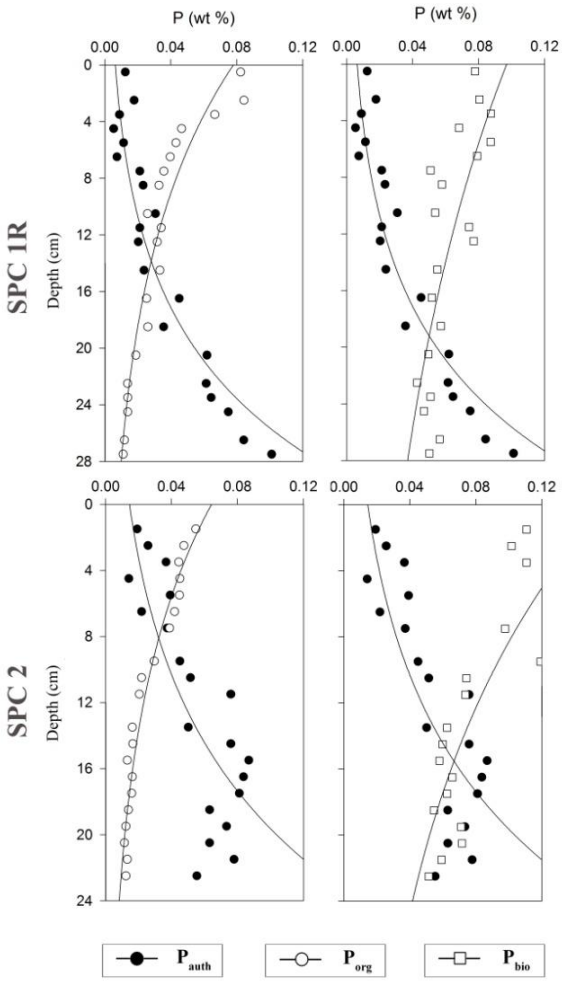

***Figure 3.11**: Solid-phase profiles of P_{auth}, P_{org} and P_{bio} (all in wt. %) and their best fit curves*

The Trapezoidal numerical integration method was used to calculate the area under the graph. This method approximates the integration over an interval by breaking the area down into trapezoids with more easily computable areas. The depth integrated P_{auth} formation and deficit of P_{org} and P_{bio} were calculated from these values (similar to the approach followed in Ruttenberg and Berner, 1993). The equation for conversion from the area to integrated P gain/deficit and R^2 values for the best fit are given in the **Table 3.6**. From the data, it is clear that the P_{auth} formation (SPC 1R - 0.99, SPC 2-1.09 gP/cm^2) is higher than the P_{org} deficit in both SPC 1R and SPC 2 (SPC 1R-0.82, SPC 2-0.51 gP/cm^2) indicating that organic matter degradation is not the only process responsible for the authigenic apatite formation but the biogenic P dissolution also acts as a major contributor. In both sites, however, the sum of P_{org} and P_{bio} deficit (SPC 1R-2.36, SPC 2-2.19 gP/cm^2) exceeds the integrated P_{auth} values, suggesting that the excess release of P from organic matter degradation and fish debris dissolution are responsible for the high benthic fluxes in these locations and P_{Fe} exerts only a minor role in authigenesis and benthic fluxes here. In SPC 4R, however, curve fitting was not possible and a downcore profile of P_{react} (sum of P_{bio}, P_{Fe} and P_{org}) and $P_{auth\ is}$ drawn **(Fig. 3.12)**. Both the profiles follow a similar trend

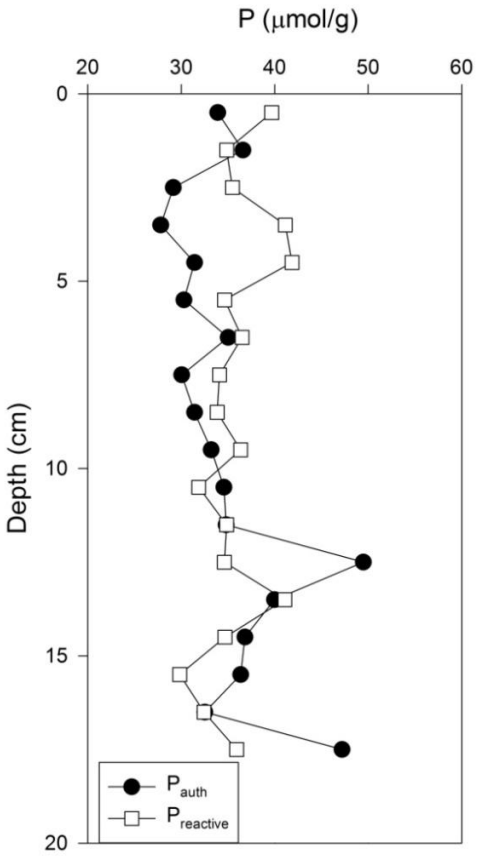

***Figure 3.12**: Downcore profiles of P_{react} (Sum of, P_{bio}, P_{Fe} and P_{org}) and P_{auth} in SPC 4R (unit in µmol/g).*

indicating the lack of significant diagenetic transformation of P_{react} to P_{auth} phase. The depletion of other reactive fractions (P_{bio},P_{Fe} and P_{org}) is not large enough to account for the high P_{auth} content of SPC 4R and may involve an external source such as atmospheric deposition.

Atmospheric deposition and controls on P geochemistry in SPC-4R

In addition to contribution from fish debris and organic matter, atmospheric deposition can contribute Ca-P minerals to the P_{auth} pool (Eijsink et al., 2000; Faul et al., 2005; Palastanga et al., 2011; Kraal et al., 2012; März et al., 2014; Ni et al., 2015). Kraal et al., (2012) have in fact reported an important role of atmospheric dust in P deposition in the western Arabian Sea. Atmospheric input of P_{auth} is likely in these sediment cores sited on topographic highs. In core SPC 4R the depositional pattern is different than the other two northern cores as revealed by downcore elemental variation **(Fig. 3.10)**. While the downcore variation of refractory elements (Ti, Th, Zr, Rb) is low and show a near uniform pattern in cores SPC 1R and SPC 2, the concentrations of these elements are high and shows distinct downcore peaks in SPC 4R, documenting periods/episodes of change in lithogenic sedimentation. Incidentally, downcore variation of some P phases including that of P_{det} and P_{auth} (with a slight offset) also follows the trend of refractory elements corroborating that the P deposition is dominantly driven by depositional change.

The episodic changes in depositional conditions can either be due to lateral advection of lithogenic material from land or due to eolian input. Lateral advection is unlikely, however, as the distance of the core from shore is about 200 km, and therefore atmospheric deposition may be driving the changes in elemental content. The high Ti and Zr content

which are good proxies for dust deposition (see Nath, 2001 and references therein), at SPC 4R may be a result of high atmospheric deposition in this area.

The clay mineral palygorskite that is typical of atmospheric deposition was reported to be present in a broad band of sediments extending from Arabia to the southern tip of India (Kolla et al., 1976). A good correlation of peaks in palygorskite content with topographic highs was noticed and attributed to reflect eolian processes. The trajectories of dust-bearing winds reconstructed for the Holocene has shown a plume reaching from the coast of Yemen up to the southern tip of India (Sirocko et al., 1991) in agreement with the studies of Kolla et al., (1976). The plume is influenced by long-distance transport by north-westerly and westerly winds from Arabia and the Persian Gulf (the Shamal) across the Arabian Sea (Sirocko and Sarnthein, 1989). Palygorskite-rich aerosols move at heights well above the low level southwest monsoon trajectories and transport dust throughout the Arabian Sea (Sirocko et al., 1991). Palygorskite derived from Arabia and Somalia was also reported in the southwest coast of India (Chauhan, 1996), little south of the present studied site.

The Arabian Sea receives relatively large fluxes of P through atmospheric input (Okin et al., 2011). According to Kraal et al. (2012), 60%~of the background Ca-P concentration may be of atmospheric origin in the western Arabian Sea. Thus, the likely reason for higher P_{auth} values throughout core SPC 4R in conjunction with the lack of direct relation between P_{auth} and other reactive P phases may be to the result of deposition of atmospheric dust containing P_{auth}. A P-speciation study of settling particles reveals a significant fraction of total P (~ 25%, ranging from 3–78%) is carried from the upper ocean to the sediments as authigenic P (Faul et al., 2005) providing evidence that the remineralization of organic P and the exchange with other forms of P may begin in the water

column, and continue in the sediments. A considerable transformation from the organic to the inorganic P pool in the water column was also reported (Paytan et al., 2003).

Though the P-speciation data do not show clear evidence of sink-switching within core SPC 4R, down core depletion of porewater P indicates the utilization of P possibly for authigenic P formation. The highest peak of P_{auth} content was observed at 12.5 cm bsf where a depletion in P_{org} and porewater DIP occurs suggesting in situ precipitation of CFA. Thus, in addition to significant atmospheric deposition, authigenic precipitation of CFA is likely taking place in the sediment.

The third process considered here for the high P_{auth} content in SPC 4R is winnowing. While Shimmield et al. (1990) and Pedersen et al. (1992) have attributed the high P concentration in the top sediment layers of Oman Margin to winnowing, Schenau et al. (2000) have ruled out the role of winnowing for the high P concentrations in the western Arabian Sea sediments. In winnowing, the high specific gravity of phosphatic precipitate (2.9 g/cm^3) compared to other sediment particles (1.5-2.5 g/cm^3), removes the finer and lighter particles, which leads to the concentration of phosphatic precipitates (Follmi, 1996; Schenau et al., 2000). While no visible phosphatic grains/pellets were found in the core, extrapolated sedimentation rates (AMC ^{14}C dates of forams) of the core tops yield an age of ~700 years BP for SPC 4R compared to 45 years and near zero age for cores SPC 1R and SPC 2, respectively suggesting an intense winnowing at SPC 4R. The high carbonate content (75-83 wt.%) and coarse grained texture along with the high C_{org}/N ratio in the top section of SPC 4R (Table 3.5) (see Schenau et al., 2000) compared to the other two cores also support higher winnowing activity in the area **(Fig. 3.13)**.

In summary, the combination of eolian input and water column precipitation, early diagenesis within the sediments, and winnowing in that order seems to be responsible for the high P_{auth} content in core SPC 4R.

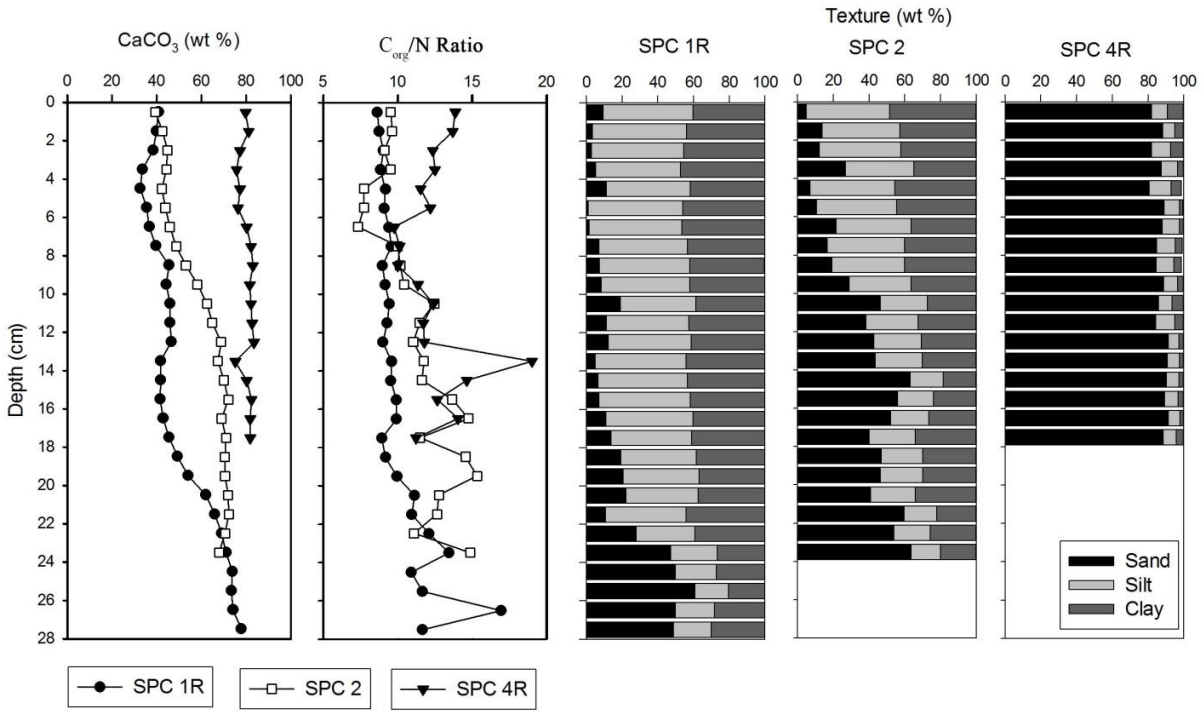

Figure 3.13: Downcore variation of $CaCO_3$, C_{org}/N ratio and texture of SPC 1R, 2 and 4R.

Schenau et al. (2000) reported present-day phosphogenesis in the northern part of the Eastern Arabian Sea off the Pakistan coast. The study presented in this work represents the first report of the occurrence of phosphogenesis in the western continental margin of India. While the geochemical evidence of phosphogenesis is found, but no phosphatic pellets/crusts/concretions were recovered in the studied cores. As mentioned in the introduction, all the phosphorites/concretions/phosphatic limestones recovered so far from the Indian continental margin are of older age (Nair, 1985; Borole et al., 1987; Rao et al.,

1995; Rao and Rao, 1996; Rao and Lamboy, 1996; Vaz et al., 1996), with Rao et al. (1995) ruling out the possibility of their recent formation from a P speciation study of the sediments from the same latitudes as the present study in the Eastern Arabian Sea but from more shallow locations (depth ~25 m), Acharya et al. (2016) report the absence of active phosphatizationin the area and attribute the lack of authigenic P according to low total P content and the dominance of detrital non-reactive fraction of P**.** The absence of active phosphatization/phosphogenesis in their study area is possibly due to the unsuitable locations chosen to study the occurrence of phosphogenesis. The sampling locations are close to the coast in shallow water depth (25 and 26 m). Such areas receive high terrigenous sediment input and bottom waters are well oxygenated. At such water depths, seasonal anoxia occur 2-3 months in a year but well oxygenated during the remaining parts of the year (Naqvi et al., 2009). The oxic bottom water promotes the adsorption of P on iron oxyhydroxide and limits the release of phosphate to the porewater and the subsequent authigenesis. The high sedimentation rates and high terrigenous input to the inner shelf regions will lead to the deposition of non-reactive P. In contrast the topographic highs impinged by less oxygenated waters, such as site studied in this work, may be suitable for phosphogenesis. Eastern Arabian Sea has several such structural highs (e.g., Mukhopadhyay et al., 2008; Rao et al., 2010), which can be potential sites for the occurrence of phosphogenesis and phosphorite formation.

3.4 Conclusions

Porewater phosphate and solid-phase P speciation results indicate that rapid regeneration of P is occurring in the sediments on topographic highs that are impinged by poorly oxygenated waters in the eastern Arabian Sea. Benthic regeneration of P is induced by high rate of organic matter degradation and fish debris dissolution. Redox cycling of iron has a limited influence on the sedimentary P cycling in this area. High concentrations of authigenic P (suggesting CFA precipitation) were measured in the sediment. Molar C_{org}/P_{org} and $C_{org}/P_{reactive}$ ratios indicate the transformation from reactive P to authigenic P. In addition to the enhanced degradation of organic material and the dissolution of fish debris, low sedimentation rates and oxygen depleted conditions favor the ongoing phosphogenesis.

The finding of present-day phosphogenesis in this work and the earlier reports of occurrence of older phosphorites that formed during different periods of the Pleistocene collectively indicate that the marginal highs overlain by poorly oxygenated waters in the Eastern Arabian Sea could be important sites of P burial, in particular during periods of increased productivity. At one of the study sites, atmospheric input of P and formation of authigenic P in the water column may have contributed to the high concentrations of authigenic P observed in the sediment.

Table 3.1: Sampling details, sedimentation rates, bottom water oxygen concentration, diffusive flux of P and its burial efficiency.

Station Name	Latitude (N)	Longitude (E)	Depth (m)	Sedimentation Rate (cm/ky)	Bottom water oxygen concentration (µmol /L)	Diffusive flux of P (mmol m^{-2} yr^{-1})	Burial Efficiency (PBE) (%)
SPC 1R	14˚46.10'	72˚ 40.35'	347	3.8	6.29	-16	2.1
SPC 2	14˚16.25'	72˚ 52.45'	325	2.1	7.49	-22	2.6
SPC 4R	12˚55.10'	73˚ 33.46'	279	26.5	9.32	-1.1	90

Table 3.2: Downcore concentrations of porewater DIP in all the 3 cores Depth-wise variation in dissolved oxygen and DIP content in seawater.

Station Name	Sediment mid-depth (cm)	Porewater DIP (µmol/L)	Water column Depth (m)	Dissolved Oxygen (ml/L)	Seawater DIP (µmol/L)
SPC1R	1	14.59	328	0.14	1.93
	3	20.09	318	0.21	5.35
	5	22.31	241	0.17	4.88
	7	14.86	175	0.17	4.42
	9	12.38	105	0.33	3.83
	11	11.67	12.7	4.88	0.67
	13	11.45			
	15	7.19			
	17	7.12			
	19	7.38			
	21	5.74			
	23	4.05			
	25	2			
SPC2	1	21.07	315	0.17	2.54
	3	28.06	304	0.16	2.43
	5	34.7	294	0.15	2.43
	7	25.55	275	0.19	2.37
	9	15.57	250	0.18	2.25
	11	9.74	225	0.19	2.13
	13	9.02	205	0.17	2.13
	15	7.27	175	0.20	1.96
	17	7.84	125	0.29	1.55
	19	7.58	75	1.15	0.96
	21	7.78	35	4.52	0.03
	23	7.86	5	5.09	0.03
SPC4R	1	7.05	271	0.21	2.81
	3	6.2	264	0.21	2.63
	5	3.53	258	0.21	2.69
	7	4.58	250	0.28	2.63
	9	4.06	225	0.25	2.57
	11	0	200	0.22	2.40
	13	0.24	175	0.21	2.28
	15	1.11	125	0.19	2.34
			74	1.60	1.23
			49	4.47	0.23
			34	4.84	0.12
			4	4.98	0.18

Table 3.3: Solid-phase phosphorus species in the 3 sediment cores.

Station Name	Mid-depth (cm)	P_{bio}	P_{Fe}	P_{auth}	P_{det}	P_{org}	P_{total}	P_{react}
		(μmol/g)						
SPC1R	0.5	25.1	7.8	4.0	5.5	26.6	69.0	63.5
	2.5	26.0	8.9	5.8	5.5	27.2	73.4	67.9
	3.5	28.2	9.2	2.9	4.5	21.5	66.3	61.8
	4.5	22.0	8.1	1.8	3.5	15.1	50.4	46.9
	5.5	28.2	14.2	3.7	2.7	13.9	62.8	60.1
	6.5	25.5	9.2	2.4	1.9	12.8	51.9	50.0
	7.5	16.4	10.3	6.9	1.8	11.6	46.9	45.2
	8.5	18.7	6.9	7.5	2.4	10.6	46.1	43.7
	10.5	17.3	4.9	9.9	1.5	8.4	42.0	40.5
	11.5	24.0	13.6	6.9	2.0	11.1	57.5	55.5
	12.5	24.9	15.6	6.6	2.1	10.3	59.4	57.3
	14.5	17.8	16.1	7.7	2.1	10.8	54.4	52.3
	16.5	16.7	6.6	14.6	1.8	8.2	47.8	46.0
	18.5	18.4	4.3	11.5	2.0	8.4	44.7	42.7
	20.5	16.0	5.7	20.0	2.2	6.1	49.9	47.8
	22.5	13.8	4.8	19.9	1.7	4.5	44.6	42.8
	23.5	16.4	12.1	20.8	1.9	4.5	55.8	53.9
	24.5	15.1	7.5	24.2	7.9	4.5	59.2	51.3
	26.5	18.2	14.2	27.2	1.9	3.9	65.4	63.5
	27.5	16.2	7.1	32.7	3.3	3.6	62.9	59.5

Table3.3: Continued

Station Name	Depth (cm)	P_{bio}	P_{Fe}	P_{auth}	P_{det}	P_{org}	P_{total}	P_{react}
		(µmol/g)						
SPC2	1.5	35.8	14.0	6.2	3.1	17.7	76.8	73.7
	2.5	32.8	14.4	8.3	3.2	15.3	74.1	70.9
	3.5	35.8	19.5	11.8	4.0	14.3	85.5	81.5
	4.5	41.2	15.7	4.6	2.8	14.6	78.9	76.1
	5.5	43.3	17.4	12.7	3.7	14.5	91.6	87.9
	6.5	42.5	23.3	7.1	3.2	13.5	89.6	86.4
	7.5	31.6	17.4	12.1	2.6	12.6	76.2	73.6
	9.5	38.5	16.7	14.5	3.2	9.6	82.5	79.3
	10.5	24.0	15.3	16.6	2.9	7.1	65.9	63.0
	11.5	23.8	15.0	24.5	6.9	6.6	76.8	69.9
	13.5	20.2	23.7	16.2	3.5	5.3	68.8	65.4
	14.5	19.4	11.0	24.5	7.7	5.4	68.0	60.3
	15.5	18.7	11.2	28.1	5.3	4.3	67.5	62.2
	16.5	21.3	12.7	27.0	5.5	5.3	71.8	66.3
	17.5	20.2	12.3	26.2	5.3	5.1	69.1	63.8
	18.5	17.7	26.7	20.4	6.0	4.5	75.3	69.2
	19.5	22.9	22.0	23.7	5.8	4.0	78.4	72.6
	20.5	23.1	22.2	20.4	5.8	3.7	75.2	69.4
	21.5	19.1	15.9	25.1	7.0	4.3	71.5	64.5
	22.5	16.6	25.6	17.9	4.8	4.0	68.9	64.1
SPC4R	0.5	20.1	15.7	33.9	6.6	3.9	80.1	73.6
	1.5	18.0	12.9	36.6	11.1	3.9	82.5	71.4
	2.5	17.8	12.4	29.1	8.9	5.2	73.5	64.6
	3.5	18.1	16.9	27.8	7.3	6.1	76.2	68.9
	4.5	19.4	16.8	31.4	6.8	5.6	80.1	73.3
	5.5	18.7	11.0	30.3	8.2	4.9	73.1	64.9
	6.5	16.9	13.7	35.0	8.0	5.9	79.5	71.5
	7.5	18.1	11.0	30.0	10.0	5.0	74.1	64.1
	8.5	19.0	10.7	31.4	7.4	4.1	72.6	65.2
	9.5	17.8	12.9	33.2	10.9	5.6	80.4	69.5
	10.5	18.0	9.2	34.6	7.4	4.6	73.8	66.4
	11.5	17.6	13.7	34.8	3.5	3.6	73.1	69.6
	12.5	19.2	11.3	49.5	9.3	4.1	93.4	84.1
	13.5	25.4	11.8	40.0	12.0	3.9	93.1	81.1
	14.5	18.3	12.3	36.8	11.5	4.1	83.0	71.5
	15.5	15.3	10.9	36.4	4.8	3.6	71.0	66.2
	16.5	17.6	10.6	32.5	10.7	4.3	75.6	64.9
	17.5	19.4	12.4	47.2	11.7	4.1	94.9	83.1

Table 3.4: Relative percentage of solid-phase phosphorus species and molar C_{org}/P_{org} and Molar C_{org}/P_{react} ratios for the sediment cores of this study.

Station Name	Depth (cm)	Relative Percentage of P (%)					Molar C_{org}/P_{org}	Molar C_{org}/P_{react}
		P_{bio}	P_{Fe}	P_{auth}	P_{det}	P_{org}		
SPC 1R	0.5	36	11	6	8	39	269	113
	2.5	35	12	8	7	37	290	116
	3.5	43	14	4	7	32	397	138
	4.5	44	16	3	7	30	566	182
	5.5	45	23	6	4	22	579	134
	6.5	49	18	5	4	25	607	156
	7.5	35	22	15	4	25	622	160
	8.5	40	15	16	5	23	618	150
	10.5	41	12	24	3	20	776	160
	11.5	42	24	12	3	19	604	120
	12.5	42	26	11	4	17	634	114
	14.5	33	30	14	4	20	654	135
	16.5	35	14	30	4	17	846	151
	18.5	41	10	26	5	19	626	124
	20.5	32	11	40	4	12	668	85
	22.5	31	11	45	4	10	732	76
	23.5	29	22	37	3	8	633	53
	24.5	26	13	41	13	8	515	45
	26.5	28	22	42	3	6	561	34
	27.5	26	11	52	5	6	502	30

Table 3.4: Continued

Station Name	Depth (cm)	Relative Percentage of P (%)					Molar C_{org}/P_{org}	Molar C_{org}/P_{react}
		P_{bio}	P_{Fe}	P_{auth}	P_{det}	P_{org}		
SPC 2	1.5	47	18	8	4	23	417	100
	2.5	44	19	11	4	21	401	87
	3.5	42	23	14	5	17	441	78
	4.5	52	20	6	4	18	422	81
	5.5	47	19	14	4	16	432	71
	6.5	47	26	8	4	15	449	70
	7.5	41	23	16	3	16	445	76
	9.5	47	20	18	4	12	419	51
	10.5	36	23	25	4	11	483	54
	11.5	31	20	32	9	9	444	42
	13.5	29	34	24	5	8	490	40
	14.5	28	16	36	11	8	403	36
	15.5	28	17	42	8	6	467	32
	16.5	30	18	38	8	7	429	34
	17.5	29	18	38	8	7	375	30
	18.5	23	35	27	8	6	438	28
	19.5	29	28	30	7	5	456	25
	20.5	31	29	27	8	5	426	23
	21.5	27	22	35	10	6	372	25
	22.5	24	37	26	7	6	282	18
SPC 4R	0.5	25	20	42	8	5	407	21
	1.5	22	16	44	13	5	416	23
	2.5	24	17	40	12	7	380	31
	3.5	24	22	36	10	8	374	33
	4.5	24	21	39	8	7	373	29
	5.5	26	15	41	11	7	452	34
	6.5	21	17	44	10	7	308	25
	7.5	24	15	41	13	7	323	25
	8.5	26	15	43	10	6	391	25
	9.5	22	16	41	14	7	321	26
	10.5	24	12	47	10	6	340	24
	11.5	24	19	48	5	5	436	22
	12.5	21	12	53	10	4	380	18
	13.5	27	13	43	13	4	601	29
	14.5	22	15	44	14	5	460	27
	15.5	22	15	51	7	5	404	22
	16.5	23	14	43	14	6	388	26
	17.5	20	13	50	12	4	379	19

Table 3.5 Total carbon (TC), total inorganic carbon (TIC), organic carbon (C_{org}), Fe, Th, Ti, Zr, Rb content, U/Th ratio, Molar C_{org}/N ratio, $CaCO_3$ (wt.%), Sand%, Silt % and Clay% for the sediment cores studied here.

Station Name	Depth (cm)	TC (wt.%)	TIC (wt.%)	C_{org} (wt.%)	Fe (wt.%)	Th (µmol/g)	Ti (µmol/g)	Zr (µmol/g)	Rb (µmol/g)	U/Th ratio	C_{org}/N ratio	$CaCO_3$ (wt.%)	Sand %	Silt %	Clay %
	0.5	13.50	4.91	8.59	4.76	0.02	69.32	0.69	0.51	0.76	8.65	40.90	9.39	50.36	40.25
	1.5	14.28	4.81	9.47	4.35	0.02	58.70	0.64	0.48	0.88	8.76	40.03	3.25	52.81	43.92
	2.5	14.09	4.62	9.46	4.31	0.02	58.29	0.66	0.48	0.96	9.06	38.51	2.90	51.68	45.43
	3.5	14.29	4.04	10.25	3.86	0.02	57.91	0.67	0.49	1.14	8.86	33.67	5.25	47.52	47.23
	4.5	14.16	3.93	10.23	3.73	0.02	54.85	0.67	0.49	2.21	9.19	32.70	11.14	47.14	41.72
	5.5	13.96	4.27	9.68	3.51	0.02	56.98	0.66	0.52	1.98	9.10	35.59	1.07	52.99	45.78
	6.5	13.75	4.41	9.34	3.28	0.02	70.15	0.76	0.56	1.51	9.44	36.74	1.65	51.92	46.44
	7.5	13.43	4.78	8.65	3.26	0.02	54.61	0.65	0.52	2.24	9.58	39.83	7.18	49.33	43.50
	8.5	13.34	5.48	7.86	3.42	0.02	58.89	0.69	0.54	2.12	9.00	45.65	7.25	50.72	41.78
	9.5	13.52	5.32	8.20	3.35	0.02	56.33	0.70	0.52	2.00	9.18	44.32	8.46	49.37	42.14
	10.5	13.32	5.52	7.80	3.43	0.02	57.67	0.70	0.53	1.95	9.45	45.98	19.05	42.17	38.77
	11.5	13.53	5.52	8.01	3.48	0.03	56.09	0.70	0.58	2.06	9.31	45.98	11.30	46.15	42.54
	12.5	13.42	5.61	7.81	3.45	0.02	57.26	0.69	0.53	2.36	9.03	46.71	12.22	46.38	41.39
SPC1R	13.5	13.82	5.01	8.81	3.07	0.02	52.39	0.66	0.40	2.60	9.61	41.76	4.99	50.81	44.21
	14.5	13.49	5.02	8.47	3.44	0.03	59.01	0.75	0.57	2.73	9.54	41.78	6.62	50.02	43.35
	15.5	13.35	4.99	8.36	3.47	0.03	58.46	0.72	0.57	2.76	9.92	41.60	7.07	51.19	41.74
	16.5	13.47	5.16	8.31	3.60	0.03	56.89	0.70	0.58	2.54	9.92	42.99	10.87	48.74	40.39
	17.5	13.10	5.48	7.62	3.66	0.03	58.10	0.71	0.59	2.54	8.95	45.65	13.88	45.11	41.01
	18.5	12.27	5.93	6.34	3.60	0.03	57.81	0.72	0.59	2.46	9.19	49.43	19.39	42.11	38.48
	19.5	12.48	6.50	5.99	3.34	0.03	57.67	0.71	0.56	2.24	9.97	54.12	20.68	42.53	36.77
	20.5	12.32	7.44	4.88	3.45	0.02	62.29	0.76	0.56	2.16	11.14	61.98	22.11	40.59	37.30
	21.5	12.10	7.92	4.17	3.28	0.02	61.52	0.72	0.56	2.30	10.95	66.01	10.62	45.35	44.03
	22.5	12.21	8.30	3.91	4.09	0.03	64.34	0.79	0.61	2.30	12.10	69.16	28.05	32.72	39.22
	23.5	11.98	8.54	3.43	3.31	0.02	46.59	0.61	0.44	2.30	13.47	71.15	47.29	26.13	26.57
	24.5	11.67	8.89	2.79	3.90	0.03	50.10	0.84	0.68	2.25	10.94	74.02	49.76	23.05	27.16
	25.5	11.50	8.82	2.68	3.65	0.03	52.33	0.70	0.51	2.26	11.69	73.50	60.68	19.02	20.30
	26.5	11.51	8.91	2.60	3.78	0.03	59.66	0.78	0.54	2.30	16.97	74.25	49.82	21.90	28.28
	27.5	11.52	9.36	2.17	4.79	0.03	77.34	0.96	0.67	2.21	11.68	77.93	48.85	21.00	30.15

Table 3.5 Continued

Station Name	Depth (cm)	TC (wt.%)	TIC (wt.%)	C_{org} (wt.%)	Fe (wt.%)	Th (µmol/g)	Ti (µmol/g)	Zr (µmol/g)	Rb (µmol/g)	U/Th ratio	C_{org}/ N ratio	$CaCO_3$ (wt.%)	Sand %	Silt %	Clay %
SPC2	0.5	13.25	4.71	8.54	3.64	0.02	52.31	0.57	0.44	2.19	9.49	39.22	4.75	46.65	48.58
	1.5	13.93	5.08	8.85	3.40	0.02	52.92	0.59	0.44	2.35	9.58	42.34	13.84	43.56	42.61
	2.5	12.73	5.36	7.37	3.44	0.02	52.78	0.67	0.52	2.24	9.06	44.62	12.31	45.61	42.00
	3.5	12.88	5.29	7.59	3.27	0.02	61.46	0.68	0.52	1.93	9.48	44.10	26.78	38.47	34.76
	4.5	12.42	5.05	7.37	3.50	0.02	51.59	0.65	0.52	1.99	7.69	42.10	6.90	47.42	45.69
	5.5	12.74	5.24	7.50	3.60	0.02	52.63	0.66	0.51	2.18	7.70	43.65	10.66	44.90	44.40
	6.5	12.78	5.48	7.30	3.49	0.03	61.65	0.66	0.53	2.09	7.30	45.66	21.47	42.15	36.38
	7.5	12.54	5.83	6.71	3.64	0.03	57.62	0.70	0.57	2.61	9.96	48.52	16.52	43.45	40.02
	8.5	12.23	6.34	5.89	3.98	0.03	79.12	0.71	0.55	2.55	10.12	52.80	19.23	40.58	40.19
	9.5	11.77	6.96	4.80	4.36	0.03	77.75	0.77	0.60	2.19	10.38	58.01	24.45	34.75	36.34
	10.5	11.57	7.48	4.09	4.33	0.03	59.98	0.78	0.60	2.08	12.42	62.29	46.32	26.34	27.34
	11.5	11.30	7.77	3.53	4.64	0.03	64.66	0.85	0.62	2.30	11.43	64.69	38.26	29.27	32.47
	12.5	11.27	8.24	3.03	4.26	0.03	68.69	0.86	0.65	2.33	11.00	68.63	42.62	26.56	30.81
	13.5	11.17	8.06	3.11	4.66	0.03	54.56	0.66	0.51	2.52	11.70	67.15	43.50	26.23	30.27
	14.5	10.98	8.39	2.59	4.85	0.03	69.43	0.81	0.63	2.38	11.58	69.88	63.05	18.58	18.37
	15.5	11.03	8.63	2.40	4.29	0.03	58.47	0.70	0.53	2.56	13.62	71.90	55.93	20.04	24.02
	16.5	10.97	8.26	2.71	4.93	0.03	62.24	0.76	0.56	2.60	14.71	68.80	52.06	21.38	26.56
	17.5	10.81	8.50	2.31	4.79	0.03	71.67	0.86	0.67	2.42	11.46	70.83	40.18	25.68	34.14
	18.5	10.80	8.44	2.36	6.34	0.03	66.04	0.68	0.60	2.32	14.52	70.28	46.98	23.07	29.95
	19.5	10.63	8.44	2.19	7.22	NA	NA	NA	NA	NA	15.30	70.33	46.29	23.72	29.99
	20.5	10.51	8.62	1.90	NA	NA	NA	NA	NA	NA	12.72	71.77	40.81	25.07	34.12
	21.5	10.56	8.65	1.91	NA	NA	NA	NA	NA	NA	12.61	72.07	59.68	18.24	22.09
	22.5	9.80	8.45	1.35	NA	NA	NA	NA	NA	NA	11.05	70.39	53.86	20.35	25.78
	23.5	10.18	8.13	2.05	NA	NA	NA	NA	NA	NA	14.84	67.70	63.51	16.59	19.89

NA - Not analysed

Table 3.5 Continued

Station Name	Depth (cm)	TC wt.%	TIC wt.%)	C_{org} (wt.%	Fe wt.%	Th µmol/g	Ti µmol/g	Zr (µmol /g)	Rb µmol/g	U/Th ratio	C_{org}/ N ratio	$CaCO_3$ (wt.%)	Sand %	Silt %	Clay %
SPC4 R	0.5	11.45	9.56	1.88	6.34	0.04	87.11	0.99	0.67	2.00	13.91	79.67	81.98	8.76	9.23
	1.5	11.70	9.74	1.96	7.22	0.08	153.65	1.72	1.14	2.04	13.73	81.11	88.17	6.91	4.89
	2.5	11.64	9.26	2.37	5.74	0.04	85.99	0.98	0.65	1.73	12.39	77.17	82.08	10.56	7.18
	3.5	11.83	9.08	2.75	5.47	0.03	71.74	0.79	0.54	1.83	12.54	75.61	87.43	9.07	3.47
	4.5	11.79	9.27	2.52	5.49	0.04	85.09	0.90	0.64	1.82	11.57	77.18	80.56	12.40	5.76
	5.5	11.79	9.16	2.63	5.28	0.04	83.77	0.93	0.64	1.84	12.23	76.31	88.99	8.58	1.79
	6.5	11.81	9.63	2.19	6.14	0.04	95.85	1.06	0.73	1.92	9.81	80.19	87.95	9.63	2.39
	7.5	11.79	9.85	1.93	6.19	0.04	91.74	1.01	0.69	2.19	10.16	82.09	84.71	10.52	4.07
	8.5	11.89	9.95	1.94	5.70	0.06	142.30	1.56	1.04	2.60	10.05	82.91	84.52	10.06	4.05
	9.5	11.96	9.79	2.17	6.34	0.07	163.19	1.81	1.17	2.03	11.40	81.56	88.79	7.61	3.59
	10.5	11.75	9.86	1.89	6.00	0.04	85.86	0.99	0.62	2.28	12.43	82.11	85.95	7.58	6.47
	11.5	11.78	9.91	1.86	5.76	0.06	145.70	1.72	1.07	2.32	11.76	82.57	84.32	10.55	4.92
	12.5	11.87	10.02	1.86	6.57	0.07	151.98	1.74	1.12	2.07	11.82	83.43	91.39	6.03	2.56
	13.5	11.84	9.01	2.83	4.66	0.03	65.02	0.88	0.49	2.19	19.05	75.06	90.88	6.57	2.53
	14.5	11.91	9.63	2.28	6.08	0.04	86.14	0.92	0.64	2.35	14.67	80.18	90.22	7.16	2.48
	15.5	11.65	9.89	1.76	6.71	0.08	155.90	2.68	1.11	1.82	12.69	82.34	89.20	7.67	2.89
	16.5	11.81	9.81	1.99	6.64	0.07	154.28	1.75	1.15	2.26	14.07	81.74	91.29	6.46	2.23
	17.5	11.66	9.81	1.85	NA	NA	NA	NA	NA	NA	11.26	81.72	88.58	7.28	4.19

Table 3.6: The equations used for integration of area under the curve for cores SPC-1R and SPC-2. Also tabulated are depth integrated P_{auth} content increase versus depth integrated P_{org} and P_{bio} decrease using these equations.

Station	Depth interval (cm) of integration	Integrated P_{org} deficit (gP/cm^2)	Integrated P_{bio} deficit (gP/cm^2)	Integrated P_{auth} increase (gP/cm^2)
SPC 1R	0-28	0.82±0.01	1.54±0.02	0.99±0.02
SPC 2	0-23	0.51±0.005	1.68±0.005	1.09±0.01

1. The equations for the curves integrated for SPC 1R:

P_{org} $y = -13.59\ln(x) - 34.675$ $R^2 = 0.93$

P_{bio} $y = -29.02\ln(x) - 67.707$ $R^2 = 0.59$

P_{auth} $y = 9.2889\ln(x) + 47.023$ $R^2 = 0.84$

2. The equations for the curves integrated for SPC 2:

P_{org} $y = -11.76\ln(x) - 32.269$ $R^2 = 0.94$

P_{bio} $y = -17.91\ln(x) - 32.923$ $R^2 = 0.74$

P_{auth} $y = 10.19\ln(x) + 43.103$ $R^2 = 0.65$

3. The integrated areas under the curves have been converted from units of (g P/g x cm) to units of (gP/cm^2) using the following equation:

$gP/cm^2 = (I- \Phi)\rho$ (g/cm^3)Area (gP/g x cm) where $\Phi = 0.65$ and $\rho = 2.65$ g/cm^3 (Ruttenberg and Berner, 1993).

Chapter 4

Phosphorus cycling and diagenesis in the Western Bay of Bengal

Chapter 4

4.1. Introduction

The major source of P to the oceans is fluvial input both as weathered products as well as in the dissolved phases. However, the major fraction of riverine P is locked up in estuaries and continental margins and only 30% of the fluvial P is biologically available for marine primary productivity (Compton et al., 2000). In this context, Bay of Bengal (BoB) assumes importance as it is a major recipient of dissolved elements and suspended material from major rivers draining the Himalaya and Peninsular India (Holeman, 1968; Milliman and Meade, 1983; Subramanian, 1985) and the riverine fluxes strongly influence the biogeochemistry of BoB (Ittekkot et al., 1991; Rao et al., 1994). Similar to the Arabian Sea, BoB is also characterized by an intense oxygen minimum zone (OMZ) at intermediate depths (Rao et al., 1994; Sardessai et al., 2007), but which is weak, denitrification free and at much shallower depths (e.g., Naqvi et.al., 1996; Paulmier and Ruiz-Pino, 2009; Al Azhar et.al., 2017; Sarma and Udaya Bhaskar, 2018). The river inputs are the principal source of nutrients to the BoB and the phosphate supply from rivers in the region constitutes about 10% of world total inorganic P (Datta et al., 1999; Stoll et al., 2007).

Vaz (1995) first reported the occurrence of phosphorites from the eastern continental margin of India off Chennai at about 150 m water depth. Later, Vaz et al. (1999) and Rao et al. (1998, 2000, 2002) found phosphorite from 30 to 300 m water depth in about 636 km^2 area in the same region. This is, so far, the largest phosphorite field reported on the continental margin of India (Vaz et al., 1999; Rao and Kessarkar, 2001). These phosphorites

were associated with microfossils belonging to upper Cretaceous-lower Eocene (foraminifera) and pelecypod fossil cast of upper Cretaceous to Miocene age (Vaz, 1995) but have been attributed to microbial origin possibly during low stands of upper Pleistocene. Similarly, Rao et al. (2000) too have invoked the microbial processes, with microbial mats forming on the outer shelf, during conditions of low sea level in the Quaternary age, which have been phosphatized subsequently. Based on subsequent work, Vaz et al. (1999) have proposed the occurrence of four episodes of phosphatization commencing from the Eocene period, but has ruled out the phosphatization during the late Pleistocene and early Holocene period. Rao et al. (2007) have identified them to represent phosphatized microbial mats (phosphate stromatolites) of shallow water settings and consider them to be of Quaternary age. According to Rao et al., 2007, during high energy levels these phosphate stromatolites were fragmented into phosphate clasts of different sizes and then reworked into shelf margin depressions with clayey sediments. Thus, unlike in the Arabian Sea (Schenau et al., 2000; Linsy et al., 2018a), it is not known whether the present-day phosphogenesis or recent phosphatization is occurring in the BoB.

Further, authigenic apatite formation was found to occur in non-upwelling, high sedimentation rate area such as Mississippi Delta (Ruttenberg and Berner, 1993) but not in shallow continental shelf off India with high sedimentation rates (Acharya et al., 2016; see Linsy et al., 2018a). As mentioned above, the BoB is an area receiving high fluvial sediment fluxes but their role in P diagenesis is not known. Thus, this study has been undertaken to assess the P regeneration and burial in the western BoB using porewater and solid phase speciation geochemistry of P.

Four short sediment cores (SSK50/SPC5, SSK50/SPC7, SSK50/SPC13 and SSK59/SPC3) from the southern part of eastern continental margin of India (Fig. 4.1; Table 2.5). Two cores among them (SSK50/SPC5, SSK50/SPC7) are from the phosphorite bearing field off Chennai. All the four locations chosen are overlain by oxygen-depleted water (Fig. 4.1), in order to study the impact of OMZ on the benthic regeneration of P and authigenic apatite formation in high fluvial sedimentation areas. In addition to porewater phosphate and P fractionation in sediments, sediments were also analyzed for organic carbon (C_{org}), total nitrogen, and calcium carbonate content. Bottom water phosphate was measured in all the locations in order to calculate the benthic fluxes of P across the sediment-water interface. Unpublished porosity and density data have also been used for the interpretations.

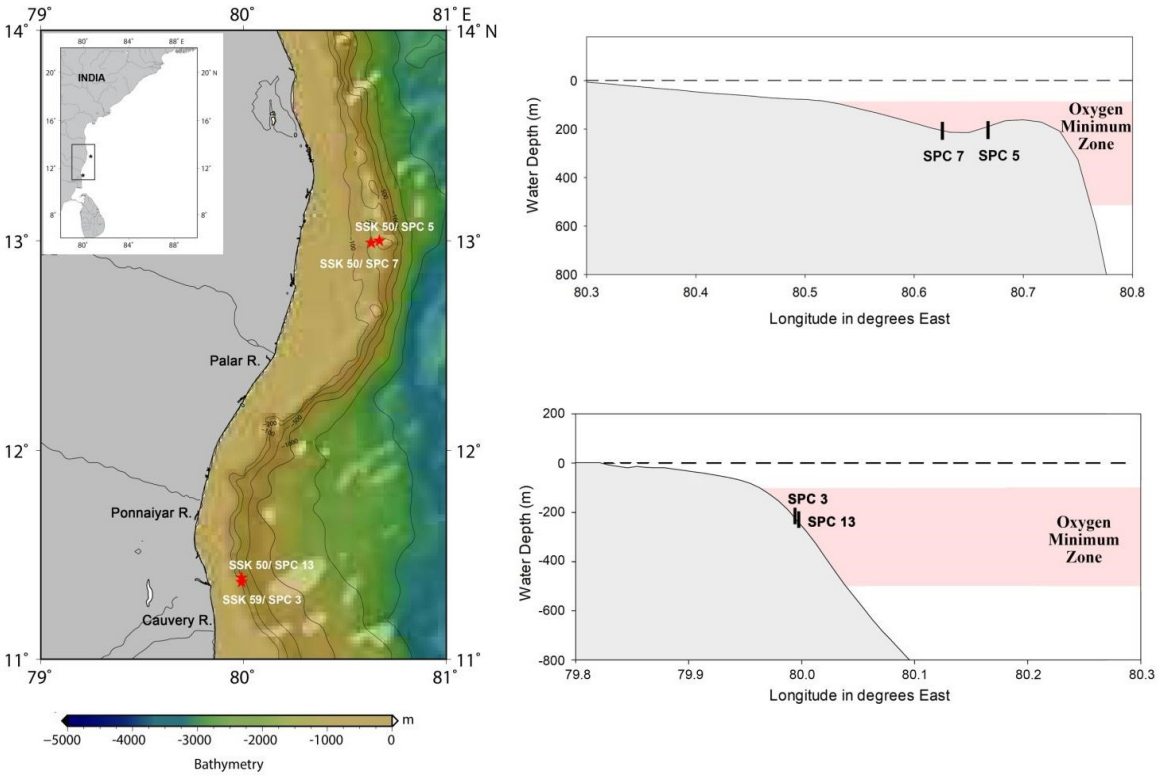

Figure 4.1: Sampling location of the present study; (b) cross bathymetric profile of sampling locations.

4.2 Results

The C_{org} content varies between 0.31 and 2 wt.% **(Fig. 4.2)** with an average of 1.01 wt.%. Higher C_{org} content occurs in core SPC5 (average 1.56 wt.%). The C_{org} content does not show any prominent downcore decrease except at the station SPC13, where C_{org} content decreases from 1.16 at the surface to 0.41 wt.% to the bottom **(Fig. 4.2).** The $CaCO_3$ content ranges from 4.9 to 40.26 wt.% with an average of 17.1 wt.% (Fig. 4.2). Compared to southern stations (SPC3 and SPC13), $CaCO_3$ content is relatively high in sediment cores SPC5 and SPC7 in the north. The $CaCO_3$ content increases with depth in core SPC5. N_{total} content decreases with sediment depth at all stations and varies between 0.032 and 0.164 wt.% (average - 0.095 wt.%). The sediment core SPC3 has lower N_{total} content (average - 0.037 wt.%) compared to other stations **(Fig. 4.2).**

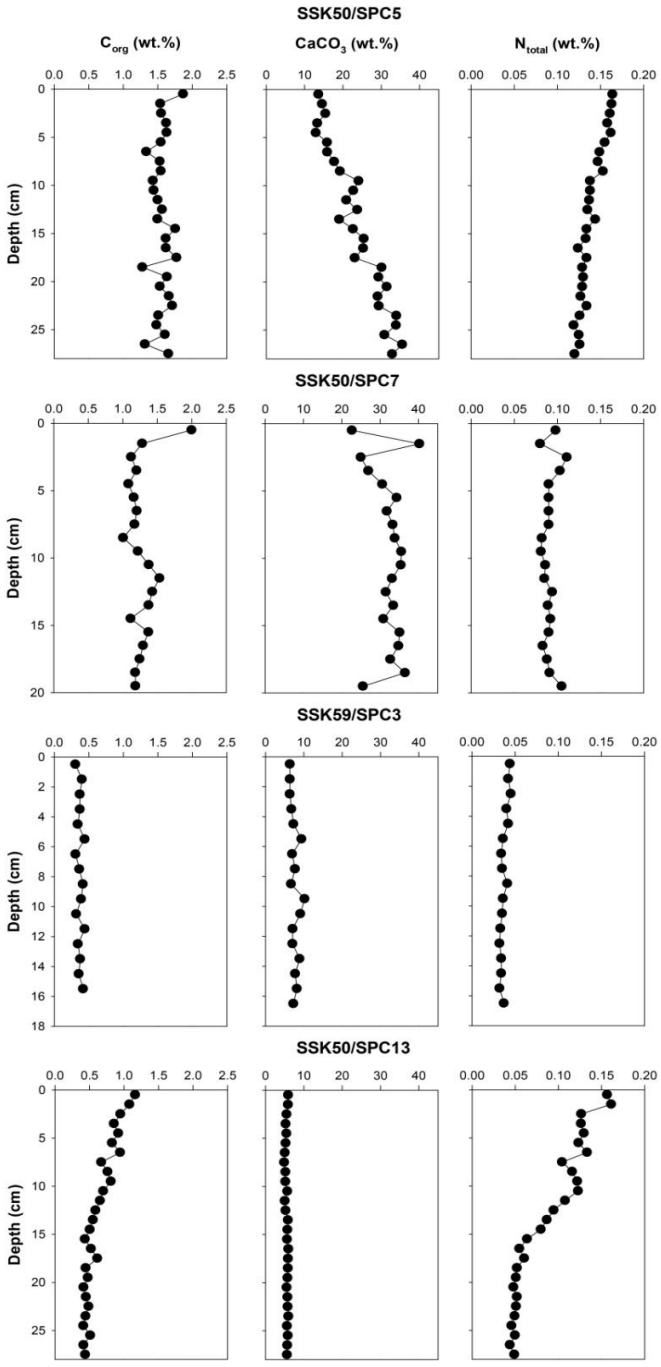

Figure 4.2: Downcore variation of C_{org}, $CaCO_3$ and N_{total} (units wt.%) in four sediment cores.

DIP concentration in the porewater varies between 4 and 32 µmol/L with an average of 12.4 µmol/L **(Fig. 4.3)**. DIP profiles mostly show higher values at the surface which gradually decrease with depth, with the decrease being more prominent in sediment cores SPC 7 and SPC 13. DIP concentration at SPC5 shows a rapid decrease at 3 cm depth after a surface enrichment and then it shows a gradual increase with depth up to 13 cm **(Fig. 4.3)**. Bottom water DIP concentration varies between 0.65 and 2.72 µmol/L and lowest concentration was observed at SPC3 station (Table. 4.1; Fig. 4.3).

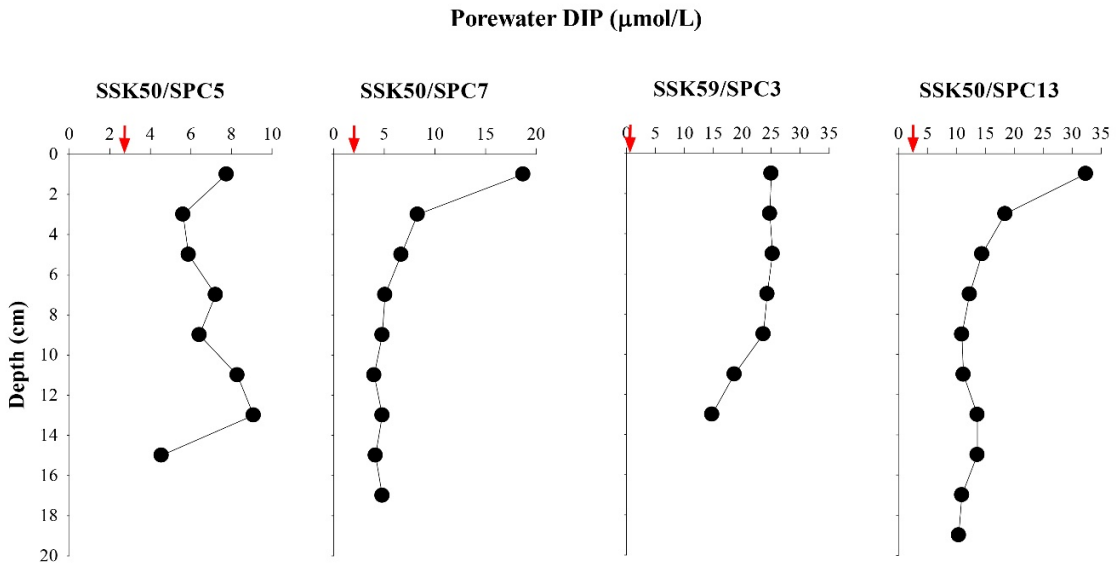

Figure 4.3: Downcore profile of dissolved phosphate (µmol/L) in porewater. Arrows on x-axis represent the bottom water dissolved phosphate values.

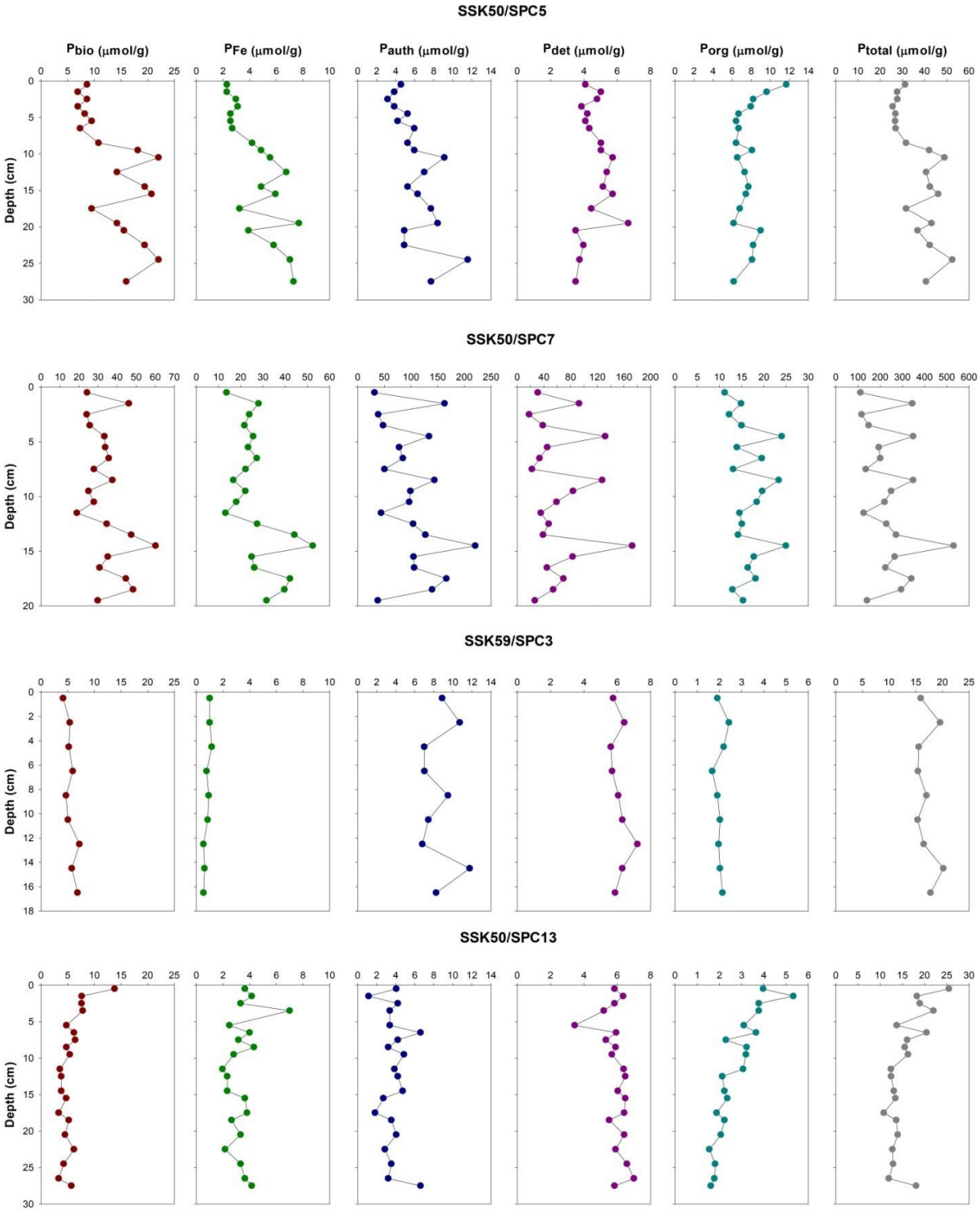

Figure 4.4: Down core variation of total phosphorus and P in five geochemically separable phases (units in µmol/g).

P_{total} content in the cores ranges between 17.2 and 531.2 µmol/g **(Fig. 4.4; Table 4.2)** with an average of 91.3 µmol/g. It shows significant variation between stations and highest values were found in core SPC7, in which the concentration varies between 112 and 531 µmol/g (average - 242 µmol/g). P_{bio} contents range between 3.3 and 60.2 µmol/g accounting for 9.5 to 46% of the P_{total} **(Fig. 4.5; Table 4.3),** with a slight subsurface increase in cores SPC5 and SPC3. P_{bio} content is relatively high at station SPC7 and varies from 19 to 60.2 µmol/g with an average of 34.5 µmol/g. The concentrations of P_{Fe} are very low (average10.5 µmol/g) and account for 11% (average) of the P_{total}. Profiles of P_{Fe} content show noteworthy variation between stations. At SPC3, P_{Fe} content decreases with depth and it accounts 2.3-5.5% of the P_{total} **(Fig. 4.5; Table 4.3)**. Relatively high P_{Fe} content is observed at SPC7 station which varies between 13.2 and 52.5 µmol/g **(Table 4.2**).

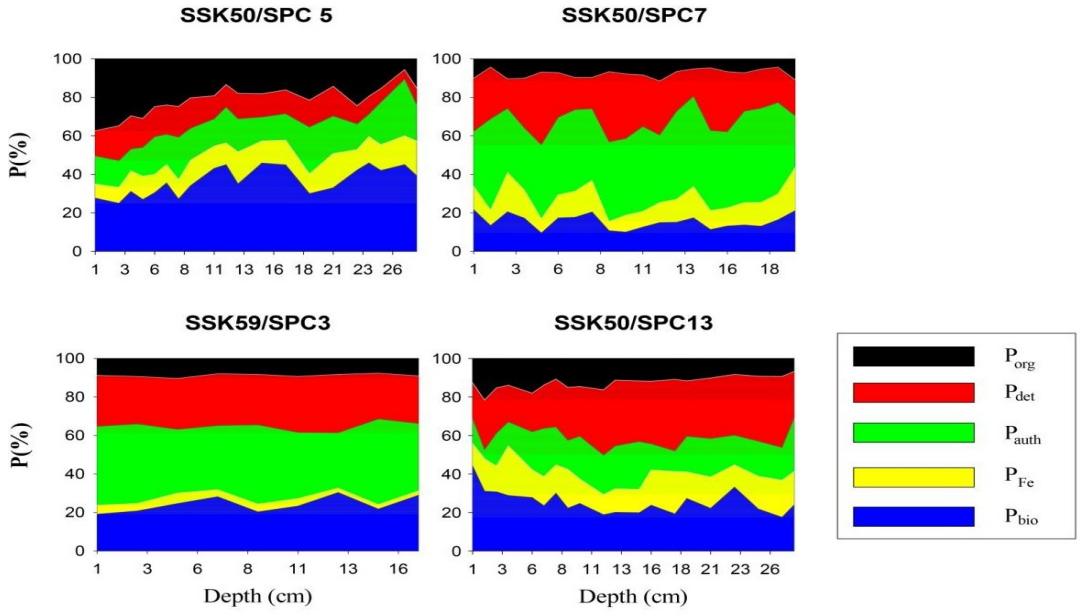

Figure 4.5: Relative percentages of solid P phases with sediment depth in four cores.

The P_{auth} content varies from 1.2 to 221 µmol/g and accounts for 4.7 - 49 % of the P_{total}. It is the major form of sedimentary P reservoir at SPC7 and SPC3 locations and constitutes 40 and 37% (average) of the P_{total}, respectively. It does not show any prominent downcore trend, except at SPC5 station where it slightly increases with depth from 2.3 to 17.2 µmol/g. The P_{det} fraction represents the second largest sedimentary P reservoir in the present study. P_{det} contents vary between 3.5 and 173 µmol/g and accounts for 4.9 to 38 % of the P_{total}. The station SPC7 has highest P_{det} content with a range between 11.2 and 25 µmol/g.

The P_{org} content is very low, ranges between 1.55 and 24.98 µmol/g (with an average of 8.11 µmol/g) and constitutes ~12.6% (average) of the P_{total}. At SPC5, P_{org} shows a gradual decrease from surface (11.7 µmol/g) to a depth of 6 cm (6.4 µmol/g). The concentration is nearly similar until 20 cm before showing a gradual decrease again. The station SPC13 shows a gradual decrease of P_{org} with depth. At station SPC3, after a rapid decrease at the surface, P_{org} content show enrichment with depth. Compared to other stations, SPC7 does not show any prominent downcore trend of P_{org} with depth and accounts for 7.7 % (average) of the P_{total}.

4.3 Discussion

4.3.1 Nature and degradation of organic matter

Molar C_{org}/N ratio can be used to characterize the source of organic matter in sediments where freshly precipitated organic matter of marine origin has a ratio of 6-9 (Bordovskiy, 1965; Prahl et al., 1980, 1994; Perdue and Koprivnjak, 2007), while the terrestrial vascular plants have molar C_{org}/N ratio of 12-14 or above (Gearing, 1988; Jia and Peng, 2003). The molar C_{org}/N ratio in the present study **(Fig. 4.6;Table 4.4)** indicates that most of the organic

matter in this area is terrigenous in nature, which is consistent with the stable isotope-based findings of dominant allochthonous organic matter in the eastern continental margin of India (Krishna et al., 2013) . However, the presence of terrestrially derived organic matter in sediments of BoB is not surprising as it receives large lithogenic flux by rivers draining from the Himalayas and Peninsular India (Bird et al., 2008; Tripathy et al., 2014). In BoB, the annual riverine supply of sediment is about 1350×10^6 tons which accounts ~ 8% of the global value (Milliman and Syvitski, 1992; Tripathy et al., 2014). A high molar C/N ratio (average-16.5) is observed at the SPC7 station **(Fig. 4.6, Table 4.4)** suggesting high terrigenous input at this site than other stations. High molar C/N ratio at SPC7 is consistent with the high P_{det} content at this site, while the lower ratios observed at the SPC13 station (average 9) indicates that most of the organic matter is marine in origin.

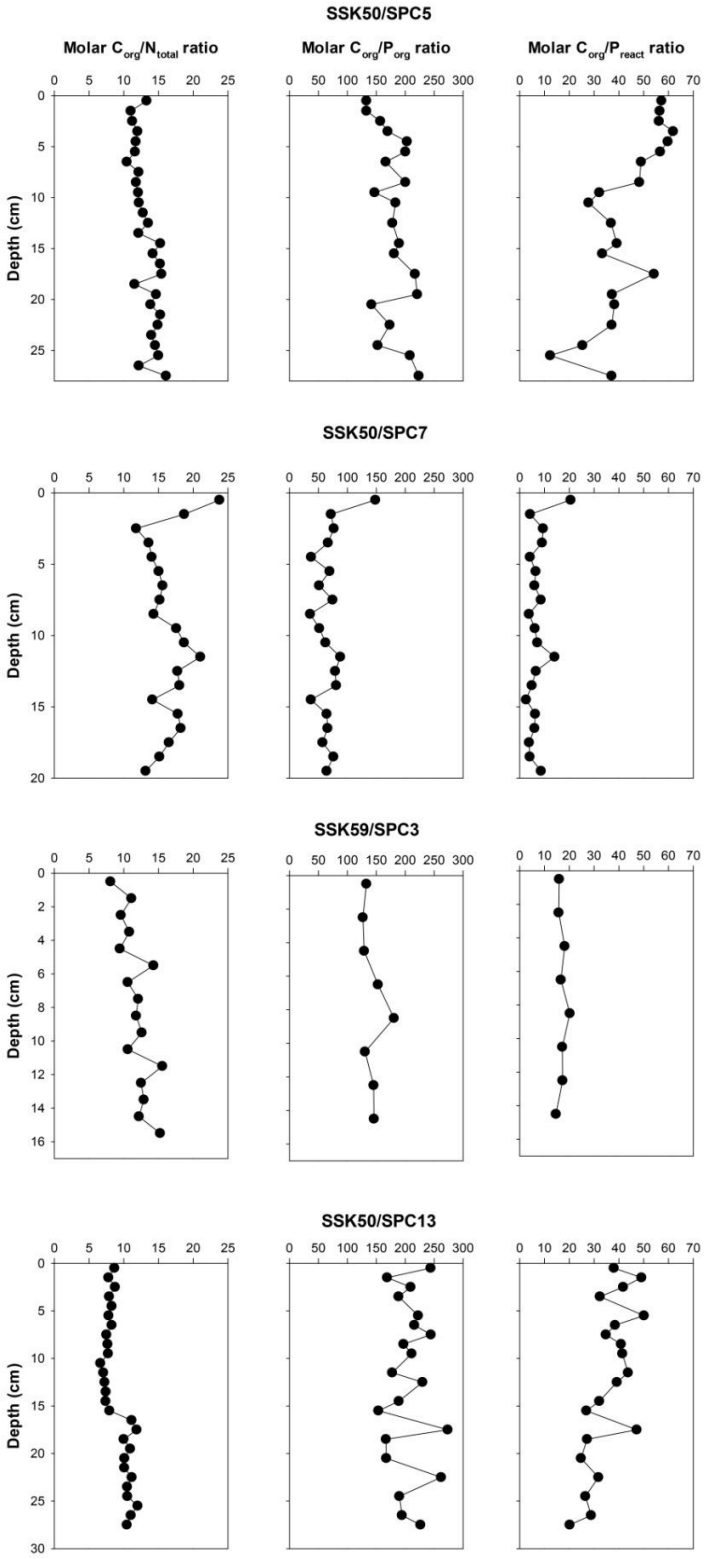

Figure 4.6: Downcore variation of molar C_{org}/N_{total}, C_{org}/P_{org} and C_{org}/P_{react} ratios in four cores.

Freshwater induced stratification and weak wind forces over the BoB together restrict the vertical mixing of seawater to a shallow depth and inhibit the nutrient transport below the mixed layer resulting in low productivity in the BoB (Prasanna Kumar et al., 2002). Due to the low productivity, marine-derived organic matter in BoB sediments is low. The downcore decrease of C_{org} and P_{org} contents at SPC13 station indicates degradation of organic matter and release of P into the porewater. However, no such degradation is observed at the other sites which are dominated by terrestrial organic matter. The marine organic matter is more reactive than the terrestrial organic matter and undergoes efficient remineralization (Burdige, 2005), while most of the terrestrial organic matter undergoes burial. Along with this, high sedimentation rate of BoB also enhances the preservation of organic matter (Galy et.al. 2007).

Molar C_{org}/P_{org} and C_{org}/P_{react} ratios in marine sediments can also be used to understand the source of organic matter and its behavior in sediments (Ruttenberg, 2003; Kraal et al., 2012; Yang et al., 2017). The low molar C_{org}/P_{org} ratio (average - 68) at SPC7 site **(Fig. 4.6; Table 4.3)** is probably due to the presence of terrestrially derived organic matter which can contain refractory material rich in P (van der Zee et al., 2002; Yang et al., 2017). This is also evident from the downcore profiles of C_{org} **(Fig. 4.2)** and P_{org} **(Fig. 4.4),** where the signatures of remineralization of organic matter with depth are not seen.

Comparatively high C_{org}/P_{org} ratio at the SPC13 site suggests the degradation of organic matter and release of P. At the station SPC5, a slight increase in C_{org}/P_{org} ratio from the surface to a 10 cm down the core (Fig 4.6) with a corresponding decrease in P_{org} (Fig 4.2) is observed, which implies the preferential release of P relative to carbon. At all these sites, the sediments are overlain by oxygen-depleted water (Table 4.1). Preferential release

of P from organic matter is more enhanced under the oxygen-depleted conditions (Ingall and Jahnke, 1994). The molar C_{org}/P_{react} ratio is an indicator of P burial in sediments (Kraal et al., 2012) and is a good tool to study the fate of sedimentary P buried in sediments (Anderson et al., 2001). Low molar C_{org}/P_{react} ratio in the present study **(Fig. 4.5)** indicates that most of the sedimentary P phases are undergoing burial rather than regeneration. Thus in this region, the benthic regeneration of P is limited due to the enhanced burial of organic matter.

4.3.2 Authigenic apatite formation

Formation of authigenic apatite is the major pathway through which the reactive P is buried in the sediments. The sink switching of P from labile to authigenic phase is more common in upwelling areas characterized by oxygen-depleted water (Ruttenberg and Berner, 1993; Anderson et al., 2001; Ruttenberg, 2003). Present-day carbonate fluorapatite (CFA) formation at the expense of organic matter degradation was also reported in the non-upwelling areas such as the Long Island Sound and the shallow Mississippi Delta (Ruttenberg and Berner, 1993). In the present study, highest P_{auth} content is found at SPC7 station, but without any significant downcore change in other reactive phases **(Fig. 4.4)**. Porewater profile of SPC7 shows decrease of DIP concentration close to the surface **(Fig. 4.3)**, but a corresponding increase of P_{auth} is not observed, indicating that porewater is not used up for the CFA formation. P_{auth} profile of SPC7 has a remarkable fit with the P_{det} profile, suggesting that most of P_{auth} fraction is detrital in origin. SPC7 is located in the continental margin off Chennai coast where phosphorites were reported earlier and that could be linked to lower sea levels during the upper Quaternary period (Vaz et al., 1999; Rao et al., 2002, 2000). This area is characterized with weak upwelling and relict sediment is rich in carbonates (Vaz et al., 1999). Texture and density data of sediments in the present

study (**Fig. 4.7**) also suggest the presence of coarse-grained sediments at SPC7 sampling location. Among the two sediment cores from this region off Chennai, compared to SPC5, P_{auth} content is high at SPC7, as the latter is situated on the shelf marginal depressions in which the abundance of phosphorites has been reported earlier (Rao et al., 2002). The cross bathymetric profiles **(Fig. 4.1)** also shows that SPC7 is situated on the shelf marginal depression, whereas SPC5 is sited a little away and possibly receives less terrigenous materials compared to SPC7.

P_{auth} content is low at SPC13 station which is dominated by P_{det}. The core SPC13 was collected from the margin off Kollidam River mouth and the riverine sediment input may have curtailed the formation of authigenic apatite. At the adjoining sampling site SPC3, P_{auth} contents are predominant, while P_{det} is the second largest fraction. However, decrease of other reactive phases is not observed at this site. This suggests that most of the P_{auth} content at SPC3 is also detrital in origin. The variability of P speciation at SPC3 and SPC13 mainly reflects the difference in the depositional environment.

Results of the study indicate that in the BoB, local variability in oceanographic settings plays a major role in controlling the P geochemistry of continental margin sediments. High detrital input and low productivity in the area limit the release of P to the porewater and thereby restrict the in situ formation of authigenic apatite in the BoB sediments. Two prerequisites that are speculated for authigenic apatite formation are the saturation of phosphate in porewater and the sedimentary condition which favors the nucleation of phosphate in the porewater (Schenau et al., 2005; Van Cappellen and Berner, 1988; van der Zee et al., 2002). Thus, unfavorable conditions like the low input of reactive P

and their rapid burial by ballasting effect seem to inhibit the sink switching of P from labile to authigenic phases.

4.3.3 Burial of phosphorus in sediments of BOB

Burial of fish debris consisting of hydroxyapatite is the potential source of reactive P to the sediments (Schenau and De Lange, 2000; Suess, 1981). Dissolution of fish debris enhances the benthic porewater phosphate fluxes in highly productive areas and may lead to P_{auth} formation (Suess, 1981; Schenau and De Lange, 2001; Linsy et al., 2018a). P_{bio} content is relatively low at SPC13 and SPC3 stations. The productivity of the Bay of Bengal is relatively low (40 - 502 mg C m^{-2} d^{-1} Madhupratap et al., 2003) compared to the Arabian Sea (770-1782 mg C m^{-2} d^{-1} – Prasanna Kumar et al., 2001). Lower productivity is expected to lower the fish production in BoB leading to a reduced burial rate of P_{bio}. However, no significant downcore decrease of P_{bio} is observed **(Fig. 4.4)** at these sites, suggesting the preservation of P_{bio} with depth.

P_{bio} phase extracted in this study also can contain carbonate associated P and exchangeable P (see Schenau and De Lange, 2000; Babu and Nath, 2005). Relatively high P_{bio} at the site SPC5 and SPC7 (Fig. 4.4) could be mainly due to the carbonate associated P. Sediments at these sites are comprised of relict carbonate sediments of Cretaceous origin (Vaz et al., 1999; Rao et al., 2000) and the variation of P_{bio} is exactly matching with other phases implying a common source. $CaCO_3$ content at these stations is relatively high compared (Fig. 4.2) to the other two stations. Dissolution of P_{bio} is playing a weak role in the benthic regeneration of P in BoB, where most of P_{bio} is undergoing burial rather than regeneration.

Iron oxides have a high affinity for P and scavenge dissolved P from water column and sediments and thus redox cycling of iron plays a crucial role in P cycling in marine sediments (Slomp et al., 1996). But under reducing conditions, iron oxyhydroxides undergo reduction and release phosphate to the porewater / overlying water; thereby enhancing the benthic porewater fluxes and facilitate the P_{auth} formation in sediments (e.g., Slomp et al., 1996; Filippelli, 2001). Based on near bottom water oxygen concentration **(Table 4.1)** and classification of oxygenation conditions by Naqvi et al. (2010), the bottom waters at all four stations of the present study fall in hypoxic category ($4.46 < O2 \leq 62.49$ μM). P_{Fe} constitutes only a minor fraction of the total P in the present study (average − 12% of the P_{total}) and except at SPC7 station, the values are comparable with the previously reported values in the BoB (Babu and Ramaswamy, 2017). Highest P_{Fe} contents (Fig. 4.4) are found at SPC7 station which is dominated by the detrital input. Other sedimentary phases are also high at this station, and the high P_{Fe} content may be due to the difference in depositional flux. In this study, even under reducing condition P_{Fe} contents at SPC5 and SPC7 do not show a prominent downcore decrease with depth **(Fig. 4.4)**, and distinct downcore peaks are exactly matching with the P_{det} variation indicating the change in the deposition. Iron oxides derived from terrigenous sources are more crystalline compared to the freshly precipitated iron oxyhydroxides. Most of these stations are dominated by detrital input, which makes P_{Fe} a minor contributor to the P_{total} **(Fig. 4.5)**.

Despite the intense OMZ, denitrification in the water column is not common in BoB (Madhupratap et al., 2003; Rao et al., 1994; Bristow et al., 2017). Low bacterial respiration and rapid burial of organic matter are attributed as reasons for the absence of denitrification in the Bay of Bengal compared to the Arabian Sea (Rao et al., 1994; Naqvi et al., 1996;

Sarma et al., 2013). Due to the low bacterial respiration, microbial reduction of iron oxyhydroxides is also low in BoB, making redox cycling of iron only a minor player in the P geochemistry in the BoB. Along with this, the low adsorption capacity of terrigenously derived iron oxides also makes P_{Fe} a minor sedimentary phase. A slight decrease of P_{Fe} content with depth at SPC3 is attributed to the conversion of amorphous iron oxides to more crystalline form. Thus the findings of the present study suggest that Fe redox cycling plays only a limited role on the P geochemistry in this area. However, it is in contrast with the earlier study of Babu and Ramaswamy (2017) where P accumulation was found associated with intense diagenetic iron-oxide cycling in sediments of eastern BoB.

4.3.4 Porewater profiles and benthic porewater fluxes

The estimated porewater fluxes in this area (Table 4.1) are comparable with the previously reported values in the Arabian Sea (Linsy et al., 2018a). High benthic fluxes of phosphate in the Arabian Sea are mainly attributed to the dissolution of fish debris and preferential release of P from organic matter (Schenau and De Lange, 2001; Linsy et al., 2018a); whereas high P fluxes in the BoB sediments originate from substantially high porewater phosphate concentration at the sediment-water interface **(Fig. 4.3)**. Due to low productivity, P_{bio} and P_{org} content in the BoB sediments are very low and along with this, high sedimentation rate also limits the release of P. The flux of particulate organic and inorganic P in the Indian Ocean through riverine input is 0.2 and 1.5×10^6 tons per year, respectively (Ramesh et al., 1995). The BoB receives a large amount of phosphate (0.08 ± 0.02 Tg yr^{-1}) than the Arabian Sea (0.03 ± 0.007 Tg yr^{-1}) through riverine input (Krishna et al., 2016). Despite the low benthic release of P through organic matter degradation and dissolution of P_{bio}, high benthic porewater phosphate fluxes at the sediment-water interface

in BoB are mainly due to high particulate phosphate supply through rivers. Relatively high benthic fluxes are seen at SPC7 and SPC3 sites (Table 4.1) which receive high terrigenous input compared to other two stations.

The porewater DIP profiles **(Fig. 4.3)** shows the highest values at the surface except at SPC5 station. High DIP concentrations at the surface of the sediments are attributed to the release of P from easily degradable organic matter deposited at the sediment-water interface. The increase of DIP concentration with depth and a corresponding decrease of P_{org} content at SPC5 station indicate the preferential release of P from organic matter. At stations SPC7 and SPC13, depletion of porewater DIP with depth is observed **(Fig. 4.3)** but a corresponding increase of P_{auth} content **(Fig. 4.4)** is not found. While the P_{auth} corresponds to P_{det} profile, in-situ formation of authigenic apatite is not reflected in the downcore profile.

4.3.5 Comparison of P geochemistry in Bay of Bengal with the Arabian Sea

The northern Indian Ocean comprises of the Arabian Sea and BoB with similar geographical settings but different hydrographical and hydrochemical characteristics (Gauns et al., 2005) and thereby leading to the difference in sedimentary cycling of P. The major difference in the P geochemistry arise primarily because of variability in the input of P. In the BoB fluvial input is the major source of P through high river runoff ($1.6\times10^{12}m^3\ yr^{-1}$) compared to the Arabian Sea ($0.3\times10^{12}m^3\ yr^{-1}$) (Sarin et al., 1990; Gauns et al., 2005). The atmospheric deposition of inorganic P in the Arabian Sea and BoB also varies considerably with the Arabian Sea receiving low input (8 - 21 Gg- P yr^{-1}) compared to BoB (6 – 50 Gg- P yr^{-1}) (Srinivas and Sarin, 2015). Such variability in the input of P is reflected in detrital-P loads in sediments; which is higher in BoB (this study) as compared to Arabian Sea (Schenau and De Lange, 2001; Babu and Nath, 2005; Linsy et al., 2018a).

Another factor controlling the P geochemistry of the sediments is the primary productivity which controls the depositional flux of photosynthetically derived particulate material to the sediments. Low productivity leads to lower depositional flux of P_{bio} in the BoB whereas in the Arabian Sea, P_{bio} represents the major sedimentary P phase and its dissolution plays a key role on the benthic fluxes of phosphate (Schenau and De Lange, 2001, Linsy et.al. 2018a). Despite the low productivity, downward flux of organic matter in the BoB is high due to the low water column degradation of organic matter through its incorporation into rapidly sinking matter by ballast effect, as a result of the massive inputs of terrigenous matter in the BoB (Gauns et al., 2005; Naqvi et al., 1996). Even though the P_{org} and C_{org} contents of the BoB are comparable with the Arabian Sea (Babu and Nath, 2005; Babu and Ramaswamy, 2017), organic matter degradation plays a minor role in the benthic porewater release. The low bacterial respiration rate and less degradable terrestrially derived organic matter may be leading to the fast burial rather than decomposition. The high influx of organic matter in sediments resulting from monsoon-driven primary production and its degradation with depth make P_{org} a key factor controlling benthic phosphate release in the Arabian Sea sediments (Schenau and De Lange, 2001; Babu and Nath, 2005; Linsy et al., 2018a). Along with this intense Arabian Sea, OMZ also enhances the preferential release of P relative to C_{org} (Babu and Nath, 2005; Linsy et al., 2018a) since the preferential release of P from organic matter is most extensive under oxygen-depleted condition (Ingall and Jhanke, 1994). Though the bottom water DO values at the sites studied here are low, the high terrestrially derived fluvial sediment fluxes seem to hinder the redistribution of sedimentary P phases but enabling the burial rather than regeneration.

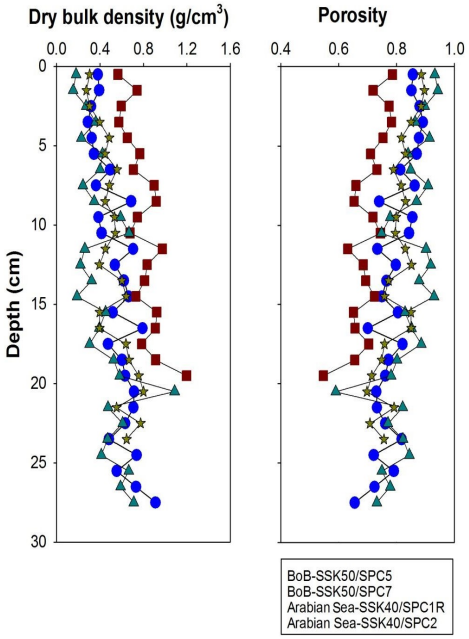

Figure 4.7: *Comparison of downcore variation of dry bulk density (g/cm^3) and porosity in BoB sediments (SSK50/SPC5 and SSK50/SPC7) with Arabian Sea Sediments (SSK40 /SPC1R and SSK40/SPC2-Linsy et al 2018a).*

The differences in physical properties of sediments may be playing an important role in the regeneration of different species of P in these two areas. The areas witnessing significant phosphogenesis in the eastern Arabian Sea (Linsy et al., 2018a) are composed of sediments with higher carbonate content, higher porosity and lower density compared to the sediments studied here from the western BoB (Fig. 4.2 and Fig. 4.7). The abundant lithogenic clays supplied by Himalayan and the peninsular Indian rivers perhaps play a key role in defining the physical properties which in turn affect the degradation of labile P phases and hinders the authigenic precipitation.

Conclusions

Downcore porewater profiles and solid phase P speciation data indicate that sedimentary cycling of P in the BoB is mostly regulated by the input of lithogenic fluxes in the area. Despite the moderate organic matter flux, the low decomposition rate of organic matter in the water column as well as in sediments and abundance of terrestrial organic matter make P_{org} a minor player for the P cycling. Unfavorable conditions such as low input of reactive P, high input of non-reactive P through river runoff and their rapid burial by ballasting effect inhibits the sink switching of P from labile to authigenic phase. Thus, most of the P_{auth} extracted here is terrigenous in origin. P_{Fe} content plays only a minor role in the benthic regeneration of P in the present study due to the weak OMZ resulting from low bacterial respiration. This limits microbial reduction of iron oxyhydroxides which in combination with low adsorption capacity of terregenous iron oxide make redox cycling of iron a weak player. Compared to the Arabian Sea, the BoB exhibits large variability in the modes of P cycling owing to multiple factors including low primary productivity, high lithogenic flux, and possibly due to different physical characteristics of the sediments.

Table 4.1: Table showing bottom water dissolved oxygen concentration, bottom water DIP, porewater DIP at the sediment-water interface, diffusive flux of phosphate and C_{org} and $CaCO_3$ in the core top sediments (0-1 cm).

Station Name	**Bottom water dissolved oxygen (µmol/L)**	**C_{org} (wt.%)**	**$CaCO_3$ (wt.%)**	**Bottom water DIP (µmol/L)**	**Porewater DIP at the sediment-water interface (µmol/L)**	**Benthic Flux of Phosphate (µmol cm^{-2} yr^{-1})**
SSK50/SPC5	11.7	1.87	13.6	2.73	7.75	-0.53
SSK50/SPC7	9.9	2.00	22.7	2.19	18.72	-1.50
SSK50/SPC13	12.0	1.16	5.9	2.51	32.36	-
SSK59/SPC3	8.3	0.31	6.4	0.65	25.00	-1.13

Table 4.2 Solid-phase phosphorus species in the studied sediment cores.

Station Name	Depth (cm)	**P_{bio}**	**P_{Fe}**	**P_{auth}**	**P_{det}**	**P_{org}**	**P_{total}**	**P_{react}**
		(µmol/g)						
SSK50/SPC5	0.5	8.7	2.3	4.6	4.1	11.7	31.3	27.2
	1.5	6.9	2.3	3.9	5.0	9.6	27.7	22.7
	2.5	8.7	3.0	3.2	4.8	8.2	27.8	23.0
	3.5	6.9	3.1	3.9	3.9	8.0	25.7	21.9
	4.5	8.2	2.6	5.3	4.2	6.7	27.0	22.7
	5.5	9.5	2.6	4.2	4.1	6.4	26.8	22.7
	6.5	7.4	2.7	6.0	4.3	6.7	27.0	22.7
	8.5	10.8	4.2	5.3	5.0	6.4	31.7	26.7
	9.5	18.2	4.9	6.0	5.0	8.1	42.1	37.1
	10.5	22.1	5.5	9.1	5.7	6.6	49.0	43.3
	12.5	14.3	6.8	7.0	5.4	7.3	40.7	35.4
	14.5	19.5	4.9	5.3	5.2	7.7	42.5	37.3
	15.5	20.8	5.9	6.3	5.7	7.5	46.2	40.5
	17.5	9.5	3.2	7.7	4.4	6.8	31.7	27.3
	19.5	14.3	7.7	8.4	6.7	6.2	43.2	36.6
	20.5	15.6	3.9	4.9	3.5	9.0	36.9	33.4
	22.5	19.5	5.8	4.9	4.0	8.2	42.4	38.4
	24.5	22.1	7.0	11.6	3.7	8.1	52.5	48.8
	27.5	16.0	7.3	7.7	3.5	6.2	40.7	37.2

Table 4.2 Continued

Station Name	Depth (cm)	P_{bio}	P_{Fe}	P_{auth}	P_{det}	P_{org}	P_{total}	P_{react}
		(μmol/g)						
SSK50/SPC 7	0.5	16.0	7.3	7.7	3.5	6.2	40.7	37.2
	1.5	24.2	13.6	31.9	31.0	11.2	112.0	81.0
	2.5	46.2	28.1	163.3	92.9	14.9	345.3	252.4
	3.5	24.1	23.9	38.9	18.0	12.2	117.0	99.0
	4.5	25.7	21.7	48.1	38.5	15.0	148.9	110.4
	5.5	33.3	25.6	134.2	132.1	24.0	349.2	217.2
	6.5	33.8	23.4	78.1	45.1	13.9	194.3	149.1
	7.5	35.6	27.3	85.1	33.6	19.5	201.2	167.6
	8.5	27.8	22.2	50.6	22.1	13.1	135.8	113.7
	9.5	37.5	16.7	144.2	127.6	23.4	349.4	221.8
	10.5	25.0	22.1	99.2	83.9	19.6	249.9	166.0
	11.5	27.8	18.0	97.0	59.1	18.4	220.3	161.2
	12.5	18.9	13.2	44.2	35.5	14.5	126.3	90.8
	13.5	34.6	27.4	104.3	47.3	15.1	228.6	181.4
	14.5	47.4	44.2	127.4	38.9	14.2	272.1	233.2
	15.5	60.2	52.5	220.8	172.7	25.0	531.2	358.5
	16.5	35.1	25.0	105.0	83.2	17.8	266.1	182.9
	17.5	30.8	26.1	106.3	44.7	16.4	224.4	179.6
	18.5	44.6	42.2	166.7	69.4	18.1	341.1	271.6
	19.5	48.4	39.7	140.0	54.1	12.9	295.2	241.0

Table 4.2 Continued

Station Name	Depth (cm)	P_{bio}	P_{Fe}	P_{auth}	P_{det}	P_{org}	P_{total}	P_{react}
		(μmol/g)						
SSK50/SPC13	0.5	13.8	3.6	4.1	5.8	4.0	31.4	25.5
	1.5	7.7	4.2	1.2	6.4	5.3	24.7	18.3
	2.5	7.6	3.3	4.2	5.8	3.8	24.8	19.0
	3.5	7.8	7.0	3.4	5.2	3.8	27.2	22.0
	5.5	4.8	2.5	3.4	3.5	3.1	17.2	13.8
	6.5	6.2	4.0	6.6	5.9	3.6	26.4	20.5
	7.5	6.4	3.2	4.2	5.3	2.3	21.4	16.1
	8.5	4.8	4.3	3.2	5.9	3.2	21.5	15.6
	9.5	5.4	2.8	4.9	5.7	3.2	22.0	16.3
	11.5	3.6	2.0	3.9	6.4	3.1	18.9	12.5
	12.5	3.8	2.3	4.2	6.5	2.1	19.0	12.5
	14.5	3.8	2.3	4.7	6.0	2.2	19.1	13.1
	15.5	4.7	3.6	2.7	6.5	2.4	20.0	13.5
	17.5	3.3	3.8	1.8	6.4	1.9	17.3	10.8
	18.5	5.2	2.6	3.6	5.5	2.2	19.2	13.7
	20.5	4.5	3.3	4.1	6.4	2.1	20.4	14.0
	22.5	6.2	2.2	2.9	5.9	1.5	18.7	12.8
	24.5	4.3	3.3	3.6	6.6	1.8	19.5	12.9
	26.5	3.3	3.6	3.2	7.0	1.8	19.0	12.0
	27.5	5.7	4.2	6.6	5.8	1.6	24.0	18.1
SSK59/SPC3	0.5	4.2	1.0	8.9	5.8	1.9	21.7	16.0
	2.5	5.4	1.0	10.7	6.4	2.4	26.0	19.6
	4.5	5.2	1.2	7.0	5.6	2.2	21.2	15.6
	6.5	6.0	0.8	7.0	5.7	1.7	21.1	15.5
	8.5	4.7	0.9	9.5	6.1	1.9	23.1	17.1
	10.5	5.1	0.9	7.4	6.3	2.0	21.7	15.4
	12.5	7.2	0.5	6.8	7.2	2.0	23.8	16.5
	14.5	5.8	0.6	11.8	6.3	2.0	26.5	20.2
	16.5	6.9	0.5	8.3	5.9	2.1	23.7	17.8

Table 4.3: Relative percentage of solid-phase phosphorus species and molar C_{org}/P_{org} and molar C_{org}/P_{react} ratios for the sediment cores of this study.

Station Name	Depth (cm)	Relative Percentage of P					Molar C_{org}/P_{org}	Molar C_{org}/P_{react}
		P_{bio}	P_{Fe}	P_{auth}	P_{det}	P_{org}		
SSK50/SPC5	0.5	27.6	7.3	14.6	13.1	37.4	133.1	57.2
	1.5	24.9	8.3	13.9	18.1	34.7	133.1	56.5
	2.5	31.1	10.7	11.4	17.3	29.6	157.1	56.2
	3.5	26.9	12.1	15.0	15.0	31.0	169.8	61.9
	4.5	30.5	9.5	19.5	15.6	24.8	203.1	59.7
	5.5	35.5	9.6	15.7	15.3	24.0	200.3	56.7
	6.5	27.2	10.0	22.1	16.0	24.7	166.3	49.0
	8.5	34.1	13.2	16.6	15.9	20.3	200.4	48.3
	9.5	43.1	11.6	14.2	11.9	19.2	147.1	32.1
	10.5	45.0	11.3	18.6	11.7	13.4	183.3	27.8
	12.5	35.0	16.6	17.2	13.2	18.0	177.9	36.9
	14.5	45.8	11.5	12.4	12.1	18.2	189.5	39.2
	15.5	44.9	12.9	13.7	12.4	16.1	180.9	33.3
	17.5	30.0	10.2	24.3	14.0	21.5	216.9	54.2
	19.5	33.0	17.8	19.5	15.4	14.3	220.8	37.3
	20.5	42.2	10.6	13.3	9.5	24.4	141.9	38.2
	22.5	45.9	13.7	11.6	9.4	19.4	173.4	37.1
	24.5	42.0	13.4	22.0	7.1	15.4	152.5	25.3
	25.5	45.1	14.9	29.5	4.9	5.6	208.3	12.3
	27.5	39.3	17.9	19.0	8.6	15.2	223.5	37.1

Table 4.3: Continued

Station Name	Depth (cm)	Relative Percentage of P					Molar C_{org}/P_{org}	Molar C_{org}/P_{react}
		P_{bio}	P_{Fe}	P_{auth}	P_{det}	P_{org}		
SSK50/SPC7	0.5	21.6	12.2	28.5	27.7	10.0	148.6	20.6
	1.5	13.4	8.1	47.3	26.9	4.3	71.8	4.2
	2.5	20.6	20.4	33.2	15.4	10.4	76.7	9.4
	3.5	17.2	14.6	32.3	25.9	10.1	66.7	9.1
	4.5	9.5	7.3	38.4	37.8	6.9	37.6	4.2
	5.5	17.4	12.0	40.2	23.2	7.2	69.4	6.5
	6.5	17.7	13.6	42.3	16.7	9.7	51.3	6.0
	7.5	20.5	16.3	37.2	16.3	9.6	74.6	8.6
	8.5	10.7	4.8	41.3	36.5	6.7	35.9	3.8
	9.5	10.0	8.9	39.7	33.6	7.9	51.7	6.1
	10.5	12.6	8.2	44.0	26.8	8.4	62.3	7.1
	11.5	15.0	10.4	35.0	28.1	11.5	87.9	14.1
	12.5	15.1	12.0	45.6	20.7	6.6	79.0	6.6
	13.5	17.4	16.2	46.8	14.3	5.2	80.8	4.9
	14.5	11.3	9.9	41.6	32.5	4.7	37.2	2.6
	15.5	13.2	9.4	39.5	31.3	6.7	64.4	6.3
	16.5	13.7	11.6	47.4	19.9	7.3	65.9	6.0
	17.5	13.1	12.4	48.9	20.4	5.3	57.2	3.8
	18.5	16.4	13.4	47.4	18.3	4.4	76.1	4.1
	19.5	21.1	22.4	26.9	18.8	10.8	64.4	8.6

Table 4.3: Continued

Station Name	Depth (cm)	Relative Percentage of P					Molar C_{org}/P_{org}	Molar C_{org}/P_{react}
		P_{bio}	P_{Fe}	P_{auth}	P_{det}	P_{org}		
SSK50/SPC13	0.5	44.1	11.6	13.0	18.6	12.7	244.0	38.0
	1.5	31.0	16.9	4.7	25.8	21.6	168.8	49.1
	2.5	30.7	13.4	17.1	23.6	15.2	209.5	41.7
	3.5	28.8	25.7	12.5	19.1	13.9	188.7	32.4
	5.5	27.8	14.4	19.7	20.1	18.0	222.5	50.1
	6.5	23.5	15.2	25.1	22.5	13.8	215.9	38.5
	7.5	30.0	14.8	19.7	24.8	10.7	244.4	34.8
	8.5	22.3	20.2	15.0	27.5	15.0	197.1	40.9
	9.5	24.7	12.8	22.2	25.8	14.5	211.3	41.4
	11.5	18.8	10.4	20.5	33.9	16.3	177.6	43.7
	12.5	20.1	12.2	22.3	34.2	11.2	230.0	39.2
	14.5	19.9	12.1	24.8	31.5	11.6	189.0	32.1
	15.5	23.8	18.3	13.6	32.5	11.8	153.8	26.9
	17.5	19.3	22.1	10.7	37.2	10.8	273.5	47.2
	18.5	27.3	13.8	18.5	28.8	11.6	166.9	27.2
	20.5	22.2	16.3	19.9	31.5	10.1	167.4	24.7
	22.5	33.2	11.6	15.4	31.6	8.3	262.2	31.8
	24.5	21.8	17.0	18.2	33.7	9.3	190.0	26.5
	26.5	17.5	19.2	17.0	36.9	9.4	194.5	28.8
	27.5	23.9	17.4	27.6	24.4	6.7	226.5	20.2
SSK59/SPC3	0.5	19.1	4.7	40.9	26.5	8.8	133.0	15.9
	2.5	20.8	3.9	41.3	24.7	9.3	126.9	15.7
	4.5	24.6	5.5	33.0	26.5	10.3	129.1	18.2
	6.5	28.2	3.7	33.2	26.9	7.9	152.9	16.6
	8.5	20.3	4.0	41.1	26.2	8.3	180.6	20.2
	10.5	23.3	3.9	34.3	29.1	9.3	130.6	17.2
	12.5	30.4	2.3	28.7	30.4	8.3	145.5	17.3
	14.5	21.8	2.3	44.4	23.8	7.6	146.1	14.7
	16.5	29.0	2.3	34.9	24.8	9.0		

Table 4.4: Total inorganic carbon (TIC), $CaCO_3$ (wt.%), N_{total} (wt.%), C_{org} (wt.%) and Molar C_{org}/N ratio for the sediment cores studied here.

Station Name	Depth (cm)	TIC (wt.%)	$CaCO_3$ (wt.%)	N_{total} (wt.%)	C_{org} (wt.%)	C_{org}/N_{total} ratio
SSK50/SPC5	0.5	1.64	13.63	0.16	1.87	13.3
	1.5	1.75	14.58	0.16	1.54	11.0
	2.5	1.86	15.46	0.16	1.55	11.2
	3.5	1.60	13.35	0.16	1.62	12.0
	4.5	1.55	12.95	0.16	1.63	11.7
	5.5	1.91	15.89	0.16	1.55	11.6
	6.5	1.91	15.92	0.15	1.33	10.4
	7.5	2.13	17.74	0.15	1.53	12.2
	8.5	2.31	19.25	0.15	1.55	11.8
	9.5	2.89	24.11	0.14	1.43	12.1
	10.5	2.73	22.74	0.14	1.44	12.2
	11.5	2.51	20.91	0.14	1.50	12.8
	12.5	2.85	23.77	0.14	1.56	13.5
	13.5	2.29	19.05	0.14	1.50	12.1
	14.5	2.72	22.64	0.13	1.75	15.3
	15.5	3.06	25.47	0.13	1.62	14.2
	16.5	3.04	25.32	0.12	1.62	15.2
	17.5	2.77	23.10	0.13	1.77	15.4
	18.5	3.61	30.11	0.13	1.28	11.6
	19.5	3.52	29.31	0.13	1.63	14.7
	20.5	3.77	31.44	0.13	1.53	13.9
	21.5	3.49	29.09	0.13	1.66	15.3
	22.5	3.53	29.38	0.13	1.71	14.9
	23.5	4.08	33.95	0.13	1.51	14.0
	24.5	4.07	33.88	0.12	1.48	14.5
	25.5	3.70	30.85	0.13	1.61	15.0
	26.5	4.26	35.48	0.13	1.31	12.2
	27.5	3.95	32.88	0.12	1.66	16.1

Table 4.4: Continued

Station Name	Depth (cm)	TIC (wt.%)	$CaCO_3$ (wt.%)	N_{total} (%)	C_{org} (%)	C_{org}/N_{total} ratio
SSK50/SPC7	0.5	2.72	22.65	0.10	2.00	23.8
	1.5	4.83	40.26	0.08	1.28	18.7
	2.5	3.00	24.96	0.11	1.12	11.8
	3.5	3.23	26.94	0.10	1.20	13.6
	4.5	3.67	30.56	0.09	1.08	14.0
	5.5	4.12	34.33	0.09	1.16	15.0
	6.5	3.81	31.75	0.09	1.20	15.6
	7.5	3.99	33.28	0.09	1.17	15.2
	8.5	4.06	33.81	0.08	1.01	14.3
	9.5	4.26	35.52	0.08	1.22	17.6
	10.5	4.25	35.40	0.09	1.38	18.7
	11.5	3.97	33.11	0.09	1.53	21.0
	12.5	3.78	31.49	0.09	1.43	17.7
	13.5	4.02	33.46	0.09	1.38	18.0
	14.5	3.71	30.87	0.09	1.11	14.1
	15.5	4.21	35.10	0.09	1.37	17.8
	16.5	4.18	34.79	0.08	1.30	18.2
	17.5	3.92	32.67	0.09	1.25	16.5
	18.5	4.38	36.51	0.09	1.18	15.1
	19.5	3.06	25.52	0.11	1.18	13.2

Table 4.4: Continued

Station Name	Depth (cm)	TIC (wt.%)	$CaCO_3$ (wt.%)	N_{total} (%)	C_{org} (%)	C_{org}/N_{total} ratio
SSK50/SPC13	0.5	0.71	5.95	0.16	1.16	8.7
	1.5	0.71	5.90	0.16	1.08	7.8
	2.5	0.66	5.53	0.13	0.95	8.8
	3.5	0.63	5.28	0.13	0.86	7.9
	4.5	0.66	5.50	0.13	0.92	8.3
	5.5	0.63	5.29	0.12	0.83	7.8
	6.5	0.61	5.08	0.13	0.95	8.3
	7.5	0.59	4.89	0.10	0.67	7.5
	8.5	0.63	5.24	0.12	0.76	7.7
	9.5	0.63	5.22	0.12	0.81	7.8
	10.5	0.69	5.73	0.12	0.70	6.6
	11.5	0.61	5.06	0.11	0.65	7.1
	12.5	0.63	5.27	0.09	0.59	7.3
	13.5	0.71	5.89	0.09	0.55	7.4
	14.5	0.69	5.76	0.08	0.51	7.4
	15.5	0.68	5.67	0.06	0.43	8.0
	16.5	0.72	5.99	0.05	0.52	11.1
	17.5	0.71	5.91	0.06	0.61	11.9
	18.5	0.70	5.87	0.05	0.45	10.0
	19.5	0.69	5.79	0.05	0.48	10.9
	20.5	0.67	5.55	0.05	0.42	10.1
	21.5	0.69	5.77	0.05	0.45	10.1
	22.5	0.70	5.81	0.05	0.49	11.2
	23.5	0.72	5.99	0.05	0.44	10.5
	24.5	0.68	5.63	0.05	0.41	10.5
	25.5	0.70	5.85	0.05	0.51	12.0
	26.5	0.69	5.71	0.04	0.41	11.0
	27.5	0.68	5.63	0.05	0.44	10.5

Table 4.4: Continued

Station Name	Depth (cm)	TIC (wt.%)	$CaCO_3$ (wt.%)	N_{total} (%)	C_{org} (%)	C_{org}/N_{total} ratio
SSK59/SPC3	0.5	0.77	6.38	0.04	0.31	8.1
	1.5	0.77	6.38	0.04	0.40	11.1
	2.5	0.76	6.36	0.05	0.37	9.6
	3.5	0.81	6.79	0.04	0.37	10.8
	4.5	0.88	7.31	0.04	0.34	9.4
	5.5	1.13	9.41	0.04	0.44	14.3
	6.5	0.84	6.98	0.03	0.31	10.6
	7.5	0.93	7.72	0.04	0.36	12.1
	8.5	0.80	6.70	0.04	0.41	11.8
	9.5	1.23	10.21	0.04	0.39	12.6
	10.5	1.09	9.11	0.04	0.32	10.6
	11.5	0.85	7.10	0.03	0.44	15.6
	12.5	0.85	7.06	0.03	0.34	12.5
	13.5	1.07	8.92	0.03	0.38	12.9
	14.5	0.93	7.77	0.03	0.36	12.2
	15.5	0.99	8.21	0.03	0.42	15.2
	16.5	0.87	7.28	0.04		

Chapter 5

Distribution and diagenesis of phosphorus in the deep-sea sediments of the Central Indian Basin

Chapter 5

5.1 Introduction

Even though over 90% of the global ocean floor is covered by deep-sea sediments, geochemical information regarding P cycling in deep-sea settings is scarce as most of the studies have been focused on continental margins. The cycling of P in an open ocean environment is entirely different compared to the continental margin settings. The reactive P burial in the continental margin sediments accounts for about 60% of the oceanic output, with deep sea sediments nearly equivalent as a sink (Filippelli and Delaney, 1996). Iron bound-P (P_{Fe}) is an important P-bearing component in deep-sea and modifies the redistribution of phosphate liberated by organic matter and thereby leading to the accumulation of large dissolved P at deeper depths (Tsandev et al., 2012). The dissolved P in the open ocean is about 3×10^{15} mol, of which 2.9×10^{15} mol are in deep water and only $\sim0.1\times10^{15}$ mol are in surface water (Broecker and Peng, 1982; see the review of Paytan and McLaughlin, 2007).

The oligotrophic setting with low organic matter flux in the deep-sea lead to a chemically inert condition where no oxide dissolution or authigenic P formation occurs (Tsandev et al., 2012). In contrast, earlier studies have documented that major P-bearing component in the deep-sea sediments is the authigenic phase (Morse and Cook, 1978; Filippelli and Delaney, 1995, 1996). The authigenic phase extracted in these studies also includes biogenic P, which may have been a reason for the elevated P_{auth} content. However, published studies have attributed this high P_{auth} content to the atmospheric deposition (Eijsink et al., 2000; Faul et al., 2005). Most of the deep-sea sediments are organic carbon (C_{org}) poor since much of the organic matter degradation takes place within the water

column. Under severe C_{org} depletion and oxic condition, phosphate solubilizing bacteria stimulate liberation of P by dissolving insoluble inorganic forms into soluble P and making it biologically re-available (Chen et al., 2006; Das et al., 2007; Biche et al., 2017).

Most of the efforts to understand P cycling at the deep-sea sediment-water interface were confined to study of pore water and diffusive flux of phosphate (Atlantic Ocean - De Lange, 1986a, 1986b; Hensen et al., 1998, 2000; Zabel et al., 1998; Pacific Ocean - Emerson et al., 1980; Jahnke et al., 1982; Indian Ocean- Nath and Mudholkar, 1989; Grandel et al., 2000) with a view to assess the early diagenetic processes. The information on pathways of P burial and solid phase P-speciation in deep-sea sediments, however, is limited to very few studies in the Pacific (Morse and Cook, 1978; Filippelli and Delaney, 1995, 1996; Tsandev et al., 2012; Ni et al., 2015) and only one in the Atlantic (Kraal et al., 2010), leaving a major gap in our understanding of other abyssal areas of the Indian and Atlantic oceans.

Most of P-cycling and solid-P speciation studies in the Indian Ocean are confined to its northern part, principally to study the biogeochemical cycling in unique monsoon-driven regions of the Arabian Sea and Bay of Bengal (Schenau et al., 2000, 2005; Schenau and De Lange, 2001; Babu and Nath, 2005; Kraal et al., 2012, 2015; Acharya et al., 2016; Babu and Ramaswamy, 2017; Sudheesh et al., 2017; Linsy et al., 2018). In an attempt to understand the cycling and the pathways of P burial in abyssal areas we present a P geochemical study of the Central Indian Basin (CIB) sediments systematically collected in a one-degree by one-degree grid spacing.

The CIB is a large abyssal basin, which is rich in ferromanganese nodules and bounded by ridges on 3 sides and is open to sediment input from the Bay of Bengal in the north-east

(see Nath et al., 1989). The past studies on the CIB sediments have reported total P (P_{total}) content (Banakar et al., 1998; Pattan and Jauhari, 2001), related sedimentary P to explain the calcium-bearing phases (Nath et al., 1989) or have used organic C to P relation to assess the recovery of benthic ecosystem after a disturbance experiment (Nath et al., 2012). However, the processes that control P diagenesis and quantitative estimates of diffusive fluxes and P fractionation in chemically separable phases are not known. This study aims to fill this knowledge gap as well as to understand early diagenetic processes associated with the burial of P in oligotrophic environments. For this, 29 surface sediments and 9 short cores were studied (Fig. 5.1 and see Table 2.3 and 2.6 in Chapter 2 for the locations) solid phase speciation for P in five chemically separable phases, total P, Fe, Ti, Zr and organic carbon, porewater (only in cores) and bottom waters (at 3 locations) were analyzed for DIP.

The five P fractions separated are same as those described in previous chapters and thus the same abbreviations are used here too (e.g., P_{bio} denoting P bound to biogenic fraction). The chemical scheme followed here for extracting the P fractions is described in Chapter 2 and presented in Table 2.5. Fe was measured in citrate-dithionite-bicarbonate (CDB) extract to estimate the amount bound as iron oxides in 3 sediment cores. In addition to studying two major sediment types, the siliceous ooze/clay and red/pelagic clay, hydrothermally altered sediments from the flank of a seamount were also studied for phosphorus geochemistry.

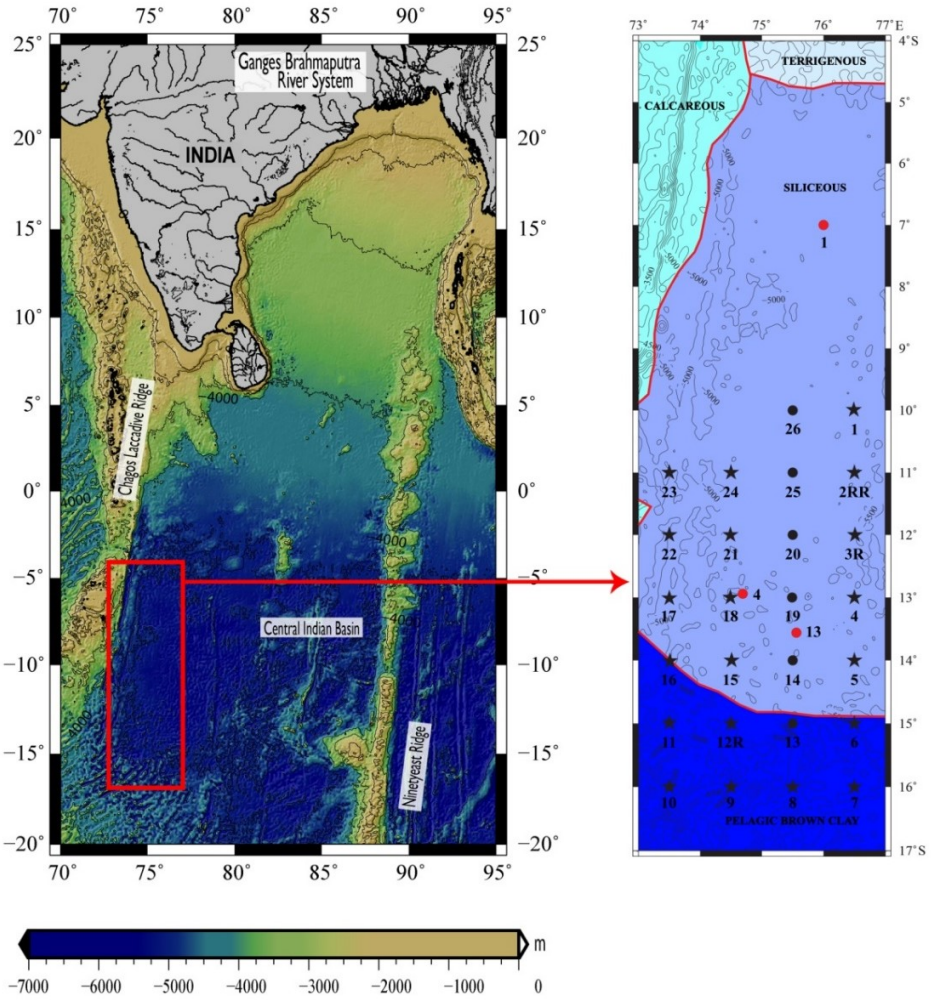

Figure 5.1: *Sampling locations in the Central Indian Basin. (Circles = core samples, stars = surface samples, Red color = cruise SS 13, black = cruise AA 61). The red line in sampling location map (here and subsequent figures) separates the siliceous ooze from pelagic clay, the two principal sediment domains in the area.*

5.2 Results

5.2.1. Regional variation of sedimentary P phases

The surface sediment P speciation data (see Fig. 5.1 for locations) of equi-spaced stations are used to assess the regional distribution patterns of pathways of phosphorus deposition. Station-wise distribution pattern of different phases of P and their relative contribution to P_{total} are shown in Fig. 5.2 (Table 5.1 and Table 5.2). The P_{total} content of the surface sediments varies between 23.8 and 81.4 µmol/g with an average of 33.7 µmol/g. The highest P_{total} content is at AA/8 station and the lowest content is found at AA/12R station **(Fig. 5.2, Table 5.1&5.2**), both the stations falling in pelagic/red clay sediment domain.

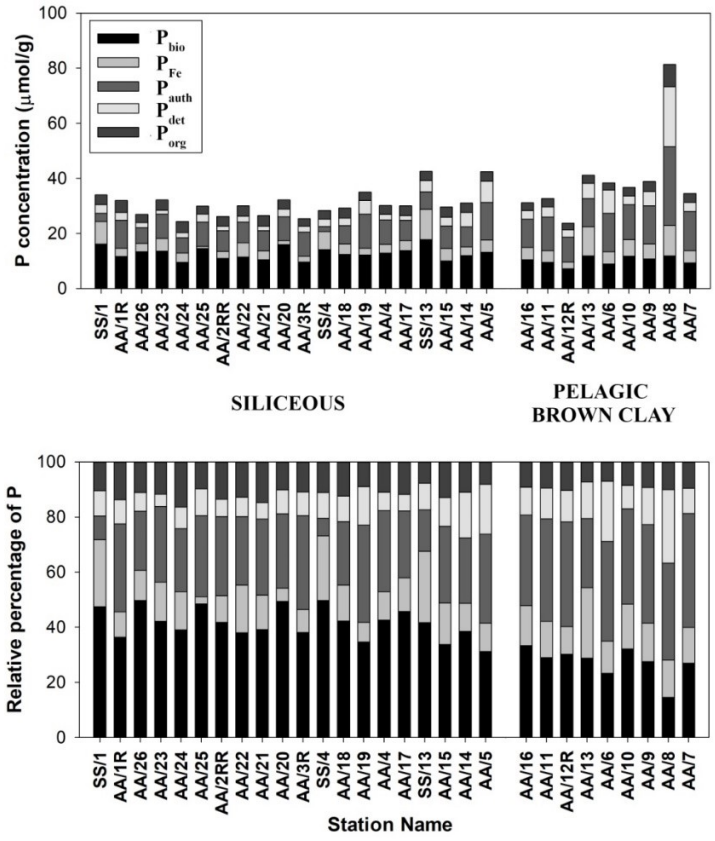

Figure 5.2 *Concentrations (top) and relative percentage (bottom) of different phases of P in the surface sediments of the CIB. Station numbers correspond to those shown in Figure 5.1.*

The P_{bio} content in the surface sediments varied between 7.17 and 17.7 µmol/g (average 11.95 µmol/g) and in general showed a spatial gradient with higher values in the northern part of the study area that has siliceous oozes and lowest in the southern part where pelagic clays are dominant **(Fig. 5.3)**. In contrast, other phases, viz., P_{Fe}, P_{auth} and $P_{det,}$ have followed a spatial distribution pattern similar to that of P_{total} with higher content in pelagic clays than that in siliceous oozes. The P_{auth} content ranges from 1.80 to 28.59 µmol/g (average - 9.64 µmol/g) and is the second largest pool of sedimentary P, making up an average 28 % of P_{total} **(Fig. 5.4, Table 5.2)**, which is slightly lower than that reported in the Central Pacific Ocean (**Table 5.3**) (Ni et al., 2015). The P_{Fe} content ranges between 0.79 and 11.11 µmol/g and constituted 13% of P_{total} **(Fig. 5.4 and Table 5.2)**. The P_{det} content ranges from 1.43 to 21.66 µmol/g with an average of 3.96 µmol/g. The P_{det} content ranges from 1.43 to 21.66 µmol/g (average 3.96 µmol/g) and is highest at station AA/8 (seamount flank) similar to P_{total}. P_{org} content in surface sediments varies from 2.46 to 8.21 µmol/g and constitutes about 7-16.4 % of the sedimentary P_{total} **(Fig. 5.2)**.

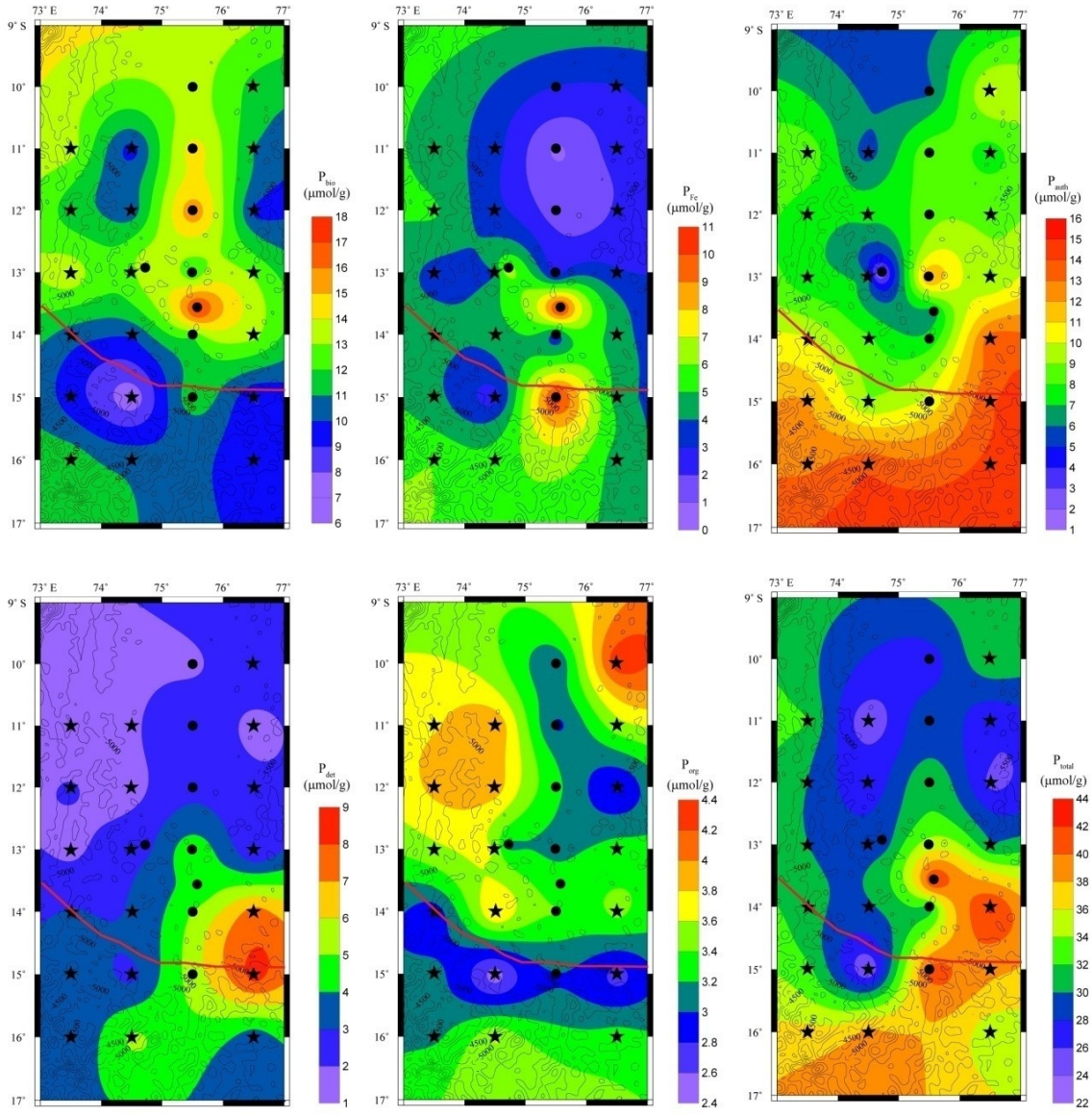

Figure 5.3: *Spatial distributions of different sedimentary phosphorus species, including total phosphorus (P_{total}), biogenic (P_{bio}), iron bond (P_{Fe}), authigenic P (P_{auth}), detrital P (P_{det}) and organic P (P_{org}), in the study area (all in µmol/g-dried-sediment).*

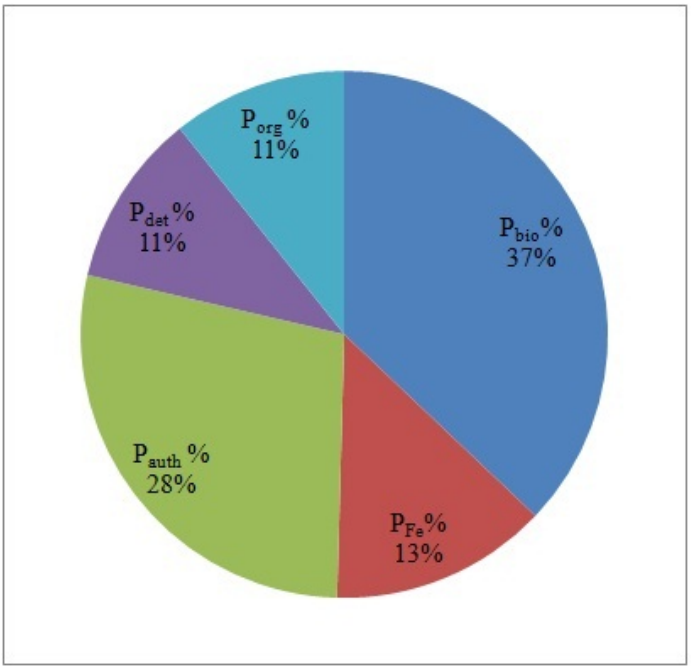

Figure 5.4: *Phase partitioning of different sedimentary phosphorus species in the CIB, biogenic P (P_{bio}), iron bound P (P_{Fe}), authigenic P (P_{auth}), detrital P (P_{det}) and organic P (P_{org}) based on average data.*

5.2.2 Downcore profiles of porewater DIP and sedimentary P phases

The DIP concentration in the porewater varies between 0.08 and 3.7 µmol/L **(Fig. 5.5)**. Generally, DIP in the porewater shows slightly lower values than that of overlying seawater in this area. In most of the locations, DIP concentrations remain relatively constant with depth except at location AA/3 where a mid-depth depletion of DIP is observed.

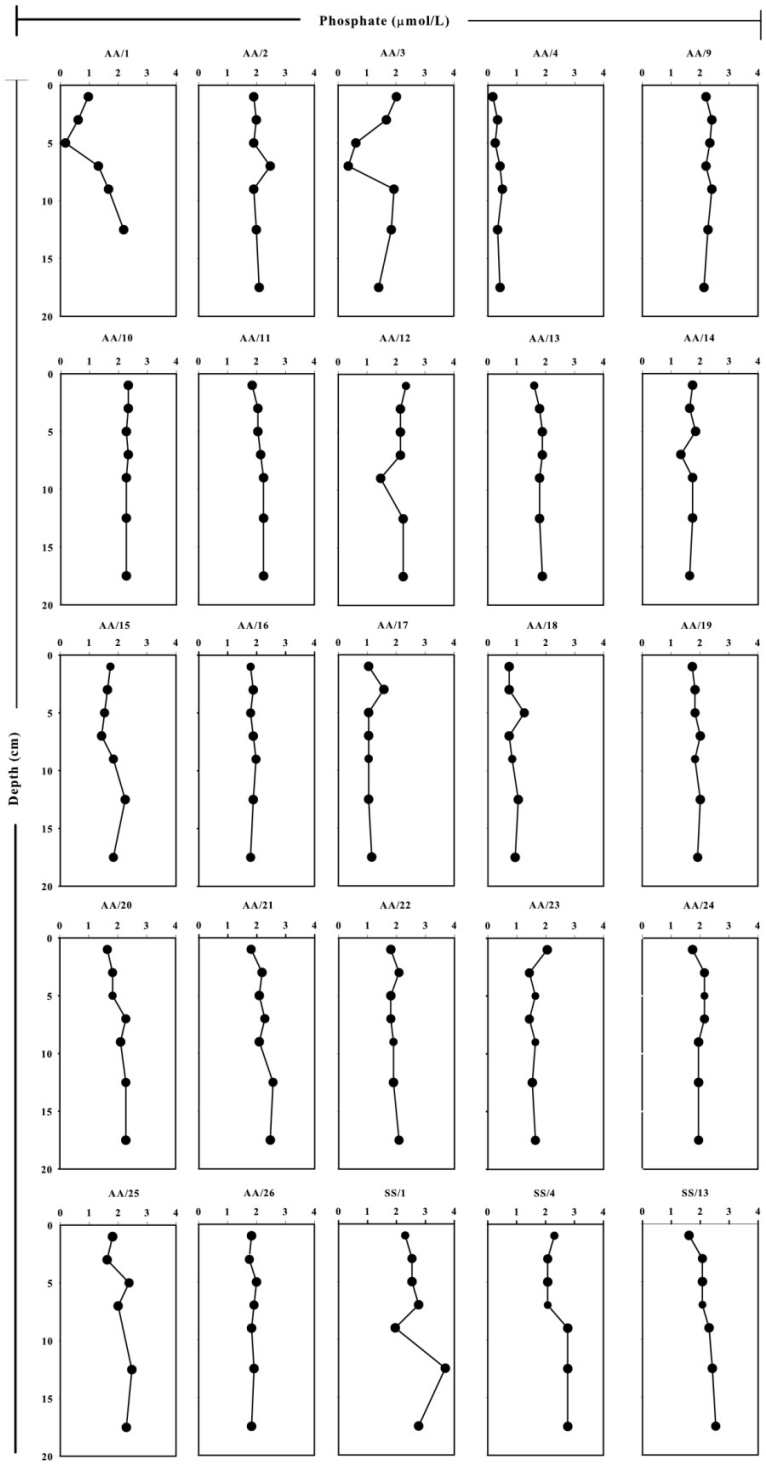

Figure 5.5: *Porewater profiles of dissolved phosphate (µmol/L).*

In all the locations, P_{total} **(Fig. 5.6)** decreased with depth except for station SS/13 where there is an enrichment of P with depth. After an initial downcore decrease, P_{total} content in cores AA/13 and AA/14 are higher at deeper depths.

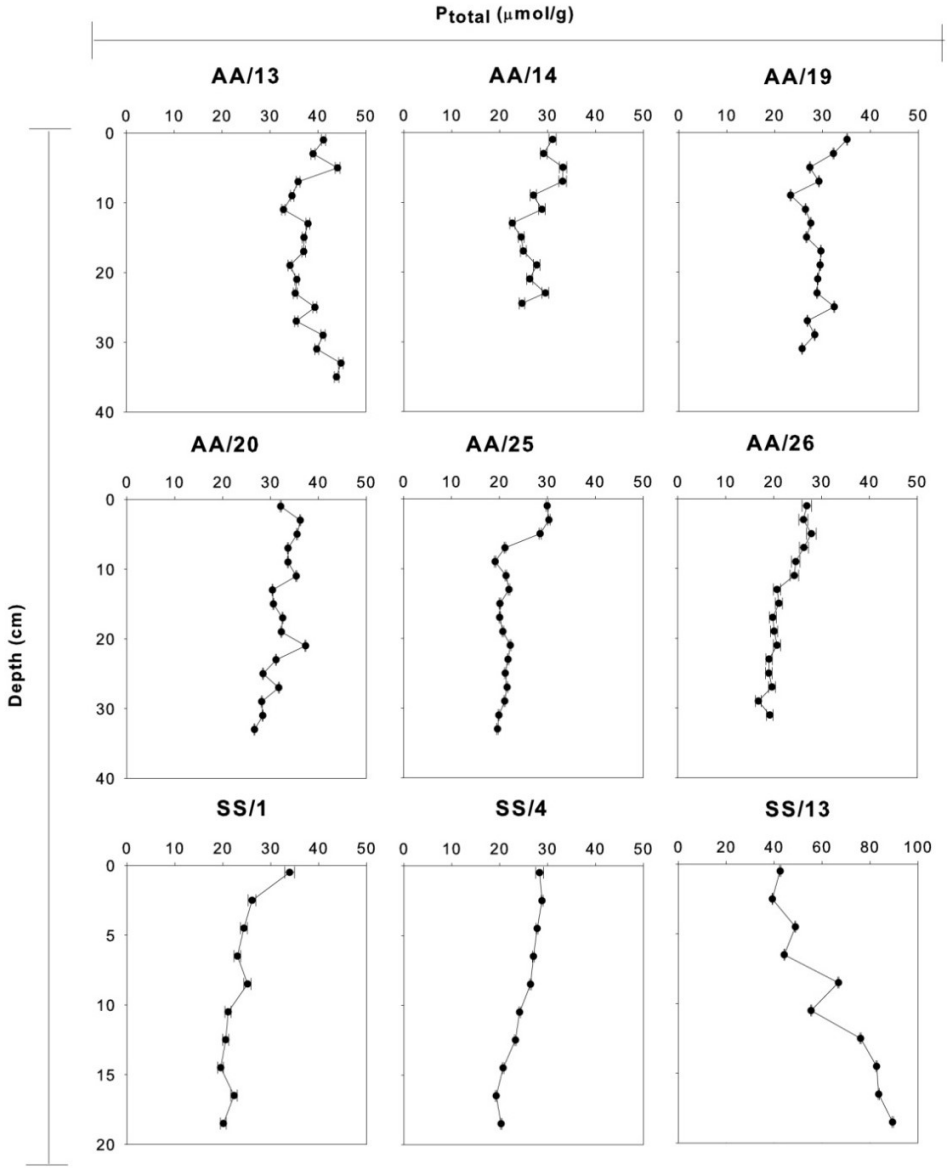

Figure 5.6: *Downcore variation of total P (P_{total}) in µmol/g).*

C_{org} content in the cores varies between 0.02 and 0.55 wt.%. In all stations, C_{org} content generally decreases with depth except at station AA/25 where no consistent trend with depth is observed.

P_{bio} is the major pool of P in the study area and accounts for 26-47% of P_{total}. P_{bio} values range between 7.8 and 40.5 μmol/g **(Table 5.4)** and generally shows a decrease **(Fig. 5.7)** with depth at sites AA/25, AA/26, SS/1, and SS/4. However, a rapid decrease occurs from 3 cm to approximately 9 cm at site AA/25. P_{bio} content below 9 cm shows a slight increase, which then follows a nearly constant pattern with depth. At sites AA/13 and SS/13, P_{bio} content increases with depth. The P_{Fe} content is between 0.13 and 15.3 μmol/g, which accounts for 0.4-29.7 % of the P_{total}. The P_{Fe} content generally decreases with depth except for sites SS/13 and AA/13, where P_{Fe} content is higher at deeper depths **(Fig. 5.7 and Table 5.4)**. The P_{Fe} content in core AA/13 decreases from 3 to 7 cm, is relatively constant between 7 and 21 cm but increases below this depth. At station SS/1, P_{Fe} content is high at surface and then shows a slight decrease but at site SS/4 it remains relatively constant till 11 cm depth and then shows a decrease. P_{auth} content is between 0.3 and 27.9 μmol/g, which account for 1.2-35.2 % of the P_{total}, and is high at the sediment-water interface at locations AA/13, AA/19, AA/25, and AA/26. But in SS/13, P_{auth} content increases with depth. P_{det} content was very low (1.5-15.7 μmol/g) **(Table 5.4)** that accounts for < 23% of P_{total} **(Fig. 5.6)**. P_{org} content ranges between 1.5 and 3.5μmol/g, which accounts for 2-13.8% of the P_{total}. P_{org} contents are low and decrease with depth at all stations in a manner similar to C_{org}.

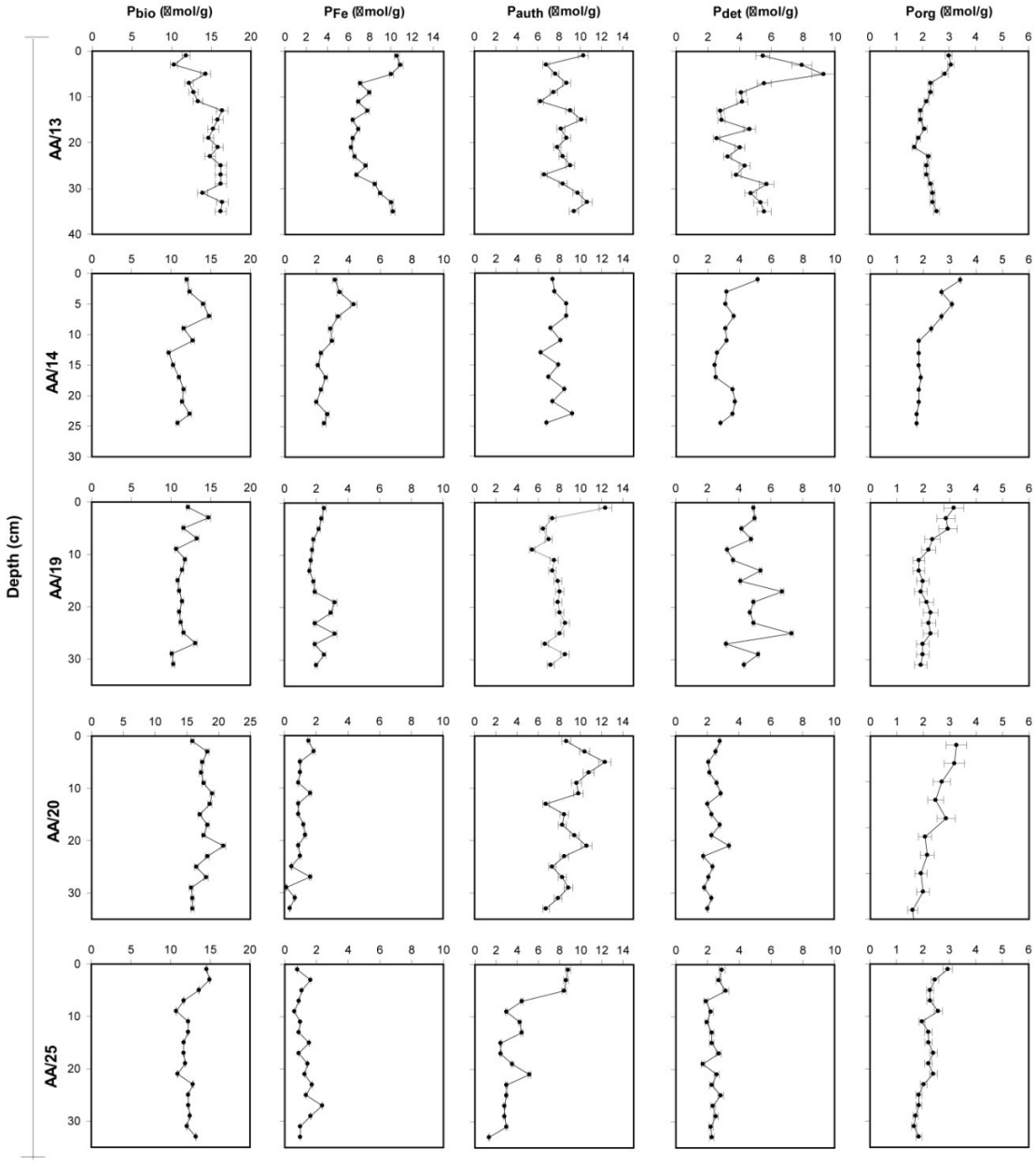

Figure 5.7: *Down core variation of P in five geochemically separable phases (units in µmol/g).*

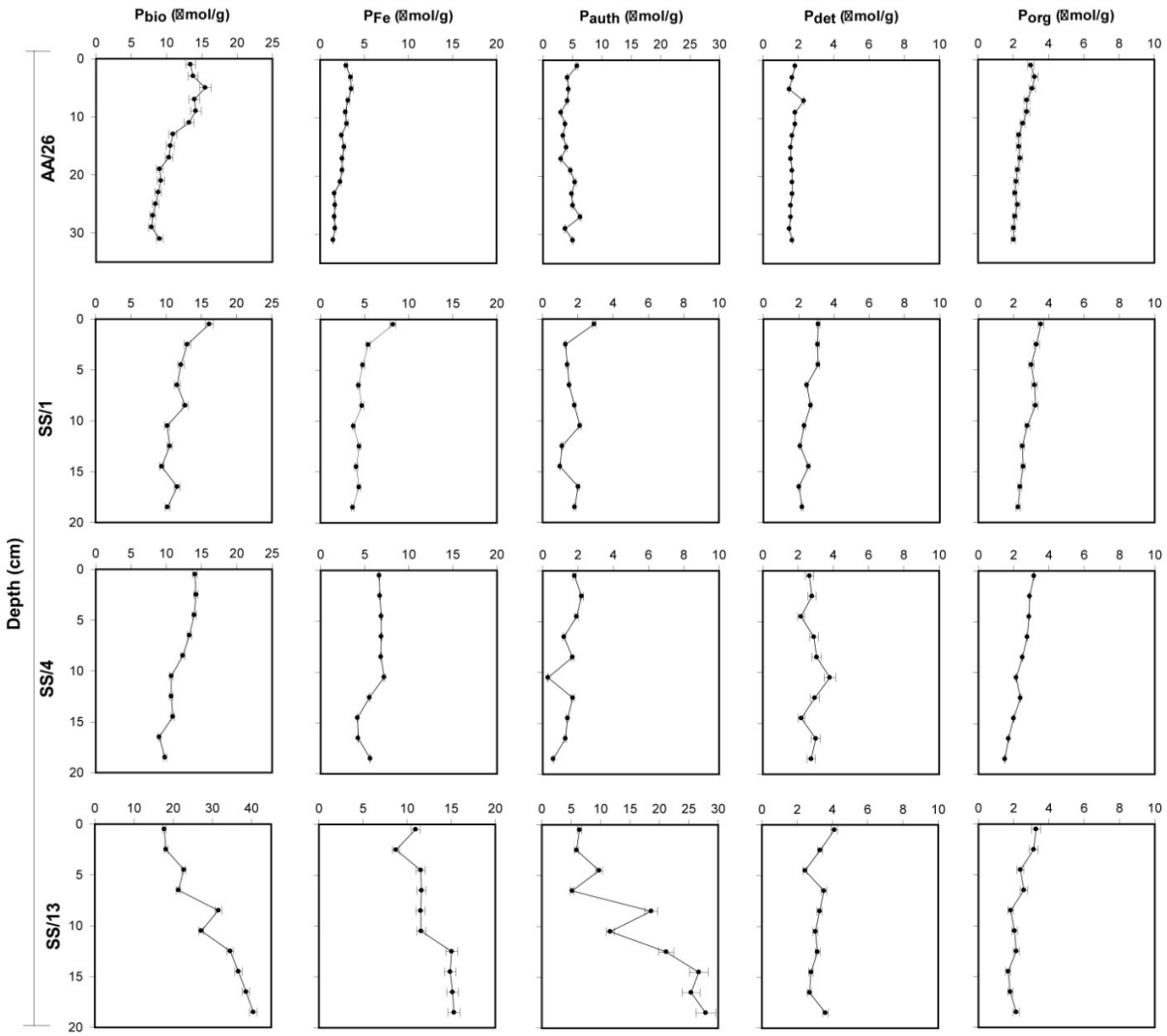

***Figure 5.7** (Cont)*

5.3. Discussion

5.3.1. Regional variation of particulate-P species

P_{total} content of the CIB sediments (average 33.7 μmol/g) is comparable with the previously reported values for siliceous ooze and pelagic red clays of the Indian Ocean

(Nath et al., 1989, Baturin, 2003), but are marginally lower than that of Central Pacific sediments (Ni et al., 2015).

The relative proportion of different P species in the CIB sediments is in the order $P_{bio}>P_{auth}>P_{Fe}>P_{det}>P_{org}$ (**Fig. 5.4**). These observations are consistent with P speciation results from other deep sea settings of the Equatorial Pacific and Central Arabian Sea (Filippelli and Delaney, 1996; Schenau et al., 2005) **(Table 5.3)**. P_{bio} is found to be a most important sedimentary pool of P in the study area. The highest value of P_{bio} observed between 12° and 14° S latitude, where highest biogenic silica content was reported earlier (Nath et al., 1989; Pattan et al., 1992), reflects the influence of higher biological productivity in the surface waters. High biological productivity leads to enhanced fish production and enrichment of biogenic apatite in this area. Relatively low values of P_{bio} associated with pelagic red clays are due to lower productivity in the overlying waters (30 to 50 mg C m^{-2} day^{-1} corresponding to 10.95 to 18 g C m^{-2} $year^{-1}$) (Matondkar et al., 2005; Das et al., 2011a).

The ammonium chloride leach used to determine P_{bio} can also extract loosely adsorbed fraction (Schenau and De Lange, 2000). The high particle reactivity of P promotes its sorption on the surface of fine-grained constituents like clays. Along with this high bottom water phosphate (~3µmol/L) and low sedimentation rate can fuel the adsorption process (Ni et al., 2015). The clay-sized sediment content in the area is high (up to 81% by weight) (Biche et al., 2017) and the sedimentation rates in the CIB are extremely low (2-3 mm kyr^{-1}, rarely exceeding 1 cm kyr^{-1}) (Banakar et al., 1991; Borole, 1993; Nath et al., 2013; Mascarenhas-Pereira et al., 2016) typical of deep-sea pelagic sediments. Thus, fine-grained

sediments with very low sedimentation rates in the CIB promote the adsorption of P, and this adsorbed fraction could be an important sink of P from the water column.

P_{auth} is the second largest pool of sedimentary P in the CIB **(Fig. 5.4)**. These results are comparable with previous studies from the Arabian Sea (Babu and Nath, 2005; Schenau et al., 2005) but much lower than that found in the Equatorial Pacific (Filippelli and Delaney, 1996) **(Table 5.3**). In the Equatorial Pacific, higher P_{auth} was attributed to sink switching of P from organic matter and iron oxyhydroxides to the precipitation of CFA whereas the sink switching of P is not active in the CIB (as mentioned elsewhere in the chapter). The lack of significant remobilization could be due to deeper water depths in the CIB. The deeper depths (average 5152 m) of the basin compared to Equatorial Pacific (average 3295 m) may have promoted enhanced re-mineralization of P within the water column and burial of P with more residual phase.

The degradation and dissolution process of P from the reactive phases can control the P_{auth} formation. Earlier studies have shown that in addition to in-situ precipitation, atmospheric input also contributes CFA to the sedimentary pool of P (Eijsink et al., 2000; Faul et al., 2005; Kraal et al., 2012; Ni et al., 2015). The aerosol content was found to increase with latitude in the southern hemisphere Indian Ocean, and the maximum was observed at 20°S. Rajeev et al. (2000) attributed this to a combination of aerosol transport through the western and eastern parts of the tropical Indian Ocean, sea salt production due to high wind speed and transport of Australian dust. Increased deposition of clay-sized sediments together with a concomitant increase in kaolinite content in the CIB, during the periods of the prevalence of arid conditions in Australia, has been attributed to the wind deposition (Nath et al., 2013). Kaolinite-rich dust from Western Australia is blown into the

eastern Indian Ocean (Griffin et al., 1968; Fagel, 2007) as a result of the prevailing easterly winds (McTainsh, 1989; Gingele et al., 2001).

Distribution of kaolinite (Fig. 5.8) in the CIB (using the clay mineral data of Valsangkar, 2011) shows distinctly high content in the south-eastern part of the study area and follows the general Indian Ocean trend (Griffin et al., 1968; Fagel, 2007) and implies the eolian contribution from Australia. In addition, a relatively high content of possible eolian proxies (Nath, 2001 and references therein) Ti and Zr in the study area (Fig. 5.9) and positive Eu anomaly observed in the CIB sediments (Banakar et al., 1998) can be attributed to the eolian input. Highest P_{auth} contents are observed south of 15°S latitude mimicking the distribution of Ti and Zr contents (Fig.5.9). Thus, the high P_{auth} content in the CIB pelagic clays could be atmospheric in origin. This is similar to the previous finding that 63% of CFA content is associated with atmospheric deposition in the Central Pacific Ocean (Ni et al., 2015), which has a similar physiographic setting.

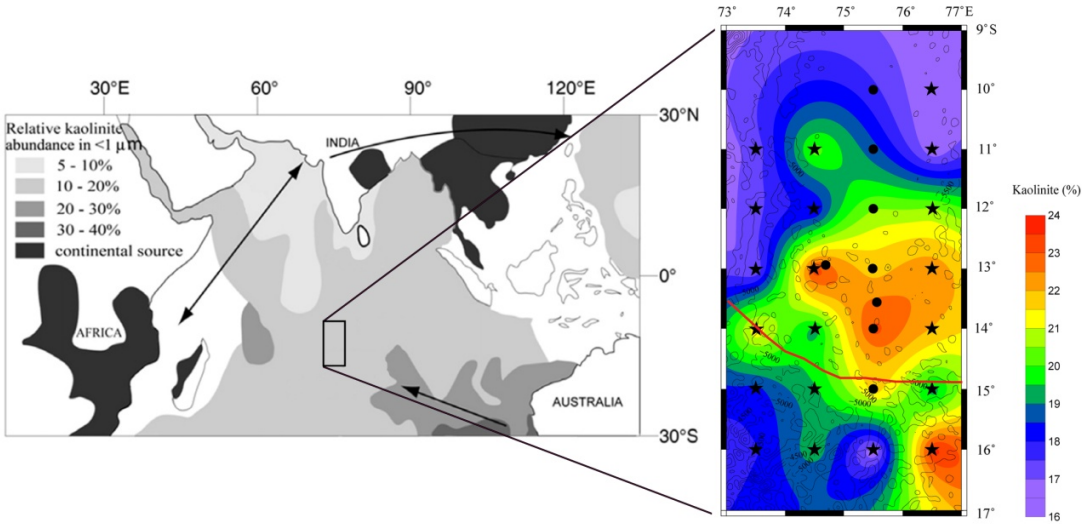

Figure 5.8: *Distribution of kaolinite content in surface sediments of the CIB and inset map were taken from Nath et al. (2013), showing relative percentage of kaolinite in <1 µm clay size fraction in sediments of the Indian Ocean and surrounding seas. Arrows depict jet stream transport pathways in the Asian subcontinent, and tropospheric transport path from the Australian continent to the CIB and between Arabia and Africa. The main map shows the kaolinite content of <2 µm in surficial sediments in the same stations studied here for P geochemistry (data from Valsangkar, 2011). Central and southeastern locations show high kaolinite content likely from Australia.*

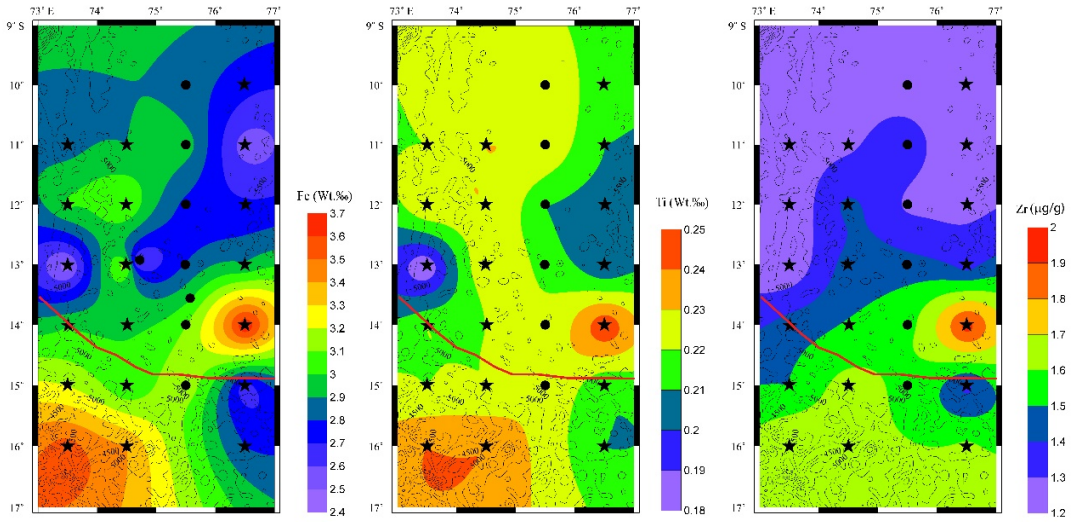

Figure 5.9. *Spatial distribution of Total iron (Fe), Ti and Zr contents in surface sediments of the CIB.*

P_{Fe} constitutes the third largest pool of P_{total} in the CIB sediments (**Fig. 5.4**), which is consistent with other deep-sea setting of the Equatorial Pacific where 11% of the sedimentary P is associated with iron oxyhydroxides (Filippelli and Delaney, 1996) (Table 5.3). The presence of iron largely affects the burial and diagenesis of P in the sediments (e.g., Slomp et al., 1996). Iron oxyhydroxides provide a sorption site for P and under reducing condition, they undergo reductive dissolution and release phosphate to the porewater. The oxygenated bottom water of the CIB promotes the adsorption of P onto the surface of iron oxyhydroxides. The distribution of P_{Fe} **(Fig. 5.3)** and total Fe (**Fig. 5.9**) indicates that the concentration increases towards the southern part of the basin, where pelagic red clays are dominant and the sediments from this region bear the signature of hydrothermal activity (Iyer et al., 2007; Nath et al., 2008; Mascarenhas-Pereira and Nath,

2010; Das et al., 2011b). This influence of hydrothermal activity results in the enrichment of Fe in the pelagic region.

The high smectite content in the pelagic clay of CIB also indicates the alteration from local basinal rocks (Rao and Nath, 1988; Fagel et al., 1994; Iyer, 1999). Fe-rich montmorillonites occur in the CIB (Rao and Nath, 1988) with higher content in siliceous oozes compared to pelagic red clays with a part of Fe being utilized in their formation in the siliceous sediments (authigenic precipitation of Fe reacting with silica released from opal dissolution). Furthermore, atmospheric process can also contribute a significant amount of Fe to the sedimentary pool in the pelagic region. This is because eolian input is a major source of Fe to the surface oceanic waters and contributes 32 x 10^{12} g yr^{-1} Fe to the global ocean (Gao et al., 2001). A previous study has shown that the main component of Fe in aerosols is not only Fe (III) oxide, but also Fe (III) phosphate (Longo et al., 2016). Distribution of P_{total} and P_{Fe} also mimics the kaolinite distribution **(Fig. 5.8**) suggesting a possible role of atmospheric deposition of P_{Fe} to pelagic red clay sediments.

P_{det} is found to be a minor fraction of the P_{total} pool in the study area. These findings are consistent with the deep Arabian Sea settings where 12% of sedimentary P phases are associated with detrital matter (Schenau et al., 2005) and greatly varied from the Central Pacific where P_{det} represents 46% of the total (Ni et al., 2015) (**Table 5.3**). The CIB receives terrigenous influx, from the Ganges and Brahmaputra rivers, decreases towards the south and has been traced up to 8°S (Nath et al., 1989, 1992a; Nath, 2001). The low P_{det} content in the CIB is similar to that observed in the Equatorial Pacific Ocean (Filippelli and Delaney, 1996). The highest P_{det} content is observed south of 15°S where the sediments are dominated by pelagic red clays. The estimated higher terrigenous sediment content (Sensarma et al.,

2017) in the CIB pelagic clays may, in fact, reflect the presence of higher lithogenic material in these sediments and not necessarily from the terrigenous sources (Nath, 2001). The sediments in the south (14° S) has higher ^{232}Th concentrations (3.88 dpm/g) compared to the northern locations (2.76 dpm/g at 12° S) (Borole, 1993). ^{232}Th can be a good tracer for lithogenic clays (Nath, 2001 and references therein). The southern portion of the basin with pelagic clays, in fact, has sediments with shale-normalized REE patterns identical to those of mid-ocean ridge basalts (MORB) (Nath et al., 1992a). The high lithogenic material can either be from eolian source or from halmyrolitic processes involving oceanic rocks. Higher P_{det} in pelagic clay area, thus, could be from atmospheric input or supplied from altered volcanic rocks from the South Eastern Indian Ridge and basinal rocks.

Organic matter is the principle shuttle of P to sediments and during its degradation, phosphate is released to the porewater, which then undergoes various biogeochemical processes (Froelich et al., 1988; Filippelli et al., 1994; Ingall and Jahnke, 1994). In an oxic environment, most labile organic matter undergoes degradation within the water column, resulting in low P_{org} and C_{org} contents in the sediments (Ni et al., 2015). The P_{org} and C_{org} contents of the CIB sediments are comparable with previously reported values for deep-sea sediments of the Pacific Ocean (Ingall and Van Cappellen, 1990; Filippelli and Delaney, 1996; Ni et al., 2015) (**Figs. 5.10 and 5.11**). The CIB sediments are depleted in C_{org} and a weak correlation of C_{org} with P_{org} (**Fig**. **5.11**) indicates the variation in source and status of organic matter degradation (Ni et al., 2015).

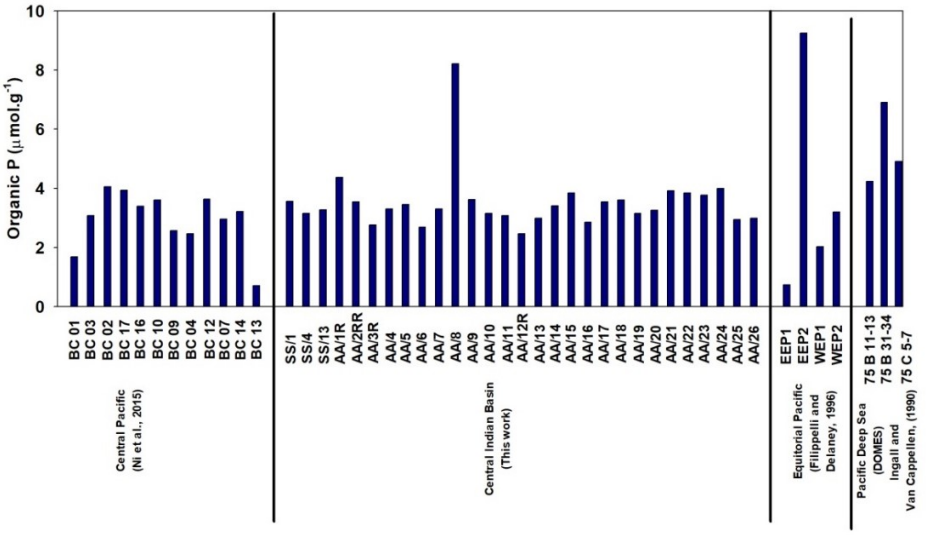

Figure 5.10. *The concentration of P_{org} in the CIB compared with that of the Pacific sediments.*

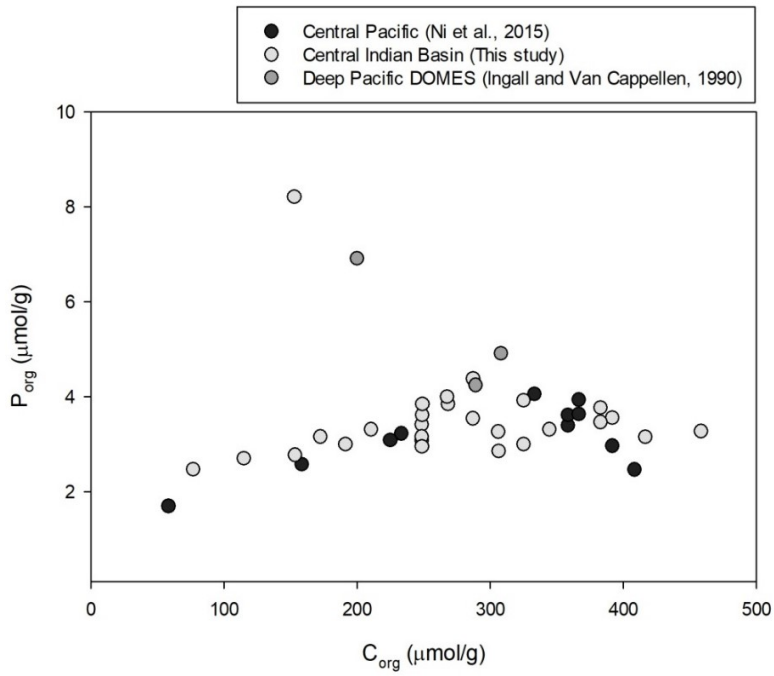

Figure 5.11. *C_{org} and P_{org} bi-plot of surface sediments in the CIB and comparison with the Central Pacific Sediments (Ni et al., 2015) and the Pacific deep sea sediments (Ingall and Van Cappellen, 1990).*

Molar C_{org}/P_{org} and C_{org}/P_{react} ratios in sediments can driven by the redox conditions and diagenetic redistribution of organic matter (Anderson et al., 2001; Kraal et al., 2012; Yang et al., 2017). In the CIB samples, C_{org}/P_{org} ratio varied from 31 to 140 with an average of 82 (excluding the low ratio of sediment core AA/8 with distinct hydrothermal signatures) with highest ratios in surface sediments dominated by siliceous oozes. Similarly, C_{org}/P_{react} ratio is higher in the northern part (with siliceous oozes) than in the southern part with pelagic/red clays (**Fig. 5.12**). Among the 26 core tops studied for regional distribution, 13 of them had C_{org}/P_{org} ratio closer to the Redfield ratio (80-140) and four of them had a ratio <60 (Fig. 5.12). The lower ratio is consistent with other slowly deposited pelagic sediments (organic C/P ratio of 49-63 in areas with sedimentation rates < 0.002 cm/y; Ingall and Van Capellen, 1990), Unlike the C_{org}, which vary with the sediment type and has a distinct N-S variation (**Fig. 5.12**), no such regional variation is seen in P_{org} (**Fig. 5.3**). Further, the

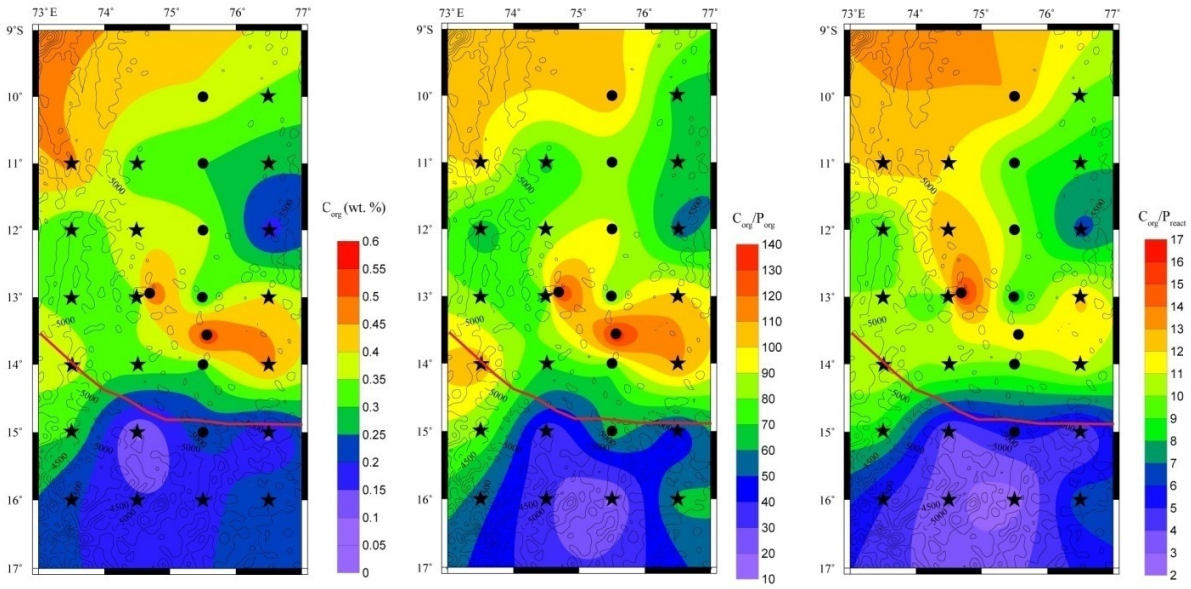

Figure 5.12: *Spatial distribution of C_{org}, molar C_{org}/P_{org} and C_{org}/P_{react} ratio in the surface sediments of the CIB.*

C_{org}/P_{org} correlates well with C_{org} (**Fig. 5.13**) (R^2 – 0.86) but not with P_{org}.

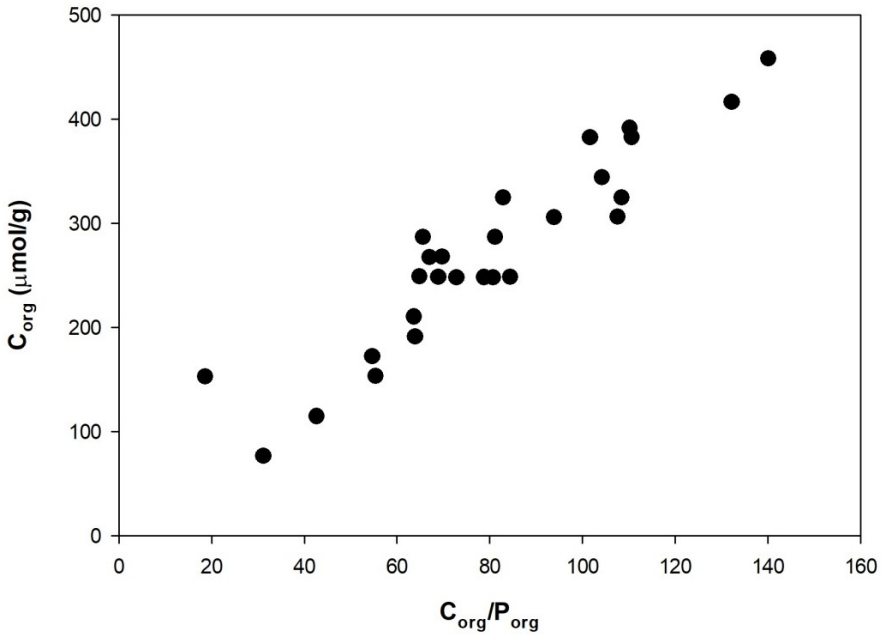

Figure 5.13. *Scatter plot between C_{org} and C_{org} /P_{org} ratio showing a remarkable positive relation.*

This apparent discrepancy was attributed to the utilization and conversion of detrital organic matter by benthic organisms into low C/P biomass (Ingall and Van Capellen, 1990). Lower sedimentation rates and oxygenated bottom waters in pelagic environment lead to the oxic diagenesis, complete oxidation of the organic matter and produce residual organic material with low C/P, which may either contain stable P-rich organic compounds (Froelich et al., 1982) or in-situ synthesized bacterial remains with low C/P ratios (Ingall and Van Cappellen, 1990 and references therein). The formation of polyphosphate and subsequent transformation to non-metabolizable organic P such as phosphate esters and phosphonates results in enrichment of P_{org} relative to C_{org} (Dale et al., 2016 and references are therein).

Thus the low C_{org}/P_{org} ratio in some of the CIB sediments are likely due to extensive degradation of organic matter coupled with low sedimentation rates in the area (Borole, 1993; Nath et al., 2013) and long exposure to oxygen (Nath et.al., 2012). These factors may have resulted in an in-situ formation of non-metabolizable P_{org} via polyphosphate intermediate and residual P_{org}. Low values of C_{org}/P_{react} ratio in red/pelagic clay domain again, indicate the presence of refractory P derived from the atmospheric input.

5.3.2 Contribution of hydrothermal activity to P species in the CIB

Hydrothermal activity and submarine weathering of basalt can act as either source or sink of P to the ocean (Baturin, 1982; Föllmi, 1996). The scavenging of P in hydrothermal areas occurs via co-precipitation/sorption onto volcanogenic ferric oxyhydroxides or by authigenic apatite formation (e.g., Wheat et al., 1996; Ruttenberg, 2003). Thus, the submarine hydrothermal processes constitute an additional sink for marine dissolved phosphate rather than a source (Froelich et al., 1977, 1982; Feely et al., 1990; Wheat et al., 1996, 2003; Paytan and McLaughlin, 2007) and strongly affect the overall geochemical balance of P in the world ocean (Bloch, 1978; Wheat et al., 2003).

The highest P_{total} content (81.4 μmol/g) is observed at location AA/8. The possibility of an intraplate volcanism due to reactivation of tectonic activity was reported at this station which is located on the flanks of a seamount and is in the vicinity of 76°30′ E fracture zone (Mascarenhas-Pereira et al., 2006). The depletion in C_{org}, dissolution features of radiolarian skeletons, presence of minerals such as smectite and zeolites and distinctly different magnetic properties in the altered sediments have been attributed to the hydrothermal alteration in the same location (Nath et al., 2008). The sediments have all the geochemical

characters typical of metalliferous nature (Mascarenhas-Pereira and Nath, 2010). Furthermore, in this location, a doubling of ^{14}C uptake, a 250 times increase in the number of autotrophic nitrifiers, a four-fold lowering in the number of aerobic sulphur oxidizers and a higher order of denitrifiers were found when compared to the northern CIB. These were attributed to the prevalence of a potentially autotrophic microbial community in response to hydrothermal activity (Das et al., 2011b). Thus the highest P_{total} content observed at location AA/8 may be related to hydrothermal activity. In hydrothermal systems, the plume particulates can have P as high as 5% which correlates well with Fe (e.g., Feely et al., 1991). To see if the data of one station with high P (#AA/8) are unusual, P in metalliferous sediments of Bauer Deep and EPR (Froelich et al., 1977) is plotted against Fe **(Fig. 5.14)**. And the AA/8 data with high P fall exactly in the field of metalliferous sediments. High P may have been incorporated into the sediments by adsorption or co-precipitation from seawater and/or by the precipitation of P originating in hydrothermal solutions themselves (Froelich et al., 1977). Enrichment of P occurs in hydrothermal sediments largely due to co-precipitation rather than adsorption (Poulton and Canfield, 2006) and results in an enrichment of Fe and P_{Fe}.

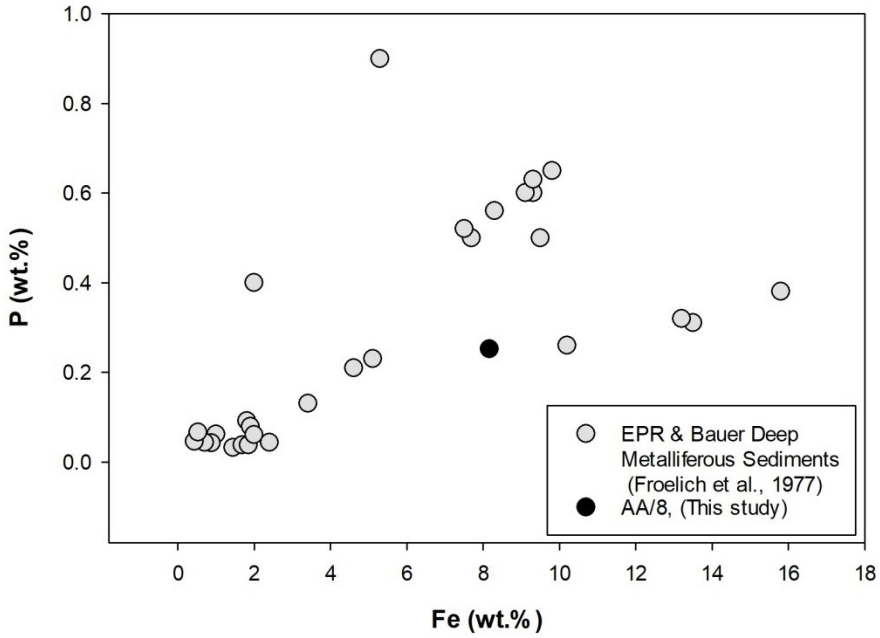

Figure 5.14. *P and Fe bi-plot showing hydrothermally altered AA/8 sediment in relation to metalliferous sediment data of Bauer Deep and EPR (Froelich et al., 1977).*

P_{auth} is the largest pool of sedimentary P at location AA/8 and accounts for 35 % of the P_{total}. The authigenic apatite formation was reported earlier at some ridge flank sediments where porewater phosphate and fluoride gradient provided evidence for their growth (Wheat et al., 1996; Ruttenberg, 2003). The hydrothermal iron oxyhydroxides undergo diagenesis and primary ferrihydrite precipitate gets transformed to goethite which is a more stable mineral. During this transformation, scavenged P will be incorporated into secondary goethite or precipitates as authigenic apatite (Poulton and Canfield, 2006) and leads to an enrichment of P_{auth} content. High P_{org} content in these sediments may be a result of microbial activity.

Chemosynthetic activity was reported earlier at this site (Das et al., 2011b). Chemosynthetic bacteria use chemical energy to produce biomass and such microbial processes were reported earlier at the hydrothermal vent of Loihi seamount (Karl et al.,

1989), an intraplate region such as in the CIB. The P content in the bacterial mats in the area was 2.4 wt.% and SEM-EDS analysis indicated that bacterial mat is comprised predominantly of Fe with a significant content of P and Ca. Some bacteria store P as polyphosphate under aerobic condition, these are then converted into nearly non-metabolizable organic P such as phosphate esters and phosphonates (Dale et al., 2016). This microbial sink switching leads to lower C_{org}/P_{org} and C_{org}/P_{react} ratio and the ratio obtained at AA/8 station is low compared to previously reported values for oxic sediments (Ingall et al., 1993; Dale et al., 2016). Thus, hydrothermal processes seem to locally exert a major role in P cycling in this part of the basin.

5.3.3. P in the sediment cores - interpreting the role of diagenesis in P cycling

Porewater profiles reflect the diagenetic remobilization of P in sediments with dissolution and remineralization processes releasing P to the porewater. Organic matter degradation and reduction of iron oxyhydroxides are major processes that affect the porewater DIP concentration (e.g., Ingall and Jahnke, 1994; Slomp et al., 1996). However, the deep-sea environments are characterized by a low input of photosynthetically produced organic matter (e.g., Suess et al., 1980; Das et al., 2011a; Nath et al., 2012). Most of the organic matter degradation occurs during its transport through the water column and deep-sea sediments receive only ~1 – 5% of the organic matter exported from surface waters (e.g., Broecker and Peng, 1982). The organic matter depleted sediments of the CIB limit the DIP concentration in sediments. The oxic bottom water condition of the CIB sites promotes adsorption of P by iron oxyhydroxides and presence of fine-grained particles such as clay effectively adsorbs P from porewater. Thus, the porewater DIP becomes low and reduces the release of P from sediments to the water column (see Biche et al., 2017).

The porewater DIP values measured in the investigated area **(Fig. 5.5**) were of similar magnitude reported earlier for the CIB (Nath and Mudholkar, 1989; Biche et al., 2017) but very low compared to continental margin sediments of the northern Indian Ocean (Grandel et al., 2000; Woulds et al., 2009; Kraal et al., 2012; Linsy et al., 2018). Nath and Mudholkar (1989) have attributed the downcore gradient of DIP concentrations in the porewater of the CIB sediments to the mobilization of iron oxyhydroxides. The mid-depth depletion of DIP observed at location AA/3 indicates that phosphate is adsorbed or co-precipitated (e.g., Noffke et al., 2012) (**Fig. 5.5**). The relatively low values and constant depth profiles of porewater DIP in most of the stations indicate that the diagenetic remobilization of phosphate is currently not active in the study area. The low influx of C_{org} and highest adsorption of P by fine-grained particles hinders the remobilization of phosphate in the sediments of the CIB and making them a sink for phosphate from the water column.

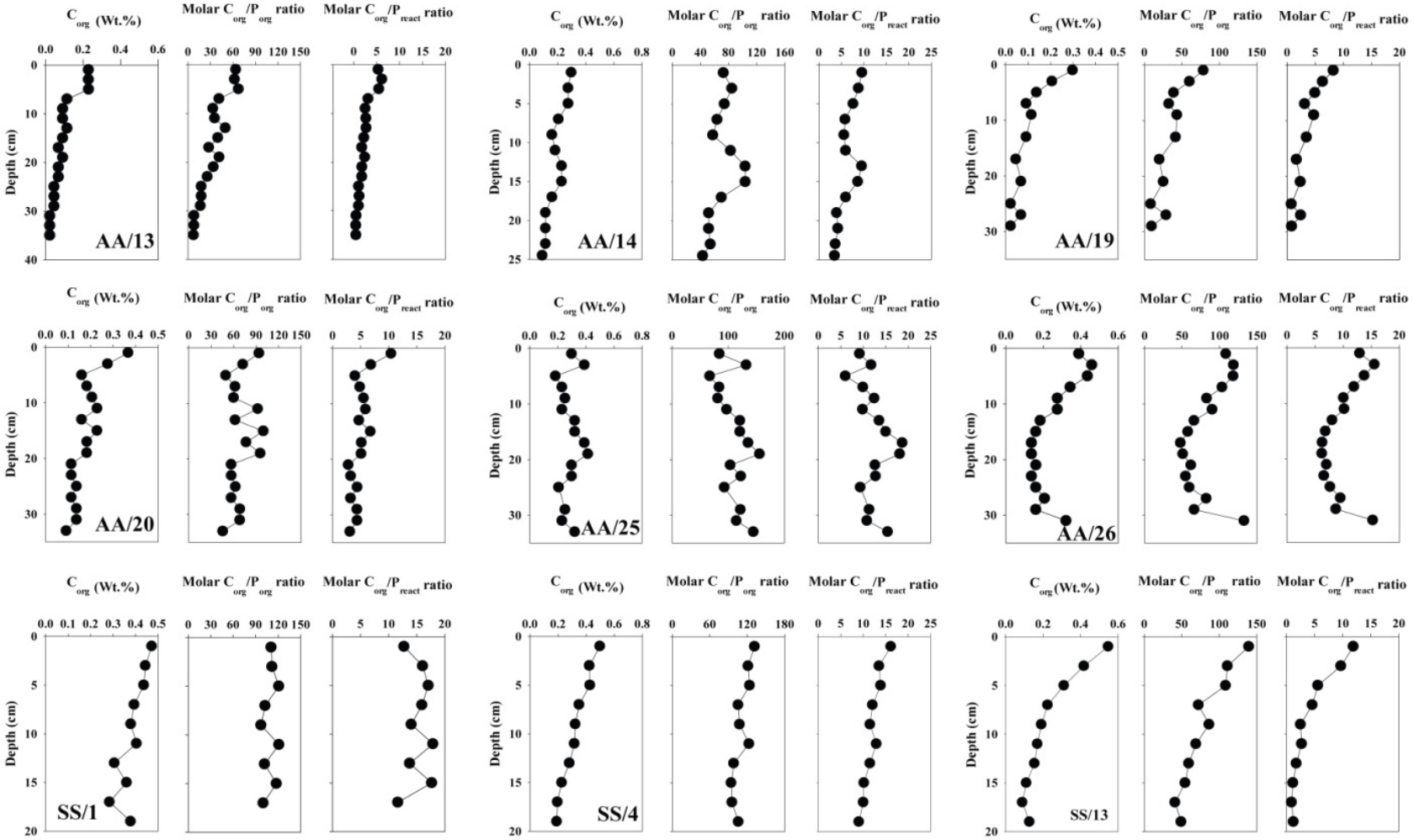

Figure 5.15: *Downcore variation of total organic carbon (C_{org} in wt.%) molar C_{org}/P_{org} and C_{org}/P_{react} ratio*

The downcore decrease of P_{org} and C_{org} contents **(Fig. 5.15**) with depth indicates the degradation of organic matter but the extent of degradation is not high compared to sediments from the continental margin. Even though a degradation of organic matter occurs, the molar C_{org}/P_{org} ratio decreases with depth, which could be explained in two ways viz., (1) bacteria can store P as polyphosphate under aerobic condition which can lead to low C_{org}/P_{org} ratio in sediments; (2) extensive oxidation of sedimentary organic matter leads to the formation of residual organic phases with low C/P ratios (Ingall et al., 1993). The low C_{org}/P_{org} and C_{org}/P_{react} ratios at AA/13 site are indicative of a more refractrory material derived from atmospheric deposition. The low C_{org} and P_{org} contents indicate that organic matter degradation plays a minor role in P cycling in the CIB.

In the present study, relatively high P_{Fe} content (**Fig. 5.7**) indicates that iron oxyhydroxides are potential P carriers to the CIB sediments. The decrease in P_{Fe} content with depth is related to recrystallization and microbial degradation with age (Filippelli and Delaney, 1996; Lucotte et al., 1994). In AA/13, P_{Fe} content decreases with depth till ~20 cm, below which it increases. All other phases also show enrichment with depth indicating a change in depositional pattern. High P_{Fe} content in pelagic clay sediments (at the AA/13 site) compared to the siliceous sediments indicates that iron oxyhydroxides control the burial of P in pelagic clays. In AA/26, a decrease in P_{Fe} is accompanied by an increase in P_{auth} content suggesting the precipitation of authigenic apatite at the expense of P_{Fe}. The adsorption of P is more at the surface of amorphous iron oxyhydroxides such as ferrihydrite due to their large surface area (Slomp et al., 1996). Thus, molar Fe/P ratio in the CDB extract can be used to understand the nature of the associations of P with Fe in sediments (Anschutz et al., 1998). The molar ratio of $(Fe/P)_{CDB}$ in three cores (SS/1, SS/4, and SS/13) varies between

1.7 and 10. (**Fig. 5.16**). The relatively low $(Fe/P)_{CDB}$ ratios in the CIB sediments indicate the presence of iron oxyhydroxides with high adsorption capacity (Anschutz et al., 1998).

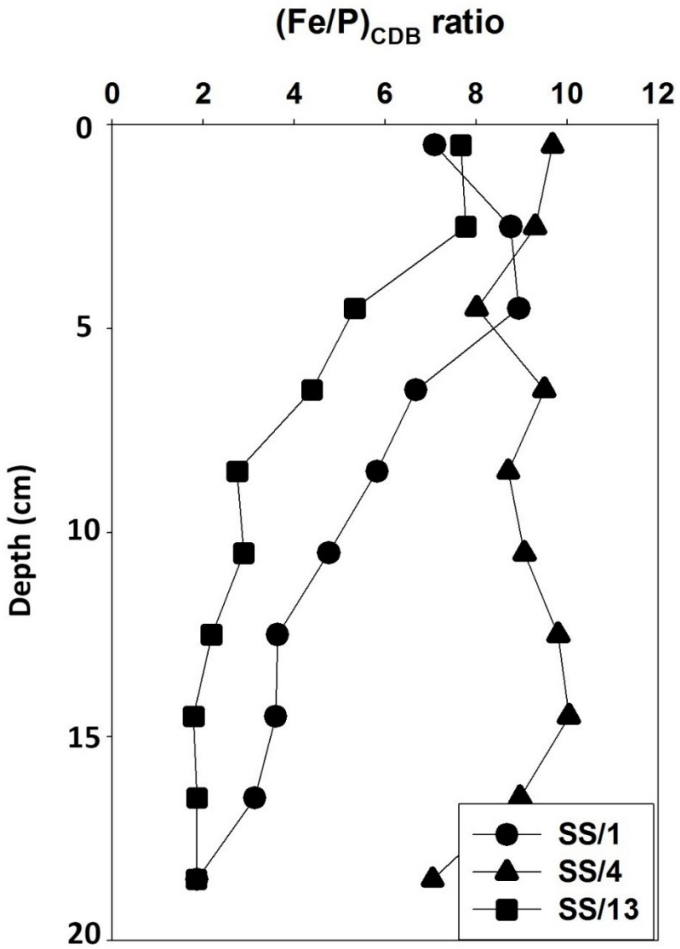

Figure 5.16. *Down core variation of molar $(Fe/P)_{CDB}$ ratio in cores SS/1, SS/4 and SS/13.*

The precipitation of CFA in sediments is a permanent sink for P_{react} in the ocean (Froelich et al., 1982; Ruttenberg and Berner, 1993; Ni et al., 2015). The solid phase downcore P_{auth} profile indicates that CFA locally forms in the CIB sediments. A gradual reduction in P_{bio}, $P_{Fe,}$ and P_{org} in AA/26 is accompanied by an increase in P_{auth} (Fig. 5.7)

indicating the formation of authigenic apatite. The peak observed at ~7 cm in P_{auth} profile (Fig. 5.7) at location AA/14 and a corresponding depletion of porewater DIP (Fig. 5.5) suggest utilization of porewater DIP for the formation of CFA in this area. The low concentration and lack of well-defined trend of P_{auth} with depth in SS/1 and SS/4 suggest that authigenesis is possibly playing only a minor role in the burial of P at these two northern sites mainly floored by siliceous oozes/clays. The surface enrichment and relatively constant P_{auth} contents below the surface are attributed to the depositional changes at AA/19 and AA/25 locations. Out of nine sediment cores studied here, eight of them fall in the siliceous ooze/clay zone while only AA/13 location falls in the pelagic clay zone (close to the siliceous – pelagic boundary Fig. 1). Minor variations are observed in downcore profiles of sedimentary P phases except for the P_{Fe} phase between these two sedimentary settings (Fig. 5.7). The sedimentation rates (Mascarenhas-Pereira et al., 2016) at the studied locations are nearly similar except at AA/13 (0.413 cm/kyr) and AA/26 (0.834 cm/kyr) and are relatively higher than in other cores (Table 5.5). The water depths at sampling sites fall in a narrow range between 4840 and 5307 m and may not be a critical factor between siliceous ooze and pelagic clay settings. The downcore profiles (Fig. 5.15) show a large reduction in C_{org} values in pelagic clays (10-fold compared to ~2-3 times in siliceous clays) showing different degrees of diagenetic processes in these two types of sediments. Low C_{org} values, however, can also reflect an intense water column dissolution and dissolution within the sediments due to low sedimentation rates (long oxygen exposure times - OET - Nath et al., 2012 and the references therein). Thus, the main difference in diagenetic process between siliceous oozes/clays and the pelagic clays seems to be mainly related to iron. Both the P_{Fe} content and P accumulation rate (mainly driven by P_{Fe}) are higher in pelagic clays (**Table 5.6**). As

described in the surface sediment section, diagenetic processes involving Fe are predominant in siliceous oozes. Fe in siliceous clays/oozes reacts with biogenic silica diagenetically to form Fe-rich smectites (Lyle et al., 1977; Rao and Nath, 1988; Nath et.al., 1994) and thus manganese nodules occurring in this sediment domain are Fe-poor (Rao, 1987) compared to those found in pelagic clays (Nath et.al., 1992b; 1994). Lesser biogenic silica content in pelagic red clays may be allowing the availability of Fe both for incorporation in manganese nodules (making them Fe-rich compared to those in siliceous oozes which are Mn-rich - e.g., Nath et.al., 1994) and for Fe-P adsorption**.**

5.4 P burial rate and benthic phosphate flux at the sediment water interface

The accumulation of sediment is the ultimate process by which P is removed from the ocean. The mass accumulation rate of phosphorus (PAR) was estimated using sedimentation rate (S), dry bulk density (DBD) and P content (C) in sediments (see section 2.6 in Chapter 2 for the equations used).

The P_{total} accumulation rate ranged between 0.6 and 11.7 μmol.cm^{-2}.kyr^{-1} (Table 5.5). The P accumulation rate estimated here is slightly lower than that in the Equatorial Pacific Ocean sediments (Filippelli and Delaney, 1996). Compared to deep ocean sediments, the accumulation rate is far higher in continental margin sediments due to high surface productivity and higher sedimentation rates there. The PAR is highest at location AA/13, which is floored by pelagic red clays. In the CIB, 42 % of buried P is in the form of P_{bio} and the burial rate of P_{bio} is 0.72 μmol cm^{-2}.kyr^{-1}(average) at the surface.

The burial rate of P in the entire study area was calculated using an average accumulation rate at the surface and area of the studied site (0.4×10^6 km^2), which was found

to be 0.724×10^{7}mol P yr^{-1}. The area of the CIB is 5.7×10^{6} km^{2} (Nath et al., 1989) and the calculated burial flux in the CIB is roughly 0.01×10^{10} mol P yr^{-1} which is very low compared to the equatorial Pacific (0.6×10^{10} mol P yr^{-1}) (Filippelli and Delaney, 1996). The global burial flux of P in the siliceous ooze ranges between 0.108 and 0.152 Mt yr^{-1} while the pelagic red clays constitute 0.463-0.530 Mt P yr^{-1} (Baturin, 2003). The global burial rate of P (calculated by Filippelli and Delaney, 1996) is 21×10^{10} mol yr^{-1}. Even though the CIB represents roughly about 1.5% of the global area, the burial of P contributed by the CIB accounts to only about 0.05 % of the global value.

The benthic flux of phosphate calculated for three sediment cores (SS/1, SS/4, and SS/13) ranged between 0.0093 and 0.133 μmol cm^{-2} kyr^{-1}. The positive value indicates that flux of phosphate is from the water column to sediments and thus the sediment is a sink for P. Thus, result of this study indicate that P reaching the CIB sediments undergoes burial without much regeneration. However, the remobilization of P must be taking place within the water column.

Conclusions

The results of sequential chemical extraction studies of P in the CIB sediments indicate that the dominant P bearing component is P_{bio} followed by P_{auth}, P_{Fe}, P_{det}, and P_{org}. The high P_{bio} content associated with siliceous oozes is due to high primary productivity. P_{auth} is mainly deposited by atmospheric input with a relatively low in situ precipitation. The oxic bottom water condition and hydrothermal activity in the CIB promote the adsorption of P by iron oxyhydroxides and makes P_{Fe} an important pool of sedimentary P phases. Low C_{org} and P_{org} contents indicate a minor role of organic matter in P diagenesis. The C_{org}/P_{org} ratios lower than the Redfield ratio are either due to the degradation of organic matter within the water column or supply of refractory material derived from the atmospheric deposition. A low influx of C_{org} and the highest adsorption of P by fine-grained particles and iron oxyhydroxides hinder the remobilization of P in the CIB sediments and limit the porewater DIP concentration.

A two-fold increase in P_{total} and high P_{auth} at AA/8 location (on a seamount flank in the vicinity of a fracture zone) is seen in hydrothermally altered sediments suggest the role of hydrothermal activity in P accumulation in the southern part of the study area. The burial flux of P in the CIB is 0.01×10^{10} mol P per year which accounts for 0.05% of the global value. Results of benthic flux calculation indicate that the deep-sea sediments of the CIB are an important burial sink for P.

Table: 5.1 Solid-phase phosphorus species and molar C_{org}/P_{org} and Molar C_{org}/P_{react} ratios in surface sediments.

Station Name	P_{bio}	P_{Fe}	P_{auth}	P_{det}	P_{org}	P_{total}	P_{react}	C_{org}	Molar C_{org}/P_{org}	Molar C_{org}/P_{react}
	µmol/g							(wt.%)		
SS/1	16.13	8.24	2.93	3.11	3.55	33.96	30.85	0.47	110.19	12.70
SS/4	14.07	6.65	1.81	2.65	3.15	28.32	25.67	0.50	132.26	16.23
SS/13	17.72	10.97	6.42	4.11	3.27	42.49	38.37	0.55	140.14	11.94
AA/1R	11.62	2.93	10.21	2.78	4.38	31.92	29.14	0.34	65.62	9.86
AA/2RR	10.91	2.53	7.51	1.66	3.54	26.15	24.49	NA	NA	NA
AA/3R	9.67	2.13	8.66	2.18	2.77	25.41	23.22	0.18	55.38	6.60
AA/4	12.86	3.13	8.86	2.03	3.31	30.18	28.15	0.41	104.22	12.24
AA/5	13.21	4.39	13.70	7.65	3.46	42.41	34.76	0.46	110.65	11.02
AA/6	8.96	4.46	13.89	8.40	2.69	38.41	30.00	0.14	42.62	3.83
AA/7	9.31	4.46	14.27	3.16	3.31	34.51	31.35	0.25	63.66	6.71
AA/8	11.80	11.12	28.59	21.67	8.21	81.39	59.72	0.18	18.62	2.56
AA/9	10.72	5.39	13.89	5.26	3.61	38.87	33.62	NA	NA	NA
AA/10	11.79	5.98	12.73	3.08	3.15	36.74	33.66	0.21	54.64	5.12
AA/11	9.48	4.32	12.15	3.68	3.08	32.71	29.03	0.30	80.73	8.56
AA/12R	7.18	2.39	9.05	2.71	2.46	23.79	21.09	0.09	31.16	3.64
AA/13	11.83	10.57	10.30	5.47	2.99	41.16	35.69	0.23	63.88	5.36
AA/14	11.97	3.16	7.36	5.14	3.41	31.04	25.89	0.30	72.86	9.59
AA/15	10.02	4.46	8.28	3.08	3.84	29.69	26.60	0.32	69.79	10.08
AA/16	10.38	4.53	10.22	3.16	2.85	31.13	27.98	0.37	107.60	10.95
AA/17	13.75	3.66	7.32	1.81	3.54	30.08	28.27	0.34	81.14	10.16
AA/18	12.34	3.80	6.73	2.71	3.61	29.17	26.47	0.30	68.92	9.40
AA/19	12.15	2.51	12.36	4.91	3.15	35.08	30.16	0.30	78.77	8.24
AA/20	15.89	1.53	8.67	2.79	3.26	32.14	29.35	0.37	93.93	10.43
AA/21	10.38	3.33	7.31	1.58	3.92	26.52	24.94	0.39	82.94	13.04
AA/22	11.44	5.19	7.51	2.11	3.84	30.08	27.98	0.30	64.81	8.90
AA/23	13.56	4.59	8.85	1.43	3.76	32.21	30.77	0.46	101.69	12.44
AA/24	9.49	3.39	5.57	1.88	3.99	24.33	22.44	0.32	67.03	11.93
AA/25	14.54	0.79	8.80	2.90	2.94	29.98	27.08	0.30	84.47	9.19
AA/26	13.39	2.94	5.78	1.81	3.00	26.93	25.11	0.39	108.49	12.95

Table 5.2: Relative percentage of solid-phase phosphorus species in the surface sediments.

Station Name	Relative Percentage				
	P_{bio}%	P_{Fe}%	P_{auth} %	P_{det} %	P_{org} %
SS/1	47.49	24.26	8.62	9.16	10.47
SS/4	49.67	23.47	6.39	9.36	11.12
SS/13	41.70	25.82	15.10	9.68	7.70
AA/1R	36.42	9.18	31.98	8.71	13.71
AA/2RR	41.74	9.67	28.71	6.34	13.53
AA/3R	38.06	8.38	34.08	8.58	10.90
AA/4	42.61	10.36	29.35	6.73	10.95
AA/5	31.15	10.35	32.30	18.05	8.16
AA/6	23.32	11.61	36.17	21.88	7.02
AA/7	26.99	12.92	41.36	9.15	9.58
AA/8	14.50	13.66	35.13	26.62	10.09
AA/9	27.58	13.85	35.74	13.52	9.30
AA/10	32.08	16.29	34.65	8.39	8.59
AA/11	28.99	13.21	37.14	11.25	9.41
AA/12R	30.19	10.06	38.03	11.37	10.35
AA/13	28.73	25.67	25.02	13.30	7.27
AA/14	38.57	10.17	23.70	16.57	10.99
AA/15	33.76	15.02	27.90	10.38	12.95
AA/16	33.35	14.54	32.82	10.14	9.15
AA/17	45.73	12.17	24.32	6.01	11.76
AA/18	42.28	13.01	23.06	9.27	12.38
AA/19	34.63	7.14	35.23	14.01	8.99
AA/20	49.44	4.76	26.97	8.69	10.14
AA/21	39.14	12.55	27.57	5.97	14.78
AA/22	38.02	17.25	24.95	7.01	12.77
AA/23	42.12	14.25	27.49	4.45	11.69
AA/24	39.01	13.95	22.89	7.74	16.42
AA/25	48.50	2.65	29.36	9.66	9.82
AA/26	49.72	10.94	21.48	6.74	11.13

Table 5.3. Partitioning of relative percentage of P phases in the deep Pacific sediments (Filippelli and Delaney, 1996; Ni et al., 2015), central Arabian Sea (Schenau et al., 2005), Central Indian Basin (present study), parts of eastern and western Arabian Sea (Schenau and De Lange, 2001), western continental margin of India, Arabian Sea (Babu and Nath, 2005) and the Bay of Bengal (Babu and Ramaswamy, 2017).

P sink	Central Pacific	Equtorial Pacific	Central Arabian Sea	Northern Arabian Sea	Eastern Arabian Sea	Eastern continental margin of India	Present Study
P_{org}	7 %	5 %	12 %	22 %	14 %	29 %	11 %
P_{Fe}	3 %	11 %	15 %	24 %	6 %	24 %	13 %
P_{det}	46 %	1 %	12 %	18 %	15 %	19 %	11 %
P_{ads}	1 %	5 %	32 %	28 %	41 %	18 %	37 %
P_{fish}	43 %	78 %					
P_{auth}			29 %	8 %	24 %	10 %	28 %

Table 5.4: Solid-phase phosphorus species and molar C_{org}/P_{org} and Molar C_{org}/P_{react} ratios for the sediment cores.

Station Name	Sediment Depth (cm)	P_{bio} (µmol/g)	P_{Fe} (µmol/g)	P_{auth} (µmol/g)	P_{det} (µmol/g)	P_{org} (µmol/g)	P_{total} (µmol/g)	C_{org} (wt. %)	Molar C_{org}/P_{org}	Molar C_{org}/P_{react}
BC-13	1	11.8	10.6	10.3	5.5	3.0	41.2	0.23	64	5
	3	10.3	10.9	6.8	7.9	3.1	39.0	0.23	62	6
	5	14.3	10.0	7.7	9.3	2.8	44.1	0.23	67	6
	7	12.2	7.1	8.7	5.5	2.3	35.9	0.11	42	3
	9	12.8	8.0	7.5	4.1	2.3	34.6	0.09	33	3
	11	13.3	6.9	6.2	4.2	2.1	32.8	0.09	36	3
	13	16.4	7.8	9.1	2.8	1.9	37.9	0.11	50	3
	15	15.8	6.4	10.1	2.9	1.9	37.1	0.09	40	2
	17	15.2	6.9	8.2	4.6	2.1	37.1	0.07	28	2
	19	14.7	6.4	8.7	2.6	1.8	34.2	0.09	42	2
	21	15.8	6.3	7.8	4.0	1.7	35.6	0.07	34	2
	23	14.9	6.6	8.4	3.2	2.2	35.3	0.07	26	2
	25	16.2	7.6	9.1	4.3	2.1	39.4	0.05	18	1
	27	16.2	6.8	6.6	3.8	2.1	35.5	0.05	18	1
	29	16.2	8.5	8.4	5.7	2.3	41.1	0.05	17	1
	31	13.9	9.0	9.8	4.7	2.4	39.8	0.02	8	1
	33	16.4	10.1	10.7	5.3	2.4	44.8	0.02	8	0
	35	16.2	10.2	9.4	5.5	2.5	43.9	0.02	8	0
BC-14	1	12.0	3.2	7.4	5.1	3.4	31.0	0.30	73	10
	3	12.3	3.4	7.5	3.2	2.7	29.2	0.28	85	9
	5	14.0	4.3	8.7	3.1	3.1	33.2	0.28	74	8
	7	14.8	3.4	8.7	3.6	2.7	33.1	0.21	64	6
	9	11.6	2.9	7.2	3.1	2.3	27.0	0.16	58	6
	11	12.7	3.0	8.1	3.2	1.8	28.8	0.18	83	6
	13	9.7	2.3	6.2	2.6	1.8	22.6	0.23	104	10
	15	10.3	2.1	7.9	2.4	1.8	24.5	0.23	104	9
	17	11.0	2.6	7.0	2.5	1.9	25.0	0.16	70	6
	19	11.6	2.3	8.5	3.6	1.8	27.8	0.11	52	4
	21	11.4	2.0	7.3	3.7	1.8	26.3	0.11	52	4
	23	12.3	2.7	9.2	3.6	1.8	29.5	0.11	54	4
	24.5	10.8	2.5	6.8	2.8	1.8	24.7	0.09	43	4

Table 5.4 continued

Station Name	Sediment Depth (cm)	P_{bio} (µmol/g)	P_{Fe} (µmol/g)	P_{auth} (µmol/g)	P_{det} (µmol/g)	P_{org} (µmol/g)	P_{total} (µmol/g)	C_{org} (wt.%)	Molar C_{org}/P_{org}	Molar C_{org}/P_{react}
BC-19	1	12.1	2.5	12.4	4.9	3.2	35.1	0.30	79	8
	3	14.7	2.3	7.3	5.0	2.9	32.3	0.21	60	6
	5	11.6	2.2	6.5	4.2	2.9	27.3	0.14	39	5
	7	13.3	1.8	7.0	4.8	2.3	29.2	0.09	33	3
	9	10.7	1.8	5.4	3.3	2.2	23.3	0.11	44	5
	11	11.8	1.7	7.5	3.6	1.8	26.4			
	13	11.4	1.6	7.3	5.4	1.8	27.5	0.09	42	3
	15	10.9	1.8	7.9	4.1	2.0	26.6			
	17	11.0	1.9	8.0	6.7	1.9	29.6	0.05	20	2
	19	11.4	3.2	7.9	4.9	2.1	29.5			
	21	11.0	2.9	8.0	4.7	2.3	29.0	0.07	25	2
	23	11.2	1.9	8.6	4.9	2.2	28.8			
	25	11.6	3.2	8.0	7.3	2.3	32.4	0.02	8	1
	27	13.1	1.9	6.7	3.2	2.0	26.8	0.07	29	2
	29	10.1	2.5	8.6	5.2	2.0	28.4	0.02	10	1
	31	10.3	2.0	7.2	4.3	1.9	25.7			
BC-20	1	15.9	1.5	8.7	2.8	3.3	32.1	0.37	94	10
	3	18.2	1.9	10.4	2.5	3.2	36.2	0.28	72	7
	5	17.4	1.0	12.3	2.1	2.7	35.6	0.16	50	4
	7	17.3	1.0	10.8	2.1	2.5	33.7	0.18	62	5
	9	17.7	0.9	9.6	2.6	2.9	33.7	0.21	60	6
	11	19.0	1.6	9.8	2.9	2.1	35.4	0.23	92	6
	13	18.6	0.9	6.7	2.0	2.2	30.4	0.16	62	5
	15	17.1	0.9	8.5	2.3	1.9	30.6	0.23	100	7
	17	18.3	1.2	8.3	2.8	2.0	32.5	0.18	77	5
	19	17.7	1.3	9.4	2.3	1.6	32.3	0.18	96	5
	21	20.8	0.9	10.6	3.4	1.7	37.3	0.11	57	3
	23	18.2	1.0	8.5	1.8	1.7	31.2	0.11	57	3
	25	16.5	0.5	7.3	2.3	1.8	28.5	0.14	63	4
	27	18.1	1.6	8.3	2.1	1.7	31.7	0.11	57	3
	29	15.7	0.1	8.9	1.8	1.7	28.2	0.14	68	4
	31	15.9	0.7	7.9	2.3	1.7	28.4	0.14	68	4
	33	15.9	0.3	6.7	2.0	1.7	26.7	0.09	46	3

Table 5.4 continued

Station Name	Sediment Depth (cm)	P_{bio} (µmol/g)	P_{Fe} (µmol/g)	P_{auth} (µmol/g)	P_{det} (µmol/g)	P_{org} (µmol/g)	P_{total} (µmol/g)	C_{org} (wt. %)	Molar C_{org}/P_{org}	Molar C_{org}/P_{react}
BC-25	1	14.5	0.8	8.8	2.9	2.9	30.0	0.30	84	9
	3	14.9	1.6	8.6	2.7	2.5	30.3	0.39	132	12
	5	13.6	1.1	8.4	3.1	2.3	28.5	0.18	67	6
	7	11.7	0.9	4.4	1.9	2.3	21.2	0.23	84	10
	9	10.7	0.6	3.0	2.2	2.6	19.1	0.25	82	12
	11	12.2	1.0	4.2	2.0	2.0	21.4	0.23	97	10
	13	12.2	0.9	4.4	2.3	2.2	22.0	0.32	121	14
	15	11.7	1.5	2.4	2.3	2.2	20.1	0.32	121	15
	17	11.7	0.9	2.4	2.7	2.4	20.1	0.39	136	19
	19	11.8	1.4	3.5	1.7	2.2	20.7	0.41	156	18
	21	10.9	1.3	5.2	2.6	2.4	22.3	0.30	104	13
	23	12.8	1.7	3.0	2.3	2.0	21.8	0.30	123	13
	25	12.2	1.3	3.0	2.8	1.8	21.2	0.21	93	9
	27	12.2	2.4	2.8	2.3	1.9	21.6	1.01	455	44
	29	12.4	1.6	2.8	2.5	1.7	21.1	0.25	122	11
	31	12.1	1.0	3.0	2.2	1.7	19.9	0.23	115	11
	33	13.2	1.0	1.3	2.3	1.8	19.6	0.32	145	15
BC-26	1	13.4	2.9	5.8	1.8	3.0	26.9	0.39	108	13
	3	13.8	3.5	4.1	1.6	3.2	26.2	0.46	119	16
	5	15.5	3.5	4.3	1.5	3.1	27.9	0.44	118	14
	7	14.0	3.2	4.1	2.3	2.8	26.3	0.34	103	12
	9	14.1	2.9	3.0	1.8	2.8	24.6	0.28	83	10
	11	13.2	3.0	3.8	1.8	2.5	24.3	0.28	90	10
	13	10.9	2.4	3.4	1.6	2.3	20.7	0.18	66	8
	15	10.5	2.7	4.0	1.6	2.3	21.1	0.16	58	7
	17	10.3	2.5	3.0	1.6	2.4	19.8	0.14	48	6
	19	9.0	2.5	4.7	1.6	2.2	20.1	0.14	51	6
	21	9.2	2.3	5.4	1.6	2.2	20.7	0.16	62	7
	23	8.8	1.6	4.9	1.7	2.1	19.1	0.14	55	7
	25	8.4	1.7	5.1	1.6	2.2	19.0	0.16	60	8
	27	8.1	1.6	6.3	1.6	2.1	19.7	0.21	82	10
	29	7.9	1.7	3.8	1.5	2.0	16.8	0.16	66	9
	31	9.0	1.5	5.1	1.6	2.0	19.2	0.32	133	15

Table 5.4 continued

Station Name	Sediment Depth (cm)	P_{bio} (µmol/g)	P_{Fe} (µmol/g)	P_{auth} (µmol/g)	P_{det} (µmol/g)	P_{org} (µmol/g)	P_{total} (µmol/g)	C_{org} (wt.%)	Molar C_{org}/P_{org}	Molar C_{org}/P_{reac}
SS/1	0.5	16.1	8.2	2.9	3.1	3.6	34.0	0.47	111	13
	2.5	13.0	5.4	1.3	3.1	3.3	26.1	0.44	112	16
	4.5	12.1	4.8	1.4	3.1	3.0	24.4	0.44	121	17
	6.5	11.6	4.3	1.5	2.5	3.2	23.1	0.39	103	16
	8.5	12.7	4.7	1.8	2.7	3.2	25.2	0.38	97	14
	10.5	10.2	3.7	2.1	2.3	2.8	21.1	0.40	121	18
	12.5	10.5	4.4	1.1	2.1	2.5	20.6	0.31	102	14
	14.5	9.4	4.1	1.0	2.6	2.6	19.6	0.36	118	18
	16.5	11.6	4.4	2.0	2.0	2.4	22.4	0.28	100	12
	18.5	10.2	3.7	1.8	2.2	2.3	20.1	0.38	_	
SS/4	0.5	14.1	6.6	1.8	2.7	3.2	28.3	0.50	132	16
	2.5	14.2	6.7	2.2	2.8	2.9	28.8	0.42	121	14
	4.5	14.0	6.9	1.9	2.2	2.9	27.8	0.43	124	14
	6.5	13.3	6.9	1.2	2.9	2.8	27.0	0.35	106	12
	8.5	12.3	6.8	1.7	3.1	2.5	26.4	0.32	108	12
	10.5	10.7	7.2	0.3	3.8	2.1	24.2	0.32	123	13
	12.5	10.7	5.5	1.7	3.0	2.4	23.3	0.28	98	12
	14.5	10.9	4.2	1.4	2.2	2.0	20.7	0.23	94	10
	16.5	9.0	4.2	1.3	3.0	1.7	19.3	0.20	96	10
	18.5	9.8	5.6	0.6	2.7	1.5	20.3	0.19	106	9
SS/13	0.5	17.7	11.0	6.4	4.1	3.3	42.5	0.55	140	12
	2.5	18.2	8.7	5.9	3.3	3.1	39.2	0.42	111	10
	4.5	22.7	11.5	9.7	2.5	2.4	48.8	0.31	109	6
	6.5	21.3	11.6	5.2	3.5	2.6	44.2	0.22	72	5
	8.5	31.5	11.5	18.6	3.3	1.8	66.8	0.19	87	3
	10.5	27.2	11.6	11.6	3.0	2.1	55.5	0.17	69	3
	12.5	34.6	15.1	21.2	3.2	2.2	76.1	0.15	59	2
	14.5	36.6	14.9	26.7	2.8	1.7	82.7	0.11	55	1
	16.5	38.6	15.2	25.4	2.7	1.8	83.7	0.09	41	1
	18.5	40.5	15.3	27.9	3.6	2.1	89.4	0.13	49	1

Table 5.5 Table showing the sedimentation rates and mass accumulation rates of P_{total}, P_{react}, P_{auth}, P_{Fe}, P_{bio}, and P_{org} at the surface

Station name & sediment domain	Sedimentation rate ($cm^{-2}\,kyr^{-1}$)	Mass accumulation rate ($g\,cm^{-2}kyr^{-1}$)	P_{total} mass accumulation rate ($\mu mol.cm^{-2}.kyr^{-1}$)	P_{react} mass accumulation rate ($\mu mol.cm^{-2}.kyr^{-1}$)	P_{auth} mass accumulation rate ($\mu mol.cm^{-2}.kyr^{-1}$)	P_{Fe} mass accumulation rate ($\mu mol.cm^{-2}.kyr^{-1}$)	P_{bio} mass accumulation rate ($\mu mol.cm^{-2}.kyr^{-1}$)	P_{org} mass accumulation rate ($\mu mol.cm^{-2}.kyr^{-1}$)
AA/13 - Pelagic red clay	0.41	0.10	3.98	3.45	1.00	1.02	1.14	0.29
AA/14 - Siliceous ooze/clay	0.27	0.02	0.69	0.57	0.16	0.07	0.26	0.08
AA/19 Siliceous ooze/clay	0.23	0.02	0.81	0.69	0.28	0.06	0.28	0.07
AA/20 Siliceous ooze/clay	0.23	0.06	1.98	1.81	0.53	0.09	0.98	0.20
AA/25 Siliceous ooze/clay	0.23	0.05	1.54	1.39	0.45	0.04	0.75	0.15
AA/26 Siliceous ooze/clay	0.83	0.07	1.87	1.74	0.40	0.20	0.93	0.21

Table 5.6 Table showing a comparison of different geochemical parameters in the pelagic and siliceous sedimentary settings

	Pelagic			siliceous		
Parameter	Minimum	Maximum	Average	Minimum	Maximum	Average
P_{bio} (µmol /g)	10.3	16.4	14.6	7.9	40.0	14.2
P_{Fe} (µmol /g)	6.3	10.9	8.1	0.1	15.0	3.5
P_{auth} (µmol /g)	6.2	10.4	8.5	0.3	27.9	7.0
P_{det} (µmol /g)	2.6	9.3	4.8	1.5	7.3	3.0
P_{org} (µmol /g)	1.7	3.1	2.3	1.5	3.6	2.3
P_{total} (µmol /g)	32.8	44.8	38.3	16.8	89.4	29.5
C_{org} (wt.%)	0.02	0.22	0.09	0.03	0.25	1.00
Molar C_{org}/P_{org}	7.6	67.4	33.3	8.4	155.0	82.9
Molar C_{org}/P_{react}	0.5	6.2	2.4	0.8	18.7	8.4
porewater DIP (µmol /L)	0.1	3.7	1.8	0.1	2.5	1.9
P accumulation rate (µmol.cm $^{-2}$·kyr^{-1})	4.0	10.7	7.6	0.7	4.4	2.0

Chapter 6

Quantification of the diffusive flux of phosphate in the Northern Indian Ocean

Chapter 6

6.1 Introduction

Phosphorus (P) plays a vital role in the marine primary productivity since it acts as a limiting nutrient over a geological timescale. Enhanced regeneration of P induces high primary productivity in the photic zone mainly in shallow areas, thereby recycling of P in sediment received much attention. Recycling of P from sediments is regulated by bottom water oxygen concentration and the benthic regeneration of P is more extensive under oxygen-depleted condition (Ingall and Jahnke, 1994). Presence of iron oxyhydroxides in the sediment can limit the benthic release of P by adsorbing dissolved P from porewater. Under reducing condition iron oxyhydroxides undergo microbially induced reductive dissolution and thereby enhances the concentration of P in sediment porewater (Slomp et al., 1996). Another factor controlling the regeneration process is the flux of organic matter and their degradation. During the degradation of organic matter, P would be released to porewater. Further, enhanced regeneration of P relative to carbon will occur under reducing condition (Ingall and Jahnke, 1997). In addition to these processes, microorganisms accumulate P in the form of polyphosphate under oxic condition and releases phosphate under oxygen-depleted condition (Gächter and Meyer, 1993).

Among the sources and sinks of P, the regeneration flux from sediments as a source is not well constrained. There are very few regional estimates of diffusive regeneration/return fluxes of phosphate from marine sediments to overlying bottom waters (e.g., Hensen et al., 1998; Zabel et al., 1998), while the global estimates are rare. The most comprehensive global estimate is based on only 193 published pore water phosphate profiles (Colman and Holland, 2000) (Fig. 6 .1). The total pre-agricultural return flux of P from

marine sediments was estimated by those authors to be ca. 12 x 10^{11} mol P/yr, which is more than an order of magnitude larger than the riverine flux of total dissolved P to the oceans (ca. 0.3 x 10^{11} mol P/yr). The current estimates of phosphate contained in the present day ocean is much less than that present in several giant phosphorite deposits on land (Froelich et al., 1982) which either may mean that the present day ocean is impoverished or phosphate contained in some reservoirs is underestimated. Wheat et al., (2003) argued that the modern P budget is unbalanced with total sinks outpacing sources. While, agreeing to the imbalance in marine P budget of the prehuman modern ocean, with P accumulation exceeding the inputs, Wallmann, (2010) found that the P turnover at continental margins is well balanced. As the estimates of Coleman and Holland (2000) are based on less than 200 locations, there is a need for new measurements in other regions and depositional environments and collation with other results published in the last 18 years for a possible revised estimate. One of the major gaps is the lack of quality data from the Indian Ocean, which make the global estimates incomplete.

Here, an attempt is made to assess the benthic regeneration fluxes of P in the Northern Indian Ocean. Both, Arabian Sea and the Bay of Bengal in the Northern Indian Ocean are characterized by perennial oxygen minimum zone (e.g., McCreary et al., 2013) and seasonal anoxia is also reported in the eastern Arabian Sea (Naqvi et al., 2009). The present study of Northern Indian Ocean assumes importance as the previous studies of Coleman and Holland (2000), Wallmann (2010) and others have also found that the phosphate return fluxes, scaled to carbon regeneration fluxes (say C:P ratios), are significantly greater from highly reduced sediments than from highly oxidized sediments. Moreover, the benthic fluxes from continental margins contributed more than 70% of total

dissolved phosphate to pre-human global oceans. In the current rate of increase in CO_2 emission ratio, the P weathering and sedimentary P release is expected to strongly enlarge the marine P inventory and a multi-fold increase in the suboxic water volume on millennial timescales (Niemeyer et al., 2017). Thus, there is a need for global estimates of P being released by sediments from all parts of the ocean.

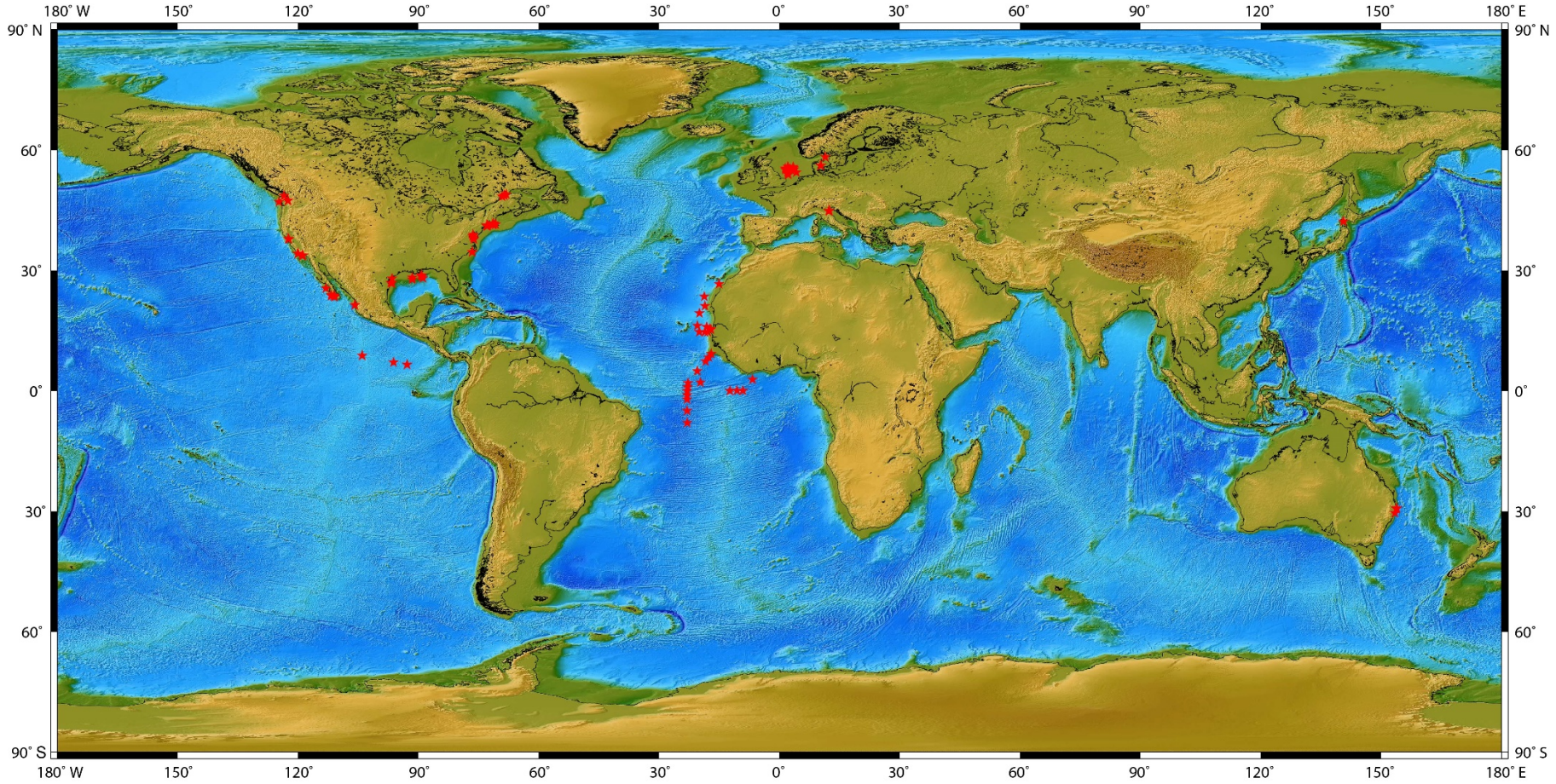

Figure 6.1: Map showing the locations used for global P diagenetic flux estimation by Colman and Holland, (2000). The lack of data from the Indian Ocean is clearly seen.

Along with the intense oxygen minimum zone at intermediate depth, vigorous circulation during the south-west monsoon affects a very large area where nutrient-rich subsurface water is brought to the surface enhancing biological production and contributes to the formation of oxygen-depleted condition along the western continental shelf of India and some part of Pakistan shelf (Banse, 1968; Sankaranarayanan, 1978; Naqvi et al., 2000; Habeebrehman et al., 2008). Thus, a need of benthic nutrient dynamics study is essential for the northern Indian Ocean. High benthic regeneration of P is known to occur in the OMZ of Arabian Sea (Schenau and De Lange 2001 and Woulds et. al., 2009). Previously, benthic P fluxes in the Arabian Sea were studied by Grandel et al. (2000), Schenau and De Lange (2001) and Woulds et al. (2009). Grandel et al. (2000) studied the benthic P fluxes in the abyssal areas of the Arabian Sea and reported that benthic P fluxes were showing distinct spatial and regional variation. In upwelling regions, fish debris will be an important source of P (Suess, 1981) and highest P flux obtained at continental slope of the Arabian Sea underlying low bottom water condition is reported to be mainly induced by the dissolution of fish debris (Schenau and De Lange, 2001). To the author's knowledge, no known reports of benthic P fluxes are available for the Bay of Bengal.

In this context, a comprehensive study of benthic P dynamics in the Northern Indian Ocean was undertaken by estimating the diffusive flux of P using porewater phosphate concentration in sediments from varying oceanographic settings. This study aims to (1) assess the P regeneration fluxes at the sediment-water interface in varying depositional environment, (2) understand the processes controlling the benthic releases of P, (3) and construct a mass balance for P in the upper sediments of the Northern Indian Ocean. For this, the diffusive fluxes of phosphate were estimated at 95 stations (Fig. 6.2) using the

bottom water and porewater concentrations. Also analyzed were total P, Fe, and organic carbon content in bulk sediments from the locations where the porewater was extracted, for assessing the controls on P regeneration fluxes.

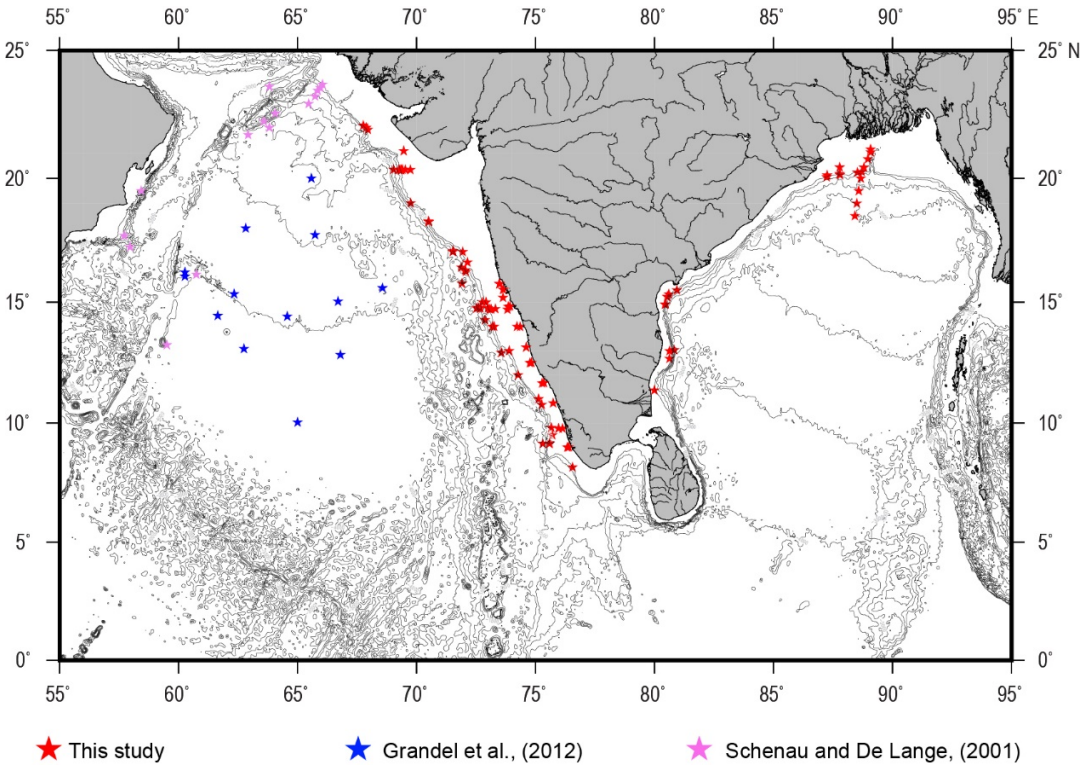

Figure 6.2: Map showing the sampling locations of the study.

6.2 Results

6.2.1 Bottom Water Dissolved Oxygen (DO) concentration

DO concentrations in the study area vary between 0 and 208.28 µmol/L and are shown in Table 6.1 and Fig. 6.3. Most of the shallow station (All SSD27 stations) sampling from the Arabian Sea was undertaken during November when the coastal anoxia was strong (e.g., Naqvi et al., 2000). Compared to the Arabian Sea, Bay of Bengal oxygen minimum zone are less intense. .

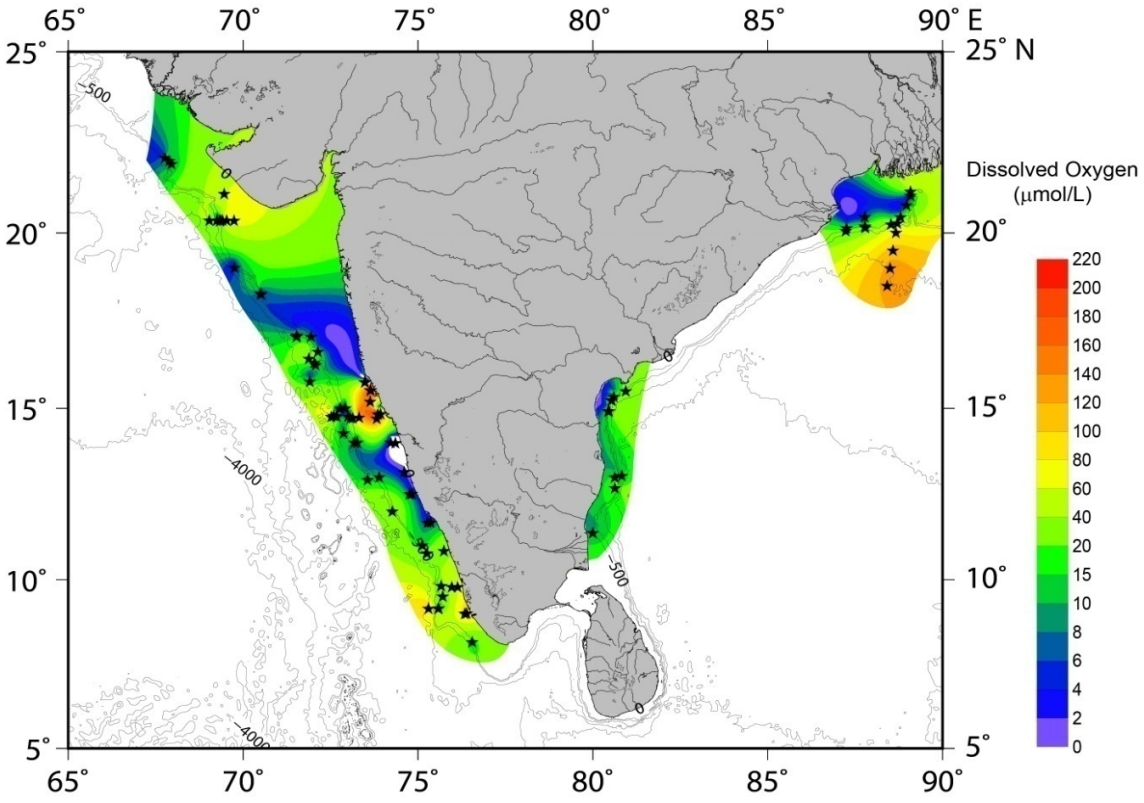

Figure 6.3: Spatial distribution of bottom water oxygen concentrations in the studied sites.

6.2.2 Phosphate Concentration in near-bottom water and porewater

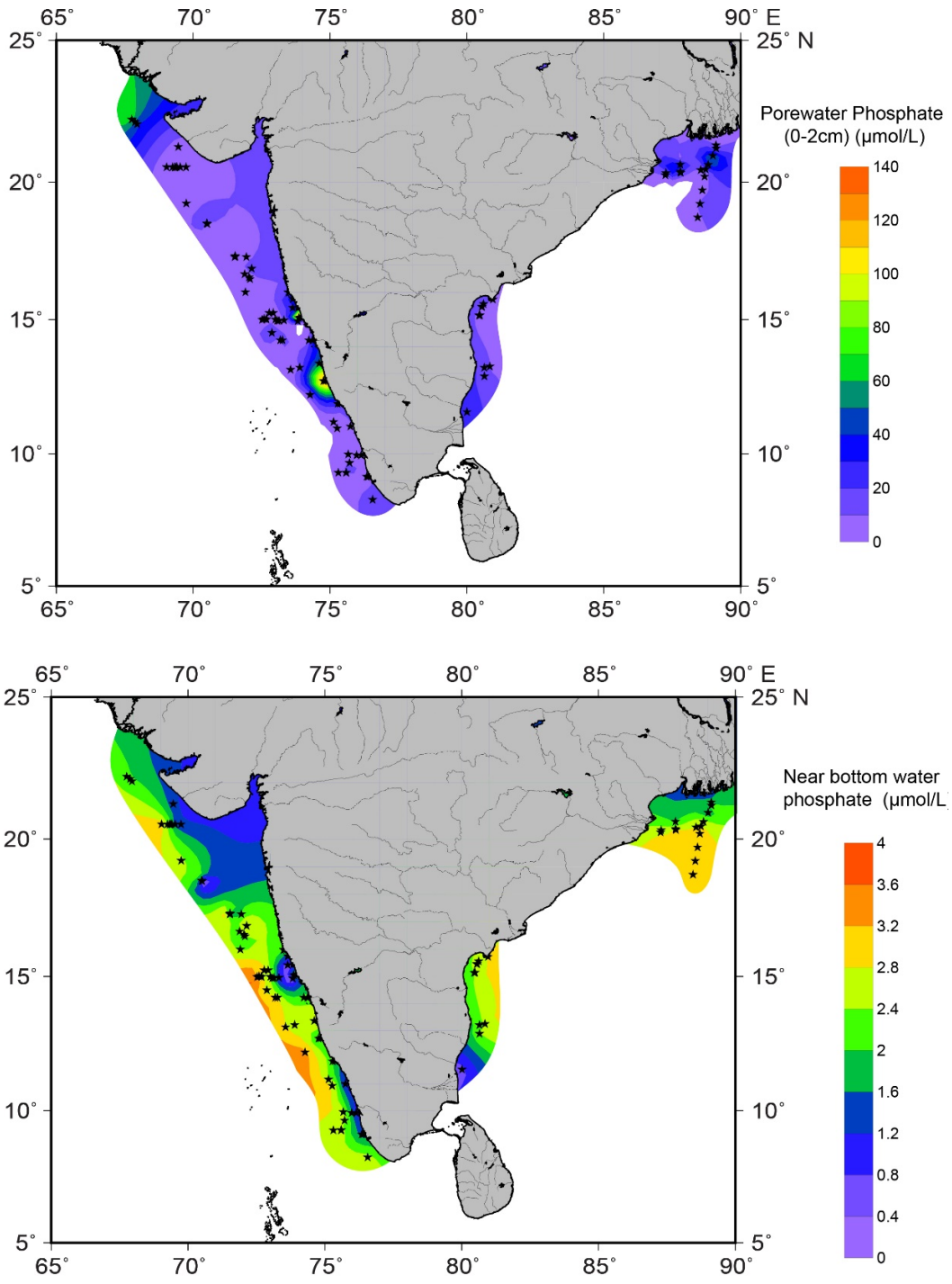

Figure 6.4: Spatial distribution of DIP in the near-bottom water and porewater in the studied sites.

Phosphate concentration in the bottom water varies from 0.2 to 3.72 µmol/L (Fig. 6.4 and Fig. 6.5). However, the values do not show significant variation with depth. Bottom water DIP concentrations in the Arabian Sea are comparable with the Bay of Bengal. Porewater DIP concentration at the upper 0-2 cm of sediment ranges from 1.61 to 165 µmol/L and higher concentrations are found in shallow stations from the Arabian Sea, affected by coastal anoxia (Fig. 6.5). In most of the stations, porewater DIP concentration increases with sediment depth and some profiles show subsurface maxima and decline in concentration after subsurface maxima. In some stations DIP concentrations show downcore decrease indicating that the porewater DIP is being used up.

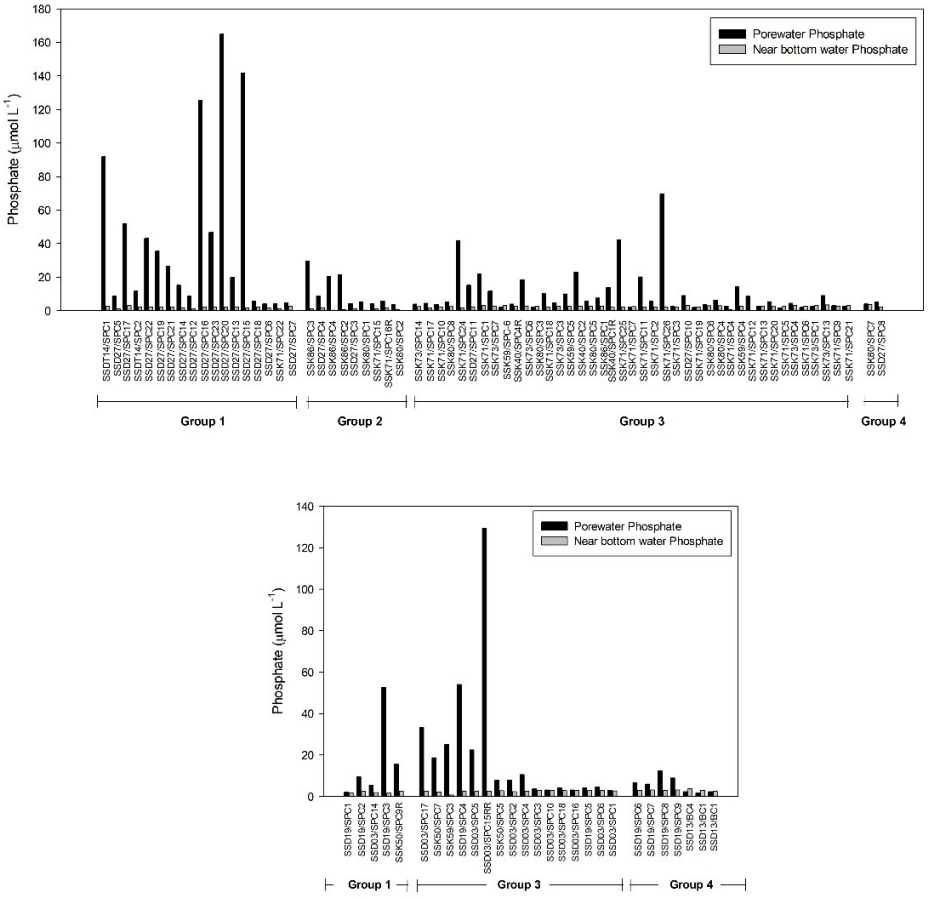

Figure 6.5 Bar diagram showing the DIP concentrations in near bottom water and porewater.

6.2.3 Sediment total P (P_{total})

The P_{total} inventory in the top 1 cm sediment varies between 13.84 and 107.29 µmol/g (Table 6.1, Fig. 6.6) except at two stations (SSK71/SPC7 - 500.51 and SSK71/SPC-18-255.83 µmol/g). P_{total} content is generally low in the deeper area (>1500 m water depth) of the Northern Indian Ocean (28.83 µmol/g) whereas high in continental slope (150-400 m water depth) sediments (72.74 µmol/g). Compared to the Bay of Bengal (27.28 µmol/g), P_{total} content in the Arabian Sea (average 55.18 µmol/g) is generally high. P_{total} content in the shallowest stations (28-150 m water depth) ranges between 13.84 and 62.86 µmol/g.

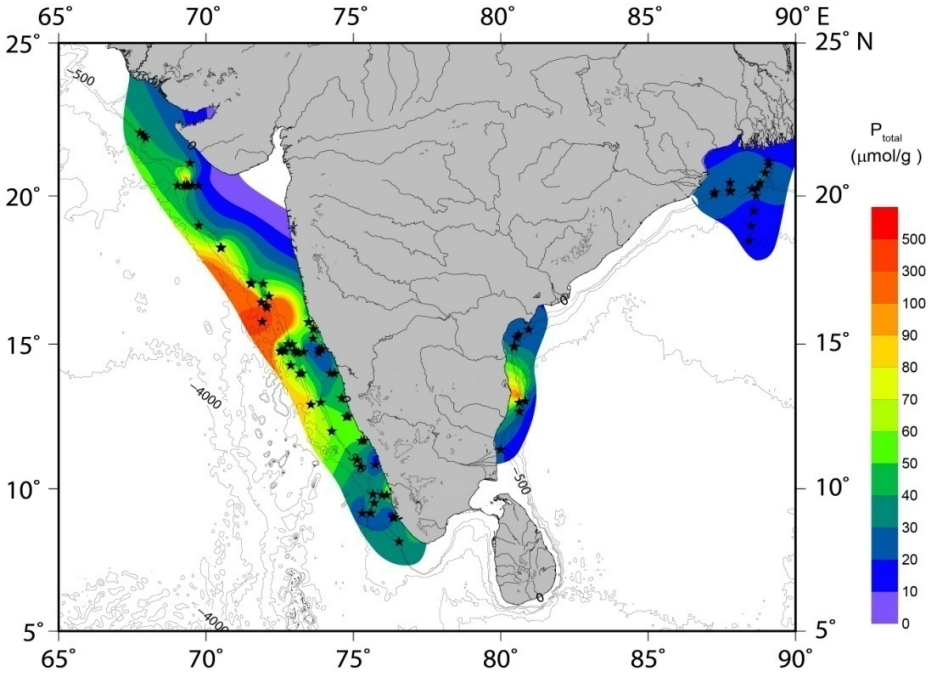

Figure 6.6: Figure showing the spatial distribution of P_{total} content in the studied sediment core tops.

6.2.4. Total Fe

Fe_{total} concentration in the study area ranges between 12.9 and 1246 µmol/g with an average of 565.8 µmol/g (Table 6.1 and Fig. 6.7). Highest Fe_{total} content is obtained at shallow stations of the Arabian Sea (<150m water depth) with an average of 749 µmol/g whereas in the Bay of Bengal the value is 569 µmol/g. But the concentration in the deeper area (>900 m water depth) is slightly low and values are in between 12.9 and 636 µmol/g in Arabian Sea sediments. In Bay of Bengal highest Fe_{total} content was obtained at continental slope sediments with water depth between 400 and 900 m (average 884 µmol/g).

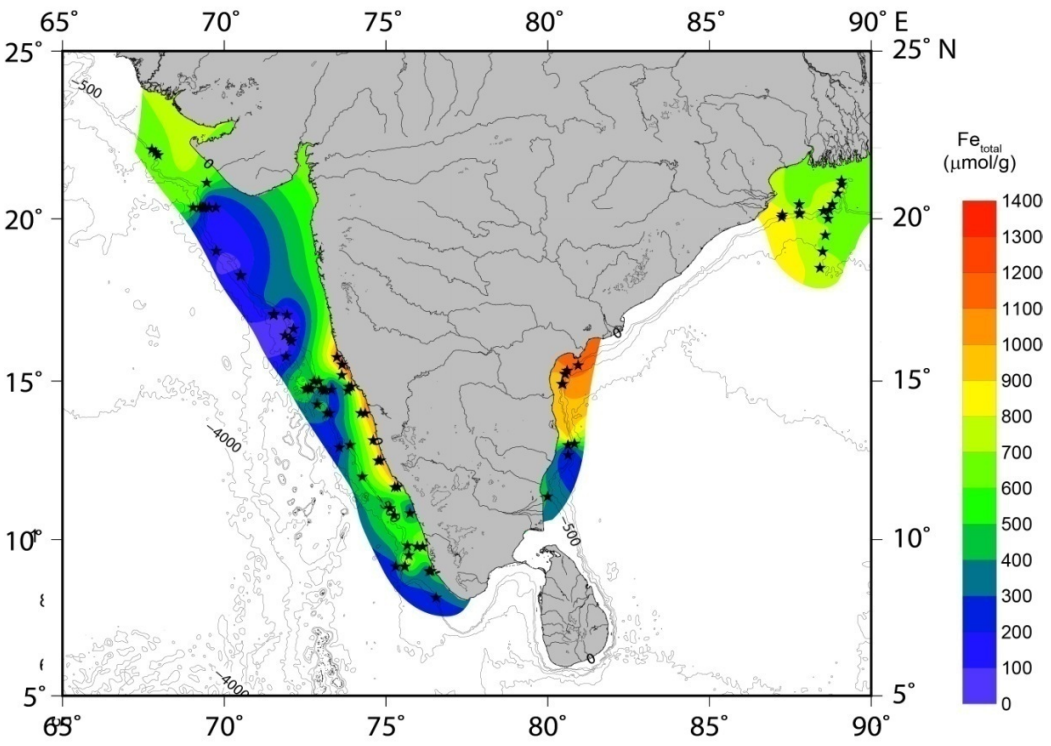

Figure 6.7: Spatial distribution of Fe_{total} content of surface sediment (top 0-1 cm) in the Northern Indian Ocean.

6.2.5. Total Organic Carbon (C_{org}) and Total Inorganic Carbon (TIC)

The C_{org} content of the study area varies between 0.32 and 9.17.wt.% and has an average of 2.86 wt.% (Table 6.1 and Fig. 6.8). The C_{org} content is low at shallow water depths (28-150 m) and increases with water depth and then starts decreasing after 1000 m depth. C_{org} content is generally high in Arabian Sea sediments (average 3.5 wt.%) compared to the Bay of Bengal (average 1.4 wt.%). TIC content varies between 0.045 and 10.45 wt.% with an average of 3.8 wt.%. Highest TIC content is obtained in Arabian Sea sediments (average 5.13 wt.%) compared to the Bay of Bengal (average 0.97 wt.%). and TIC content is high in continental slope sediments compared to the shelf and deep-sea sediments.

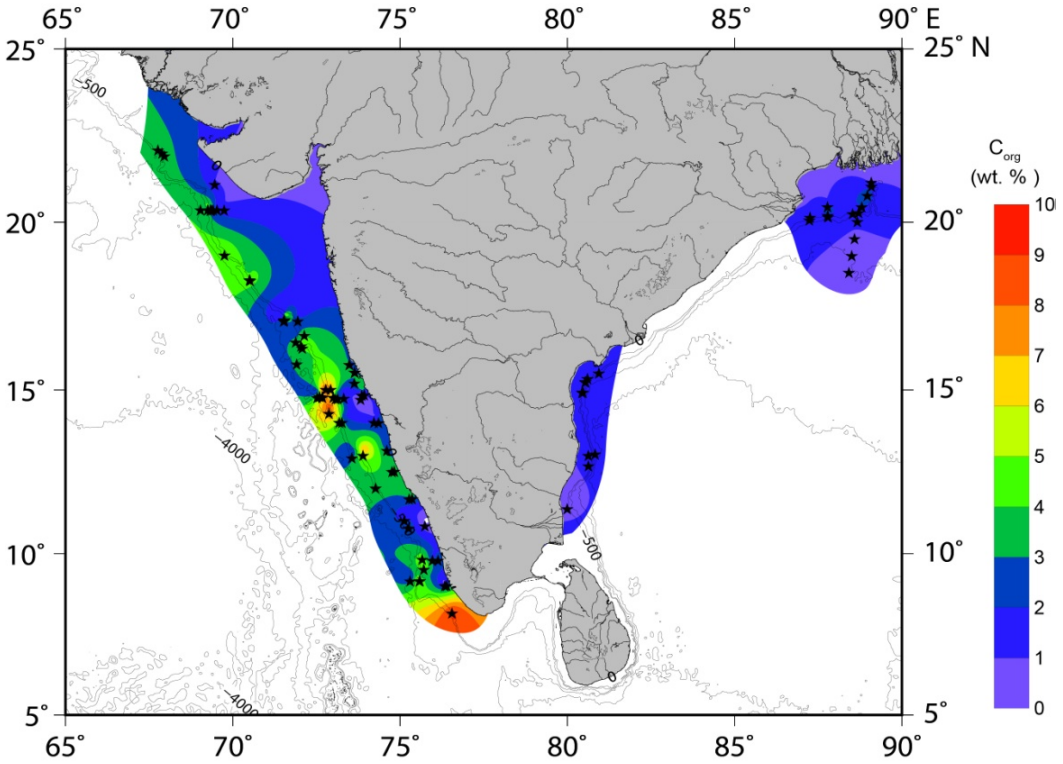

Figure 6.8: Spatial distribution of C_{org} content of surface sediment (top 0-1 cm) in the Northern Indian Ocean.

6.2.5. Benthic Phosphate flux at the sediment-water interface

Benthic flux of P calculated from porewater data is shown in the Table 6.1. Except for few stations, all other stations show negative flux which indicates the movement of phosphate from sediment to the water column. The magnitude of diffusive flux ranged from 0.01 to 25 µmolcm^{-2}yr $^{-1}$ with an average of 2.22 µmolcm^{-2}yr^{-1}. Fluxes are generally high at stations close to the shelf and high values (13.24 - 25.25 µmol cm^{-2} yr^{-1}) obtained at four stations where the water depth is below 50 m and are oxygen depleted. Except for some shallow stations (below 50m water depth) all stations having higher benthic flux lie below oxygen minimum zone (DO value <0.12 ml/L). In the deeper area, the magnitude of benthic fluxes decreases and most of the positive fluxes obtained are in the deeper area (Fig. 6.9).

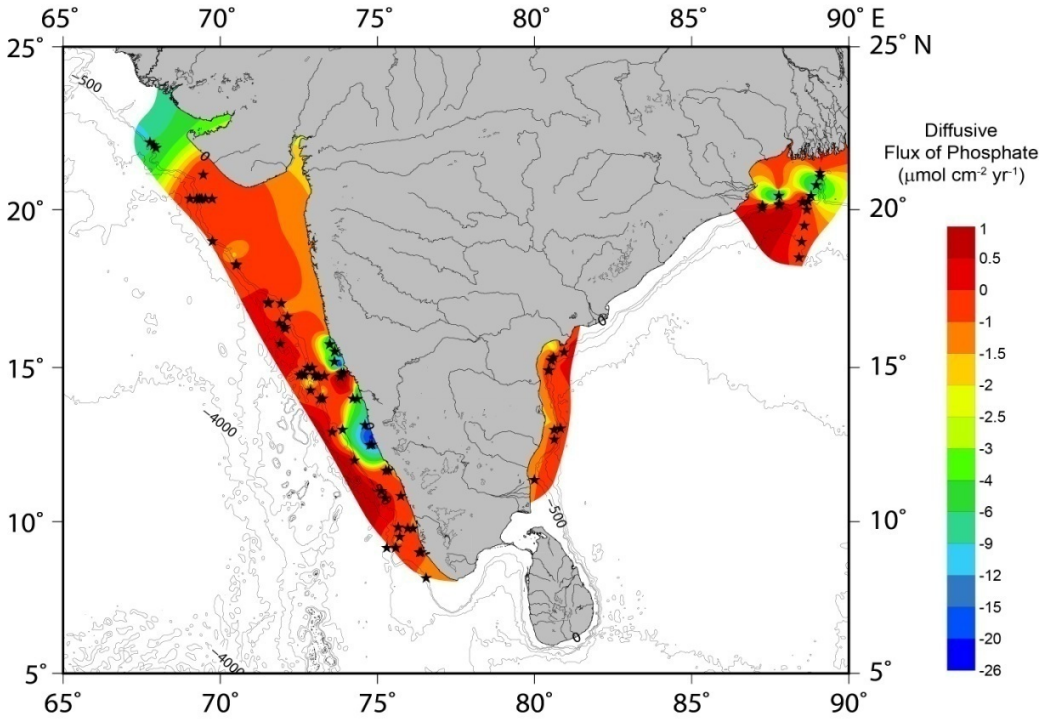

Figure 6.9: Spatial distribution of the diffusive flux of phosphate at the sediment-water interface.

6.3. Discussion

6.3.1. Diffusive flux of phosphate at the sediment-water interface

Benthic flux calculated in this study area is generally similar to the previously reported values in the Arabian Sea (Grandel et al., 2000; Schenau and De Lange, 2001) and South Atlantic Ocean (Hensen et al., 1998). The flux obtained in the shelf region is similar to the Northwestern Shelf of Black Sea (Friedl et al., 1998) and the values are shown in the table 6.2.

To present the estimated DIP flux in the context of different bottom water oxygen conditions and water depth, the data are divided into four groups (modified after Mort et al., 2010; Jilbert et al., 2011; Viktorsson et al., 2013). The group 1 includes DIP fluxes from seasonal anoxic to hypoxic condition ($0 \leq O_2 \leq 62.49$ μM – Naqvi et al 2010) in the depth range between 25 and 150 m; group 2 includes fluxes from oxic bottom condition in the depth range 25-150 m; group 3 includes fluxes from perennial OMZ in the depth range 150-1,250 m; group 4 includes fluxes from deeper region >1,250 m depth in which sediments overlain by oxic bottom water lie (Table 6.1).

The DIP flux was found to increase with decreasing bottom water oxygen concentration and this is consistent with the previous study from the Arabian Sea (Fig. 6.9) (Schenau and De Lange, 2001). The findings of the relatively high DIP fluxes from the group 1 stations are in agreement with the previous findings by Jilbert et al., (2011) and Mort et al., (2010). This high DIP fluxes from the group 1 stations are due to the remobilization of temporary P sink which is formed only stable under oxic condition (Viktorsson et al., 2013 and references therein). To understand this seasonal variation we have measured benthic fluxes at two different seasons one in September 2015

(SSDT14/SPC1-during the anoxia time) and another during January 2016 (SSK86/SPC3) at one station. The DIP flux estimated shows high flux during September. The western Indian continental shelf experiences intense hypoxia (O_2 < 22 μM) during late summer and autumn resulting in accumulation of N_2O and H_2S in the water column (Naqvi et al., 2000).

Comparatively high DIP flux at hypoxic condition during September suggests the remobilization of P from temporary sinks. Among the group 1 stations, high benthic fluxes were observed under anoxic to suboxic condition and porewater profiles (Table 6.1) of these stations also show surface enrichment of DIP concentration. This also indicates the remobilization of temporary P sinks. Highest flux measured in group 1 stations coincides with the highest concentration of Fe indicating that microbial reduction of iron oxyhydroxides is a possibility for the elevated fluxes in the shallow shelf stations. High concentrations of Fe at the sediment-water interface in the shelf area may be due to the high deposition rate of iron oxyhydroxides during the periods of bottom water oxygenation (Noffke et al., 2012), where the release of P by Fe is mainly controlled primarily by the bottom water oxygen concentration and the availability of reactive Fe (Pakhomova et al., 2007; Severmann et al., 2010). Compared to the Arabian Sea, bottom water dissolved oxygen concentrations are relatively high in BoB (Table 6.1). Thus, less intense OMZ leads to comparatively lower DIP flux in group 1 stations of the BoB.

Relatively low C_{org} contents in group 1 stations compared to group 3 stations are due to the seasonal exposure of the former group to O_2 that does not occur within the perennial OMZ (Cowie et al., 2014). The enrichment of porewater DIP with depth indicates degradation of organic matter and corresponding release of phosphate to the porewater.

Thus, in the group 1 stations, degradation of organic matter partly contributes to the regeneration fluxes.

Our DIP fluxes from group 2 stations averaged 1.3 μmol cm^{-2} $yr^{-1}$and relatively low values of DIP flux compared to the oxygen-depleted shelf sediments are due to the presence of iron oxyhydroxides. In almost all group 2 stations, DIP concentrations are low at the surface and enriched with depth indicating the release of P during the organic matter degradation. Along with this, low molar C_{org}/P_{total} ratio in the oxygenated shelf sediments also indicates the extensive degradation of organic matter. Generally, molar C_{org}/P_{org} ratios are used to understand the diagenetic change. Due to the lack of P_{org} data, we have used the molar C_{org}/P_{total} ratio. The low molar C_{org}/P_{total} ratio of the present study is in close agreement with the previous study of the shelf sediments of the Arabian Sea (Babu and Nath 2005). Relatively low molar C_{org}/P_{total} ratio in group 2 stations indicate remineralization of organic matter during O_2 exposure.

Compared to the seasonal hypoxic stations, benthic fluxes are high in group 3 stations in which sediments overlain by perennial OMZ. Burial of organic matter is the major pathway by which the reactive P would have reached the sediments overlain by OMZ (Ingall and Jahnke 1994). Relatively high C_{org} content in the group 3 sites indicates the preservation of organic matter under oxygen-depleted condition. Relatively high C_{org}/P_{total} ratios in these stations suggest the preferential release of P relative to C. Schenau and De Lange (2001) have suggested that the high benthic flux of Arabian Sea is mainly due to the degradation of organic matter. The C_{org}/P_{org} ratio of Babu and Nath (2005) also provide evidence of preferential regeneration of P from organic matter in the surface sediments of Arabian Sea. Compared to the Arabian Sea, group 3 stations of the Bay of Bengal have low

C_{org} content which may be due to the low surface productivity in the Bay of Bengal. Stratification resulting from high freshwater input and together with weak wind forces over the BoB restrict the vertical mixing to a shallow depth and inhibit the nutrient transport below the mixed layer resulting in low productivity in the BoB (Kumar et al., 2002).

Compared to shelf stations, Fe concentrations in the continental slope are low in stations which are impinged by the perennial OMZ. These low concentrations indicate that the iron oxides have already been reduced in the water column or at the sediment-water interface. A weak role of iron on the benthic release of P in the continental margin sediments of Arabian Sea impinged by perennial OMZ was suggested by Linsy et al., (2018), who have also suggested the possibility of the formation of reduced Fe (II) mineral, vivianite. Due to less intense OMZ and low bacterial respiration (Rao et al., 1994; Naqvi et al., 1996; Sarma et al., 2013), reductive dissolution of iron oxyhydroxides is weak in the BoB. Therefore, reductive dissolution of iron oxyhydroxides and release of P to the porewater is weak in the perennial OMZ. Thus, in the continental slope sediments overlain by perennial OMZ, organic matter degradation is the primary controlling factor for the benthic P release.

Apart from the degradation of organic matter and redox cycling of iron, dissolution of fish debris also explains the high P flux in the Northern Indian Ocean. High accumulation rate of P_{bio} was reported for the Northern Indian Ocean continental slope (Babu and Nath, 2005; Linsy et al., 2018) owing to the high fish production rates in the surface water and reduced biogenic apatite dissolution rate in the water column (Schenau and De Lange, 2000, 2001).

The benthic fluxes of P are low in group 4 stations (water depth > 1,250 m) which are overlain by oxic bottom water in the deeper areas of the Northern Indian Ocean. DIP fluxes in the deeper areas of the Northern Indian Ocean are relatively low compared to the shelf, slope sediments. C_{org} content of group 4 stations is relatively low compared to other groups. These lower burial rates of C_{org} are very likely due to the increased water column remineralization during its transport. Fish debris also undergoes dissolution during exposure to O_2 and water column transport (Schenau and De Lange, 2001) and this also leads to the lower fluxes. Oxic bottom water condition of the deep-sea promotes the adsorption of P on the surface of iron oxyhydroxides (Slomp et al., 1996). Thus the presence of iron oxyhydroxides limits the release of phosphate to the porewater and thereby reduces the DIP fluxes from sediments to the overlying water.

6.3.2. P mass balance in the Northern Indian Ocean

The mass balance of P is controlled by input from the continents, by internal uptake, transport, regeneration of P, and by burial of reactive P in a number of the sedimentary sinks (Delaney, 1998).

1) Internal load of P to the Northern Indian Ocean

Along with the external load of P (river input and atmospheric deposition), internal load (reflux from sediments) also controls the water column DIP pool (Viktorsson et al., 2013) and thus the estimation of the internal load is important. Here I have estimated the magnitude of the internal DIP load to the Northern Indian Ocean based on diffusive flux measurements. Using the average DIP flux from sediments (Table 6.3), a regional

extrapolation of the internal DIP load to the water column of the Arabian Sea and BoB was made.

The Arabian-Sea OMZ is the second-most intense OMZ in the world tropical ocean (Kamykowski and Zentara, 1990). In view of the role of OMZs as a major P source of the global ocean, total diffusive fluxes as well as an average diffusive flux in the Arabian Sea including the Laccadive Sea were estimated to provide an estimate of P return flux contribution of the Arabian Sea to the global ocean. The total area of the Arabian Sea including the Laccadive Sea is about 4.68 million km^2 and out of this about 20.4% consist of continental margin (<2000 m depth). The average flux in the continental margin is 27.95 mmol m^{-2} yr^{-1} and the minimum and maximum values are 0.2 and 252.5 mmol m^{-2} yr^{-1}, respectively. The total annual diffusive flux of phosphate from the continental margins of the Arabian Sea is 0.268 x 10^{11} mol/yr which is about 68% of the total release of phosphate from the Arabian Sea, and consistent with earlier studies of importance of margins in P release (Wallmann, 2010). The western continental shelf of India covers an area of 0.31x 10^6 km^2. The total annual diffusive flux of phosphate in this shelf is about 0.152 x 10^{11} mol/yr and account 39% of the annual reflux from the Arabian Sea.

The regeneration of phosphate is found to be enhanced from sediments underlying hypoxic or anoxic water (Jilbert et al., 2011). During September to October, almost the entire western continental shelf of India was bathed by oxygen-depleted water and this covers an area of 0.18 x 10^6 km^2 (Naqvi et al., 2000). The estimated diffusive flux of phosphate from this period is 0.118 x 10^{11} mol/yr and this contributes 30% of the total annual diffusive flux of the Arabian Sea. In this study, all the stations are shallower than 2200 m water depth and hence to quantify the flux in the deeper areas (> 2000 m), the data

of previously reported values from the deeper part of the Arabian Sea (Grandel et al., 2000; Schenau and De Lange, 2001) are included. The estimated annual diffusive flux of phosphate from the deep-sea sediments of the Arabian Sea is about 0.118 x 10^{11} mol/yr. Though, the abyssal regions occupy 79.6 % of Arabian Sea, P flux contribution from the abyssal sediments is much lower compared to continental margins. Total annual diffusive flux of P from the Arabian Sea, including the earlier data published, is 0.39 x 10^{11} mol/yr and this is about 3.16 % of the global value 12 x 10^{11} mol/yr (Colman and Holland, 2000). However, in an another estimate (Wallmann, 2003), the pre-anthropogenic return flux of P from sediments is slightly higher at 13.4 x 10^{11} mol/yr. The total annual return flux of P obtained in the Arabian Sea is comparable with flux reported in the South Atlantic Ocean by Hensen et al. (1998).

The estimated return flux of P from sediments of the eastern continental shelf of India is 0.02 x 10^{11} mol/yr and which is very low compared to the western continental shelf of India. The diagenetic return flux in the continental margin of BoB (covers an area of 0.60 x 10^6 km^2) was calculated using the average diffusive flux of phosphate 17.93 mmol m^{-2} yr^{-1}. The estimated flux of P from the continental margin of BoB is 0.108 x 10^{11} mol/yr. The extrapolated flux for the entire BoB (total area of the BoB is 2.172 x 10^6 km^2) is 0.378 x 10^{11} mol/yr and accounts for 3.1% of the global value. The value is nearly comparable with the Arabian Sea (3.16). However, the estimation of the return flux of the BoB is very uncertain owing to the lack of deep-sea data.

Combining the above, total annual diagenetic return flux of P in the Northern Indian Ocean estimated here is 0.77 x 10^{11} mol/yr and the global estimate may have to be revised by increasing about 6.3% of the current global value. Even though the Northern Indian

Ocean covers only about 1.66% of the global ocean floor and has so far not been accounted for, this work shows it may account for additional 6.3% to the global diagenetic flux.

2) External load of Phosphorus to the Northern Indian Ocean

i) River input of P

A major share of P reaching into the ocean is from the continents primarily in the dissolved and particulate phases via river input (Baturin, 2003; Paytan and McLaughlin, 2007). The Northern Indian Ocean receives an immense supply of fresh water from the glacial and monsoonal rivers. The major rivers reaching into the Arabian Sea are the Indus, Narmada, and Tapti. The estimate of river runoff into the Arabian Sea is ~0.347x10^3 km^3 of water (Krishna et al., 2016; Ramesh et al., 2015) and is ~0.8 - 1% of the global value (35 - 44 x 10^3 km^3) (Baturin, 2003). Among the other rivers, Indus alone discharges 0.238x10^3 km^3 (69% of the total) of water annually (Krishna et al., 2016). The river discharge is more during the time of southwest monsoon and negligible during other times. Compared to the Arabian Sea, BoB receives a larger supply of freshwater (1.63 x10^3 km^3; Subramanian, 1993) from the glacial and monsoonal rivers of India, Bangladesh, and Myanmar (Krishna et al., 2016).

The annual river flux of DIP in to the Arabian Sea is estimated to be 0.213x10^{10} mol/yr (estimated from the data provided by Subramanian, 1993; Ramesh et al., 2015; Krishna et al., 2016) which is 4.5-8% of the global value (0.8 and 1.4 x 10^{12} g/yr (Compton et al., 2000). The average DIP concentration in the river water is 0.33 mg/L (Krishna et al., 2016) which is higher than the global value (0.007-.01 mg/L) of the unpolluted river

(Compton et al., 2000) indicating the anthropogenic influence. The annual DIP flux into the Bay of Bengal is ~0.67 x 10^{10} mol/yr and which is three times higher than that of the Arabian Sea due to the higher discharge to the former. The total river flux of DIP into the Northern Indian Ocean is ~0.88x 10^{10} g/yr and out of that 0.26 x 10^{10} mol/yr is contributed by the monsoonal rivers (Krishna et al., 2016).

The present-day dissolved organic phosphorus (DOP) river flux into the Arabian Sea can be calculated as 0.0141 x 10^{10}mol/yr from a dissolved organic carbon (DOC) flux of 4.37 x 10^{12}g/yr and an average DOM C/P weight ratio of 1000 (Meybeck, 1982; Compton et al., 2000). DOC content of the major Indian rivers reported by Krishna et al., (2016) and Ramesh et al., (2015) are used for the estimation of organic carbon flux. The export flux of DOC into the Bay of Bengal is 6.02 x 10^{12}g/yr and the calculated export flux of DOP into this area is 0.0194 x 10^{10} mol/yr. Compared to the Arabian Sea, DOP flux into the Bay of Bengal is high due to the high discharge of rivers. The total DOP flux into the Northern Indian Ocean is 0.03 x 10^{10} mol/yr and accounts for 5.2% of the global value (.0.065x 10^{11} mol/yr Meybeck, 1982; Compton et al., 2000). The monsoonal river itself contributes 0.077 x 10^{9} mol/yr DOP to the Northern Indian Ocean (Fig. 6.10).

Particulate organic phosphate flux (POP) into the Arabian Sea can be calculated using POC flux values and POM C/P wt ratio of 193 (Ramirez and Rose, 1992; Compton et al., 2000). Averge POC content of 3.14 wt.% (Ramesh et al., 1995; Sarma et al., 2014) was used for the estimation of POP river flux into the Arabian Sea. POC flux into the Arabian Sea is 5.14 x 10^{12} g/yr and the calculated POP flux is 0.086 x 10^{10} mol/yr. The export flux of POC into the BoB is estimated to be ~26.94 X 10^{12} g/yr, from the average POC content of 2.08 wt.%. Total annual flux of POP into the Bay of Bengal is ~0.450 x 10^{10} mol/yr which

~5 times higher than that of the Arabian Sea. In the BoB, Ganges-Brahmaputra annually discharge 1060 x 10^6 tones suspended load (Ramesh et al., 2015) and high flux into the BoB is due to this high suspended load. The total annual flux of POP into the Northern Indian Ocean by the rivers is ~ 0.510 x 10^{10} mol/yr (Fig. 6.10, Table 6.3).

The present-day particulate inorganic phosphate (PIP) flux into the Bay of Bengal is estimated to be 4.07 x 10^{10} mol/yr and which is calculated using the average PIP content 974 µg/g. Due to the lack of PIP data from the rivers discharging into the Arabian Sea, the total PIP flux into the Northern Indian Ocean was also estimated using the same average. The extrapolated PIP flux into the Northern Indian Ocean is 4.5 x 10^{10} mol/yr. The total annual fluvial flux of P (including DIP, DOP, POP, and PIP) into the Northern Indian Ocean is ~ 6.0 x 10^{10} mol/yr and it accounts 6-10.5 % of the global value (57.2–98.2 x 10^{10} mol/yr, Compton et al., 2000).

ii) Atmospheric deposition of P

Atmospheric input is the significant source of P to the open ocean as well as coastal zone. Atmospheric deposition contributes approximately 5% of the pre-anthropogenic input of about 3.2 x 10^{10} mol P/yr (Paytan and McLaughlin, 2007and references are therein). In the marine environment, atmospheric deposition may provide an additional source of nutrient and thereby increase primary productivity (Paytan and McLaughlin, 2007; Srinivas and Sarin, 2015). The Arabian Sea receives eolian input from the arid regions of North Africa, Arabia, Pakistan, and India (Ramaswamy et al., 1991), whereas the BoB receives

mineral-dust supply from the Indo-Gangetic plain and South-East Asia through the advective transport during NE monsoon (Srinivas and Sarin, 2013).

The dry deposition rate of water-soluble inorganic phosphate to the Northern Indian Ocean was estimated and the soluble P deposition rate in the Arabian Sea is ~0.045 x 10^{10} mol P/ yr (Srinivas and Sarin, 2012, 2013, 2015). While the Bay of Bengal is two-fold higher than that of the Arabian Sea and the estimated dry deposition rate of DIP to the BoB is 0.071 x 10^{10} mol P/ yr (Srinivas and Sarin, 2012) , the aerosol DIP from the Arabian Sea is low owing to the lower fractional solubility of the mineral dust over the Arabian Sea (Srinivas and Sarin, 2013). In the Bay of Bengal, 75% of this aerosol is contributed by the anthropogenic sources, viz. biomass burning emissions and fertilizers from the Indo-Gangetic plain and contrary to this the contribution of anthropogenic sources to the Arabian Sea is relatively low (<30%) and is dominated by dust input from desert regions mainly from Thar in India, Iran and Arabia (Srinivas and Sarin, 2013).

The dry deposition rate of DIP to the Northern Indian Ocean is ~ 0.12 x 10^{10} mol P/ yr (Srinivas and Sarin, 2015). Okin et al. (2011) also estimated the dry deposition rate of DIP into the Northern Indian Ocean of ~0.14 x 10^{10} mol P/ yr and which is nearly comparable to the value reported by Srinivas and Sarin (2012, 2013, 2015) join both sentences. The global estimate of the dry deposition rate reported by Okin et al. (2011) is ~ 0.32 Tg P/ yr. Thus the atmospheric deposition of DIP in the Northern Indian Ocean accounts for 11.25 % of the global value (Okin et al., 2011). Mahowald et al. (2008) estimated that the oceans are receiving a global average of 1.8 and 0.312 x 10^{10} mol P/ yr of atmospheric P and phosphate, respectively, and out that 5 to 15% are anthropogenic in origin. However, they have also estimated that the Northern Indian Ocean receives an

average of 0.3746 and 0.45 x 10^{10} mol P/ yr atmospheric P and water-soluble inorganic phosphate, respectively and accounts for ~21% and ~15% of the global average.

3) Primary Productivity

Primary production is the major processes by which dissolved P is converted into the particulate form. The Northern Indian Ocean is one of the highly productive regions of the tropical ocean.

The summer south-west monsoon winds lead to an intense coastal upwelling along the NE African cost due to strong offshore Ekman Transport (e.g., Wyrtki, 1973; Slater and Kroopnick, 1984). These nutrient-rich surface upwelled waters are transported throughout the Arabian Sea and stable solar irradiance leads to a summer primary productivity bloom that produces approximately 200 g C m^{-2} yr^{-1} (Nair et al., 1989). Strong North East Monsoon wind causes large-scale convective mixing and generates comparable primary productivity to the summer monsoon. These processes make the Arabian Sea as the most productive region of the world ocean and it contributes nearly ~5% of the world primary production (Qasim, 1982). The annual primary productivity of the Arabian Sea varies between 163 and 1782 mg C m^{-2} d^{-1} (Gauns et al., 2005). Compared to the Arabian Sea surface, the productivity of the BoB is relatively low. Warm sea surface temperature (SST) and low salinity (resulted from high freshwater input) lead to strong stratification preventing the entrainment of nutrients into the surface waters throughout the year (Gauns et al., 2005). Along with this, weak winds over the BOB together restrict the vertical mixing to a shallow depth and inhibit the nutrient introduction below the mixed layer (Kumar et al., 2002). The

primary productivity of the Bay of Bengal varies between 40 and 566 mg C m^{-2} d^{-1}(Gauns et al., 2005).

The assessment of P nutrient demand was developed (Monbet et al., 2007) from the primary productivity data reported by (Gauns et al., 2005). The Redfield ratio (C/P=106) was used for the estimation of P productivity. The annual P productivity of the Arabian Sea varies between 0.562 and 6.10 g P m^{-2} yr^{-1}, whereas the P productivity of the BoB ranges between 0.138 and 1.95 g P m^{-2} yr^{-1}. Estimated P nutrient demand of the Arabian Sea is 2.63 - 28.74 x 10^{12} g P yr^{-1} and the BoB is 0.30-4.24 x 10^{12} g P yr^{-1}. The total P nutrient demand of the Northern Indian Ocean varies between 2.93 and 32.97 x 10^{12} g P yr^{-1}. Our results indicate that the Arabian Sea accounts 87-90 % of the P nutrient demand of the Northern Indian Ocean.

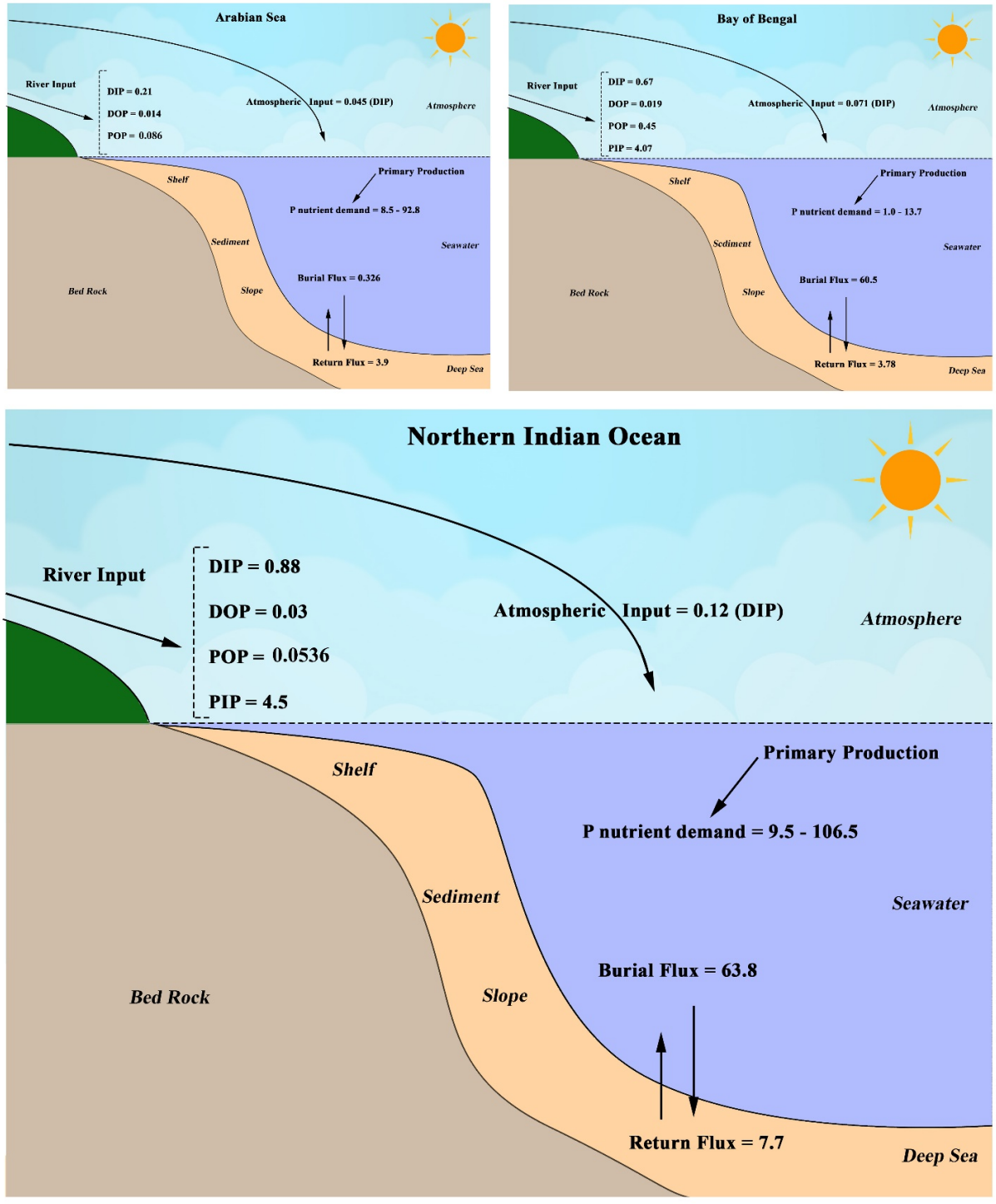

Figure 6.10: The estimated annual mass balance (in units of 10^{10} mol/year) for phosphorus in the Northern Indian Ocean (this work).

4) Burial flux of P

P_{total} accumulation rate was estimated using the sedimentation rate, surface P_{total} concentration and dry bulk density. The estimated accumulation rate in the present study ranged from 0.07 to 525 µmol cm^{-2} yr^{-1}. P_{total} accumulation rate in the BoB (average 100 µmol cm^{-2} yr^{-1}) is several times larger than the Arabian Sea due to the high fluvial sediment input in the former region. Highest P_{total} accumulation rate is obtained at stations which are located near the Swatch of No Ground canyon, which receives enormous amount of sediment from the Ganges-Brahmaputra river system (Michels et al., 2003). Accumulation rates are high in shelf area compared to the slope and decreases with increasing water column depth. P accumulation rate in the deeper areas of the Northern Indian Ocean are comparable with the previous reported values from the deep Arabian Sea (Schenau and De Lange, 2001).

P burial within the sediment is the long-term sink of P from the ocean. Thus, while considering the mass balance approach, estimation of burial rate of P in sediment is inevitable. The burial rate in the entire study area is calculated using the average P_{total} accumulation rate at the surface and area of the site. The P burial rate in the entire Arabian Sea is ~3.26 X 10^9 mol/yr, and of this, 93% is buried in the continental margin (~3.04 X 10^9 mol/yr). P burial rate in the abyssal areas of the Arabian Sea was estimated using the average P accumulation rate of 0.06 µmol cm^{-2} yr^{-1} reported by Schenau and De Lange (2001) due to the lack of deep-sea data in the present study. P burial flux in the western continental shelf of India is 1.52 X 10^9 mol/yr and which was estimated using the average accumulation rate of 4.89 µmol cm^{-2} yr^{-1}. P burial rate in the continental margin of BoB is several times larger than the Arabian Sea and estimated P burial flux in the BoB continental margin is ~60 X 10^9 mol/yr. The burial flux of P in the deep BoB estimated using the

average accumulation rate of 0.11 μmol cm^{-2} yr^{-1} is 0.156 X 10^9 mol/yr. The total burial flux of P in the entire BoB is 60.5 X 10^9 mol/yr and is nearly 20 times larger than the Arabian Sea. The total P burial rate in the Northern Indian Ocean is ~64 X 10^9 mol/yr.

The presented mass balance study (Fig. 6. 10) indicates that the major source of P to the sediment in the Arabian Sea is through the biogenic input (primary production 8.5-92.8 x 10^{10} mol P/yr) compared to the fluvial and atmospheric supply. Whereas in the BoB, fluvial input contributes a major share of P that reaches the seafloor sediments. The major portions of P reaching to the sediments of the Arabian Sea returns to the photic zone through diagenetic regeneration (3.9 x 10^{10} mol P/yr) and less than 10% is undergoing burial (0.33 x 10^{10} mol P/yr). The mass balance study of the BoB shows that most of the P reaching in the sediments undergo burial rather than regeneration. The diagenetic return flux of DIP in the Northern Indian Ocean is 7.5 times higher than external input and the excess flux indicate the extensive regeneration from sediments.

Conclusions

This study shows that benthic regeneration of P is more extensive during the oxygen-depleted condition in the bottom waters. The benthic return flux of P from the perennial OMZ is mainly contributed by the organic matter degradation and fish debris dissolution whereas in the areas witnessing seasonal hypoxia, reductive dissolution of iron oxyhydroxides plays a major role. Compared to the Arabian Sea OMZ, the diagenetic return flux of P is relatively low in the BoB OMZ. The regeneration flux from the areas influenced by seasonal hypoxia contributes 39% of the annual reflux from the Arabian Sea. The new data and estimates of diffusive fluxes from the Northern Indian Ocean sediments would

account for an additional 6.3% of the current global value to global P regeneration flux/supply. The mass balance study shows that the magnitude of diagenetic flux is larger than the fluvial flux into the Northern Indian Ocean. The results of the P nutrient demand estimates indicate that the Arabian Sea accounts for 87-90% of the Northern Indian Ocean. The burial flux of P in the BoB is 20 times larger than the Arabian Sea.

Table 6.1(a): Diffusive flux of phosphate, P_{total}, Fe_{total}, and bottom water DO of the studied locations from the Arabian Sea.

Group	Station Name	Depth (m)	Diffusive flux of Phosphate (µmol cm^{-2} yr^{-1})	P_{total} (µmol/g)	Fe_{total} (µmol/g)	Bottom Water Dissolved Oxygen (µmol/L)
Group 1	SSDT14/SPC1	28	-13.24	35.9	1245.9	4.77
	SSD27/SPC5	30	-1.26	60.8	709.6	61.08
	SSD27/SPC17	31	-7.49	48.3	909.1	0
	SSDT14/SPC2	31	-1.24	37.4	977.6	6.22
	SSD27/SPC22	32	-6.15	62.9	1136.5	0.62
	SSD27/SPC19	32	-5.29	40.2	1061.8	0
	SSD27/SPC21	32	-4.07	50.2	1115.8	4.17
	SSD27/SPC14	32	-2.26	56.2	971.3	2.42
	SSD27/SPC12	33	-0.36	14.3	285	32.92
	SSD27/SPC16	34	-21.48	45.9	1031.2	2.42
	SSD27/SPC23	35	-7.59	51.6	1090.3	3.56
	SSD27/SPC20	44	-25.25	46.2	NA	4.28
	SSD27/SPC13	44	-1.46	NA	NA	2.5
	SSD27/SPC15	45	-20.38	48	843.6	4.24
	SSD27/SPC18	46	-0.23	20.6	797.5	0
	SSD27/SPC6	50	-0.33	29.6	630.2	54.11
	SSK71/SPC22	64	-0.21	27.1	647.9	56.14
	SSD27/SPC7	106	-0.13	31.2	564.2	35.61
Group 2	SSK86/SPC3	30	-4.54	53.2	1207.9	191.33
	SSD27/SPC4	32	-0.87	43.3	579.8	97.6
	SSK86/SPC4	34	-3.39	NA	NA	182.09
	SSK86/SPC2	34	-3.56	NA	NA	200.35
	SSD27/SPC3	46	-0.19	13.8	292.9	89.95
	SSK80/SPC1	53	-0.29	17	508.4	208.28
	SSK71/SPC15	80	-0.18	17	221.4	81.05
	SSK71/SPC16R	99	-0.37	27.5	125.2	67.47
	SSK80/SPC2	110	-0.21	28.9	263.6	150.52

Table 6.1(a): Continued

Group	Station Name	Depth (m)	Diffusive flux of Phosphate (µmol cm^{-2} $yr^{-1)}$	P_{total} (µmol/g)	Fe_{total} (µmol/g)	Bottom Water Dissolved Oxygen µmol/L)
Group 3	SSK73/SPC14	158	-0.08	40	386.5	10.78
	SSK71/SPC17	195	-0.36	72.8	300.7	32.05
	SSK71/SPC10	212	-0.12	48.6	178.6	5.18
	SSK80/SPC8	217	-0.31	77.4	503.6	6.02
	SSK71/SPC24	218	-4.94	NA	NA	15.91
	SSD27/SPC11	229	-1.41	41	885.6	12.28
	SSK71/SPC1	238	-1.6	68.6	84.6	5.48
	SSK73/SPC7	243	-0.97	36.7	405.8	8.21
	SSK59/SPC-6	260	0.07	40.9	695.8	18.61
	SSK40/SPC4R	279	-0.11	80.1	230.7	9.32
	SSK73/SPC6	289	-2	54.5	171.5	4.89
	SSK80/SPC3	294	0.06	38.4	401.4	7.79
	SSK71/SPC18	297	-1.18	255.8	410.1	7.43
	SSK73/SPC3	300	-0.23	55.7	NA	6.3
	SSK59/SPC5	314	-0.65	31.1	461.7	25.86
	SSK40/SPC2	325	-2.22	55	361.9	7.33
	SSK80/SPC5	329	-0.42	51.3	522.1	4.74
	SSK86/SPC1	330	-0.63	49.7	388.7	5.08
	SSK40/SPC1R	347	-1.61	69	504	6.05
	SSK71/SPC25	353	-5.83	NA	NA	6.6
	SSK71/SPC7	399	0.02	500.5	63	3.98
	SSK71/SPC11	407	-1.73	39.7	79.6	15.61
	SSK71/SPC2	410	-0.39	47.5	73.5	34.37
	SSK71/SPC26	415	-9.16	41.4	670	5.1
	SSK71/SPC3	442	-0.05	107.3	99.4	20.49
	SSD27/SPC10	501	-0.61	36.3	553.2	16.9
	SSK71/SPC19	509	0.04	24.5	152.9	6.45
	SSK80/SPC6	541	-0.11	48.3	369.1	5.78
	SSK80/SPC4	563	-0.45	52.8	524.3	8.19

Table 6.1 (a): Continued

Group	Station Name	Depth (m)	Diffusive flux of Phosphate (µmol cm^{-2} yr^{-1})	P_{total} (µmol/g)	Fe_{total} (µmol/g)	Bottom Water Dissolved Oxygen µmol/L)
Group 3	SSK71/SPC4	630	-0.24	40.6	162.8	8.71
	SSK59/SPC4	635	-1.35	38.6	288.2	15.71
	SSK71/SPC12	751	-1	69.9	147.2	7.13
	SSK71/SPC13	774	-0.02	36.3	118.6	4.28
	SSK71/SPC20	791	-0.38	68.9	530	5.1
	SSK71/SPC5	826	0.06	48.5	372.4	3.9
	SSK73/SPC4	826	-0.12	45.3	493.8	18.48
	SSK71/SPC6	930	0.05	32.4	176	7.13
	SSK73/SPC1	951	0.07	44.9	NA	25.61
	SSK73/SPC13	973	-0.62	NA	NA	36.55
	SSK71/SPC9	1051	-0.04	38.5	12.9	23.57
Group 4	SSK71/SPC21	1544	0.02	40.6	635.7	47.28
	SSK80/SPC7	1711	-0.03	31.8	634.8	84.58
	SSD27/SPC8	1979	-0.3	23.1	276.5	98.66

Table 6.1(b): Diffusive flux of phosphate, P_{total}, Fe_{total}, and bottom water DO, of the studied locations from the Bay of Bengal.

Group	Station Name	Depth (m)	Diffusive flux of Phosphate (µmol cm^{-2} yr^{-1})	P_{total} (µmol/g)	Fe_{total} (µmol/g)	Bottom Water Dissolved Oxygen µmol/L)
Group 1	SSD19/SPC1	29	-0.03	17.9	604.4	62
	SSD19/SPC2	90	-0.6	19.2	685.8	5.4
	SSD03/SPC14	95	-0.46	21.2	636.9	5.8
	SSD19/SPC3	132	-5.92	25.3	745.2	4.3
	SSK50/SPC9R	148	-0.74	33.1	172.4	20.5
Group 3	SSD03/SPC17	175	-2.93	22	759.2	4.9
	SSK50/SPC7	202	-1.5	112	898.5	9.9
	SSK59/SPC3	224	-1.13	21.7	404.8	8.3
	SSD19/SPC4	226	-6.67	32.5	681.4	6.1
	SSD03/SPC5	230	-2.56	27	1160.6	4.5
	SSD03/SPC15RR	260	-16.4	27.8	632	5.1
	SSK50/SPC5	269	-0.53	31.3	770.7	11.7
	SSD03/SPC2	288	-0.75	22.6	942.7	5.9
	SSD03/SPC4	358	-1.09	NA	NA	5
	SSD03/SPC3	620	-0.09	21.5	1089.6	20.5
	SSD03/SPC10	632	-0.02	23.7	770.5	17.8
	SSD03/SPC18	640	-0.14	23.5	867	13.3
	SSD03/SPC16	650	-0.02	22.3	715.5	13.5
	SSD19/SPC5	719	-0.11	21.3	760.2	18.7
	SSD03/SPC6	800	-0.2	NA	NA	23.8
	SSD03/SPC1	829	-0.01	24.5	1103.2	31.3
Group 4	SSD19/SPC6	1314	-0.35	21.6	572.8	69.1
	SSD19/SPC7	1700	-0.21	18.8	724.1	98.4
	SSD19/SPC8	1954	-0.56	17.8	661.3	122.9
	SSD19/SPC9	2161	-0.39	18.7	774.8	127.3

Table 6.2: Diffusive flux of phosphate in different regions of the world ocean.

Area	**Depth (m)**	**Phosphate Flux** (mmol m^{-2} yr^{-1})	**Source**
Deep Arabian Sea	3188-4424	4-16	Grandel et al., 2000
Arabian Sea	527-4338	0.1-66.3	Schenau and De Lange 2001
Eastern South Atlantic	399-5626	0-6.02	Zabel et al.,1998
North Western shelf of the Black Sea	11-142	3.65-219	Friedl et al., 1998
Southern Atlantic Ocean	202-5697	0-23.38	Hansen et al., 1998

Table 6.3: Annual mass balance of P in the Northern Indian Ocean

Area	Diffusive flux of phosphate (x 10^{10} mol/yr)	Burial Flux of P (x 10^{10} mol/yr)	P nutrient Demand (x 10^{10} mol/yr)	Fluvial export flux of DIP (x 10^{10} mol/yr)	Fluvial export flux of DOP (x 10^{10} mol/yr)	Fluvial export flux of POP (x 10^{10} mol/yr)	Fluvial export flux of PIP (x 10^{10} mol/yr)	Atmospheric Input of DIP (x 10^{10} mol/yr)
Arabian Sea	3.9	0.326	8.5 - 92.8	0.21	0.0141	0.086		0.045
Bay of Bengal	3.78	60.5	1.0 - 13.7	0.67	0.019	0.45	4.07	0.071
Northern Indian Ocean	7.7	63.8	9.5 - 106.5	0.88	0.03	0.536	4.5	0.12

Chapter 7

Variability of phosphorus and iron geochemistry in two transects across the oxygen minimum zone in the Eastern Arabian Sea

Chapter 7

7.1 Introduction

The cycling of P and Fe is strongly coupled through iron oxyhydroxides; one of the dominant reactive Fe phases in sediments. The iron oxyhydroxides have high adsorption capacity and scavenge dissolved phosphate in oxic condition (Slomp et al., 1996). But under reducing conditions, it undergoes reductive dissolution and releases P to the overlying water (Froelich et al., 1988; Van Cappellen and Berner, 1988). While most of the reduced Fe undergoes re-oxidation, a portion of it reacts with other elements to form minerals such as Fe(II) sulfides (FeS, FeS_2), Fe(II) carbonates (siderite, ankerite), Fe(II) phosphates (vivianite), and Fe(II)-bearing authigenic clays, depending on the diagenetic conditions (Aller et al., 2004a, 2004b; Zhu et al., 2013; Egger et al., 2015; Ma et al., 2018).

Several studies were carried out of the P fractionation and cycling in the oxygen minimum zone (OMZ) of Arabian Sea (Schenau et al., 2000; Schenau and De Lange, 2001; Babu and Nath, 2005; Kraal et al., 2012, 2015; Linsy et al., 2018). The results from these studies show that the sink switching of P from labile phase to authigenic phase is more restricted to the sediments impinged by OMZ (Schenau et al., 2000; Schenau and De Lange, 2001; Kraal et al., 2012), where the preferential release of P from organic matter and reductive dissolution of iron oxyhydroxides drive the CFA formation (Schenau and De Lange, 2001; Linsy et al., 2018). The sedimentary cycling of P and Fe in the northern Arabian Sea (Murray ridge) was investigated by Kraal et al., (2012). Their model results suggest that Fe redox cycle plays a crucial role on the CFA formation and P retention in the lower boundary of the OMZ. They found large difference in P and Fe chemistry between stations within the OMZ, however, the reason for this dynamic condition is still not known completely. Information of cycling of Fe

and the impact of OMZ on the distribution of Fe bearing mineral phases in underlying sediments of the Arabian Sea is limited. Therefore, this study examines the variability of porewater P fluxes and P and Fe fractionation in sediments with changing bottom water concentration in two depth transects. To our knowledge, this study represents the first detailed investigation on the variability of P and Fe geochemistry across the OMZ of the Arabian Sea.

For this study, 16 surface sediments samples were collected from the western continental margin of India along two transects passing through the perennial OMZ, one off Gujarat (SSK71) in the northern part and another off Karwar (SSK80), in the central part (Fig. 7.1) were used. In addition to P speciation, Fe speciation was also undertaken in the surface sediments across the OMZ to assess the major Fe-bearing mineral phases favorable for P sorption and its variability with changing oxygenation. The sediment samples were also analyzed for texture, C_{org}, TIC and total nitrogen content. Dissolved oxygen and dissolved inorganic phosphate concentration in the water column were also measured for all stations.

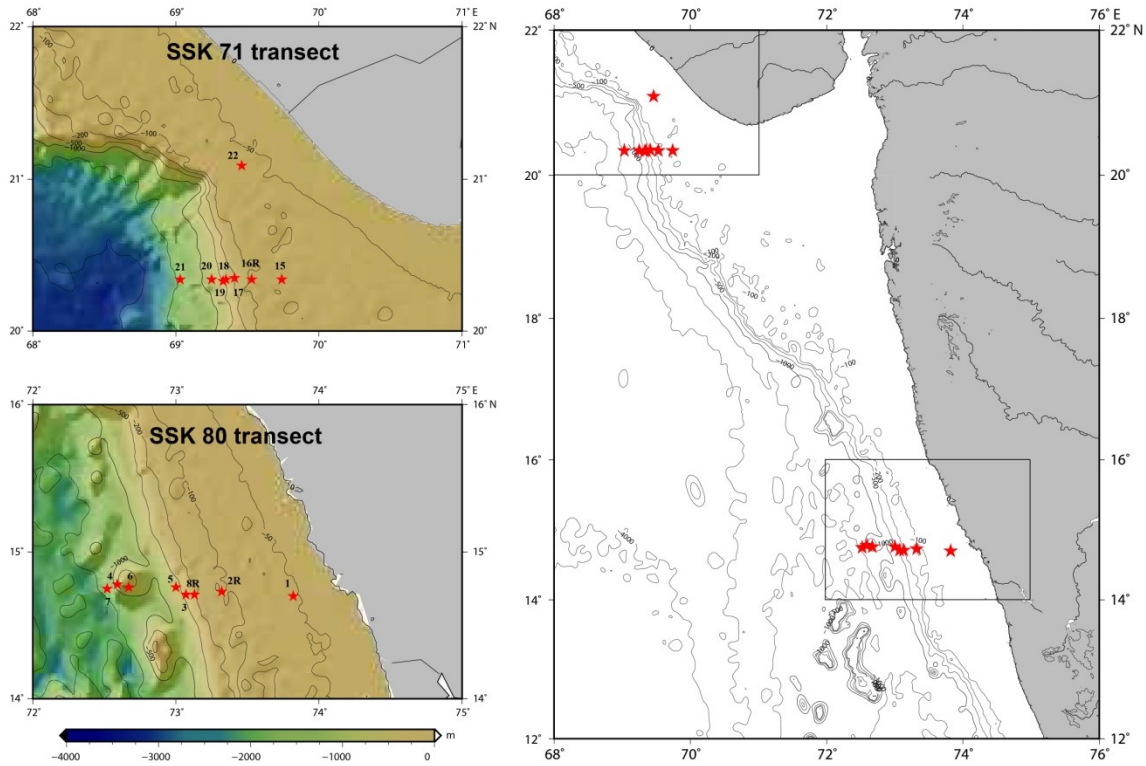

Figure 7.1*. Map of the western continental margin of India. The location of two depth transects along which sampling was done are indicated by rectangle boxes. 2. Bathymetric map of off Gujarat transect (SSK71). 3. Bathymetric map of off Karwar transect (SSK80).*

7.2. Results

7.2.1. General geochemistry of surface sediments

Figure 7.2 shows the bulk geochemistry of sediments along the two transects with OMZ boundary between 150 and 1200 m water depth. Bottom water oxygen concentration is high in shelf sediments (except at SPC22 station of SSK71 transect, which is falling in hypoxic condition) and decreases steadily from shelf to slope. After 1000 m water depth it increases and follows the general Arabian Sea trend. Compared to SSK80 transect, shelf sediments of SSK71 are underlain by more oxygen depleted water. The C_{org} contents of the study area are between 0.73 and 8 wt.% **(Fig. 7.2)** with an average value of 3.1 wt.%. Compared to SSK71 transect, the average C_{org} content of the SSK80

transect is high (SSK71: 2.36 and SSK80: 3.81). The highest C_{org} contents are associated with continental slope sediments impinged by OMZ (e.g., Nath et al., 1997). $CaCO_3$ content of the surface sediments varies between 38 and 85 wt.%. It is seen that the stations SPC15 and SPC16 of SSK71 and SPC2 of SSK80 transect fall in relict carbonate platform of early Holocene age in the outer shelf reported by Nair (1971).

7.2.2 DIP in seawater and porewater across the OMZ and diffusive fluxes of phosphate at the sediment-water interface

DIP concentration in the seawater varies between 0.15 and 3.68 µmol/L **(Fig. 7.3)** and follows the general nutrient profile in which depletion takes place in the surface and enrichment is seen at deeper depths. The seawater DIP concentrations do not show much variation across the OMZ. DIP concentrations in the porewater show a large range between 0.25 and 21 µmol/L **(Fig. 7.3)** but down core porewater DIP does not display significant variation in the shelf sediments that are overlain by oxic bottom water. In some of the hypoxic sites, DIP concentrations show a subsurface peak indicating the

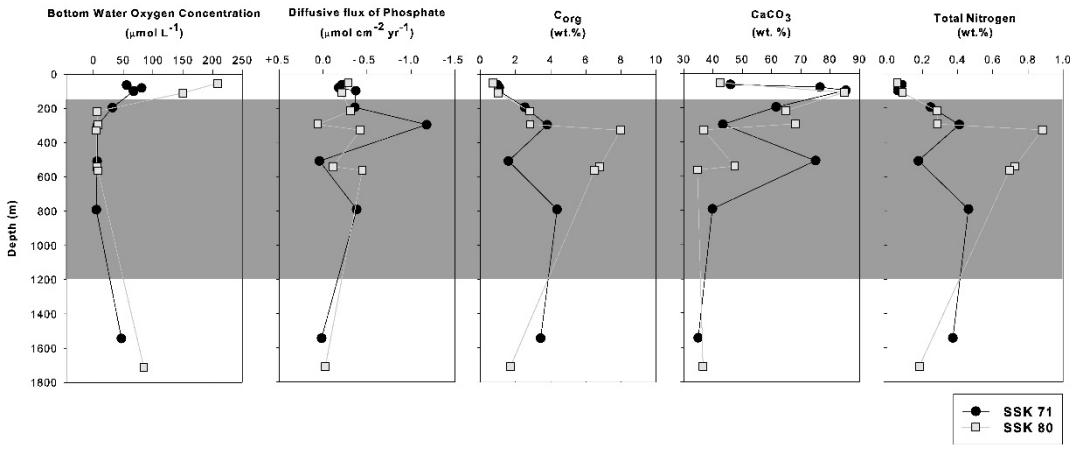

Figure 7.2: Trends with water depth for bottom water oxygen concentration, diffusive flux of phosphate at the sediment water interface and solid phase C_{org}, $CaCO_3$, and total nitrogen contents in the surface sediments. The grey color indicates the station falling in the OMZ

enhanced release of P **(Fig. 7.3)**. After the subsurface increase, a mid-depth depletion of porewater DIP is also observed at these sites.

Diffusive flux of phosphate calculated at the sediment-water interface varies between 0.017 and 1.17 μmol cm^{-2} yr^{-1} **(Fig.7.2)**. The negative values indicate that flux of phosphate is from sediment to the water column (except at three stations SPC19, SPC21of SSK71 transect and SPC3 of SSK80 transect). Highest benthic flux values are observed at hypoxic stations and lowest are observed at deeper sites (Fig. 7.3 and Table. 7.1).

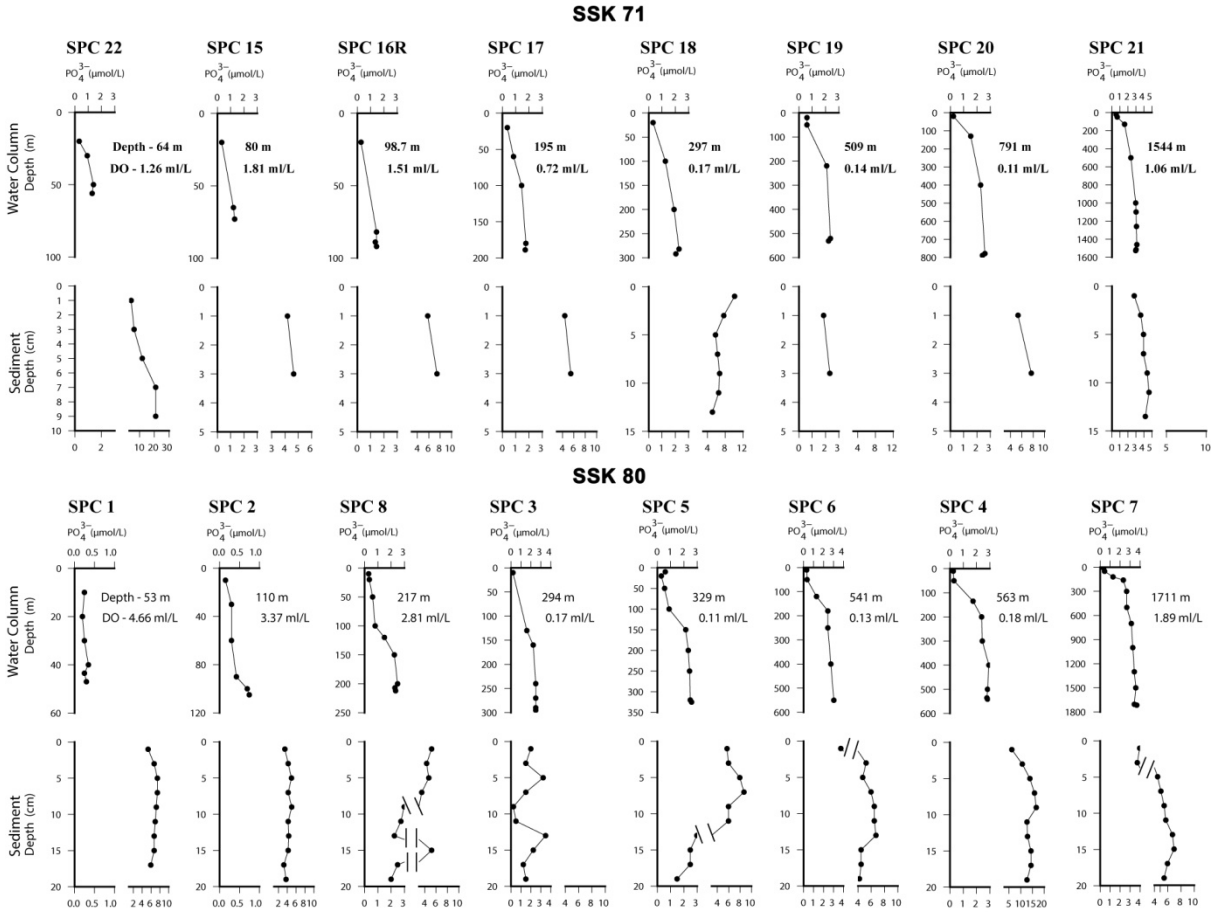

Figure 7.3*: Dissolved phosphate (µmol/L) in seawater (with depth) and porewater (with sediment depth) across the two transects.*

7.2.3 Speciation of Solid Phase P

P_{total} content in the study area ranges between 16.3 and 77.8 µmol g^{-1} **(Fig. 7.4)** except for one station with very high value (SPC18: 244 µmol g^{-1}) and the values are generally high in the sediments lying under the oxygen-depleted waters compared to the stations lying under oxic bottom water. The P_{total} values are comparable with previously reported values in the Arabian Sea (Schenau and De Lange, 2001; Babu and Nath, 2005).

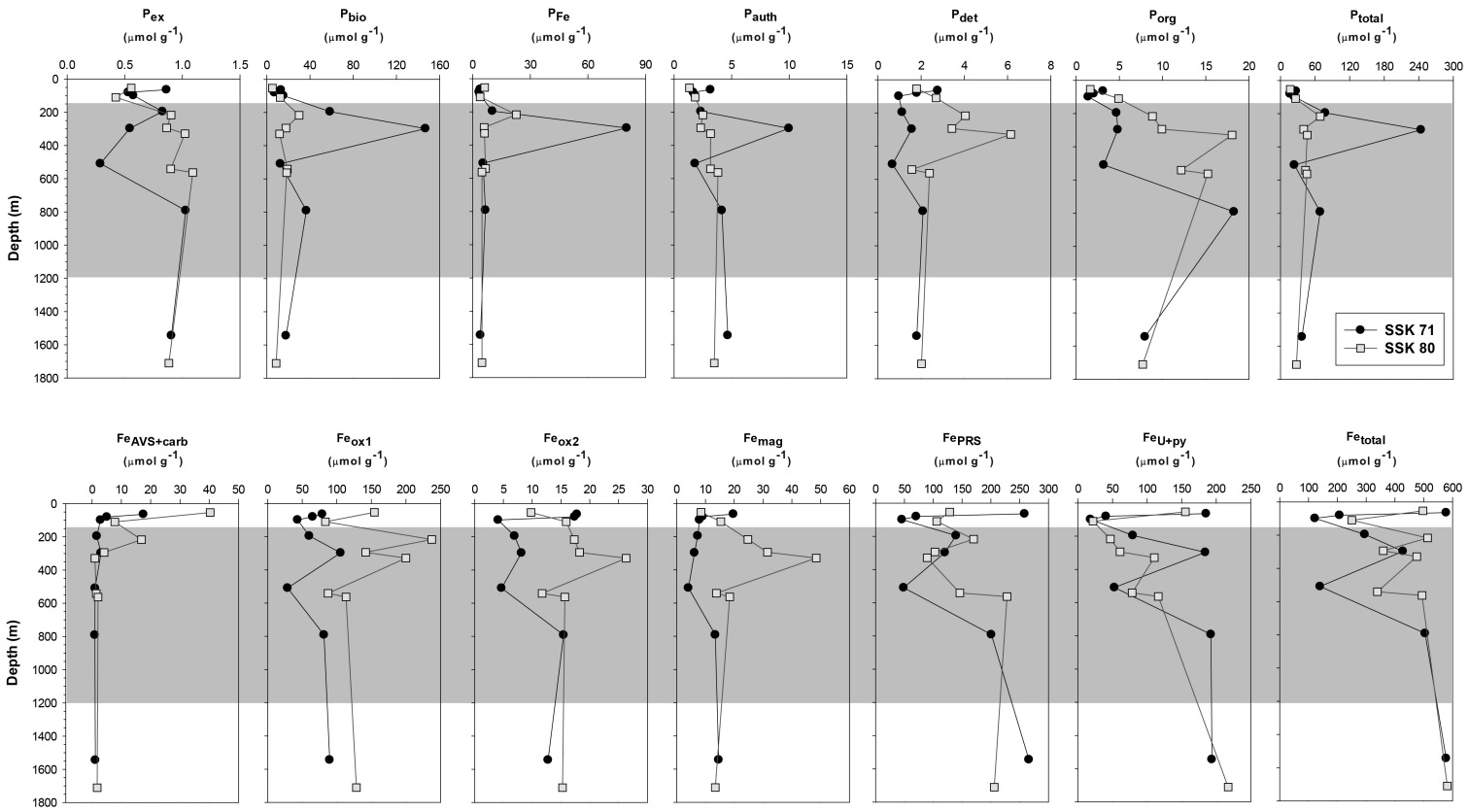

***Figure 7.4**: Trend with water depth for total P, total Fe and sequentially extracted phases of Fe and P (units in μmol/g) in sediments across the OMZ (shown as a grey band).*

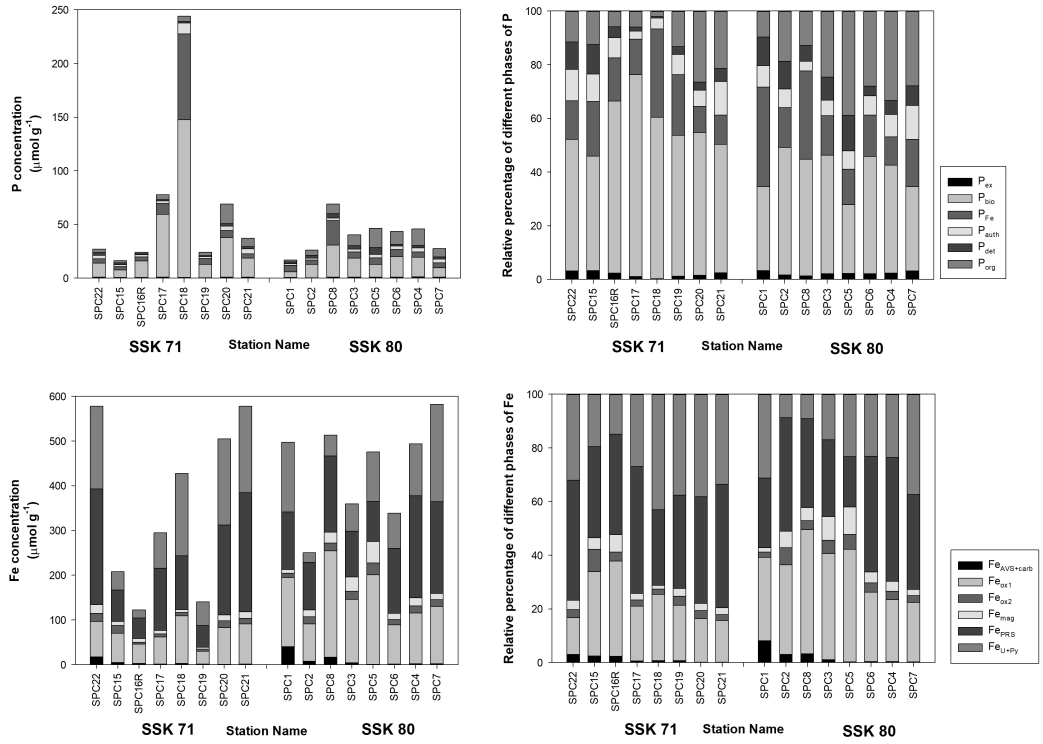

Figure 7.5: *Concentrations (left) and relative percentage (right) of different phases of P and Fe across the OMZ.*

Different phases of P in the two transects are shown in figure **(Fig. 7.5)**. P_{ex} concentrations range between 0.29 and 1.09 µmol g^{-1} with an average value of 0.76 µmol g^{-1}. P_{ex} fractions are negligible at all stations and account for 0.2-3.3% of the P_{total}. P_{bio}, largest pool of sedimentary P phase in the study area, concentrations are range from 5.25 to 146.95 µmol g^{-1} (average 30 µmol g^{-1}) and accounts for 25.6-75.3% of the P_{total}. Highest P_{bio} contents are found at the surface sediments overlain by oxygen-depleted water. The concentration of P_{Fe} is in the range of 3.35 to 80.16 µmol g^{-1} (average 11.19 µmol g^{-1}) and accounts for 9.7-37.2% of the P_{total}. The P_{org} content is low in SSK71 transect (2-26.5% of the P_{total}) compared to SSK80 transect (9.7-38.9% of the P_{total}). In SSK71 transect, P_{det} accounts for 0.6-11.01% of the P_{total} with an average of 4.75% while in SSK80 transect, it accounts for

3.6-13.25% of the P_{total} (average 8%). The P_{auth} content in the present study varies between 1.3 and 10 µmol g^{-1} and the highest values are found at the OMZ region. The P_{auth} content is low in SSK80 transect (average 2.7 µmol g^{-1}) compared to SSK 71 transect (average 3.7 µmol g^{-1}). Molar C_{org}/P_{org} ratio are high in all the samples and the values range from 175 to 632 **(Fig. 7.6)**. Molar C_{org}/P_{react} ratio ranges between 13 and 165 and is relatively high in SSK80 transect (average 82) compared to SSK71 transect (average 46).

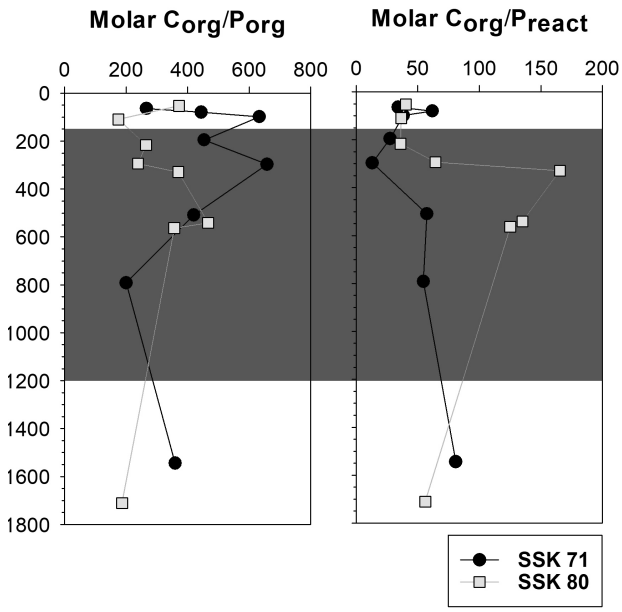

Figure 7.6: *Variation of molar C_{org}/P_{org} and C_{org}/P_{react} in the surface sediments across the OMZ (shown as a grey band).*

7.2.4 Speciation of Solid Phase Fe

Fe_{total} content of the surface sediments vary between 122 and 582 µmol g^{-1} **(Fig. 7.4)** with an average of 398 µmol g^{-1}.which is slightly lower than that of value reported in the western continental shelf of India (average 628 µmol g^{-1}- Kurian et al., 2013). The partitioning of solid phase Fe between various pools in two transects is shown in figure 7.5. The $Fe_{AVS+carb}$ content is in the range of 1-40.3 µmol g^{-1} (average 1.70 µmol g^{-1}) and the average $Fe_{AVS+carb}$ /Fe_{total} ratio is 0.017. $Fe_{AVS+carb}$ concentrations are relatively low compared with other fractions in most of the stations with higher values in shallow areas compared to the deeper areas. The second largest pool of Fe is $Feox_1$ and ranges between 28.9 and 237.5 µmol g^{-1} (average 106.3 µmol g^{-1}) with an average Fe_{ox1}/Fe_{total} ratio of 0.275. Fe_{ox1} concentrations are high in continental slope sediments. The Fe_{ox2} content in the transects vary between 4.1 and

26.3 µmol g^{-1} (average 13.6 µmol g^{-1}). The Fe_{ox2} phase is relatively low in both the transects and accounts only 3.7% of the Fe_{total} The Fe_{mag} content in the surface sediments vary from 4.1 to 48.5 µmol g^{-1} (average 4.07 µmol g^{-1}) and accounts 4.2% of the Fe_{total} with highest values at SPC3 and SPC5 of SSK80 transect sites. The Fe_{PRS} content is in the range of 45.7 -266 µmol g^{-1} (average 145.5 µmol g^{-1}) and the average Fe_{PRS}/Fe_{total} ratio is 0.36. The Fe_{U+py} content range between 18.2 and 217.3 µmol g^{-1} with an average 109.7 µmol g^{-1} and accounts 26% of Fe_{total}. The average relative percentage of the six Fe phases follows the order: Fe_{PRS} > Fe_{ox1} > Fe_{U+py} > Fe_{mag} > Fe_{ox2} > $Fe_{AVS+carb}$.

7.3. Discussion

7.3.1 Phosphorus cycling across the OMZ

Notwithstanding the variation in sampling interval, the DIP concentration profiles in seawater of both the transects (**Fig. 7.3**) show similar trend with lower values at surface down to about 100-200 m with a gradual increase towards the bottom, the changes being prominently seen in the southern transect (SSK-80). The increase at ~100 m possibly corresponds to water mass change with reducing influence of high salinity Persian Gulf water (e.g., Morrison et al., 1998). One reason for higher DIP content in the deeper water irrespective of location and DO content (within and outside OMZ) could be because of the benthic supply. This is reflected by higher porewater DIP concentrations in most of the locations compared to the bottom waters (**Fig. 7.3**).

The porewater profiles provide quantitative and semi-qualitative information on P remobilization in sediments (e.g., Ogrinc and Faganeli, 2006). The Arabian Sea which is characterized by intense OMZ and redox changes are reflected in the porewater profiles presented here. The oxygen-depleted condition leads to the preferential release of P from

organic matter. The dissolution of iron-oxyhydroxides and the release of P adsorbed by the iron oxyhydroxides leads to the enrichment of DIP in the porewater. The near constant porewater profile in the shelf sediments at depths (SPC1 and SPC2 of SSK80 with oxic bottom water DO values of 208 and 150 µmol/L; Table 7.1) shallower than OMZ (**Fig. 7.3**) implies that benthic remobilization is weak in this area, where high sedimentation rate in the shelf region and oxic water condition hinders the remobilization processes (see Linsy et al., 2018). This is consistent with the previous findings in the northern Arabian Sea, where the oxic sediments were associated with low benthic regeneration (Schenau and De Lange, 2001). The increasing porewater DIP in the continental slope sediments of the Eastern Arabian Sea indicate that remobilization of P is more at the OMZ impinged depths which may be linked to the phosphate release due to the microbially mediated reductive dissolution of iron oxyhydroxides (Woulds et al., 2009). The mid-depth depletion in porewater observed at the sediments overlain by oxygen-depleted waters indicates the precipitation of CFA (Froelich et al., 1988). The decrease in porewater profile is more prominent at the site SPC5 where ongoing phosphogenesis was reported by Linsy et al. (2018). The stations deeper than 1500 m water depth, where the bottom water is relatively oxic, shows a slight increase in the porewater DIP which may either be due to the preferential release of P from organic matter or the dissolution biogenic apatite.

Benthic flux of P calculated from porewater data are shown in Table: 7.1 and **Figure 7.2**. Except for three stations, the other stations show negative flux indicating the movement of phosphate from sediment to the water column and the magnitude of diffusive flux ranged from 0.017 to 1.17 µmol cm^{-2} yr^{-1}. The benthic flux calculated in the EAS is generally similar to the previously reported values in the Arabian Sea (Grandel et al., 2000; Schenau

and De Lange, 2001) and South Atlantic Ocean (Hensen et al., 1998) and less than that of the Peruvian OMZ.

At the deeper areas of the present study benthic flux is low due to the oxic nature of the bottom water, which enhances adsorption processes and limits the release of P to the sediments. The positive correlation of phosphate fluxes with P_{bio} and P_{Fe} reflect the major role of fish debris and iron oxyhydroxides dissolution in the release of P across the OMZ. The positive values were seen in two stations in the northern transect (water depths of #SPC19 -509 m within the OMZ and #SPC21-1544 m beneath the OMZ) and one station in the southern transect (water depth #SPC3-294 m within the OMZ) (Table 7.1). While in SPC19, the bottom water and the porewater values were nearly similar and thus no gradient, in SPC21 the porewater DIP content was in general higher than the seawater except at the sediment-water interface (top 2cm) (Fig. 7.3). In the southern transect, the negative gradient is clearly due to multiple-depth depletion within the sediments (**Fig. 7.3**) possibly reflecting the episodes of P authigenesis.

Deposition of organic matter is the principal source of reactive P to the sediments. The Arabian Sea is one of the highly productive regions in the world ocean, thus the deposition of organic matter plays a major role in the cycling P in the sediments of the Arabian Sea. The C_{org} values obtained here are comparable with the previously reported values from the Arabian Sea (Calvert et al., 1995; Paropkari et al., 1992; Babu and Nath, 2005; Cowie et al., 2014). Despite the high productivity in the SSK71 region (Madhupratap et al., 1996), the C_{org} contents are higher in the southern (SSK80) transect **(Fig.7.2)** which is consistent with the previous findings (Babu and Nath, 2005). Intense remineralization of organic matter was previously reported in the NE Arabian Sea (Sarma et al., 1996; Hupe et al., 2001), which

could be the reason for the lower C_{org} content in the SSK71 transect. The high C_{org} content in the continental slope sediments impinged by OMZ was attributed to enhanced organic matter preservation under the oxygen-depleted condition and progressive decay of organic matter with increasing O_2 exposure below the OMZ (e.g., Cowie et al., 2014). According to Cowie et al. (2014), low C_{org} content in the shelf sediments is due to the extensive reworking and/or winnowing of organic matter from carbonate sand deposits on the mid- and outer shelf, or to dilution of near-shore muds with organic-poor terrestrial clays. Below the lower boundary of the permanent mid-water OMZ, there is a progressive drop of C_{org} content indicating the degradation of organic matter within the water column.

The molar C_{org}/P_{org} is a good indicator of P burial in sediments and redox-dependent regeneration of P from organic matter (Babu and Nath, 2005; Kraal et al., 2012). The molar C_{org}/P_{org} ratio in surface sediments is greater than the Redfield ratio (106) and shows large variation within the OMZ with values ranging between 175 and 657. The high ratios is similar to those found in OMZ sediments of Pakistan margin (318 ±86; Filippelli and Cowie, 2017) and closer to the mean sediment ratio of 430 (Mach et al., 1987). The high C_{org}/P_{org} ratio is usually attributed to the preferential release of P relative to C. As these sediments are surficial, the preferential loss of P_{org} must be occurring either in the water column (e.g., Paytan and McLaughlin, 2007; Benitez-Nelson, 2000) or during residence in surficial sediments, as several recent studies have indicated that the transformation process of P_{org} is rapid (Filippelli and Cowie, 2017 and references therein). High C_{org}/P_{org} ratio in SSK71 transect compared to SSK80 transect reflects that the preferential regeneration of P_{org} relative to C is more intense in the NE Arabian Sea where the OMZ is more intense compared to the SE Arabian Sea (Babu and Nath, 2005). Due to the efficient transfer of P_{org}

to other sedimentary P phases, C_{org}/P_{react} ratio can be used to study the diagenetic redistribution of P in sediments (Anderson et al., 2001) and it reflects the overall burial efficiency of P in sediments (Kraal et al., 2012). The high P_{react} and relatively low C_{org}/P_{react} ratio (less than Redfield Ratios (13-80) in OMZ **(Fig.7.6)** sediments from the SSK71 transect indicate the diagenetic transformation of labile forms of P to the authigenic phase.

Iron oxyhydroxides are the potential carrier of reactive P to the sediment, where oxic conditions favor the adsorption of dissolved phosphate on the surface of iron oxyhydroxides (Slomp et al., 1996). Thus the presence of iron oxyhydroxides scavenges upward diffusing phosphate released by the dissolution processes and limits the release of P to overlain water. But under reducing conditions, these iron oxyhydroxides undergo reductive dissolution and P is released to the surrounding water. Enrichment of reactive iron may occur at the sediment-water interface due to re-precipitation of upward diffusing Fe^{2+} mobilized under reducing condition, as the oxic-suboxic interface is located close to the sediment surface (Schenau and De Lange, 2001). Relatively high percentage of P_{Fe} content in the SSK71 reflects the re-adsorption of phosphate released upward during organic matter degradation or reduction of iron oxyhydroxides at the deeper depths (Babu and Nath, 2005). Another possible reason for the high P_{Fe} content is the transport of iron oxyhydroxides through the water column and its subsequent adsorption with P from the water column. The relative percentage of P_{Fe} content is low at the stations (SPC3, SPC4, SPC5, SPC6) overlain by oxygen-depleted water. This decrease is accompanied by an increase in porewater DIP concentration at the subsurface indicating the dissolution of iron oxyhydroxides and corresponding release of P to the porewater. Thus, reductive dissolution of iron oxyhydroxides plays a key role on the benthic porewater fluxes in the OMZ sediments of the

Arabian Sea. The P concentration associated with fish debris is the largest pool of P in the study area and the results are comparable with previous studies (Schenau and De Lange, 2001; Babu and Nath, 2005; Linsy et al., 2018). High productivity (600 mg cm^{-2} d^{-1}) of the Arabian Sea enhances the fish production (Madhupratap et al., 2001) and their debris forms a potential source of reactive P to the sediments which consists of 60-70% of hydroxyapatite (Suess, 1981; Van Cappellen and Berner, 1988). Previous studies have found out that high benthic phosphate fluxes in continental margin sediments of the Arabian Sea are, to a large extent, a result of biogenic apatite dissolution (Schenau and De Lange, 2001; Linsy et al., 2018). Compared to shelf sediments, P_{bio} content is highest at slope sediments impinged by OMZ and can be attributed to the high fish production rates in the surface waters and reduced biogenic apatite dissolution rates in the water column in comparison to the deep Arabian Sea (Schenau and De Lange, 2001, 2000). Compared to southern transect (SSK80), P_{bio} content is higher in the SSK71 transect in the north due to high primary productivity in that area (807 mg cm^{-2} d^{-1}) compared to south (335 mg cm^{-2} d^{-1}) (Madhupratap et al., 1996) and the enhanced preservation of fish debris under more intense OMZ of the NE Arabian Sea.

Sink switching of P is the key processes leading to the formation of CFA in sediments (Föllmi, 1996; Ruttenberg and Berner, 1993). The release of phosphate from the microbial degradation of organic matter (Froelich et al., 1988; Ruttenberg and Berner, 1993), desorption of iron oxyhydroxides (Slomp et al., 1996) and dissolution of fish debris (Suess, 1981; Schenau and De Lange, 2000) results in the enrichment of DIP concentration in the porewater. When the porewater is saturated with DIP, precipitation of CFA will occur. Coastal upwelling and the presence of OMZ in the Arabian Sea make it a suitable site for

CFA formation. However, this sink switching of P and formation of CFA is mostly restricted to the OMZ of the Arabian Sea (Schenau et al., 2000; Babu and Nath, 2005; Kraal et al., 2012; Linsy et al., 2018).

High P_{auth} content observed at the continental slope of Arabian Sea implies the precipitation of authigenic apatite. A study by Faul et al., (2005) suggest that precipitation of CFA in the water column resulted by the organic matter remineralization and its subsequent settling also contribute to the CFA pool in the sediment. Thus at the sediment-water interface, settling of CFA from the water column may play a significant role. The mid depth depletion of porewater phosphate concentration also indicates the precipitation of Ca-P minerals and is more pronounced at SPC5 (SSK80), where Linsy et al., (2018) found evidence of ongoing phosphogenesis. The degradation of organic matter and dissolution of fish debris are the key processes controlling the Ca-P mineral formation here (Linsy et al., 2018). The low concentrations of P_{auth} at the deep sites implies that limited role of P_{auth} in the sequestration of P released from labile sedimentary pools (Kraal et al., 2012). Recent studies from the Arabian Sea suggest that other than in situ precipitation, atmospheric deposition may also contribute CFA mineral to the sediment pool (Kraal et al., 2012; Linsy et al., 2018).

The P_{det} is low in all the samples (average 6.4% of the total) and is highest in the shelf sediments and at the station SSK80 SPC5 situated on the marginal high, where the P_{det} mainly comes through the atmospheric input (Linsy et al., 2018). High P_{det} content in the SSK80 transect is consistent with the earlier study (Babu and Nath, 2005), indicating the high terrigenous influence in this region. In the northern transect, two stations on the shelf with low P_{det} content are on the carbonate bank with no terrestrial sediment deposition (Nair, 1971).

7.3.2 Iron Cycling across the OMZ

The sodium acetate extract (pH 4.5) used for leaching first Fe fraction (Poulton and Canfield, 2005) is capable of extracting both acid volatile iron sulfide Fe (II)$_{AVS}$ and Fe (II) carbonate (Zhu et al., 2012) and this pool ($Fe_{AVS+carb}$) only accounts for an average of 1.7% of $Fe_{total.}$. The low concentration suggests that the formation of both the Fe_{AVS} and Fe_{carb} phases is not active in the study area where most of the upward diffusing Fe^{2+} undergoes re-oxidation at the sediment-water interface. Siderite formation occurs only in Fe rich non-sulfidic suboxic-anoxic environment where microbial Fe reduction is strongly coupled to organic matter oxidation (Zhu et al., 2012). Since the Arabian Sea is a denitrification zone, and sulfidic conditions are not been reported so far in this area, the Fe_{AVS} contribution is ruled out. Relatively, the highest concentrations are mainly seen in shallow shelf stations close to coast in both transects (Fig. 7.4), which probably may represent the leaching of Fe-oxide present as coatings/infilling of carbonate skeletons.

The iron oxyhydroxides in sediments can either be contributed from terrestrial sources or through the oxidation and precipitation of upward diffusing Fe^{2+} at the sedimentary oxic/suboxic redox boundary (Henkel et al., 2018 and references are therein). Compared to other oxide minerals, amorphous iron oxyhydroxides such as ferrihydrite and lepidocrocite are more reactive towards sulfide. In anoxic environment, iron oxide/oxyhydroxide undergoes reduction either by microbial iron reduction coupled to organic matter oxidation or by chemical iron reduction mainly through dissolved sulfide produced by sulfate reduction (Canfield et al, 2005; Jing et al., 2017). In the present study, Fe_{ox1} phase representing ferrihydrite and lepidocrocite is the second largest pool of the sedimentary iron phase. In both transects, highest Fe_{ox1} concentrations are obtained between 200 and 350 m

water depth. Despite the hypoxic conditions, high concentration of Fe_{ox1} is found in the surface sediments studied here, which is consistent with earlier work in the Northern Arabian Sea (Kraal et al., 2012). High Fe_{ox1} phase in the surface sediments of the Arabian Sea is likely in part caused by re-oxidation of upward diffusing Fe^{2+} (Kraal et al., 2012).

Recent studies found that iron oxide plays an important role in the preservation of organic carbon against microbial degradation in sediments (Lalonde et al., 2012; Zhao et al., 2016). Iron oxides have high sorption capacity (110-140 mg C_{org} $g^{-}1$) for C_{org} retention through inner-sphere complexation (Zhao et al., 2016; Ma et al., 2018). The complexation of Fe-C_{org} sterically inhibits reductive dissolution (Barber et al., 2017). In an earlier study, Witter et al., (2000) showed that Fe(III) was more complexed with organic ligands in the Arabian Sea OMZ than in many other oceanic environments. Thus, high Fe_{ox1} in the sediments of the Arabian Sea likely results from Fe-C_{org} complex formation.

The cycling of Fe is strongly coupled with S cycling and the formation of pyrite and subsequent burial are the major pathways for their permanent removal from the ocean (Berner, 1982). In marine sediments, pyrite formation occurs by the reaction of dissolved sulfide produced during the sulfate reduction with reactive iron compound via iron monosulfide intermediate (Berner, 1982; Wilkin and Barnes, 1996; Wijsman et al., 2001). The major factor limiting the pyrite formation in sediments is the availability of dissolved sulfide, reactive iron minerals, and metabolizable organic matter (e.g. Berner, 1970; Passier et al., 1997) whereas in anoxic environments, pyrite formation is commonly limited by the availability of reactive iron phases where iron oxides are already reduced and sulfidised in the water column (Raiswell and Berner, 1985; Boesen and Postma, 1988; Calvert et al., 1991; Middelburg, 1991; Lallier-Vergès et al., 1997; Schenau et al., 2002).

In our study, Fe_{U+py} phase includes both residual Fe and pyrite, which contributes an average of 26% of the Fe_{total} (Fig.7.5). Previous studies in the Arabian Sea found that pyrite formation in the Arabian Sea is limited in the upper centimeters of the sediment column (Emeis et al., 1991; Passier et al., 1997; Schenau et al., 2002; Kraal et al., 2012). The low rate of sulfate reduction in the Arabian Sea limits pyrite formation (van der Weijden et al., 1999). Even though the Arabian Sea is oxygen-depleted, sulfate reduction is not taking place in the shelf (Naqvi, 2008) and no euxinic conditions were found to develop in the Arabian Sea during the last 120 kyr (Schenau et al., 2002). A study by Law et al. (2009) suggests that the abundance of Fe-oxides and Mn-oxides together with the associated metal reducing microbial communities, may act to suppress rates of sulfate reduction in the OMZ of Arabian Sea by consuming available metabolites to levels below threshold concentrations commonly tolerated by sulfate-reducing bacteria. Extremely low $Fe_{AVS+carb}$ phase in the present study also suggests low rate of sulfate reduction in the OMZ. This indicates that a large fraction of Fe_{U+py} phase in the surface sediments is most likely is in residual form in the sulfide-poor setting of the Arabian Sea.

The $Fe_{ox2,}$ representing goethite, akaganeite and hematite in the present study is relatively lower than the Fe_{ox1} (Fig.7.5). Though, there is a tendency of mineral transformation from ferrihydrite to secondary iron mineral phases such as goethite, lepidocrocite, siderite, and akaganeite (Adhikari et al., 2017 and references therein), the formation of more crystalline Fe_{ox2} from amorphous iron oxyhydroxides occurs mainly in the deeper sections of the core. The variation of Fe_{ox2} in this study follows P_{det} variations indicating a detrital source for Fe_{ox2} for the surface sediments and its variation across the OMZ is mainly due to the difference in the depositional flux of lithogenic material.

The Fe_{mag} content is high in SSK80 transect compared to SSK71 off Gujarat (Fig.7.4). In the SSK71 transect, the highest Fe_{mag} content is found in the shelf region and it decreased with increasing water depth. Whereas in the SSK80 transect, the high content is seen at a depth between 200 and 350 m within the OMZ. Detrital magnetite from igneous terrains is one of the major sources of sedimentary magnetite (Zhu et al., 2012). The chemical weathering of titanomagnetite-rich Deccan Volcanic Province and its subsequent transport by the Narmada and Tapti Rivers bring magnetite rich sediments to the shelf off Gujarat (SSK71) (Kolla et al., 1981; Shankar et al., 1987). Biogenic magnetite is another source of Fe_{mag} in the sedimentary environment which can be formed in two ways; biologically controlled and biologically induced conditions (Roh et al., 2003 and references are therein). Fe_{mag} formed by magnetotactic bacteria is biologically controlled processes whereas Fe_{mag} formation by Fe(III) reducing bacteria is biologically induced remineralization (Konhauser, 2009). Thus, high Fe_{mag} content at the sites SSK80 SPC3 (water depth 294 m & DO-7.8 µmol/L) and SSK80 SPC5 (water depth 329 m & DO-4.7 µmol/L) could be due to biogenic magnetite formation, where high C_{org} and oxygen depleted condition can favor their formation.

Majority of the iron minerals deposited in marine sediments are Fe-silicate minerals and in the present study, Fe_{PRS} contributes an average of 37% of the Fe_{total} (Fig.7.5). A good positive correlation between Fe_{PRS} and Fe_{U+py} suggests that they share a common source. Fe_{PRS} shows high content in the inner shelf sediments (SSK71 SPC22). The sediments in this region receive lithogenic flux from Narmada and Tapti rivers (Kolla et al., 1981; Rao and Wagle, 1997). However, the terrigenous flux is restricted in the shelf up to a distance of 175 km from the shore (17-60 m water depth) (Rao and Wagle, 1997). A sudden decrease in Fe_{PRS} and Fe_{U+py} is observed at the stations SPC15 and SPC16. These stations lie on the Fifty

Fathom Flat (FFF); a topographic feature which is predominantly comprised of relict carbonate sand ($CaCO_3$ 77 and 85% respectively for SPC15 and SPC16). The prevailing high energy condition in this area transports siliciclastic sediments further offshore (Rao and Wagle, 1997) limiting the modern sedimentation in the FFF. An increase of Fe_{PRS} and Fe_{U+py} is observed on crossing the FFF and can be attributed to the Indus River sediments which are transported to the deeper Arabian Sea (Rao and Rao, 1995). High smectite and low chlorite and illite contents were previously reported off Gujarat coast (Rao and Rao, 1995; Kessarkar et al., 2003) and this smectite could be the reason for the high Fe_{PRS} content in the inner shelf of SSK71 transect compared to SSK80. In SSK80 transect, high Fe_{PRS} content is observed at continental slope sediments. Low illite and chlorite content in the inner shelf and high content in the outer shelf/slope sediments were reported earlier in this region (Rao and Rao, 1995). They suggest that the high surface runoff and offshore transport of the surface water during the SW monsoons together with the narrow shelf width in this region are probably responsible for the cross-shelf transport of clay mineral and their accumulation in the outer shelf/slope sediments. The sediments in this area are derived mainly from gneissic rocks of the hinterland (Kurian et.al., 2013; Kessarkar et al., 2003 and references are therein), and thus a major fraction of Fe_{PRS} and Fe_{U+py} would have come from this source

7.3.3 Linkage of P and Fe

Iron oxyhydroxides are the primary constituents governing the P mobility in sediments. The binding mechanism includes adsorption on the surface of iron oxyhydroxides or co-precipitation with metal ion. However the adsorption capacity of iron oxyhydroxides varies with mineralogy, crystallinity, morphology and chemical composition (Kostka and Luther, 1994; Thamdrup, 2000). The adsorption of phosphate on iron oxyhydroxides involves ligand

exchange mechanism in which OH^- group on the hydrous oxides is replaced by phosphate anion in solution (Zhang and Huang, 2007). This reaction is pH dependent in which excess hydroxide ion can reduce P-retention in metal complexes (Lijklema, 1980). In anoxic settings sulfate reduction also affects the P adsorption; in which sulfate reduction produce iron OH ion and promote desorption of P (Caraco et al., 1993). But non-sulfidic reducing condition leads to the precipitation of Fe-P mineral such as vivianite (Dijkstra et al., 2014).

Iron oxide mineral such as ferrihydrite, lepidocrocite and goethite, will play a greater role in the adsorption of P in natural environment than minerals with characteristically lower surface areas, such as hematite (Torrent and Schwertmann, 1992; Slomp and van Raaphorst, 1993; Ruttenberg and Sulak, 2011). In this study, P concentrations were measured in different phases of iron to quantify the iron bound P and understanding the binding of P with different iron minerals in bottom waters with varying oxygenation conditions. Most of the P is associated with Fe_{ox1} phase (Fig 7.7) which includes easily reducible iron oxyhydroxides such as ferrihydrite and lepidocrocite. However large difference in concentration was found between Fe_{ox1}-P extracted by hydroxylamine hydrochloride (Poulton and Canfield method) and P_{Fe} extracted by citrate dithionite bicarbonate extract (SEDEX method). This may indicate that the iron bound P is overestimated in hydroxylamine hydrochloride extraction.

A previous study has found that hydroxylamine-HCl can solubilize 62% of P associated with Ca in shell and 32% of P in CFA (Mangan, 2007). Thus, in order to obtain the P associated with Fe_{ox1} phase we have subtracted the P concentration measured at Fe_{ox2} phase (goethite, akaganeite, hematite) from P_{Fe} and still found that the P concentration is high in Fe_{ox1} phase compared to $Fe_{ox2.}$ This suggests that most of the P in marine sediments is associated with easily reducible Fe oxide such as ferrihydrite (Fig. 7.7) which is poorly crystalline, and has

large micropore volume and surface site density compared to other Fe oxide minerals (Wang et al., 2013).

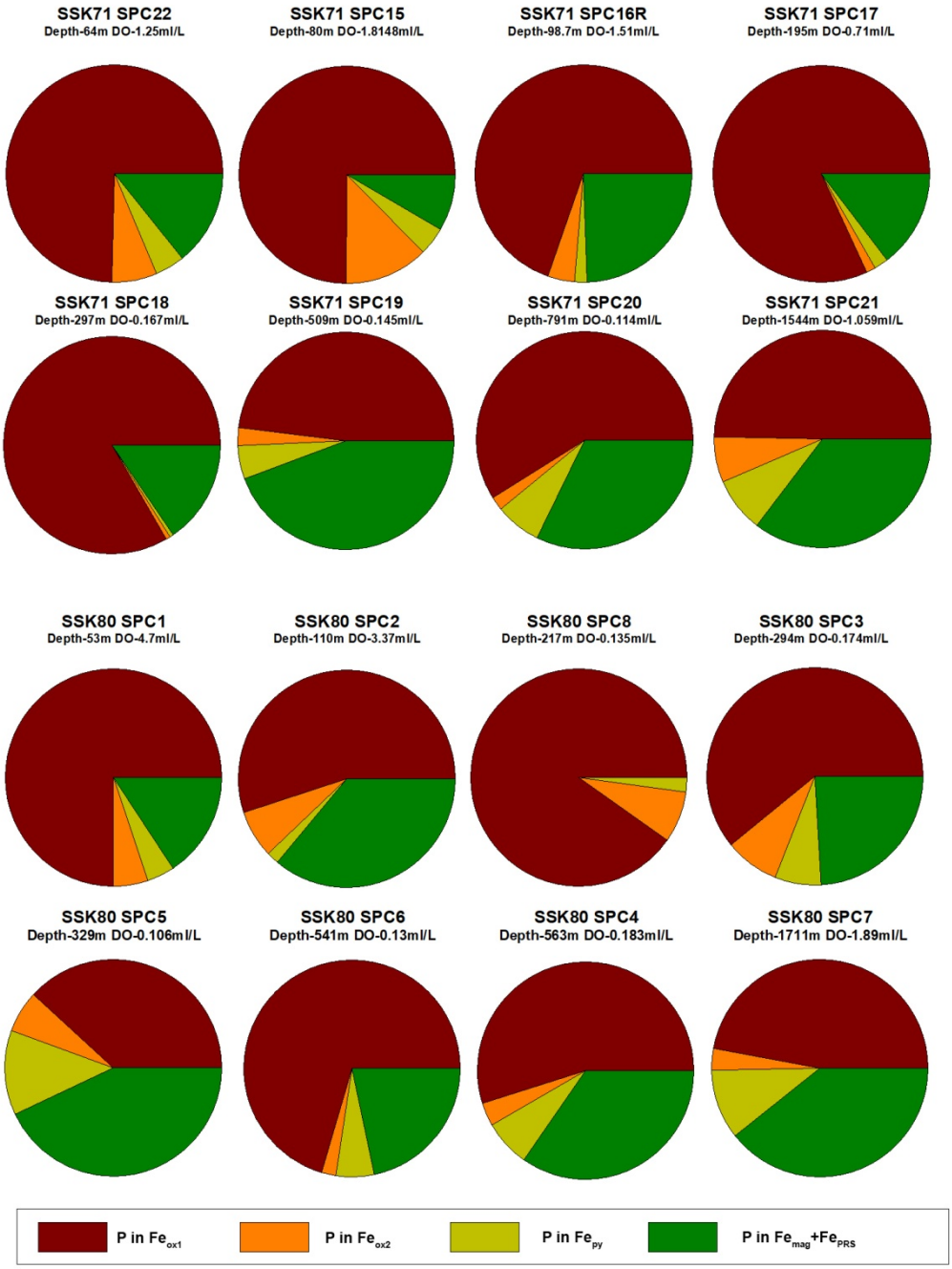

Figure 7.7: P concentrations measured in different phases of Fe.

The low concentration of P at the Fe_{ox2} phase is largely due to the presence of more crystalline iron oxyhydroxides such as goethite and hematite. The sorption of P on amorphous iron oxyhydroxides was reported to be far greater (~20-fold higher) than that of crystalline Fe (III) oxides (e.g. goethite and hematite). Therefore, ferrihydrite may play a more important role in P cycling in marine environment.

The adsorption of P in sediments will depend on several factors such as availability of iron oxyhydroxides, pH, dissolved oxygen concentration, crystallinity of available iron oxyhydroxides, organically bound iron oxy hydroxides etc. The presence of freshly precipitated amorphous iron oxyhydroxides at the surface sediments increases the adsorption of P in Arabian Sea. However, the adsorption of humic substance/fluvic acid on the surface of iron oxyhydroxides may reduce the phosphate adsorption in sediments (Sibanda and Young, 1986). One of the reasons for the persistence of Fe_{ox1} in the surface sediments of Arabian Sea is due to the presence of Fe-C_{org} which may reduce the adsorption of P on iron oxyhydroxides. A study by Zhang and Huang (2007) suggests that rather than iron oxides exchangeable phosphate governs the adsorption behavior in sediments. However poor correlation between P_{ex} and P_{Fe} indicates that P_{ex} playing minor role on the P adsorption in sediments. The results suggest that availability of ferrhydrite plays a major role on the variation of P_{Fe} in the surface sediments of Arabian Sea.

Conclusion

The porewater DIP profiles and solid phase P speciation study in two transects across the OMZ indicates that the authigenic formation of P is largely restricted to the OMZ of the

Arabian Sea, where high P remobilization from organic matter, reduction of iron oxyhydroxides and fish debris dissolution contribute to the formation. The high P_{Fe} content in the sediments overlain by oxygen depleted water is mostly due to the re-adsorption of upward diffusing phosphate. The high benthic phosphate flux and high C_{org}/P_{org} ratio in the OMZ indicate that P retention capacity of the Arabian Sea sediments is low.

Fe fractionation study indicate that even under hypoxic conditions, the formation of Fe (II) minerals such as siderite iron mono sulfide, pyrite etc are not active in the Arabian Sea due to low sulfate reduction and presence of abundant iron oxyhydroxides associated with metal reducing microbial communities. The persistence of iron oxyhydroxides in hypoxic condition is due to re-oxidation of upward diffusing Fe^{2+} or the complexation of Fe oxy hydroxides with organic matter and inhibits the reductive of dissolution of iron oxy hydroxides. The distribution of Fe_{PRS} and Fe_{U+py} in the EAS is mostly controlled by the depositional characteristics rather than diagenesis.

Table 7.1 Water depth, bottom water oxygen concentration, diffusive flux of P and total organic carbon (C_{org}) of the surface sediments of the studied sites.

Transect Name	Station Name	Water Depth (m)	Bottom Water Oxygen (µmol/L)	Diffusive flux of P (µmol cm^{-2} yr^{-1})	C_{org} (wt.%)
SSK71	SPC22	64	56.1	-0.215	0.99
	SPC15	80	81.1	-0.178	1.08
	SPC16R	98.7	67.5	-0.373	1.06
	SPC17	195	32.0	-0.362	2.54
	SPC18	297	7.4	-1.178	3.81
	SPC19	509	6.5	0.041	1.61
	SPC20	791	5.1	-0.381	4.38
	SPC21	1544	47.3	0.017	3.44
SSK80	SPC-1	53	208.3	-0.286	0.73
	SPC-2	110	150.5	-0.211	1.03
	SPC-8	217	6.0	-0.313	2.81
	SPC-3	294	7.8	0.061	2.84
	SPC-5	329	4.7	-0.423	8.00
	SPC-6	541	5.8	-0.112	6.80
	SPC-4	563	8.2	-0.447	6.52
	SPC-7	1711	84.6	-0.026	1.73

Chapter 8

Summary and Conclusions

Summary and Conclusions

This study provides a comprehensive account of dynamics of benthic phosphorous (P) in the Indian continental margins in the Northern Indian Ocean and the abyssal areas of the Central Indian Ocean. The oceanographic, climatic, surface water productivity, nature and quantum of river fluxes and geological diversity occurring in the Northern Indian Ocean on either side of India provided suitable platforms to study the variability of P geochemistry with the varying depositional environment. This is the first detailed study of the P geochemistry in the Indian Ocean by covering a large area (shelf to abyssal plain) using sediment cores from 98 stations. The benthic phosphate flux estimated here will fill the missing gaps of Indian Ocean data in the global estimate of the diagenetic return flux of P. This study also attempted to estimate the P mass balance in the Northern Indian Ocean by considering the internal and external load of DIP (dissolved inorganic phosphate).

A combined solid phase- porewater data generated here has allowed the assessment of present-day P diagenesis in the sediments. Detailed geochemical study, including the sequential chemical extraction experiments, of 16 sediment cores from the Northern and the Central Indian Ocean (shelf, slope, and abyssal plain) has been carried out here to understand the input pathways and reservoir switching of P between different phases. The data provided information regarding the early diagenetic re-distribution and pathways of P burial in sediments and its variability with varying oceanographic settings. This study presents the first report of the ongoing phosphogenesis in the Indian continental margin. This new finding is in variance with the previous studies that have ruled out the present-day formation of phosphogenesis.

Major findings and key conclusions drawn from this study are listed below.

- The results of the benthic flux calculations of new data generated in combination with the published data reveal that the sediments of the Northern Indian Ocean are the source of DIP and contributes to an additional 6.3% to the current global diagenetic return flux estimates, while the deep-sea sediments of CIB act as sinks for DIP.
- Compared to the sediments overlain by oxic bottom water, sediments overlain by anoxic/suboxic water shows extensive benthic regeneration and release of P into the water column.
- In contrast to the perennial OMZ, the benthic release of P from sediments are high in seasonal anoxic sediments and contributes about 39% of the annual reflux from the Arabian Sea.
- In the Northern Indian Ocean, benthic regeneration is induced by a high rate of organic matter degradation, reductive dissolution of iron oxyhydroxides and fish debris dissolution. While in the CIB, extensive water column re-mineralization of organic matter and effective scavenging of P by iron oxyhydroxides limit the benthic release of P.
- The mass balance study shows that the magnitude of benthic diffusive flux is larger than the fluvial flux into the Northern Indian Ocean.
- In the Arabian Sea, enhanced degradation of organic material and the dissolution of fish debris and oxygen-depleted conditions favor the present-day phosphogenesis while in the BoB low input of reactive P, a high input of non-reactive P through river runoff and their rapid burial by ballasting effect restrict the sink switch over. In the CIB, extensive water column remineralization and lack of significant diagenesis hinders

phosphogenesis while atmospheric deposition contributes a significant amount of P to the authigenic pool.

- P distribution in the surface sediments of the CIB indicates that hydrothermal processes exert a local albeit a major role on P cycling in a part of the basin. At such sites the P enrichment in the hydrothermally influenced area occurs mainly due to co-precipitation.
- Geochemical studies of the Fe-P relationship in sediments of the Arabian Sea in two transects with bottom water oxygen gradients indicate that within the oxygen minimum zone the relationship is independent of O_2 variation. In seasonal hypoxic stations, reductive dissolution of iron exerts a major role on the benthic release of P while in the perennial OMZ it plays a weak role. In the BoB, low bacterial respiration limits microbial reduction of iron oxyhydroxides this coupled with a low adsorption capacity of terrigenous iron oxides make redox cycling of iron a weak player. In the abyssal CIB, prevailing oxic condition promotes the adsorption of P on the surface of iron oxyhydroxides and and thus Fe is a major sink for P.
- Among the major iron-bearing mineral phases, ferrihydrite is found to be an important sink for P in the Arabian Sea sediments. Relative proportions of Fe-bearing oxide mineral phases were found to vary with changing bottom water oxygenation.

Bibliography

Acharya, S.S., Panigrahi, M.K., Kurian, J., Gupta, A.K., Tripathy, S., 2016. Speciation of phosphorus in the continental shelf sediments in the Eastern Arabian Sea. Cont. Shelf Res. 115, 65–75. doi:10.1016/j.csr.2016.01.005

Adhikari, P.L., White, J.R., Maiti, K., Nguyen, N., 2015. Phosphorus speciation and sedimentary phosphorus release from the Gulf of Mexico sediments: Implication for hypoxia. Estuar. Coast. Shelf Sci. 164, 77–85. https://doi.org/10.1016/j.ecss.2015.07.016

Aller, R.C., Hannides, A., Heilbrun, C., Panzeca., C., 2004a. Coupling of early diagenetic processes and sedimentary dynamics in tropical shelf environments: The Gulf of Papua deltaic complex. Cont. Shelf Res. 24, 2455–2486. https://doi.org/10.1016/j.csr.2004.07.018

Aller, R.C., Heilbrun, C., Panzeca, C., Zhu, Z., Baltzer, F., 2004b. Coupling between sedimentary dynamics, early diagenetic processes, and biogeochemical cycling in the Amazon-Guianas mobile mud belt: Coastal French Guiana. Mar. Geol. Marine Geology, 331–360. https://doi.org/10.1016/j.margeo.2004.04.027

Anderson, L.D., Delaney, M.L., 2000. Sequential extraction and analysis of phosphorus in marine sediments: Streamlining of the SEDEX procedure. Limnol. Oceanogr. 45, 509–515. doi:10.4319/lo.2000.45.2.0509

Anderson, L.D., Delaney, M.L., Faul, K.L., 2001. Carbon to phosphorus ratios in sediments: Implications for nutrient cycling. Global Biogeochem. Cycles 15, 65–79. https://doi.org/10.1029/2000GB001270

Anschutz, P., Zhong, S., Sundby, B., Mucci, A., Gobeil, C., 1998. Burial efficiency of phosphorus and the geochemistry of iron in continental margin sediments. Limnol. Oceanogr. 43, 53–64. https://doi.org/10.4319/lo.1998.43.1.0053

Atlas, E., Pytkowicx, R.M., 1977. Solubility behavior of apatites in seawater1. Limnol. Oceanogr. 22, 290–300.

Babu, C.P., Nath, B.N., 2005. Processes controlling forms of phosphorus in surficial sediments from the eastern Arabian Sea impinged by varying bottom water oxygenation conditions. Deep Sea Res. Part II Top. Stud. Oceanogr. 52, 1965–1980. doi:10.1016/j.dsr2.2005.06.004

Babu, C.P., Ramaswamy, V., 2017. Phosphorus accumulation associated with intense diagenetic metal-Oxide cycling in sediments along the Eastern Continental Margin of India. Curr. Sci. 113, 473–478. https://doi.org/10.18520/CS/V113/I03/473-478

Babu, M.T., Sarma, Y.V.B., Murty, V.S.N., Vethamony, P., 2003. On the circulation in the Bay of Bengal during Northern spring inter-monsoon (March-April 1987). Deep. Res. Part II Top. Stud. Oceanogr. https://doi.org/10.1016/S0967-0645(02)00609-4

Banakar, V.K., Gupta, S.M., Padmavathi, V.K., 1991. Abyssal sediment erosion in the Central Indian Basin: Evidence from radiochemical and radiolarian studies. Mar. Geol. 96, 167–173. https://doi.org/10.1016/0025-3227(91)90214-O

Banakar, V.K., Parthiban, G., Pattan, J.. N., .Jauhari, P., 1998. Chemistry of surface sediment along a north–south transect across the equator in the Central Indian Basin: an assessment of biogenic and detrital influences on elemental burial on the seafloor. Chem. Geol. 147, 217–232.

Bange, H.W., Rixen, T., Johansen, A.M., Siefert, R.L., Ramesh, R., Ittekkot, V., Hoffmann, M.R., Andreae, M.O., Planck, M., 2000. A revised nitrogen budget for the Arabian Sea. Global Biogeochem Cy. 14, 1283–1297.

Banse, K., 1968. Hydrography of the Arabian Sea Shelf of India and Pakistan and effects on demersal fishes. Deep Sea Res. Oceanogr. Abstr. 15, 45–48. https://doi.org/10.1016/0011-7471(68)90028-4

Barber, A., Brandes, J., Leri, A., Lalonde, K., Balind, K., Wirick, S., Wang, J., Gélinas, Y., 2017. Preservation of organic matter in marine sediments by inner-sphere interactions with reactive iron. Sci. Rep. 7, 366. https://doi.org/10.1038/s41598-017-00494-0

Baturin, G., 2003. Phosphorus cycle in the ocean. Lithol. Miner. Resour. 38, 101–119. https://doi.org/10.1023/A:1023499908601

Baturin, G.N., 1982. Phosphorites on the sea floor. Elsevier.

Baturin, G.N., 1988. Disseminated phosphorus in oceanic sediments - A review. Mar. Geol. 84, 95–104. https://doi.org/10.1016/0025-3227(88)90127-2

Benitez-Nelson, C.R., 2000. The biogeochemical cycling of phosphorus in marine systems. Earth Sci. Rev. 51, 109–135. https://doi.org/10.1016/S0012-8252(00)00018-0

Berner, R.A., 1970. Sedimentary pyrite formation. Am. J. Sci. 268, 1–23

Berner, R.A., 1982. Burial of organic carbon and pyrite sulfur in the modern ocean; its geochemical and environmental significance. Am. J. Sci. 282, 451–473. https://doi.org/10.2475/ajs.282.4.451

Biche, S.U., Das, A., Mascarenhas-Pereira, M.B.L., Nagender Nath, B., Naik, S.S., Helekar, S.P., Sharma, R., Valsangkar, A.B., Loka Bharathi, P.A., 2017. Alkaline Phosphatase: An appraisal of its critical Role in C-limited deep-sea sdiments of Central Indian Basin. Geomicrobiol. J. 34, 274–288. https://doi.org/10.1080/01490451.2016.1190804

Bird, M.I., Robinson, R.A.J., Oo, N.W., Aye, M.M., Lu, X.X., Higgitt, D.L., Swe, A., Tun, T., Lhaing Win, S., Sandar Aye, K., Mi, K., Win, M., Hoey, T.B., 2008. A preliminary estimate of organic carbon transport by the Ayeyarwady (Irrawaddy) and Thanlwin (Salween) Rivers of Myanmar. Quat. Int. 186, 113--122. https://doi.org/10.1016/j.quaint.2007.08.003

Bloch, S., 1978. Phosphorus distribution in smectite-bearing basal metalliferous sediments. Chem. Geol. 22, 353–359

Boesen, C., Postma, D., 1988. Pyrite formation in anoxic environments of the Baltic. Am. J. Sci. 288, 575–605

Bordovskiy, O.., 1965. Accumulation of organic matter in bottom sediments. Mar. Geol. 3, 33–82.

Borole, D. V, 1993. Late Pleistocene sedimentation : a case study of the central Indian Ocean Basin. Deep. Res. I 40, 761–775.

Borole, D. V, Rajagopalan, G., Somayajulu, B.L.., 1987. Radiometric ages of phosphorites from the west coast of India. Mar. Geol. 78, 161–165. doi:10.1016/0025-3227(87)90075-2

Boudreau, B.P., 1997. Diagenetic models and their implementation, Springer Berlin. https://doi.org/10.1016/S0264-8172(98)80005-6

Brand, T.D., Griffiths, C., 2009. Seasonality in the hydrography and biogeochemistry across the Pakistan margin of the NE Arabian Sea. Deep. Res. Part II Top. Stud. Oceanogr. https://doi.org/10.1016/j.dsr2.2008.05.036

Bristow, L.A., Callbeck, C.M., Larsen, M., Altabet, M.A., Dekaezemacker, J., Forth, M., Gauns, M., Glud, R.N., Kuypers, M.M.M., Lavik, G., Milucka, J., Naqvi, S.W.A., Pratihary, A., Revsbech, N.P., Thamdrup, B., Treusch, A.H., Canfield, D.E., 2017. N2 production rates limited by nitrite availability in the Bay of Bengal oxygen minimum zone. Nat. Geosci. 10, 24–29. https://doi.org/10.1038/ngeo2847

Brock, J.C., Sathyendranath, S., Platt, T., 1993. Modelling the seasonality of subsurface light and primary production in the Arabian Sea. Mar. Ecol. Prog. Ser. 101, 209–221.

Broecker, W.S., Peng, T.H., 1982. Tracers in the Sea, Eldigio, Lamont-Doherty Geol. Obs. Columbia Univ., Palisades, NY

Burdige, D.J., 2005. Burial of terrestrial organic matter in marine sediments: A re-assessment. Global Biogeochem. Cycles 19, n/a-n/a. https://doi.org/10.1029/2004GB002368

Calvert, S.E., Karlin, R.E., Toolin, L.J., Donahue, D.J., Southon, J.R., Vogel, J.S., 1991. Low organic carbon accumulation rates in Black Sea sediments. Nature 350, 692–695. https://doi.org/10.1038/350692a0

Calvert, S.E., Pedersen, T.F., Naidu, P.D., von Stackelberg, U., 1995. On the organic carbon maximum on the continental slope of the eastern Arabian Sea. J. Mar. Res. 53, 269–296. https://doi.org/10.1357/0022240953213232

Caraco, N.F., Cole, J.J., Likens, G.E., 1993. Sulfate control of phosphorus availability in lakes A test and re-evaluation of Hasler and Einsele's Model. Hydrobiologia 253, 275–280

Cha, H.J., Lee, C.B., Kim, B.S., Choi, M.S., Ruttenberg, K.C., 2005. Early diagenetic redistribution and burial of phosphorus in the sediments of the southwestern East Sea (Japan Sea). Mar. Geol. 216, 127–143. https://doi.org/10.1016/j.margeo.2005.02.001

Chakraborty, P., Vudamala, K., Chennuri, K., Armoury, K., Linsy, P., Ramteke, D., Sebastian, T., Jayachandran, S., Naik, C., Naik, R., Nath, B.N., 2016. Mercury

profiles in sediment from the marginal high of Arabian Sea: an indicator of increasing anthropogenic Hg input. Environ. Sci. Pollut. Res. 23, 8529–8538. doi:10.1007/s11356-015-5925-1

Chauhan, O.S., 1996. Aeolian deposition of Arabia and Somalia sediments on the southwestern continental margin of India. Curr. Sci. 71, 233–236. doi:10.2307/24099588

Chauhan, O.S., Gujar, A.R., 1996. Surficial clay mineral distribution on the southwestern continental margin of India: Evidence of input from the Bay of Bengal. Cont. Shelf Res. https://doi.org/10.1016/0278-4343(95)00015-S

Chen, Y.P., Rekha, P.D., Arun, A.B., Shen, F.T.F., Lai, W.A., Young, C.C.C., 2006. Phosphate solubilizing bacteria from subtropical soil and their tricalcium phosphate solubilizing abilities. Appl. Soil Ecol. 34, 33–41. https://doi.org/10.1016/j.apsoil.2005.12.002

Colman, A.S., Holland, H.D., 2000. The Global Diagenetic Flux of Phosphorus From Marine Sediments To the Oceans: Redox Sensitivity and the Control of Atmospheric Oxygen Levels. Mar. Authigenes. From Glob. to Microb. 53–75. https://doi.org/10.2110/pec.00.66.0053

Compton, J., Mallinson, D., Glenn, C.R., Filippelli, G., Follmi, K., Shields, G., Zanin, Y., 2000. Variations in the global phosphorus cycle. Mar. Authigenes. From Glob. to Microb. 21–33. https://doi.org/10.2110/pec.00.66.0021

Conkright, M.E., Gregg, W.W., Levitus, S., 2000. Seasonal cycle of phosphate in the open ocean. Deep. Res. Part I Oceanogr. Res. Pap. 47. 159-175. https://doi.org/10.1016/S0967-0637(99)00042-4

Cowie, G., Mowbray, S., Kurian, S., Sarkar, A., White, C., Anderson, A., Vergnaud, B., Johnstone, G., Brear, S., Woulds, C., Naqvi, S.W.A.A., Kitazato, H., 2014. Comparative organic geochemistry of Indian margin (Arabian Sea) sediments: Estuary to continental slope. Biogeosciences 11, 6683–6696. https://doi.org/10.5194/bg-11-6683-2014

Dale, A.W., Boyle, R.A., Lenton, T.M., Ingall, E.D., Wallmann, K., 2016. A model for microbial phosphorus cycling in bioturbated marine sediments: Significance for phosphorus burial in the early Paleozoic. Geochim. Cosmochim. Acta 189, 251–268. https://doi.org/10.1016/J.GCA.2016.05.046

Das, A., Fernandes, C.E.G.G., Naik, S.S., Nagender Nath, B., Suresh, I., Mascarenhas-Pereira, M.B.L., Gupta, S.M., Khadge, N.H., Prakash Babu, C., Borole, D. V., Sujith, P.P., Valsangkar, A.B., Shashikant Mourya, B., Biche, S.U., Sharma, R., Loka Bharathi, P.A., 2011a. Bacterial response to contrasting sediment geochemistry in the Central Indian Basin. Sedimentology 58, 756–784. https://doi.org/10.1111/j.1365-3091.2010.01183.x

Das, A., Sujith, P.P., Mourya, B.S., Biche, S.U., Loka Bharathi, P.A., 2011b. Chemosynthetic activity prevails in deep-sea sediments of the Central Indian Basin. Extremophiles 15, 177–189. https://doi.org/10.1007/s00792-010-0346-z

Das, S., Lyla, P.S., Khan, S.A., 2007. Biogeochemical processes in the continental slope of Bay of Bengal: I. Bacterial solubilization of inorganic phosphate. Rev. Biol. Trop. 55, 1–9

Datta, D.K., Gupta, L.P., Subramanian, V., 1999. Distribution of C, N and P in the sediments of the Ganges-Brahmaputra-Meghna river system in the Bengal basin. Org. Geochem. 30, 75–82. https://doi.org/10.1016/S0146-6380(98)00203-4

De Lange, G.J., 1986a. Chemical composition of interstitial water in cores from the Nares abyssal plain (Western North Atlantic). Oceanol. Acta 9, 159–169

De Lange, G.J., 1986b. Early diagenetic reactions in interbedded pelagic and turbiditic sediments in the Nares Abyssal Plain (western North Atlantic): Consequences for the composition of sediment and interstitial water. Geochim. Cosmochim. Acta 50, 2543–2561. https://doi.org/10.1016/0016-7037(86)90209-7

De Sousa, S.N., Naqvi, W.A., Reddy, G., 1981. Distribution of Nutrients in the Western Bay of Bengal. Indian J. Mar. Sci. 10, 327–331

De Sousa, S.N., DileepKumar, M., Sardessai, S., Sarma, V.V.S.S., Shirodkar, P.V., 1996. Seasonal variability in oxygen and nutrients in the central and eastern Arabian Sea. Curr. Sci. 71, 847–851

De Sousa, S.., Sardessai, S.., Babu, V.R., Murty, V.S.., Gupta, G.V.., 2001. Chemical characteristics of Central Indian Basin waters during the southern summer. Deep Sea Res. Part II Top. Stud. Oceanogr. 48, 3343–3352. https://doi.org/10.1016/S0967-0645(01)00044-3

De Vries, T.J., Pearcy, W.G., 1982. Fish debris in sediments of the upwelling zone off central Peru: a late Quaternary record. Deep Sea Res. Part A, Oceanogr. Res. Pap. 29, 87–109. doi:10.1016/0198-0149(82)90063-2

Delaney, M.L., 1998. Phosphorus accumulation in marine sediments and the oceanic phosphorus cycle. Global Biogeochem. Cycles 12, 563. https://doi.org/10.1029/98GB02263

Dijkstra, N., Kraal, P., Kuypers, M.M.M., Schnetger, B., Slomp, C.P., 2014. Are iron-phosphate minerals a sink for phosphorus in anoxic Black Sea sediments? PLoS One 9, 1–12. doi:10.1371/journal.pone.0101139

Dulk, D.M., Reichart, G.J., Memon, G.M., Roelofs, E.M.P., Zachariasse, W.J., van der Zwaan, G.J., 1998. Benthic foraminiferal response to variations in surface water productivity and oxygenation in the northern Arabian Sea. Mar. Micropaleontol. 35, 43–66. https://doi.org/10.1016/S0377-8398(98)00015-2

Egger, M., Jilbert, T., Behrends, T., Rivard, C., Slomp, C.P., 2015. Vivianite is a major sink for phosphorus in methanogenic coastal surface sediments. Geochim. Cosmochim. Acta 169. https://doi.org/10.1016/j.gca.2015.09.012

Eijsink, L.M., Krom, M.D., Herut, B., 2000. Speciation and burial flux of phosphorus in the surface sediments of the Eastern Mediterranean. Am. Jounal Sci. 300, 483–503

Emeis, K.C., Morse, J.W., Mays, L.L., 1991. Organic carbon, reduced sulfur, and iron in Miocene to Holocene upwelling sediments from the Oman and Benguela upwelling

systems. Proc. Ocean Drill. Program, Sci. Res 117. https://doi.org/10.2973/odp.proc.sr.117.155.1991

Emerson, S.R., Jahnke, R., Bender, M., Froelich, P., Klinkhammer, G.P., Bowser, C., Setlock, G., 1980. Early diagenesis in sediments from the eastern equatorial Pacific, I. Pore water nutrient and carbonate results. Earth Planet. Sci. Lett. 49, 57–80. https://doi.org/10.1016/0012-821X(80)90150-8

Fagel, N., 2007. Clay minerals, deep circulation and climate. Dev. Mar. Geol. 1, 139–184. https://doi.org/10.1016/S1572-5480(07)01009-3

Fagel, N., Alleman, L.Y., Granina, L., Hatert, F., Thamo-Bozso, E., Cloots, R., André, L., 2005. Vivianite formation and distribution in Lake Baikal sediments. Glob. Planet. Change 46, 315–336. https://doi.org/10.1016/j.gloplacha.2004.09.022

Fagel, N., Debrabant, P., André, L., 1994. Clay supplies in the Central Indian Basin since the Late Miocene: climatic or tectonic control? Mar. Geol. 122, 151–172. https://doi.org/10.1016/0025-3227(94)90209-7

Falkowski, P., Barber, R.T., Smetacek, V., Wegener, A., 1998. Biogeochemical Controls and Feedbacks on Ocean Primary Production Protein network analysis View project Earth's Metabolic Network View project. Science (80-.). 281, 200–206

Fang, T.H., Chen, J.L., Huh, C.A., 2007. Sedimentary phosphorus species and sedimentation flux in the East China Sea. Cont. Shelf Res. 27, 1465–1476. https://doi.org/10.1016/j.csr.2007.01.011

Faul, K.L., Paytan, A., Delaney, M.L., 2005. Phosphorus distribution in sinking oceanic particulate matter. Mar. Chem. 97, 307–333. https://doi.org/10.1016/j.marchem.2005.04.002

Feely, R.A., Massoth, G.J., Baker, E.T., Cowen, J.P., Lamb, M.F., Krogslund, K.A., 1990. The effect of hydrothermal processes on midwater phosphorus distributions in the northeast Pacific. Earth Planet. Sci. Lett. 96, 305–318

Filippelli, G.M., 2008. The Global Phosphorus Cycle: Past, Present, and Future. Elements 4, 89–95. https://doi.org/10.2113/GSELEMENTS.4.2.89

Filippelli, G.M., 2001. Carbon and phosphorus cycling in anoxic sediments of the Saanich Inlet, British Columbia. Mar. Geol. 174, 307–321. https://doi.org/10.1016/S0025-3227(00)00157-2

Filippelli, G.M., Cowie, G.., 2017. Carbon and Phosphorus Cycling in Arabian Sea Sediments across the Oxygen Minimum Zone. J. Oceanogr. Mar. Res. 5. https://doi.org/10.4172/2572-3103.1000171

Filippelli, G.M., Delaney, M.L., 1995. Phosphorus geochemistry and accumulation rates in the Eastern Equatorial Pacific Ocean: Results from Leg 138. Proc. Ocean Drill. Program, Sci. Results 138, 757–767.

Filippelli, G.M., Delaney, M.L., 1996. Phosphorus geochemistry of equatorial Pacific sediments. Geochim. Cosmochim. Acta 60, 1479–1495. doi:10.1016/0016-7037(96)00042-7

Filippelli, G.M., Delaney, M.L., Garrison, R.E., Omarzai, S.K., Behl, R.J., 1994. Phosphorus accumulation rates in a Miocene low oxygen basin: The Monterey Formation (Pismo Basin), California. Mar. Geol. 116, 419–430. https://doi.org/10.1016/0025-3227(94)90055-8

Föllmi, K.B.B., 1996. The phosphorus cycle, phosphogenesis and marine phosphate-rich deposits. Earth-Science Rev. 40, 55–124. https://doi.org/10.1016/0012-8252(95)00049-6

Friedl, G., Dinkel, C., Wehrli, B., 1998. Benthic fluxes of nutrients in the northwestern Black Sea. Mar. Chem. 62, 77–88. https://doi.org/10.1016/S0304-4203(98)00029-2

Froelich, P.N., Arthur, M.A., Burnett, W.C., Deakin, M., Hensley, V., Jahnke, R., Kaul, L., Kim, K.H., Roe, K., Soutar, A., Vathakanon, C., 1988. Early diagenesis of organic matter in Peru continental margin sediments: Phosphorite precipitation. Mar. Geol. 80, 309–343. doi:10.1016/0025-3227(88)90095-3

Froelich, P.N., Bender, M.L., Heath, G.R., 1977. Phosphorus accumulation rates in metalliferous sediments on the East Pacific Rise. Earth Planet. Sci. Lett. 34, 351–359

Froelich, P.N., Bender, M.L., Luedtke, N. A., Heath, G.R., DeVries, T., 1982. The marine phosphorous cycle. Am. J. Sci. https://doi.org/10.3389/fmicb.2013.00105

Gächter, R., Meyer, J.S., 1993. The role of microorganisms in mobilization and fixation of phosphorus in sediments. Hydrobiologia 253, 103–121. https://doi.org/10.1007/BF00050731

Gao, Y., Kaufman, Y.J., Tanre, D., Kolber, D., Falkowski, P.G., 2001. Seasonal distribution of aeolian iron flux to the global ocean. Geophys. Res. Lett. 28, 29–32. https://doi.org/10.1029/2000GL011926

Gauns, M., Madhupratap, M., Ramaiah, N., Jyothibabu, R., Fernandes, V., Paul, J.T., Prasanna Kumar, S., 2005. Comparative accounts of biological productivity characteristics and estimates of carbon fluxes in the Arabian Sea and the Bay of Bengal. Deep. Res. Part II Top. Stud. Oceanogr. 52, 2003–2017. https://doi.org/10.1016/j.dsr2.2005.05.009

Gearing, J.N., 1988. The use of stable isotope ratios for tracing the nearshore-offshore exchange of organic matter, in: Coastal-Offshore Ecosystem Interactions. Springer, Berlin, Heidelberg, pp. 69–101. https://doi.org/10.1007/978-3-642-52452-3_4

Gingele, F.X., De Deckker, P., Hillenbrand, C.-D., 2001. Clay mineral distribution in surface sediments between Indonesia and NW Australia — source and transport by ocean currents. Mar. Geol. 179, 135–146. https://doi.org/10.1016/S0025-3227(01)00194-3

Graham, W.F., Duce, R.A., 1979. Atmospheric pathways of the phosphorus cycle. Geochim. Cosmochim. Acta 43, 1195–1208. https://doi.org/10.1016/0016-7037(79)90112-1

Grandel, S., Rickert, D., Schlüter, M., Wallmann, K., 2000. Pore-water distribution and quantification of diffusive benthic fluxes of silicic acid, nitrate and phosphate in

surface sediments of the deep Arabian Sea. Deep. Res. Part II Top. Stud. Oceanogr. 47, 2707–2734. https://doi.org/10.1016/S0967-0645(00)00046-1

Grasshoff, K., Ehrhardt, M., Kremling, K., 1983. Methods of seawater analysis, 419 pp, Verlag Chemie, New York.

Griffin, J.J., Windom, H., Goldberg, E.D., 1968. The distribution of clay minerals in the World Ocean. Deep Sea Res. Oceanogr. Abstr. 15, 433–459. https://doi.org/10.1016/0011-7471(68)90051-X

Groves, D.G., Hunt, L.M., 1980. Ocean world encyclopedia. McGraw-Hill

Gruber, N., Sarmiento, J.L., 1997. Global patterns of marine nitrogen fixation and denitrification. Global Biogeochem. Cycles. https://doi.org/10.1029/97GB00077

Gunnars, A., Blomqvist, S., Johansson, P., Andersson, C., 2002. Formation of Fe(III) oxyhydroxide colloids in freshwater and brackish seawater, with incorporation of phosphate and calcium. Geochim. Cosmochim. Acta 66, 745–758. https://doi.org/10.1016/S0016-7037(01)00818-3

Gupta, R. Sen, Naqvi, S.W.A., 1984. Chemical oceanography of the Indian Ocean, north of the equator. Deep Sea Res. Part A, Oceanogr. Res. Pap. https://doi.org/10.1016/0198-0149(84)90035-9

Gupta, S., Jauhari, P, 1994. Radiolarian abundance and geochemistry of the surface-sediments from the Central Indian Basin: inferences to Antarctic bottom water current. Curr. Sci. 659—663

Habeebrehman, H., Prabhakaran, M.P., Jacob, J., Sabu, P., Jayalakshmi, K.J., Achuthankutty, C.T., Revichandran, C., 2008. Variability in biological responses influenced by upwelling events in the Eastern Arabian Sea. J. Mar. Syst. https://doi.org/10.1016/j.jmarsys.2008.04.002

Heller, M.I., Lam, P.J., Moffett, J.W., Till, C.P., Lee, J.-M., Toner, B.M., Marcus, M.A., 2017. Accumulation of Fe oxyhydroxides in the Peruvian oxygen deficient zone implies non-oxygen dependent Fe oxidation. Geochim. Cosmochim. Acta 211, 174–193. https://doi.org/10.1016/j.gca.2017.05.019

Henkel, S., Kasten, S., Hartmann, J.F., Silva-Busso, A., Staubwasser, M., 2018. Iron cycling and stable Fe isotope fractionation in Antarctic shelf sediments, King George Island. Geochim. Cosmochim. Acta 237, 320–338. https://doi.org/10.1016/j.gca.2018.06.042

Hensen, C., Landenberger, H., Zabel, M., Schulz, H.D., 1998. Quantification of diffusive benthic fluxes of nitrate , phosphate and silicate in the southern Atlantic Ocean. Global Biogeochem. Cycles 12, 193–210.

Hensen, C., Zabel, M., Schulz, H.D., 2000. A comparison of benthic nutrient fluxes from deep-sea sediments off Namibia and Argentina. Deep. Res. Part II Top. Stud. Oceanogr. 47, 2029–2050

Holeman, J.N., 1968. The sediment yield of major rivers of the world. Water Resour. Res. 4, 737–747. https://doi.org/10.1029/WR004i004p00737

Holland, H.D., 1978. The chemistry of the atmosphere and oceans. Wiley, New York, NY

Howarth, R.W., Jensen, H.S., Marino, R., Postma, H., 1995. Transport to and processing of P in near-shore and oceanic waters, in: Tiessen, H. (Ed.), Phosphorus in the Global Environment: Transfers, Cycles, and Management. John Wiley & Sons, Chichester, England, p. 323–345 (SCOPE; No. 54).

Howell, E.A., Doney, S.C., Fine, R.A., Olson, D.B., 1997. Geochemical estimates of denitrification in the Arabian Sea and the Bay of Bengal during WOCE. Geophys. Res. Lett. 24, 2549-2552. https://doi.org/10.1029/97GL01538

Hupe, A., Thomas, H., Ittekkot, V., Lendt, R., 2001. Inventory of released inorganic carbon from organic matter remineralization in the deeper Arabian Sea. J. Geophys. Res. 106, 31,189-31,196. https://doi.org/10.1029/2000JC000427

Ingall, E., Jahnke, R., 1994. Evidence for enhanced phosphorus regeneration from marine sediments overlain by oxygen depleted waters. Geochim. Cosmochim. Acta 58, 2571–2575. doi:10.1016/0016-7037(94)90033-7

Ingall, E., Jahnke, R., 1997. Influence of water-column anoxia on the elemental fractionation of carbon and phosphorus during sediment diagenesis. Mar. Geol. 139, 219–229. https://doi.org/10.1016/S0025-3227(96)00112-0

Ingall, E.D., Bustin, R.M., Van Cappellen, P., 1993. Influence of water column anoxia on the burial and preservation of carbon and phosphorus in marine shales. Geochim. Cosmochim. Acta 57, 303–316. https://doi.org/10.1016/0016-7037(93)90433-W

Ingall, E.D., Van Cappellen, P., 1990. Relation between sedimentation rate and burial of organic phosphorus and organic carbon in marine sediments. Geochim. Cosmochim. Acta 54, 373–386. doi:10.1016/0016-7037(90)90326-G

Ittekkot, V., Nair, R.R., Honjo, S., Ramaswamy, V., Bartsch, M., Manganini, S., Desai, B.N., 1991. Enhanced particle fluxes in Bay of Bengal induced by injection of fresh water. Nature 351, 385–387. https://doi.org/10.1038/351385a0

Iyer, S.D., Mascarenhas-Pereira, M.B.L., Nath, B.N., 2007. Native aluminium (spherules and particles) in the Central Indian Basin sediments: Implications on the occurrence of hydrothermal events. Mar. Geol. 240, 177–184. https://doi.org/10.1016/j.margeo.2007.02.004

Jacob, J., Chandramohanakumar, N., Jayaraj, K.A., Raveendran, T. V, Balachandran, K.K., Joseph, T., Nair, M., Achuthankutty, C.T., Nair, K.K.C., George, R., Ravi, Z.., 2008. Biogeochemistry of the Surficial Sediments of the Western and Eastern Continental Shelves of India. J. Coast. Res. 245, 1240–1248. https://doi.org/10.2112/06-0794.1

Jahnke, R.A., 1996. The global ocean flux of particulate organic carbon: Areal distribution and magnitude. Global Biogeochem. Cycles 10, 71–88. https://doi.org/10.1029/95GB03525

Jahnke, R.A., Emerson, S.R., Roe, K.K., Burnett, W.C., 1983. The present day formation of apatite in Mexican continental margin sediments. Geochim. Cosmochim. Acta 47, 259–266. doi:10.1016/0016-7037(83)90138-2

Jahnke, R.A., Heggie, D., Emerson, S., Grundmanis, V., 1982. Pore waters of the central Pacific Ocean: Nutrient results. Earth Planet. Sci. Lett. 61, 233–256

Jia, G.., Peng, P.., 2003. Temporal and spatial variations in signatures of sedimented organic matter in Lingding Bay (Pearl estuary), southern China. Mar. Chem. 82, 47–54. https://doi.org/10.1016/S0304-4203(03)00050-1

Jilbert, T., Slomp, C.P., Gustafsson, B.G., Boer, W., 2011. Beyond the Fe-P-redox connection: Preferential regeneration of phosphorus from organic matter as a key control on Baltic Sea nutrient cycles. Biogeosciences 8, 1699–1720. https://doi.org/10.5194/bg-8-1699-2011

Jing, T., Ma, W., Zhu, M., Li, T., Yang, R., 2017. Characterization of iron diagenesis in marine sediments using refined iron speciation and quantized iron(III)-oxide reactivity: a case study in the Jiaozhou Bay, China. Acta Oceanol. Sin. 36, 48–55. https://doi.org/10.1007/s13131-016-1083-2

Jones, B., Manning, D.A.C., 1994. Comparison of geochemical indices used for the interpretation of palaeoredox conditions in ancient mudstones. Chem. Geol. 111, 111–129. doi:10.1016/0009-2541(94)90085-X

Kader, A., Rahman, M.Z., Uddin, M.M., Hoque, M.E., Basak, S.C., 2013. Bathymetric study of the Bay of Bengal based on open source satellite and sounding data. Int. J. Geomatics Geosci. 4, 116–124

Kamykowski, D., Zentara, S.-J., 1990. Hypoxia in the world ocean as recorded in the historical data set. Deep. Res. 37, 1861–1874.

Karl, D.M., Brittain, A.M., Tilbrook, B.D., 1989. Hydrothermal and microbial processes at Loihi Seamount, a mid-plate hot-spot volcano. Deep Sea Res. Part A. Oceanogr. Res. Pap. 36, 1655–1673. https://doi.org/10.1016/0198-0149(89)90065-4

Kasten, S., Hartmann, S., Silva Busso, J., Staubwasser, A., Henkel, S., Kasten, S., Hartmann, J.F., Silva-Busso, A., Staubwasser, M., 2018. Iron cycling and stable Fe isotope fractionation in Antarctic shelf sediments, King George Island. Geochim. Cosmochim. Acta 237, 320–338. https://doi.org/10.1016/j.gca.2018.06.042

Kessarkar, P.M., Purnachandra Rao, V., Ahmad, S.M., Anil Babu, G., 2003. Clay minerals and Sr^Nd isotopes of the sediments along the western margin of India and their implication for sediment provenance. Mar. Geol. 202, 55–69. https://doi.org/10.1016/S0025-3227(03)00240-8

Kolla, V., Henderson, L., Biscaye, P.E., 1976. Clay mineralogy and sedimentation in the western Indian ocean. Deep Sea Res. Oceanogr. Abstr. 23, 949–961. doi:10.1016/0011-7471(76)90825-1

Kolla, V., Kostecki, J.., Robinson, F., Biscaye, P.., 1981. Distribution and orgin of clay minerals and quartz in surface sediments of the Arabian Sea. J. Sediment. Petrol. 51, 563–569.

Kolodny, Y., 1981. Phosphorites. The sea. 7, 981-1024.

Konhauser, K., 2009. Introduction to Geomicrobiology. John Wiley & Sons

Kostka, J.E., Luther, G.W., 1994. Partitioning and speciation of solid phase iron in saltmarsh sediments. Geochim. Cosmochim. Acta 58, 1701–1710. https://doi.org/10.1016/0016-7037(94)90531-2

Kraal, P., 2011. Redox-dependent phosphorus burial in modern and ancient marine sediments. PhD thesis

Kraal, P., Bostick, B.C., Behrends, T., Reichart, G.J., Slomp, C.P., 2015. Characterization of phosphorus species in sediments from the Arabian Sea oxygen minimum zone: Combining sequential extractions and X-ray spectroscopy. Mar. Chem. 168, 1–8. https://doi.org/10.1016/j.marchem.2014.10.009

Kraal, P., Dijkstra, N., Behrends, T., Slomp, C.P., 2017. Phosphorus burial in sediments of the sulfidic deep Black Sea: Key roles for adsorption by calcium carbonate and apatite authigenesis. Geochim. Cosmochim. Acta 204, 140–158. doi:10.1016/j.gca.2017.01.042

Kraal, P., Slomp, C.P., 2014. Rapid and Extensive Alteration of Phosphorus Speciation during Oxic Storage of Wet Sediment Samples. PLoS One 9, 1–6. doi:10.1371/journal.pone.0096859

Kraal, P., Slomp, C.P., Forster, A., Kuypers, M.M.M., 2010. Phosphorus cycling from the margin to abyssal depths in the proto-Atlantic during oceanic anoxic event 2. Palaeogeogr. Palaeoclimatol. Palaeoecol. 295, 42–54. https://doi.org/10.1016/j.palaeo.2010.05.014

Kraal, P., Slomp, C.P., Forster, A., Kuypers, M.M.M., Sluijs, A., 2009. Pyrite oxidation during sample storage determines phosphorus fractionation in carbonate-poor anoxic sediments. Geochim. Cosmochim. Acta 73, 3277–3290. doi:10.1016/j.gca.2009.02.026

Kraal, P., Slomp, C.P., Reed, D.C., Reichart, G.J., Poulton, S.W., 2012. Sedimentary phosphorus and iron cycling in and below the oxygen minimum zone of the northern Arabian Sea. Biogeosciences 9, 2603–2624. https://doi.org/10.5194/bg-9-2603-2012

Krishna, M.S., Prasad, M.H.K.K., Rao, D.B., Viswanadham, R., Sarma, V.V.S.S., Reddy, N.P.C.C., 2016. Export of dissolved inorganic nutrients to the northern Indian Ocean from the Indian monsoonal rivers during discharge period. Geochim. Cosmochim. Acta 172, 430–443. https://doi.org/10.1016/j.gca.2015.10.013

Krishnaswami, S and Sarin, M., 1976. The simultaneous determination of Th, Pu, Ra isotopes, ^{210}Pb, ^{55}Fe, ^{32}Si and ^{14}C in marine suspended phases. Anal. Chim. Acta 83, 143–156.

Kumar, P.S., Muraleedharan, P.M., Prasad, T.G., Gauns, M., Ramaiah, N., de Souza, S.N., Sardesai, S., Madhupratap, M., 2002. Why is the Bay of Bengal less productive during summer monsoon compared to the Arabian Sea? Geophys. Res. Lett. 29, 88-1-88–4. https://doi.org/10.1029/2002GL016013

Kumar, P.S., Ramaiah, N., Gauns, M., Sarma, V.V.S.S., Muraleedharan, P.M., Raghukumar, S., Dileep Kumar, M., Madhupratap, M., 2001. Physical forcing of biological productivity in the Northern Arabian Sea during the Northeast Monsoon. Deep Sea Res. Part II Top. Stud. Oceanogr. 48, 1115–1126. https://doi.org/10.1016/S0967-0645(00)00133-8

Kurian, S., Nath, B.N., Kumar, N.C., Nair, K.K.C., 2013. Geochemical and Isotopic Signatures of Surficial Sediments from the Western Continental Shelf of India: Inferring Provenance, Weathering, and the Nature of Organic Matter. J. Sediment. Res. 83, 427–442. https://doi.org/10.2110/jsr.2013.36

Lallier-Vergès, E., Hayes, J.M., Boussafir, M., Zaback, D.A., Tribovillard, N.P., Connan, J., Bertrand, P., 1997. Productivity-induced sulphur enrichment of hydrocarbon-rich sediments from the Kimmeridge Clay Formation. Chem. Geol. 134, 277–288. https://doi.org/10.1016/S0009-2541(96)00093-9

Lalonde, K., Mucci, A., Ouellet, A., Yves Gélinas, 2012. Preservation of organic matter in sediments promoted by iron. Nat. 483, 198–200

Law, G.T.W., Shimmield, T.M., Shimmield, G.B., Cowie, G.L., Breuer, E.R., Harvey, S.M., 2009. Manganese , iron , and sulphur cycling on the Pakistan margin. Deep. Res. II 56, 305–323. https://doi.org/10.1016/j.dsr2.2008.06.011

Li, Y.-H., Gregory, S., 1974. Diffusion of ions in sea water and in deep-sea sediments. Geochim. Cosmochim. Acta 38, 703–714.

Lijklema, L., 1980. Interaction of orthophosphate with iron (III) and aluminum hydroxides. Environ. Sci. Technol. 14, 537–541.

Linsy, P., Nagender Nath, B., Mascarenhas-Pereira, M.B.L., Chauhan, T., Sebastian, T., Babu, C.P., Kurian, S., Miriyala, P., Kazip, A., Borole, D. V., Khadge, N.H., 2018. Distribution and Diagenesis of Phosphorus in the Deep-Sea Sediments of the Central Indian Basin. J. Geophys. Res. Ocean. 123, 7963-7982. https://doi.org/10.1029/2018JC014386

Linsy, P., Nagender Nath, B., Mascarenhas-Pereira, M.B.L., Vinitha, P.V., Ray, D., Prakash Babu, C., Ramalingeswara Rao, B., Kazip, A., Sebastian, T., Kocherla, M., Miriyala, P., 2018. Benthic cycling of phosphorus in the Eastern Arabian Sea: Evidence of present day phosphogenesis. Mar. Chem. 199, 53–66. https://doi.org/10.1016/j.marchem.2018.01.007

Lomnitz, U., 2017. Biogeochemical cycling of iron and phosphorus under low oxygen conditions. Ph.D. Thesis

Longo, A.F., Feng, Y., Lai, B., Landing, W.M., Shelley, R.U., Nenes, A., Mihalopoulos, N., Violaki, K., Ingall, E.D., 2016. Influence of atmospheric processes on the solubility and composition of iron in Saharan Dust. Environ. Sci. Technol. 50, 6912–6920. https://doi.org/10.1021/acs.est.6b02605

Louchouarn, P., Lucotte, M., Duchemin, E., De Vernal, A., 1997. Early diagenetic processes in recent sediments of the Gulf of St-Lawrence: Phosphorus, carbon and iron burial rates. Mar. Geol. 139, 181–200. doi:10.1016/S0025-3227(96)00110-7

Lucotte, M., Mucci, A., Hillaire-Marcel, C., Tran, S., 1994. Early diagenetic processes in deep Labrador Sea sediments: reactive and nonreactive iron and phosphorus. Can. J. Earth Sci. 31, 14–27. https://doi.org/10.1139/e94-003

Lyle, M., Dymond, J., Heath, G.R., 1977. Copper-nickel-enriched ferromanganese nodules and associated crusts from the Bauer Basin, northwest Nazca Plate. Earth Planet. Sci. Lett. 35, 55–64.

Ma, W.W., Zhu, M.X., Yang, G.P., Li, T., 2018. Iron geochemistry and organic carbon preservation by iron (oxyhydr)oxides in surface sediments of the East China Sea and the south Yellow Sea. J. Mar. Syst. 178, 62–74. https://doi.org/10.1016/j.jmarsys.2017.10.009

Madhupratap, M., Gauns, M., Ramaiah, N., Prasanna Kumar, S., Muraleedharan, P.M., De Sousa, S.N., Sardessai, S., Muraleedharan, U., 2003. Biogeochemistry of the Bay of Bengal: Physical, chemical and primary productivity characteristics of the central and western Bay of Bengal during summer monsoon 2001. Deep. Res. Part II Top. Stud. Oceanogr. 50, 881–896. https://doi.org/10.1016/S0967-0645(02)00611-2

Madhupratap, M., Kumar, S.P., Bhattathiri, P., Kumar, M.D., Raghukumar, S., Nair, K., Ramaiah, N., 1996. Mechanism of the biological response to winter cooling in the northeastern Arabian Sea. Nature 384, 549. https://doi.org/10.1038/384549a0

Madhupratap, M., Nair, KNV, Gopalakrishnan, T., Haridas, P., Nair, KKC, Venugopal, P., Gauns, M., 2001. Arabian Sea oceanography and fisheries of the west coast of India. Curr. Sci. 81, 355--361.

Mahowald, N., Timothy, D.J., Alex, R.B., Paulo, A., Claudia, R.B.-N., Gilles, B., Tami, C.B., Ying, C., David, D.C., Barak, H., Nilgun, K., Remi, L., Chao, L., Willy, M., Kenneth, A.M., Gregory, S.O., Ronald, L.S., Seigen, T., 2008. Global distribution of atmospheric phosphorus sources, concentrations and deposition rates, and anthropogenic impacts Natalie. Global Biogeochem. Cycles 22, 1–19. https://doi.org/10.1029/2008gb003240

Mangan, C.., 2007. The sequestration of phosphate by iron phases in the sediments from lake rotorua, new zealand. Thesis

März, C., Hoffmann, J., Bleil, U., de Lange, G.J., Kasten, S., 2008. Diagenetic changes of magnetic and geochemical signals by anaerobic methane oxidation in sediments of the Zambezi deep-sea fan (SW Indian Ocean). Mar. Geol. 255, 118–130. doi:10.1016/j.margeo.2008.05.013

März, C., Poulton, S.W., Wagner, T., Schnetger, B., Brumsack, H.J., 2014. Phosphorus burial and diagenesis in the central Bering Sea (Bowers Ridge, IODP Site U1341): Perspectives on the marine P cycle. Chem. Geol. 363, 270–282. doi:10.1016/j.chemgeo.2013.11.004

Mascarenhas-Pereira, M.B.L., Nagender Nath, B., Iyer, S.D., Borole, D. V., Parthiban, G., Jijin, R., Khedekar, V., 2016. Multiple ash layers in late Quaternary sediments from the Central Indian Basin. J. Volcanol. Geotherm. Res. 316, 85–100. https://doi.org/10.1016/j.jvolgeores.2016.03.011

Mascarenhas-Pereira, M.B.L., Nath, B.N., 2010. Selective leaching studies of sediments from a seamount flank in the Central Indian Basin: Resolving hydrothermal, volcanogenic and terrigenous sources using major, trace and rare-earth elements. Mar. Chem. 121, 49–66. https://doi.org/10.1016/j.marchem.2010.03.004

Mascarenhas-Pereira, M.B.L., Nath, B.N., Borole, D. V., Gupta, S.M., 2006. Nature, source and composition of volcanic ash in sediments from a fracture zone trace of Rodriguez Triple Junction in the Central Indian Basin. Mar. Geol. 229, 79–90. https://doi.org/10.1016/j.margeo.2006.02.002

Matondkar, P. S.. G., Nair, K.K.C.C., Anzari, Z.. A., 2005. Biological characteristics of central indian basin waters during the southern summer. Mar. Georesources Geotechnol. 23, 299–313. https://doi.org/10.1080/10641190500446649

McCreary, J.P., Yu, Z., Hood, R.R., Vinaychandran, P.N., Furue, R., Ishida, A., Richards, K.J., 2013. Dynamics of the Indian-Ocean oxygen minimum zones. Prog. Oceanogr. 112–113, 15–37. https://doi.org/10.1016/j.pocean.2013.03.002

McTainsh, G.H., 1989. Quaternary aeolian dust processes and sediments in the Australian region. Quat. Sci. Rev. 8, 235–253. https://doi.org/10.1016/0277-3791(89)90039-5

Meybeck, M., 1982. Carbon, nitrogen, and phosphorus transport by world rivers. Am. Jounal Sci. 282, 401–450

Michels, K.H., Suckow, A., Breitzke, M., Kudrass, H.R., Kottke, B., 2003. Sediment transport in the shelf canyon “Swatch of No Ground” (Bay of Bengal). Deep. Res. Part II Top. Stud. Oceanogr. 50, 1003–1022. https://doi.org/10.1016/S0967-0645(02)00617-3

Middelburg, J.J., 1991. Organic carbon, sulphur, and iron in recent semi-euxinic sediments of Kau Bay, Indonesia. Geochim. Cosmochim. Acta 55, 815–828. https://doi.org/10.1016/0016-7037(91)90344-5

Milliman, J., Meade, R., 1983. World-wide delivery of river sediment to the oceans. J. Geol. 91, l-21

Milliman, J.D., Syvitski, J.P.., 1992. Geomorphic/tectonic control of sediment discharge to the ocean: the importance of small mountainous rivers. J. Geol. 100, 525–544

Mohanty, A.K., Bramha, S.N., Satpathy, K.K., Padhi, R.K., Panigrahi, S.N., Samantara, M.K., 2018. Geochemical distribution of forms of phosphorus in marine sediment of Bay of Bengal , southeast coast of India. Indian J. Geo Mar. Sci. 47, 1132–1141.

Mohanty, P.K., Pradhan, Y., Nayak, S.R., Panda, U.S., Mohapatra, G.N., 2008. Sediment Dispersion in the Bay of Bengal. Monit. Model. Lakes Coast. Environ. 50–78.

Monbet, P., Brunskill, G.J., Zagorskis, I., Pfitzner, J., 2007. Phosphorus speciation in the sediment and mass balance for the central region of the Great Barrier Reef continental shelf (Australia). Geochim. Cosmochim. Acta 71, 2762–2779. https://doi.org/10.1016/j.gca.2007.03.025

Morrison, J.M., Codispoti, L.A., Gaurin, S., Jones, B., Manghnani, V., Zheng, Z., 1998. Seasonal variation of hydrographic and nutrient fields during the US JGOFS Arabian

Sea Process Study. Deep. Res. Part II Top. Stud. Oceanogr. https://doi.org/10.1016/S0967-0645(98)00063-0

Morse, J.W., Cook, N., 1978. The distribution and form of phosphorus in North Atlantic Ocean deep-sea and continental slope sediment. Limnol. Oceanogr. 23, 825–830. https://doi.org/10.4319/lo.1978.23.4.0825

Mort, H.P., Slomp, C.P., Gustafsson, B.G., Andersen, T.J., 2010. Phosphorus recycling and burial in Baltic Sea sediments with contrasting redox conditions. Geochim. Cosmochim. Acta 74, 1350–1362. https://doi.org/10.1016/j.gca.2009.11.016

Mukhopadhyay, R., Batiza, R., 1994. Basinal seamounts and seamount chains of the Central Indian Ocean: Probable near-axis origin from a fast-spreading Ridge. Mar. Geophys. Res. https://doi.org/10.1007/BF01224747

Mukhopadhyay, R., Rajesh, M., De, S., Chakraborty, B., Jauhari, P., 2008. Structural highs on the western continental slope of India: Implications for regional tectonics. Geomorphology 96, 48–61. doi:10.1016/j.geomorph.2007.07.017

Murray, R.W., Leinen, M., 1993. Chemical transport to the seafloor of the equatorial Pacific Ocean across a latitudinal transect at 135°W: Tracking sedimentary major, trace, and rare earth element fluxes at the Equator and the Intertropical Convergence Zone. Geochim. Cosmochim. Acta 57, 4141–4163. doi:10.1016/0016-7037(93)90312-K

Murty, P.S.N., Reddy, C.V.G., Varadachari, V.V.R., 1968. Distribution of total phosphorus in the shelf sediments off the west coast of India, in: Proc. Nat. Inst. Sci. India. pp. 134–141.

Nair, R., 1971. Beachrock and associated carbonate sediments on the Fifty Fathom Flat, a submarine terrace on the outer continental shelf off Bombay. Proc. Indian Acad. Sci. B 73, 148–154

Nair, R., 1985. Holocene phosphorites of the western continental margin of India. Mahasagar 18, 273–279

Nair, R.R., Ittekkot, V., Manganini, S.J., Ramaswamy, V., Haake, B., Degens, E.T., Desai, B.N., Honjo, S., 1989. Increased particle flux to the deep ocean related to monsoons. Nature. 338, 749-751. https://doi.org/10.1038/338749a0

Naqvi, S.W.A., 1987. Some aspects of the oxygen-deficient conditions and denitrification in the Arabian Sea. J. Mar. Res. 45, 1049–1072. https://doi.org/10.1357/002224087788327118

Naqvi, S.W.A., 2008. The Indian Ocean, in: Capone, D.G., Bronk, D.A., Mulholland, M.R., Carpenter, E.. (Eds.), Nitrogen in the Marine Environment. Elsevier, Amsterdam; The Netherlands, pp. 631–681. https://doi.org/10.1016/B978-0-12-372522-6.00014-1

Naqvi, S.W.A., Jayakumar, A., Naik, H., Sarma, V., 2000. Increased Marine Production of N_2O Due to Intensifying Anoxia on the Indian Continental Shelf. Nature 408, 346–349. https://doi.org/10.1038/35042551

Naqvi, S.W.A., Kumar, M.D., Narvekar, P. V., De Sousa, S.N., George, M.D., D'Silva, C., 1993. An intermediate nepheloid layer associated with high microbial metabolic rates and denitrification in the northwest Indian Ocean. J. Geophys. Res. 98, 16469. doi:10.1029/93JC00973

Naqvi, S.W.A., Naik, H., Jayakumar, A., Pratihary, A.K., Narvenkar, G., Kurian, S., Agnihotri, R., Shailaja, M.S., Narvekar, P. V., 2009. Seasonal anoxia over the Western Indian continental shelf. Geophys. Monogr. Ser. 185, 333–345. https://doi.org/10.1029/2008GM000745

Naqvi, S.W.A., Shailaja, M.S., Dileep Kumar, M., Sen Gupta, R., 1996. Respiration rates in subsurface waters of the northern Indian Ocean: evidence for low decomposition rates of organic matter within the water column in the Bay of Bengal. Deep Sea Res. Part II Top. Stud. Oceanogr. 43, 73–81. https://doi.org/10.1016/0967-0645(95)00080-1

Naqvi, S.W.A., Bange, H.W., Farias, L., Monteiro, P.M.S.S., Scranton, M.I., Zhang, J., 2010. Marine hypoxia/anoxia as a source of CH_4 and N_2O. Biogeosciences 7, 2159–2190. https://doi.org/10.5194/bg-7-2159-2010

Nath, B.N., 2001. Geochemistry of sediments, in: Sen Gupta, R., Desa, E. (Eds.), The Indian Ocean : A Perspective. A.A. Balkema, pp. 645–690.Nath, B.N., Balaram, V., Sudhakar, M., Pluger, W.L., 1992a. Rare earth element geochemistry of ferromanganese deposits from the Indian Ocean. Mar. Chem. 38, 185–208

Nath, B.N., Balaram, V., Sudhakar, M., Pluger, W.L., 1992. Rare earth element geochemistry of ferromanganese deposits from the Indian Ocean. Mar. Chem. 38, 185–208.

Nath, B.N., Bau, M., Ramalingeswara Rao, B., Rao, C.M., 1997. Trace and rare earth elemental variation in Arabian Sea sediments through a transect across the oxygen minimum zone. Geochim. Cosmochim. Acta 61, 2375–2388. doi:10.1016/S0016-7037(97)00094-X

Nath, B.N., Borole, D. V., Aldahan, A., Patil, S.K., Mascarenhas-Pereira, M.B.L., Possnert, G., Ericsson, T., Ramaswamy, V., Gupta, S.M., 2008. ^{210}Pb, ^{230}Th, and ^{10}Be in Central Indian Basin seamount sediments: Signatures of degassing and hydrothermal alteration of recent origin. Geophys. Res. Lett. 35, 2–7. https://doi.org/10.1029/2008GL033849

Nath, B.N., Khadge, N.H., Nabar, S., Raghukumar, C., Ingole, B.S., Valsangkar, A.B., Sharma, R., Srinivas, K., 2012. Monitoring the sedimentary carbon in an artificially disturbed deep-sea sedimentary environment. Environ. Monit. Assess. 184, 2829–2844. https://doi.org/10.1007/s10661-011-2154-z

Nath, B.N., Mudholkar, A.V., 1989a. Early diagenetic processes affecting nutrients in the pore waters of Central Indian Ocean cores. Mar. Geol. 86, 57–66. https://doi.org/10.1016/0025-3227(89)90018-2

Nath, B.N., Rao, V.P., Becker, K.P., 1989b. Geochemical evidence of terrigenous influence in deep-sea sediments up to 8°S in the Central Indian Basin. Mar. Geol. 87, 301–313. https://doi.org/10.1016/0025-3227(89)90067-4

Nath, B.N., Roelandts, I., Sudhakar, M., Plüger, W.L., 1992b. Rare Earth element patterns of the Central Indian Basin sediments related to their lithology. Geophys. Res. Lett. 19, 1197–1200. doi:10.1029/92GL01243

Nath, B.N., Roelandts, I., Sudhakar, M., Plüger, W.L., Balaram, V., 1994. Cerium anomaly variations in ferromanganese nodules and crusts from the Indian Ocean. Mar. Geol. 120, 385–400. doi:10.1016/0025-3227(94)90069-8

Nath, B.N., Sijinkumar, A. V., Borole, D. V., Gupta, S.M., Mergulhao, L.P., Mascarenhas-Pereira, M.B.L., Ramaswamy, V., Guptha, M.V.S., Possnert, G., Aldahan, A., Khadge, N.H., Sharma, R., 2013. Record of carbonate preservation and the Mid-Brunhes climatic shift from a seamount top with low sedimentation rates in the Central Indian Basin. Boreas 42, 762–778. https://doi.org/10.1111/j.1502-3885.2012.00304.x

Nenes, A., Krom, M.D., Mihalopoulos, N., Van Cappellen, P., Shi, Z., Bougiatioti, A., Zarmpas, P., Herut, B., 2011. Atmospheric acidification of mineral aerosols: a source of bioavailable phosphorus for the oceans. Atmos. Chem. Phys 11, 6265–6272. https://doi.org/10.5194/acp-11-6265-2011

Ni, J., Lin, P., Zhen, Y., Yao, X., Guo, L., 2015. Distribution, source and chemical speciation of phosphorus in surface sediments of the central Pacific Ocean. Deep Sea Res. Part I Oceanogr. Res. Pap. 105, 74–82. https://doi.org/http://dx.doi.org/10.1016/j.dsr.2015.08.008

Niemeyer, D., Kemena, T.P., Meissner, K.J., Oschlies, A., 2017. A model study of warming-induced phosphorus-oxygen feedbacks in open-ocean oxygen minimum zones on millennial timescales. Earth Syst. Dynam 8, 357–367. https://doi.org/10.5194/esd-8-357-2017

Noffke, A., 2014. Phosphorus cycling in anoxic sediments. Math. Fak.

Noffke, A., Hensen, C., Sommer, S., Scholz, F., Bohlen, L., Mosch, T., Graco, M., Wallmann, K., 2012. Benthic iron and phosphorus fluxes across the Peruvian oxygen minimum zone. Limnol. Oceanogr. 57, 851–867. https://doi.org/10.4319/lo.2012.57.3.0851

O'Connell, D.W., Mark Jensen, M., Jakobsen, R., Thamdrup, B., Joest Andersen, T., Kovacs, A., Bruun Hansen, H.C., 2015. Vivianite formation and its role in phosphorus retention in Lake Ørn, Denmark. Chem. Geol. 409, 42–53. https://doi.org/10.1016/j.chemgeo.2015.05.002

Ogrinc, N., Faganeli, J., 2006. Phosphorus regeneration and burial in near-shore marine sediments (the Gulf of Trieste, northern Adriatic Sea). Estuar. Coast. Shelf Sci. 67, 579–588. https://doi.org/10.1016/j.ecss.2005.12.016

Okin, G.S., Baker, A.R., Tegen, I., Mahowald, N.M., Dentener, F.J., Duce, R.A., Galloway, J.N., Hunter, K., Kanakidou, M., Kubilay, N., Prospero, J.M., Sarin, M., Surapipith, V., Uematsu, M., Zhu, T., 2011. Impacts of atmospheric nutrient deposition on marine productivity: Roles of nitrogen, phosphorus, and iron. Global Biogeochem. Cycles 25. doi:10.1029/2010GB003858

Olson, D.B., Hitchcock, G.L., Fine, R.A., Warren, B.A., 1993. Maintenance of the low-oxygen layer in the central Arabian Sea. Deep Sea Res. Part II Top. Stud. Oceanogr. 40, 673–685. https://doi.org/10.1016/0967-0645(93)90051-N

Ostlund, H.G., Oleson, R., Brescher, R., 1980. GEOSECS Indian Ocean radiocarbon and tritium results (Miami). Data report

Ostrofsky, M.L., 2012. Determination of total phosphorus in lake sediments. Hydrobiologia 696, 199–203. doi:10.1007/s10750-012-1208-8

Pakhomova, S. V., Hall, P.O.J., Kononets, M.Y., Rozanov, A.G., Tengberg, A., Vershinin, A. V., 2007. Fluxes of iron and manganese across the sediment-water interface under various redox conditions. Mar. Chem. https://doi.org/10.1016/j.marchem.2007.06.001

Palastanga, V., Slomp, C.P., Heinze, C., 2011. Long-term controls on ocean phosphorus and oxygen in a global biogeochemical model. Global Biogeochem. Cycles 25, 1–19. doi:10.1029/2010GB003827

Paropkari, a L., Babu, C.P., Mascarenhas, a, 1992. A critical evaluation of depositional parameters controlling the variability of organic carbon in Arabian Sea sediments. Mar. Geol. 107, 213–226

Parsons, T.R., Malta, Y., Lalli, C.M., 1984. A Manual of Chemical and Biological Methods for Seawater Analysis. Pergamon Press New York.

Passier, H.F., Luther, G.W., De Lange, G.J., 1997. Early diagenesis and sulphur speciation in sediments of the Oman Margin, northwestern Arabian Sea. Deep. Res. Part II Top. Stud. Oceanogr. 44, 1361–1380. https://doi.org/10.1016/S0967-0645(97)00014-3

Pattan, J., Gupta, S., Mudholkar, A., Parthiban, G., 1992. Biogenic silica in space and time in sediments of Central Indian Ocean. Indian J. Mar. Sci. 21, 116–120.

Pattan, J.N., Jauhari, P., 2001. Major, trace, and rare earth elements in the sediments of the Central Indian Ocean Basin: their source and distribution. Mar. Georesources Geotechnol. 19, 85–106. https://doi.org/10.1080/10641190109353806

Pattan, J.N., Mir, I.A., Parthiban, G., Karapurkar, S.G., Matta, V.M., Naidu, P.D., Naqvi, S.W.A., 2013. Coupling between suboxic condition in sediments of the western Bay of Bengal and southwest monsoon intensification: A geochemical study. Chem. Geol. https://doi.org/10.1016/j.chemgeo.2013.02.011

Pattan, J.N., Parthiban, G., Garg, A., Moraes, N.R.C., 2017. Intense reducing conditions during the last deglaciation and Heinrich events (H1, H2, H3) in sediments from the oxygen minimum zone off Goa, eastern Arabian Sea. Mar. Pet. Geol. 84, 243–256. doi:10.1016/j.marpetgeo.2017.03.034

Paulmier, A., Ruiz-Pino, D., 2009. Oxygen minimum zones (OMZs) in the modern ocean. Prog. Oceanogr. https://doi.org/10.1016/j.pocean.2008.08.001

Paytan, A., Cade-menun, B.J., Mclaughlin, K., Faul, K.L., 2003. Selective phosphorus regeneration of sinking marine particles : evidence from 31 P-NMR. Mar. Chem. 82, 55–70. doi:10.1016/S0304-4203(03)00052-5

Paytan, A., McLaughlin, K., 2007. The oceanic phosphorus cycle. Chem. Rev. 107, 563–576. https://doi.org/10.1021/cr0503613

Pedersen, T.., Shimmield, G.., N.B, P., 1992. Lack of enhanced preservation of organic matter in sediments under the oxygen minimum on the Oman Margin. Geochim. Cosmochim. Acta 56, 545–551. doi:10.1016/0016-7037(92)90152-9

Perdue, E.., Koprivnjak, J.., 2007. Using the C/N ratio to estimate terrigenous inputs of organic matter to aquatic environments. Estuar. Coast. Shelf Sci. 73, 65–72. https://doi.org/10.1016/j.ecss.2006.12.021

Poulton, S.W., Canfield, D.E., 2006. Co-diagenesis of iron and phosphorus in hydrothermal sediments from the southern East Pacific Rise: Implications for the evaluation of paleoseawater phosphate concentrations. Geochim. Cosmochim. Acta 70, 5883–5898. https://doi.org/10.1016/j.gca.2006.01.030

Prahl, F.., Bennett, J.., Carpenter, R., 1980. The early diagenesis of aliphatic hydrocarbons and organic matter in sedimentary particulates from Dabob Bay, Washington. Geochim. Cosmochim. Acta 44, 1967–1976. https://doi.org/10.1016/0016-7037(80)90196-9

Prakash, S., Nair, T.M.B., Bhaskar, T.V.S.U., Prakash, P., Gilbert, D., 2012. Oxycline variability in the central Arabian Sea: An Argo-oxygen study. J. Sea Res. https://doi.org/10.1016/j.seares.2012.03.003

Prospero, J.M., Glaccum, R.A., Nees, R.T., 1981. Atmospheric transport of soil dust from Africa to South America. Nature 289, 570–572. https://doi.org/10.1038/289570a0

Qasim, S.Z., 1982. Oceanography of the northern Arabian Sea. Deep Sea Res. Part A, Oceanogr. Res. Pap. 29, 1041–1068. doi:10.1016/0198-0149(82)90027-9

Raiswell, R., Berner, R.A., 1985. Pyrite formation in euxinic and semi-euxinic sediments. Am. J. Sci. 285, 710–724. https://doi.org/10.2475/ajs.285.8.710

Raiswell, R., Canfield, D.E., 1998. Sources of iron for pyrite formation in marine sediments. Am. J. Sci. 298, 219--245.

Rajeev, K., Ramanathan, V., Meywerk, J., 2000. Regional aerosol distribution and its long-range transport over the Indian Ocean. J. Geophys. Res. 105, 2029. https://doi.org/10.1029/1999JD900414

Ramaswamy, V., Muraleedharan, P.M., Babu, C.P., 2017. Mid-troposphere transport of Middle-East dust over the Arabian Sea and its effect on rainwater composition and sensitive ecosystems over India. Sci. Rep. 7, 13676. https://doi.org/10.1038/s41598-017-13652-1

Ramaswamy, V., Nair, R.R., Manganini, S., Haake, B., Ittekkot, V., 1991. Lithogenic fluxes to the deep Arabian sea measured by sediment traps. Deep Sea Res. Part A, Oceanogr. Res. Pap. 38, 169–184. https://doi.org/10.1016/0198-0149(91)90078-T

Ramesh, R., Purvaja, G.R., Subramanian, V., 1995. Carbon and phosphorus transport by the major Indian rivers. J. Biogeogr. 22, 409–415. https://doi.org/10.2307/2845937

Ramesh, R., Robin, R.S., Purvaja, R., 2015. An inventory on the phosphorus flux of major Indian rivers. Curr. Sci. 108, 1294–1299.

Ramirez, A.J., Rose, A.W., 1992. Analytical geochemistry of organic phosphorus and its correlation with organic carbon in marine and fluvial sediments and soils. Am. Jounal Sci. 292, 421–454.

Rao, C.K., Naqvi, S.W.., Kumar, M.D., Varaprasad, S.J.., Jayakumar, D.A., George, M.D., Singbal, S.Y.., 1994. Hydrochemistry of the Bay of Bengal: possible reasons for a different water-column cycling of carbon and nitrogen from the Arabian Sea. Mar. Chem. 47, 279–290. https://doi.org/10.1016/0304-4203(94)90026-4

Rao, C.M., Paropkari, A.L., Mascarenhas, A., Murty, P.S.N., 1987. Distribution of phosphorus and phosphatisation along the western continental margin of India. J. Geol. Soc. India 30, 423–438.

Rao, C.M., Rajamanickam, G. V, Paropkari, A.L., Murty, P.S.N., 1978. Distribution of phosphate in sediments of the northern half of the western continental shelf of India. Indian J. Mar. Sci. 7, 146–150.

Rao, C.M., Rao, B.R., 1996. Phosphorite concretions in a sediment core from a bathymetric high off Goa, western continental margin of India. Curr. Sci. 70, 308–312.

Rao, D.G., Paropkari, A.L., Krishna, K.S., Chaubey, A.K., Ajay, K.K., Kodagali, V.N., 2010. Bathymetric highs in the mid-slope region of the western continental margin of India—Structure and mode of origin. Mar. Geol. 276, 58–70. doi:10.1016/j.margeo.2010.07.007

Rao, V.P., 1986. Phosphorites from the Error Seamount, Northern Arabian Sea. Mar. Geol. 71, 177–186. doi:10.1016/0025-3227(86)90038-1

Rao, V.P 1987. Mineralogy of polymetallic nodules and associated sediments from the Central Indian Ocean Basin. Mar. Geol. 74, 151–157.

Rao, V.P., Hegner, E., Naqvi, S.W.A., Kessarkar, P.M., Ahmad, S.M., Raju, D.S., 2008. Miocene phosphorites from the Murray Ridge, northwestern Arabian Sea. Palaeogeogr. Palaeoclimatol. Palaeoecol. 260, 347–358. https://doi.org/10.1016/j.palaeo.2007.12.003

Rao, V.P., Kessarkar, P.M., 2001. Geomorphology and geology of the Bay of Bengal and the Andaman Sea, in: The Indian Ocean: A Perspective. Oxford and IBH New Delhi, pp. 817–868.

Rao, V.P., Kessarkar, P.M., Nagendra, R., Babu, E.V.S.S.K., 2007. Origin of Cretaceous phosphorites from the onshore of Tamil Nadu, India. J. Earth Syst. Sci. 116, 525–536. doi:10.1007/s12040-007-0048-9

Rao, V.P., Lamboy, M., 1995. Phosphorites from the Oman Margin, ODP Leg 117. Oceanol. acta 18, 289–308.

Rao, V.P., Lamboy, M., 1996. Genesis of apatite in the phosphatized limestones of the western continental shelf of India. Mar. Geol. 136, 41–53. doi:10.1016/S0025-3227(96)00062-X

Rao, V.P., Michard, A., Naqvi, S.W.A., Böttcher, M.E., Krishnaswamy, R., Thamban, M., Natarajan, R., Borole, D. V., 2002. Quaternary phosphorites off the southeast coast of India. Chem. Geol. 182, 483–502. https://doi.org/10.1016/S0009-2541(01)00336-9

Rao, V.P., Nair, R.R., 1988. Microbial origin of the phosphorites of the western continental shelf of India. Mar. Geol. 84, 105–110. doi:10.1016/0025-3227(88)90128-4

Rao, V.P, Nath, B.N., 1988. Nature, distribution and origin of clay minerals in grain size fractions of sediment samples from the Central Indian Ocean Basin. Indian J. Mar. Sci. 17, 202–207.

Rao, V.P., Rao, B.R., 1995. Provenance and distribution of clay minerals in the sediments of the western continental shelf and slope of India. Cont. Shelf Res. 15, 1757–1771

Rao, V.P., Rao, C.M., Thamban, M., Natarajan, R., Rao, B.R., 1995. Origin and significance of high-grade phosphorite in a sediment core from the continental slope off Goa, India. Curr. Sci. 69, 1017–1022.

Rao, V.P., Rao, K.M., Vora, K.H., Almeida, F., Subramaniam, M.M., Souza, C.G.A., 1998. A potential phosphorite deposit on the continental margin off Chennai. Curr. Sci. 74, 574–577.

Rao, V.P., Rao, K.. M., Raju, D.S.N., 2000. Quaternary Phosphorites from the Continental Margin Off Chennai, Southeast India: Analogs of Ancient Phosphate Stromatolites. J. Sediment. Res. 70, 1197–1209. https://doi.org/10.1306/012400701197

Rao, V.P., Wagle, B., 1997. Geomorphology and surficial geology of the western continental shelf and slope of India: A review. Curr. Sci. 73

Redfield, A.C., 1958. The biological control of chemical factors in the environment. Am. Sci. 46, 230A–221.

Roh, Y., Zhang, C.L., Zhou, J., 2003. Biogeochemical and environmental factors in Fe biomineralization: Magnetite and siderite formation. Clays Clay Miner. 51, 83–95. https://doi.org/10.1346/CCMN.2003.510110

Rothe, M., Frederichs, T., Eder, M., Kleeberg, A., Hupfer, M., 2014. Evidence for vivianite formation and its contribution to long-term phosphorus retention in a recent lake sediment: a novel analytical approach. Biogeosciences 11, 5169–5180. https://doi.org/10.5194/bg-11-5169-2014

Ruttenberg, K.C., 1992. Development of a Sequential Extraction Method for Different Forms of Phosphorus in Marine Sediments. Limnol. Oceanogr. 37, 1460–1482. https://doi.org/10.4319/lo.1992.37.7.1460

Ruttenberg, K.C., 2003. The global phosphorus cycle. Treatise on Geochemistry 8, 682.

Ruttenberg, K.C., Berner, R.A., 1993. Authigenic apatite formation and burial in sediments from non-upwelling, continental margin environments. Geochim. Cosmochim. Acta 57, 991–1007. doi:10.1016/0016-7037(93)90035-U

Ruttenberg, K.C., Sulak, D.J., 2011. Sorption and desorption of dissolved organic phosphorus onto iron (oxyhydr)oxides in seawater. Geochim. Cosmochim. Acta 75, 4095–4112. https://doi.org/10.1016/J.GCA.2010.10.033

Sankaranarayanan, V.N., 1978. Some physical and chemical studies of the waters of the northern Arabian Sea. Ph. D. Thesis, Kerala University, Trivandrum, India

Sannigrahi, P., Ingall, E., 2005. Polyphosphates as a source of enhanced P fluxes in marine sediments overlain by anoxic waters: Evidence from 31P NMR. Geochem. Trans. 6, 52–59. https://doi.org/10.1063/1.1946447

Sapota, T., Aldahan, A., Al-Aasm, I.S., 2006. Sedimentary facies and climate control on formation of vivianite and siderite microconcretions in sediments of Lake Baikal, Siberia. J. Paleolimnol. 36, 245–257. https://doi.org/10.1007/s10933-006-9005-x

Sardessai, S., Ramaiah, N., Kumar, S.P., De Sousa, S.N., 2007. Influence of environmental forcings on the seasonality of dissolved oxygen and nutrients in the Bay of Bengal. J. Mar. Res. 65, 301–316.

Sarin, M.M., Borole, D.., Krishnaswami, S., 1979. Geochemistry and geochronology of sediments from the Bay of Bengal and the equatorial Indian Ocean. Proc. Indian Acad. Sci 88, 131–154.

Sarin, M.M., Krishnaswami, S., Dilli, K., Somayajulu, B.L.K., Moore, W.S., 1989. Major ion chemistry of the Ganga-Brahmaputra river system: Weathering processes and fluxes to the Bay of Bengal. Geochim. Cosmochim. Acta. https://doi.org/10.1016/0016-7037(89)90205-6

Sarin, M.M., Krishnaswami, S., Somayajulu, L.K., Moorer, W.S., 1990. Chemistry of uranium, thorium, and radium isotopes in the Ganga-Brahmaputra river system: Weathering processes and fluxes to the Bay of Bengal. Gecchimica ef Ccmmxhimifa Acta 54, 1387–1396.

Sarma, V.V.S.S., Krishna, M., Prasad, V., Kumar, B., Naidu, S., Rao, G., Viswanadham, R., Sridevi, T., Kumar, P., Reddy, N., 2014. Distribution and sources of particulate organic matter in the Indian monsoonal estuaries during monsoon. J. Geophys. Res. Biogeosciences 119, 2095–2111. https://doi.org/10.1002/2013JG002433

Sarma, V.V.S.S., Krishna, M.S., Viswanadham, R., Rao, G.D., Rao, V.D., Sridevi, B., Kumar, B.S.K., Prasad, V.R., Subbaiah, C. V., Acharyya, T., Bandopadhyay, D., 2013. Intensified oxygen minimum zone on the western shelf of Bay of Bengal during summer monsoon: Influence of river discharge. J. Oceanogr. 69, 45–55. https://doi.org/10.1007/s10872-012-0156-2

Sarma, V.V.S.S., Kumar, M.D., George, M.D., Rajendran, A., 1996. Seasonal variations in inorganic carbon components in the central and eastern Arabian Sea. Curr. Sci. 71, 852–856. https://doi.org/10.2307/24098558

Sarma, V.V.S.S., Rao, G.D., Viswanadham, R., Sherin, C.K., Salisbury, J., Omand, M.M., Mahadevan, A., Murty, V.S.N., Shroyer, E.L., Baumgartner, M., Stafford, K.M., 2016. Effects of Freshwater Stratification on Nutrients, Dissolved Oxygen, and Phytoplankton in the Bay of Bengal. Oceanography 29, 222–231. https://doi.org/10.5670/oceanog.2016.54

Schenau, S.J., De Lange, G.J., 2000. A novel chemical method to quantify fish debris in marine sediments. Limnol. Ocean. 45, 963–971. https://doi.org/10.4319/lo.2000.45.4.0963

Schenau, S.J., De Lange, G.J., 2001. Phosphorus regeneration vs. burial in sediments of the Arabian Sea. Mar. Chem. 75, 201–217. https://doi.org/10.1016/S0304-4203(01)00037-8

Schenau, S.J., Passier, H.F., Reichart, G.J., de Lange, G.J., 2002. Sedimentary pyrite formation in the Arabian Sea. Mar. Geol. 185, 393–402. doi:10.1016/S0025-3227(02)00183-4

Schenau, S.J., Reichart, G.J., De Lange, G.J., 2005. Phosphorus burial as a function of paleoproductivity and redox conditions in Arabian Sea sediments. Geochim. Cosmochim. Acta 69, 919–931. https://doi.org/10.1016/J.GCA.2004.05.044

Schenau, S.J., Slomp, C.P., De Lange, G.J., 2000. Phosphogenesis and active phosphorite formation in sediments from the Arabian Sea oxygen minimum zone. Mar. Geol. 169, 1–20. https://doi.org/10.1016/S0025-3227(00)00083-9

Schott, F.A., McCreary, J.P., 2001. The monsoon circulation of the Indian Ocean. Prog. Oceanogr. 51, 1-123. https://doi.org/10.1016/S0079-6611(01)00083-0

Sen Gupta, R., Sankaranarayanan, N., Sousa, D.E., Fondekar, S.P., 1976. Chemical oceanography of the Arabian Sea: Part III-Studies on nutrient fraction and stoichiometric relationships in the northern and the eastern basins. Indian J. Mar. Sci. 5, 58–71.

Sensarma, S., Banerjee, R., Satyanarayanan, M., Mukhopadhyay, S., 2017. Depositional environment of the surface sediments in Central Indian Basin (CIB), Indian Ocean, between 8°-18°S latitude and 72°-79°E longitude, based on their geochemical characteristics. Geol. J. 1–18. https://doi.org/10.1002/gj.2978

Setty, M., Rao, C.M., 1972. Phosphate, carbonate and organic matter distribution in sediment cores off Bombay–Saurashtra coast, India, in: Twenty-Fourth International Geological Congress, Canada. pp. 182–191.

Severmann, S., McManus, J., Berelson, W.M., Hammond, D.E., 2010. The continental shelf benthic iron flux and its isotope composition. Geochim. Cosmochim. Acta. 74, 3984-4004. https://doi.org/10.1016/j.gca.2010.04.022

Shankar, R., Subbarao, K. V., Kolla, V., 1987. Geochemistry of surface sediments from the Arabian Sea. Mar. Geol. 76, 253–279. https://doi.org/10.1016/0025-3227(87)90033-8

Shetye, S.R., Gouveia, A.D., Shenoi, S.S.C., 1994. Circulation and water masses of the Arabian Sea. Proc. Indian Acad. Sci. (Earth Planet. Sci.) 103, 107–123

Shimmield, G.B., Mowbray, S.R., Weedon, G.P., 1990. A 350 ka history of the Indian Southwest Monsoon—evidence from deep-sea cores, northwest Arabian Sea. Trans. R. Soc. Edinb. Earth Sci. 81, 289–299. doi:10.1017/S0263593300020800

Sibanda, H.M., Young, S.D., 1986. Competitive adsorption of humus acids and phosphate on goethite, gibbsite and two tropical soils. J. Soil Sci. 37, 197–204. https://doi.org/10.1111/j.1365-2389.1986.tb00020.x

Sirocko, F., Sarnthein, M., 1989. Wind-Borne Deposits in the Northwestern Indian Ocean: Record of Holocene Sediments Versus Modern Satellite Data, in: Leinen, M., Sarnthein, M. (Eds.), Paleoclimatology and Paleometeorology: Modern and Past Patterns of Global Atmospheric Transport. Springer Netherlands, Dordrecht, pp. 401–433. doi:10.1007/978-94-009-0995-3_17

Sirocko, F., Sarnthein, M., Lange, H., Erlenkeuser, H., 1991. Atmospheric summer circulation and coastal upwelling in the Arabian Sea during the Holocene and the last glaciation. Quat. Res. 36, 72–93. doi:10.1016/0033-5894(91)90018-Z

Slater, R.D., Kroopnick, P., 1984. Controls of dissolved oxygen distribution and organic carbon deposition in the Arabian Sea. Geol. Oceanogr. Arab. Sea Coast. Pakistan 305—313.

Slomp, C.P., 2011. Phosphorus Cycling in the Estuarine and Coastal Zones, Treatise on Estuarine and Coastal Science. Elsevier Inc. https://doi.org/10.1016/B978-0-12-374711-2.00506-4

Slomp, C.P., Epping, E.H.G., Helder, W., Raaphorst, W. Van, 1996a. A key role for iron-bound phosphorus in authigenic apatite formation in North Atlantic continental platform sediments. J. Mar. Res. 54, 1179–1205. https://doi.org/10.1357/0022240963213745

Slomp, C.P., Mort, H.P., Jilbert, T., Reed, D.C., Gustafsson, B.G., Wolthers, M., 2013. Coupled Dynamics of Iron and Phosphorus in Sediments of an Oligotrophic Coastal Basin and the Impact of Anaerobic Oxidation of Methane. PLoS One 8. https://doi.org/10.1371/journal.pone.0062386

Slomp, C.P., Van Der Gaast, S.J., Van Raaphorst, W., 1996b. Phosphorus binding by poorly crystalline iron oxides in North Sea sediments. Mar. Chem. 52, 55–73. https://doi.org/10.1016/0304-4203(95)00078-X

Slomp, C.P., van Raaphorst, W., 1993. Phosphate adsorption in oxidized marine sediments. Chem. Geol. 107, 477–480. https://doi.org/10.1016/0009-2541(93)90235-B

Somayajulu, Y.K., Murty, V.S.N., Sarma, Y.V.B., 2003. Seasonal and inter-annual variability of surface circulation in the Bay of Bengal from TOPEX/Poseidon altimetry. Deep. Res. Part II Top. Stud. Oceanogr. https://doi.org/10.1016/S0967-0645(02)00610-0

Srinivas, B., Sarin, M.M., 2012. Atmospheric pathways of phosphorous to the Bay of Bengal: contribution from anthropogenic sources and mineral dust. Tellus B Chem. Phys. Meteorol. 64, 1–12. https://doi.org/10.3402/tellusb.v64i0.17174

Srinivas, B., Sarin, M.M., 2013. Atmospheric deposition of N, P and Fe to the Northern Indian Ocean: Implications to C- and N-fixation. Sci. Total Environ. 456–457, 104–114. https://doi.org/10.1016/j.scitotenv.2013.03.068

Srinivas, B., Sarin, M.M., 2015. Atmospheric deposition of phosphorus to the Northern Indian Ocean. Curr. Sci. 108, 7.

Stoll, H.M., Arevalos, A., Burke, A., Ziveri, P., Mortyn, G., Shimizu, N., Unger, D., 2007. Seasonal cycles in biogenic production and export in Northern Bay of Bengal sediment traps. Deep. Res. II 54, 558–580. https://doi.org/10.1016/j.dsr2.2007.01.002

Strickland, J.D., Parsons, T.R., 1960. A manual of seawater analysis,Bulletin of the Fisheries Research Board of Canada, 125, 1-185.

Strickland, J.D., Parsons, T.R., 1972. A practical handbook of seawater analysis, 2nd ed. Fisheries Research Board of Canada.

Subramanian, V., 1985. Geochemistry of river basins in the Indian subcontinent, Part I: Water Chemistry, Chemical Erosion and Water-Mineral Equilibria, in: Egon T. Degens, Stephan Kempe, Hassan Soliman (Eds.), Transport of Carbon and Minerals in Major World Rivers. Mittilungen aus dem Geologisch- Palaeontologischen, Institut der Universitat Hamburg, pp. 495–512.

Subramanian, V., 1993. Sediment load of Indian rivers. Curr. Sci. 64, 928–930. https://doi.org/10.2307/24096213

Sudheesh, V., Movitha, M., Hatha, A.A.M., Renjith, K.R., Resmi, P., Rahiman, M., Nair, S.M., 2017. Effects of seasonal anoxia on the distribution of phosphorus fractions in the surface sediments of southeastern Arabian Sea shelf. Cont. Shelf Res. 150, 57–64. https://doi.org/10.1016/J.CSR.2017.09.011

Suess, E., 1981. Phosphate regeneration from sediments of the Peru continental margin by dissolution of fish debris. Geochim. Cosmochim. Acta 45, 577–588. doi:10.1016/0016-7037(81)90191-5

Suess, E., Muller, P.. J., Powel, H.. S., Reimers, C.. E., 1980. A closer look at nitrification in pelagic sediments. Geochem. J. 14, 129–137.

Sundby, B., Gobeil, C., Silverberg, N., Mucci, A., 1992. The phosphorus cycle in coastal marine sediments. Limnol. Oceanogr. 37, 1129–1145. https://doi.org/10.4319/lo.1992.37.6.1129

Swallow, J.C., Molinari, R.L., Bruce, J.G., Brown, O.B., Evans, R.H., 1983. Development of Near-Surface Flow Pattern and Water Mass Distribution in the Somali Basin in Response to the Southwest Monsoon of 1979. J. Phys. Oceanogr. 13, 1398–1415. https://doi.org/10.1175/1520-0485(1983)013<1398:donsfp>2.0.co;2

Tchernia, P., 1980. Descriptive regional oceanography. Pergamon.

Thamdrup, B., 2000. Bacterial Manganese and Iron Reduction in Aquatic Sediments, in: Advances in Microbial Ecology. Springer, Boston, MA, pp. 41–84. https://doi.org/10.1007/978-1-4615-4187-5_2

Thangaradjou, T., Sarangi, R.K., Shanthi, R., Poornima, D., Raja, K., Saravanakumar, A., Balasubramanian, S.T., 2014. Changes in nutrients ratio along the central Bay of Bengal coast and its influence on chlorophyll distribution. J. Environ. Biol. 35, 467–477.

Torrent, J., Schwertmann, U., 1992. Fast and slow phosphate sorption by goethite-rich natural minerals. Clays Clay Miner. 14-21.

Tripathy, G.., Singh, S.., Ramaswamy, V., 2014. Major and trace element geochemistry of Bay of Bengal sediments: Implications to provenances and their controlling factors. Palaeogeogr. Palaeoclimatol. Palaeoecol. 397, 20–30. https://doi.org/10.1016/j.palaeo.2013.04.012

Tsandev, I., Reed, D.C., Slomp, C.P., 2012. Phosphorus diagenesis in deep-sea sediments: Sensitivity to water column conditions and global scale implications. Chem. Geol. 330–331, 127–139. https://doi.org/10.1016/j.chemgeo.2012.08.012

Tyrrell, T., 1999. The relative influences of nitrogen and phosphorus on oceanic primary production. Nature 400, 525–531.

Valsangkar, A.B., 2011. Spatial distribution and longitudinal variation of clay minerals in the central indian basin. Acta Geol. Sin. (English Ed. 85, 814–825.

Van Cappellen, P., Berner, R.A., 1988. A mathematical model for the early diagenesis of phosphorus and fluorine in marine sediments; apatite precipitation. Am. J. Sci. 288, 289–333.

van der Weijden, C.H., Reichart, G.J., Visser, H.J., 1999. Enhanced preservation of organic matter in sediments deposited within the oxygen minimum zone in the northeastern Arabian Sea. Deep Sea Res. Part I Oceanogr. Res. Pap. 46, 807–830. https://doi.org/10.1016/S0967-0637(98)00093-4

van der Zee, C., Slomp, C.P., van Raaphorst, W., 2002. Authigenic P formation and reactive P burial in sediments of the Nazaré canyon on the Iberian margin (NE Atlantic). Mar. Geol. 185, 379–392. https://doi.org/10.1016/S0025-3227(02)00189-5

Vaz, G.G, Vijaykumar, P., Rao, B.L., 1999. Phosphorite from the continental margin off madras, bay of bengal. Mar. Georesources Geotechnol. 17, 33–48. https://doi.org/10.1080/106411999273990

Vaz, G.G., 1995. Phosphatic nodules in the outer continental shelf off Madras, Bay of Bengal. Indian J. Mar. Sci. 24, 8–12.

Vaz, G.G., Faruque, B., Biswas, N., Vijaykumar, P., Misra, U., Sankar, J., Rao, J., 1996. Phosphorite from the upper continental slope off Kachchh, northwest coast of India. Indian J. Mar. Sci. 25, 20–24.

Vaz, G.G., Vijaykumar, P., Rao, B.L., 1999. Phosphorite from the Continental Margin off Madras, Bay of Bengal. Mar. Georesources Geotechnol. 17, 33–48. doi:10.1080/106411999273990

Viktorsson, L., Ekeroth, N., Nilsson, M., Kononets, M., Hall, P.O.J.J., 2013. Phosphorus recycling in sediments of the central Baltic Sea. Biogeosciences 10, 3901–3916. https://doi.org/10.5194/bg-10-3901-2013

Vineesh, T.C., Nath, B.N., Banerjee, R., Jaisankar, S., Lekshmi, V., 2009. Manganese nodule morphology as indicators for oceanic processes in the Central Indian Basin. Int. Geol. Rev. 51, 27–44. https://doi.org/10.1080/00206810802622773

Wallmann, K., 2003. Feedbacks between oceanic redox states and marine productivity: A model perspective focused on benthic phosphorus cycling. Global Biogeochem. Cycles 17, n/a--n/a. https://doi.org/10.1029/2002GB001968

Wallmann, K., 2010. Phosphorus imbalance in the global ocean? Global Biogeochem. Cycles 24, 1–12. https://doi.org/10.1029/2009GB003643

Warren, B.A., 1982. The deep water of the Central Indian Basin. J. Mar. Res. 40, 823–859.

Watanabe, F.S., Olsen, S.R., 1962. Colorometric determination of phosphorus in water extracts of soils. Soil Sci. 93, 183–188.

Wheat, C.G., Freely, A.R., Mottl, M.J., 1996. Phosphate removal by oceanic hydrothermal processes: An update of the phosphorus budget in the oceans. Geochim. Cosmochim. Acta 60, 3593–3608.

Wheat, C.G., McManus, J., Mottl, M.J., Giambalvo, E., 2003. Oceanic phosphorus imbalance: Magnitude of the mid-ocean ridge flank hydrothermal sink. Geophys. Res. Lett. 30, n/a--n/a. https://doi.org/10.1029/2003GL017318

Wijsman, J.W.M.M., Middelburg, J.J., Herman, P.M.J.J., Böttcher, M.E., Heip, C.H.R.R., 2001. Sulfur and iron speciation in surface sediments along the northwestern margin of the Black Sea. Mar. Chem. 74, 261–278. https://doi.org/10.1016/S0304-4203(01)00019-6

Wilkin, R.T., Barnes, H.L., 1996. Pyrite formation by reactions of iron monosulfides with dissolved inorganic and organic sulfur species. Geochim. Cosmochim. Acta 60, 4167–4179. https://doi.org/10.1016/S0016-7037(97)81466-4

Witter, A.E., Lewis, B.L., Luther, G.W., 2000. Iron speciation in the Arabian Sea. Deep. Res. Part II Top. Stud. Oceanogr. 47, 1517–1539. https://doi.org/10.1016/S0967-0645(99)00152-6

Wollast, R., 1993. Interactions of Carbon and Nitrogen Cycles in the Coastal Zone, in: Interactions of C, N, P and S Biogeochemical Cycles and Global Change. Springer Berlin Heidelberg, Berlin, Heidelberg, pp. 195–210. https://doi.org/10.1007/978-3-642-76064-8_7

Woodward, E.M.S., Rees, A.P., Stephens, J.A., 1999. The influence of the south-west monsoon upon the nutrient bigeochemistry of the Arabian Sea. Deep. Res. II 46, 571–591.

Woulds, C., Schwartz, M.C., Brand, T., Cowie, G.L., Law, G., Mowbray, S.R., 2009. Porewater nutrient concentrations and benthic nutrient fluxes across the Pakistan margin OMZ. Deep. Res. Part II Top. Stud. Oceanogr. 56, 333–346. https://doi.org/10.1016/j.dsr2.2008.05.034

Wright, J., Seymour, R.S., Shaw, H.F., 1984. REE and Nd isotopes in conodont apatite: Variations with geological age and depositional environment, in: Clark, D.L. (Ed.), Conodont Biofacies and Provincialism. Geological Society of America, pp. 325–340. doi:10.1130/SPE196-p325

Wyrtki, K., 1973. Physical Oceanography of the Indian Ocean, in: The Biology of the Indian Ocean. Springer, Berlin, Heidelberg, pp. 18–36. https://doi.org/10.1007/978-3-642-65468-8_3

Yamagata, Y., Watanabe, H., Saitoh, M., Namba, T., 1991. Volcanic production of polyphosphates and its relevance to prebiotic evolution. Nature 352, 516–519. https://doi.org/10.1038/352516a0

Yang, B., Song, G.-D., Liu, S.M., Jin, J., 2017. Phosphorus recycling and burial in core sediments of the East China Sea. Mar. Chem. 192, 59–72

Zabel, M., Dahmke, A., Schulz, H.D., 1998. Regional distribution of diffusive phosphate and silicate fluxes through the sediment-water interface: The eastern South Atlantic. Deep. Res. Part I Oceanogr. Res. Pap. 45, 277–300. https://doi.org/10.1016/S0967-0637(97)00073-3

Zhang, J.Z., Huang, X.L., 2007. Relative importance of solid-phase phosphorus and iron on the sorption behavior of sediments. Environ. Sci. Technol. 41, 2789–2795. https://doi.org/10.1021/es061836q

Zhao, Q., Poulson, S.R., Obrist, D., Sumaila, S., Dynes, J.J., Mcbeth, J.M., Yang, Y., 2016. Iron-bound organic carbon in forest soils: quantification and characterization. Biogeosciences 13, 4777–4788. https://doi.org/10.5194/bg-13-4777-2016

Zhu, M.X., Hao, X.C., Shi, X.N., Yang, G.P., Li, T., 2012. Speciation and spatial distribution of solid-phase iron in surface sediments of the East China Sea continental shelf. Appl. Geochemistry 27. https://doi.org/10.1016/j.apgeochem.2012.01.004

Zhu, M.X., Shi, X.N., Yang, G.P., Hao, X.C., 2013. Formation and burial of pyrite and organic sulfur in mud sediments of the East China Sea inner shelf: Constraints from solid-phase sulfur speciation and stable sulfur isotope. Cont. Shelf Res. 54, 24–36. https://doi.org/10.1016/j.csr.2013.01.002